Investigation of the Biosynthesis of Exopolysaccharides within the Biofilm Matrix of *Pseudomonas aeruginosa* and *Pseudomonas syringae* pv. *actinidiea*

A thesis presented in partial fulfilment of the requirements for degree

of

Doctor of Philosophy

In

Microbiology and Genetics

At Massey University, Manawatu,

New Zealand

Shirin Ghods

2017

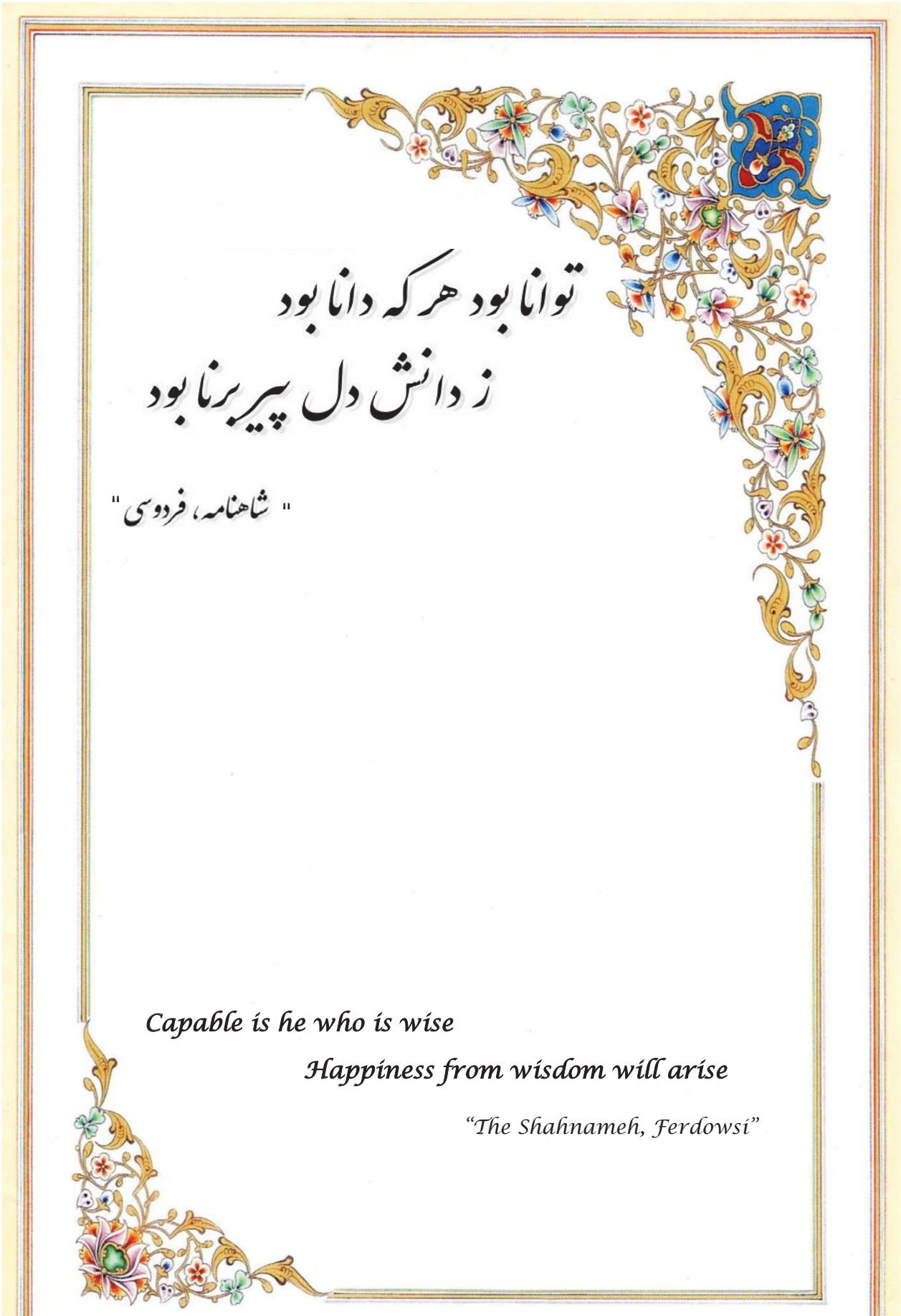

توانا بود هر که دانا بود
ز دانش دل پیر برنا بود

" شاهنامه، فردوسی "

Capable is he who is wise
Happiness from wisdom will arise

"The Shahnameh, Ferdowsi"

ABSTRACT

Polysaccharides are highly abundant natural biopolymers, which have biologically significant structural functions in living organisms. Various polysaccharides, with specific physicochemical properties, contribute to biofilm formation; defined as cell aggregations surrounded by extracellular polymeric substances. They are also important in the context of bacterial pathogenesis, while some have been harnessed for industrial and biomedical applications due to their unique chemical compositions and properties.
In present study, we aimed at studying biofilm formation by *Pseudomonas aeruginosa* and *P. syringae* pv. *actinidiae*, respectively known as human and plant pathogens. In this context we focused on the production of exopolysaccharides, which predominantly constitute the biofilm matrix of these pathogenic bacteria.

Here, we uncovered that the polysaccharide isolated from *P. syringae* pv. *actinidiae* biofilm mainly consists of rhamnose, fucose and glucose and it was cautiously introduced as a novel polysaccharide. In the context of disease control, and developing a management program, we provided some evidences for the effectiveness of chlorine dioxide and kasugamycin in the control of the bacteria living in both biofilm and planktonic modes.

Furthermore, we investigated alginate biosynthesis as major polysaccharide contributing to mucoid biofilm formation by *P. aeruginosa*. We generated various mutants producing a variety of alginates with different chemical compositions. Also, this enabled us to analyse functional relationships of protein subunits involved in multiple steps of alginate biosynthesis including alginate polymerization, modification and secretion. We present evidence that while alginate unravelled that while alginate is polymerised and translocated across the membrane by a multiprotein complex, acetylation and epimerisation events positively and negatively correlated with the polymerization of the alginate or molecular mass, respectively. Analysis of the biofilms showed that biofilm architecture and cell-to-cell interactions were differently impacted by various compositions of the alginates. Also, this study provided insights into the c-di-GMP mediated activation of alginate polymerization upon binding to c-di-GMP as well as assigning functional roles to Alg8 and Alg44 including their subcellular localization and distribution.
Here, we also used current knowledge of the alginate biosynthesis pathway to assess the production of alginate from biotechnologically accepted heterologous hosts including

Escherichia coli and *Bacillus megaterium* strains. Primarily, we evaluated the production and functionality of the minimal protein requirements in nonpathogenic heterologous hosts, required for producing alginate precursor, and proceeding into polymerization and secretion steps.

Overall, we concluded that polysaccharides play a major role in the formation of bacterial biofilms while chemical composition is a key determinant for biofilm architecture and development. This contribution to understanding the biosynthesis of bacterial polysaccharides and their properties could provide the necessary knowledge not only for developing novel therapeutics, but also for harnessing such biopolymers for various industrial applications and production via biotechnological procedures.

ACKNOWLEDGMENTS

To my supervisor Prof. Bernd H. A. Rehm, thank you very much for taking me as a doctorate student. Thank you for your encouragement, patience, wisdom and support throughout this experience and I wish all the best for you.

I wish to gratefully acknowledge Massey University Doctoral Scholarship and the Institute of Fundamental Sciences (IFS) for financial support and research facilities that have allowed me to complete this study. I would like to extend my sincere gratitude to the following people for all their help: Dr. Ian M. Sims (Victoria University of Wellington), Dr. Ian Donati (University of Trieste), Dr. Adrian Turner (University of Auckland), Dr. Lynne Howell (University of Toronto), Dr. Dennis E. Ohman (Virginia Commonwealth University), Dr. Iain D. Hay (Monash University), Dr. M. S. Savoian, Dr. Patrick Edwards, Dr. Martin A. K. Williams, Dr. Bradley W. Mansel, Dr. Jasna Rakonjac, Mr. David Lun and Mr. Trev Loo from Massey University who have supported me in different ways. Thank you to all the past and present members of IFS and the Rehm workgroup, who helped, guided and supported me technically and emotionally over the past few years. Also I would like to give my great thanks to all my great friends in my workplace who made it easier to finish this study, giving me more happiness. Patricia, Karin, Jason, Shuxiong, Yaji, Majela, Natalie and Jinping; I really appreciate you all. I am also very thankful to Ann, Cynthia, Colleen and Fiona for their help and support at all stages of this PhD program and many thanks to Paul and Geraldine for their significant effort with all ordering consumable items and suchlike. And also I am very thankful to the very nice people who are working in International Student Support office giving me lots of help at some stages of my PhD program.

Very special thanks and appreciation to my beloved husband, Fata, who is my most enthusiastic cheerleader, my amazing buddy and the best colleague in my professional life. It has been an absolute privilege to work alongside you over these past few years. I am forever grateful to you for all support, Fata. Thank you to all my previous supervisors in Iran, who changed my life by encouraging and supporting me in the past and present, and to my parents, Mr. Seifollah Ghods and Mrs. Manzar Nazemi, and my lovely sister and my great brother-in-low, Shima and Abbas azizam, for all the love and support. Finally, I would like to send my deepest gratitude to all Kiwis that let me have a very nice life experience in New Zealand.

PREFACE

Below lists the publication status of all chapters in this thesis.

Chapter I

General introduction

This chapter was written as an introductory chapter for this thesis by Shirin Ghods

Chapter II

Shirin Ghods, Ian M. Sims, M. Fata Moradali, Bernd H. A. Rehm. Bactericidal Compounds Controlling Growth of the Plant Pathogen *Pseudomonas syringae* pv. *actinidiae*, Which Forms Biofilms Composed of a Novel Exopolysaccharide. (Applied and environmental microbiology 81.12 (2015): 4026-4036)

This article was written by Shirin Ghods and reviewed by all other authors. The concept was conceived by Shirin Ghods and Bernd H. A. Rehm. Experimental design was performed by Shirin Ghods with the advice of Bernd H. A. Rehm. All experiments were performed by Shirin Ghods with the exception of some compositional analysis were planned and performed with the guidance and involvement of Ian M. Sims.

Chapter III

Shirin Ghods, M. Fata Moradali, Ivan Donati, Ian M. Sims, Bernd H. A. Rehm. Interplay of alginate polymerisation and modifications in *Pseudomonas aeruginosa* and their impact on biofilm formation (co-published in mBio 6 (3) (2015):e00453-15) (see Appendix)

This chapter was written by Shirin Ghods and reviewed by Bernd H.A. Rehm. The concept was conceived by Shirin Ghods and Bernd H. A. Rehm. Generation of some mutants and production of various alginates was performed by Shirin Ghods. Raw data of compositional analysis of various alginates were provided by Ivan Donati and Ian M. Sims. Interpretation of physicochemical properties of alginates was performed by Shirin Ghods and Fata Moradali and then approved by Bernd H.A Rehm. Setting up and analysis of biofilms results was performed by Shirin Ghods.

Chapter IV

M. Fata Moradali, Shirin Ghods, Bernd H. A. Rehm. Activation Mechanism and Cellular Localization of Membrane-Anchored Alginate Polymerase in *Pseudomonas aeruginosa.* (Applied and Environmental Microbiology 83.9 (2017): e03499-16)

This article was written by Fata Moradali and Shirin Ghods and reviewed by Bernd H. A. Rehm. The concept was conceived by Fata Moradali, Shirin Ghods and Bernd H. A. Rehm. Generation of double-gene knockout mutants, complementation, biofilm assessment, alginate quantification, and imaging was performed by Fata Moradali and Shirin Ghods. Manuscript was mainly drafted by Fata Moradali and Shirin Ghods and finalized by Bernd H. A. Rehm.

Chapter V

Shirin Ghods, Bernd H. A. Rehm. Preliminary assessment of the establishment of the alginate biosynthesis pathway in non-pathogenic heterologous hosts (Drafted manuscript, 2017)

This manuscript was written by Shirin Ghods and reviewed by Bernd H. A. Rehm. The concept was conceived by Shirin Ghods and Bernd H. A. Rehm. All Experimental design was performed by Shirin Ghods with the advice of Bernd H. A. Rehm.

This is to certify that above mentioned work was conducted by Shirin Ghods.

Signature Date	Signature Date 2/6/2017
	
Prof. Bernd H.A. Rehm	Shirin Ghods

TABLE OF CONTENTS

Page

LIST OF FIGURES

Page

Chapter I

Chapter II

Chapter III

Chapter IV

Chapter V

LIST OF TABLES

Page

Chapter I

Chapter II

Chapter III

Chapter IV

Chapter V

ABBREVIATIONS

Psa	*Pseudomonas syringae* pv. *Actinidiae*
EPS	Extracellular polymeric substances
LB	Luria Bertani
°C	Degree Celsius
mM	Millimolar
pH	Potential hydrogen
µg	Micro gram
µl	Micro litre
µg ml^{-1}	Micro gram/millilitre
Nm	Nano metre
Mm	Micro metre
Ppm	Part per million
MIC	Minimal inhibitory concentration
OD	Optical density
H	Hour
Min	Minute
CFU	Colony forming units
3D	Three-dimensional
CDM	Cell dry mass
GC-MS	Gas chromatograph mass spectrometer
HPAEC	High-performance anion-exchange chromatography
DMSO	Dimethylsulfoxide
HSQC	Heteronuclear single quantum coherence
TOCSY	Total correaltion spectroscopy
COSY	Correlation spectroscopy
NMR	Nuclear magnetic resonance spectroscopy
SSA	Solid surfaces attachment
Ap	Ampicillin
Gm	Gentamycin
Cm	Chloramphenicol
Tet	Tetracycline
Kan	Kanamycin
BSA	Bovine serum albumin
Cb	Carbenicillin
Δ Delta	Deleted
DMSO	Dimethyl sulfoxide
D_2O	Deuterium oxide
DNA	Deoxyribonucleic acid
DNAase	Deoxyribonuclease
RNAase	Ribonuclease
dNTPs	Deoxyribonucleotide triphosphates
EtOH	Ethanol
EDTA	Ethylenediaminetetraacetic acid
G	Gravity/gram
GTP	Guanosine triphosphate
HEPES	4-(2-hydroxyethyl)-1-piperazineethanesulfonic acid
HRP	Horse radish peroxidase
IPTG	Isopropyl â-D-1-thiogalactopyranoside
kDa	Kilodaltons
Λ	Lambda (wavelength or type of phage)

GFP	Green fluorescent protein
ORF	Open reading frame
PCR	Polymerase chain reaction
PIA	Pseudomonas isolation agar
PPI	Protein-protein interaction
SD	Standard deviation
SDS-PAGE	Sodium dodecyl sulfate gel electrophoresis
TBE	Tris-Borate-EDTA buffer
TE	Tris-EDTA buffer
Tm	Primer melting temperature
Tris	Tris(hydroxymethyl)aminomethane
vol/vol	Volume per volume
wt/vol	Weight per volume
X-Gal	5-bromo-4-chloro-3-indolyl-beta-D-galactopyranoside
ELISA	enzyme-linked immunosorbent assay
M	1,4-linked β-D-mannuronic acid
G	C5 epimer α-L-guluronic acid
GG-blocks	C5 epimer α-L-guluronic acid residues
PMI	Phosphomannose isomerase
GMP/GDP-MP	Guanosine diphosphate (GDP)-mannose pyrophosphorylase
PMM	Phosphomannomutase
GMD	GDP-mannose 4, 6-dehydrogenase
KEGG	Kyoto encyclopedia of genes and genomes
His	Histidine
DTT	Dithiothreitol
NAD	Nicotinamide adenine dinucleotide
NADH	Nicotinamide adenine dinucleotide - hydrogen
PGC	Porous graphitic carbon
Q-TOF	Quadrupole time of flight
SPE	Solid extraction column
MS	Mass spectrometry
OPD	O-Phenylenediamine dihydrochloride
TCA	Tricarboxylic acid
T0	Zero Time
HRP	Horseradish peroxidase

Chapter I

General Introduction

INTRODUCTION

Polysaccharides are of the most abundant biopolymers in nature. Notably, they are part of structural organization of living organisms (1). Depending on their chemical structure, various polysaccharides display specific physicochemical properties that are also biologically important for producers (1). Bacteria are major polysaccharide producers in nature. There are a wide range of bacterial exopolysaccharides with different chemical compositions (2). The composition of polysaccharides determines polymer properties and their biological function relevant to the producer. Likewise, humans discovered the usefulness of polysaccharides and harnessed their properties for a long time (3). Bacterial polysaccharides such as cellulose, alginate, xanthan, dextran and complex capsular polysaccharides are well-known bacterial exopolysaccharides (2, 4). Besides industrial applications of various microbial polysaccharides, their association with bacterial communities that impact our life have been of paramount importance. This thesis mainly studies and highlights the importance of polysaccharides associated with bacterial biofilm formation which are potentially important in the context of pathogenesis and industrial applications.

Biofilm

The lifestyle of bacteria has two major facets, motility and sessility (5). A typical example of motility is flagella-mediated swimming (6). Under specific circumstances, bacteria may lose motility apparatus and attach to surfaces and form cellular aggregations or micro colonies which are embedded in extracellular polymeric substances (EPS) constituting biofilm matrix. These structures are so called biofilms (7, 8). The biofilm matrix predominantly consists of polysaccharides, extracellular DNA, proteinaceous components and small molecules or metabolites (7).

Biofilms confer an extreme capacity for protecting bacteria from the surrounding environment and persistence against oxidative stresses, nutrient/oxygen restriction, metabolic waste accumulation, interspecies competitions, conventional antimicrobial agents and phagocytosis (9). Hence, biofilms are major form of the bacterial life style for survival. Therefore, bacteria can colonize almost all environments by forming biofilms (9). In the context of pathogenesis, they are largely associated with development of chronic infections by which bacteria persist despite antibiotic treatment and the immune system (10, 11).

Understanding the biosynthesis of polysaccharides is tremendously important. In the context of pathogenesis, these studies would inform the development of drugs for eradication of biofilms causing persisting infections, while they also inform biopolymer sciences and engineering for harnessing natural and unique properties of identified polysaccharides (2).

Generally, *Pseudomonas* species can form biofilms in various environments (9, 12-14). This thesis is mainly aimed at studying the biosynthesis of polysaccharides involved in the development of biofilms of two pathogenic bacteria in plant and human namely *Pseudomonas syringae* pv. *actinidiae* and *P. aeruginosa*. Furthermore, the possibility of harnessing bacterial polysaccharide via understood biosynthesis pathways and biotechnological production was assessed.

***Pseudomonas syringae* pv. *actinidiae* NZ- V13 strain (*Psa*)**

Pseudomonas syringae pv. *actinidiae* NZ- V13 strain (*Psa*) and related diseases have become epidemic in New Zealand. This was first detected in New Zealand in the Bay of Plenty (Te Puke) in November 2010. The main damage caused by this pathogen is canker on tree trunks and seedlings, leading to plant death. In New Zealand, it threatens the kiwi fruit industry with over 57% of the kiwi fruit orchardsbeing *Psa*-positive with different degrees of infection. It is estimated that the economic impact of *Psa* over the next 10 years will be about NZ$ 500-600 million. Therefore, understanding its disease cycle to find a solution to control the spread of this disease and remedying local infections have become important (15-20).

Infection usually occurs in xylem and phloem tissues by entering through openings and lesions in the plant, while biofilm formation is found outside and inside plants. The *Psa* symptoms are usually necrosis of the phloem-cambial, dieback, reduction in vessel size and presence of tyloses, leading to canker and plant death (19).

According to previous studies, *P. syringae* pv. *actinidiae* lives within biofilms both outside and inside host plants and the existence of a matrix (biofilm) surrounding bacteria is likely involved in different (external and internal) stages of infection (18, 21). Moreover, control strategies should address the creation of specific compounds that cope with *P. syringae* pv. *actinidiae* biofilm formation. When biofilm reaches maturation, an intercellular signalling system (quorum sensing) is activated, allowing the bacteria to

regulate the expression of specific sets of genes, such as virulence factors, and those associated with resistance to antimicrobial compounds and the host defence mechanisms (22, 23). It is well known that biofilms are able to influence many metabolic processes including several of the pathogenic steps involved in *P. syringae* infection processes (11, 24-26).

Hence, in this study for the first time, we tried to study and analyse the biofilm structure of this pathogen and predominant constitutive polymeric substances to add more valuable information on *Psa* to achieve the best strategies to its control. To achieve this goal, we evaluated the effect of two chemical compounds, kasugamycin and chlorine dioxide. Kasugamycin ($C_{14}H_{25}N_3O_9$) is an aminoglycosidic antibiotic isolated from *Streptomyces kasugaensis* and its mode of action is inhibition of translation initiation by binding to ribosomes. This antibiotic is more effective against *Pseudomonas* compared with other bacteria (27-30). Chlorine dioxide is a strong oxidizer which can inactivate cells and electron-rich centre of organic molecules (31-35).

Recently, New Zealand`s Environmental Protection Authority has approved kasugamycin for controlling *Psa* causing kiwifruit canker (http://www.epa.govt.nz) and also chlorine dioxide (ClO_2)-based formulated products have been reported to be useful against *Psa* disease in New Zealand (http://www.kvh.org.nz). However, these are not scientifically documented in regard to their efficacy against planktonic and biofilm modes of this bacterium.

Pseudomonas aeruginosa

Pseudomonas aeruginosa is an opportunistic human pathogen which can become life-threatening in immune compromised patients (9). For many years *P. aeruginosa* has been a model organism for studying various aspects of alginate biosynthesis such as polymerization, epimerization, acetylation, secretion and regulation (36). The genetics and biochemical pathways underlying alginate production will be reviewed in more detail in the next chapter. *P. aeruginosa* is the leading cause of morbidity and mortality in cystic fibrosis patients when it colonizes lung due to switching from non-mucoid phenotype to mucoid. This enables the cells to produce biofilms that predominantly consist of alginate (9). Alginate has been shown to be important for the formation of thick highly structured biofilms which protect bacterial cells from the immune system and antibiotic treatment in addition to clogging lungs (37-39). It has been identified to be necessary for the

maturation and development of *P. aeruginosa* biofilm structures and it confers a survival advantage due to its ability to reduce uptake and diffusion of antibiotics, interfere with polymorphonuclear leukocyte (PMN)-mediated killing of mucoid strains (37, 40, 41)and scavenging free radicals released by triggered mechanisms in the immune system, protecting bacteria from innate immune responses (42).

Alginate structure and physicochemical properties

Alginates are unbranched polysaccharides produced by seaweeds and bacteria belonging to *Pseudomonas* and *Azotobacter* genera. Basically, the structure of the alginates consists of two uronic acid residues including β-D-mannuronic acid (M) and its C5 epimer α-L-guluronic acid (G) linked via 1,4-glycosidic bonds (43) (Figure 1).

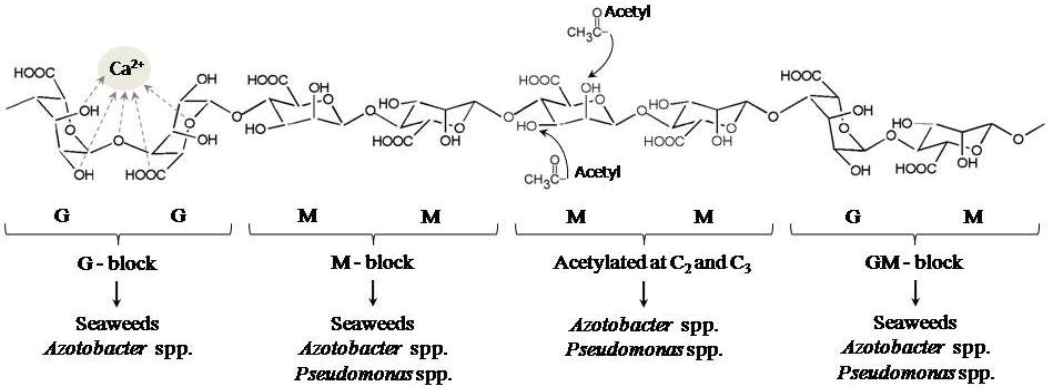

FIG. 1 Chemical structures of alginates produced by various organisms including seaweeds and bacteria belonging to the genera *Pseudomonas* and *Azotobacter*. G blocks occur only in algal alginates and *Azotobacter* spp. bind selectively with divalent cations such as calcium causing hydrogel formation. Only bacterial alginates are being acetylated at C_2 and C_3 positions increasing the interaction of polymer with water molecules and increasing water capacity and polymer extension.

In nature, alginates are usually found with heteropolymeric structures i.e. combination of both M and G residues while production of monopolymeric structure (polyM) has been reported at initial stage of alginate polymerization in bacteria (44, 45). The occurrence of M and G residues in polymeric structures varies significantly among alginates as variable numbers and lengths of M-blocks, G blocks and MG blocks. The composition of alginates and their molecular masses may differ significantly depending on the source of production and growth conditions for the producer. However, while algal alginates

usually show a high content of G-blocks, alginate produced by *P. aeruginosa* does not possess G-blocks. Another significant structural modification is natural acetylation of alginates at *O*-2 and/or *O*-3 positions which have been so far reported only in bacterial alginates (Figure 1), while acetylating algal alginates via chemical treatments has also been reported (46, 47).

The composition of polymers determines their physicochemical properties. The most important features of alginates are connected to their ability to efficiently and selectively bind divalent cations leading eventually to hydrogel formation and cross linked polymeric scaffolds (48) (Figure 1).

Application of alginates

The unique composition and properties of alginates motivated their wide applications in various industries including agriculture, food, textile, cosmetic and pharmaceutical/biomedical industries. These natural polymers have been considered as thickeners, stabilizers, viscosifier, additive, gel-and film-formers, and fertilizer (49-53). Owing to non-toxicity, biocompatibility, non-immunogenicity, hydrophilicity and biodegradability, alginates have been extensively applied for biomedical and pharmaceutical purposes (54-56). They have been traditionally applied for generating materials in dental impressions and wound dressings (57-60). However, technological advancements such as materials fabrication and processing technologies have enhanced their biomedical applications via harnessing the straightforward modification and tailoring of alginates and their synergistic interactions with other polysaccharides. Hence, alginates have been developed as nanoparticles, nanotubes, microspheres, microcapsules, sponges, hydrogels, foams, elastomers, fibers, etc. (61-67). Nowadays, various types of alginate derivatives are considered as one of the most valuable biocompatible biopolymers for drug delivery (52, 53), immobilization of enzymes (68-70), cancer therapy by functionalizing polymeric scaffolds for controlled releasing of anticancer drugs (71, 72), therapeutic cell entrapment (73-75), protection of transplanted cells from the host immune system (76-78), tissue engineering (79-81), generation of three-dimensional cell culture matrices for different laboratory assessments such as cell-drug interactions, cell growth and cell biology (82-84), and alginate formulations for preventing gastric reflux (85, 86).

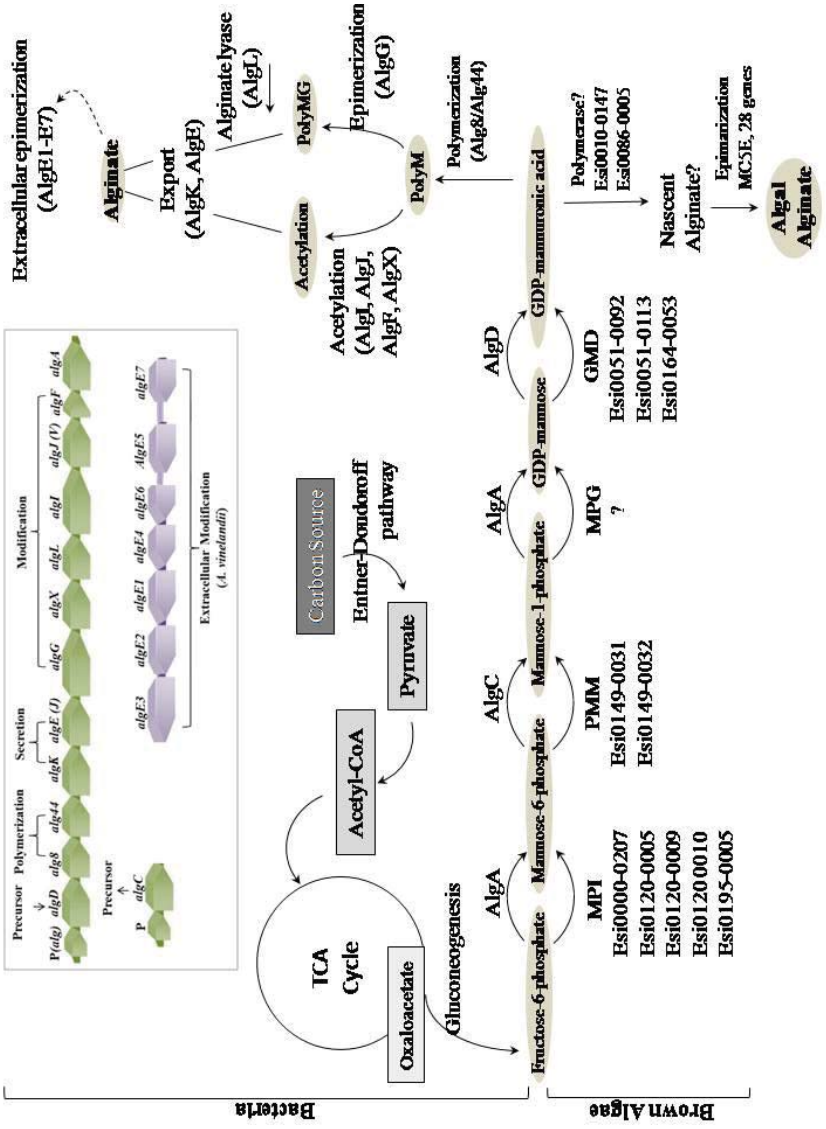

FIG. 2 Biosynthesis pathways of alginates in bacteria and algae. This pathway is mainly understood in the bacteria *P. aeruginosa* and *A. vinelandii* and some homologous genes which have been hypothetically reported in the brown alga *Ectocarpus siliculosus* (based on reference (87)). Gene clusters encoding different proteins accomplishing different steps of alginate biosynthesis are presented and functionally assigned in the frame. TCA cycle: the tricarboxylic acid cycle; MPI: mannose-6-phosphate isomerase; PMM: phosphomannomutase; MPG: mannose-1-phosphate guanosylyltransferase; GMD: GDP-mannose 6-dehydrogenase; MC5E: mannuronate C5-epimerase; PolyM: poly-mannuronate; polyMG: poly-mannuronate/guluronate.

Alginate biosynthesis

To date our knowledge about the biosynthesis of alginates is based on bacterial model organisms mainly *P. aeruginosa* whose alginate production is the hallmark of chronic infections in cystic fibrosis patients (9). Alginates produced by bacterial species are variably acetylated, and contrary to *Azotobacter* alginates which contain all types of block structures, *Pseudomonas* alginates only possess M and MG blocks, but not G blocks, indicating their different biological role (88) (Figure 1).

Genetics of alginate biosynthesis

To date at least 24 genes have been found to be directly involved in alginate production in *P. aeruginosa* (37). With the exception of *algC* all the structural genes involved in alginate biosynthesis are clustered in a single operon (89). This cluster consists of 12 genes including *algD, alg8, alg44, algK, algE, algG, algX, algL, algI, algJ, algF*, and *algA* located at approximately 3.96 Mb on the PAO1 genome map and this operon is under the tight control of a promoter located upstream of *algD* (37, 90, 91) (Figure 2).
These genes encode those enzymes catalyzing the synthesis of the precursor GDP-mannuronic acid from fructose 6-phosphate, and those subunits constituting the alginate polymerization/secretion multiprotein complex residing in the bacterial envelope and by which polymerization, translocation, modification and secretion of alginate take place (37).
In terms of structure, localization and function, proteins constituting the alginate polymerization/secretion multiprotein complex can be divided into different groups shown in Table 1.

Alginate precursor

The synthesis of the precursor GDP-mannuronic acid in the cytosol of *Pseudomonas aeruginosa* is the best understood part of alginate biosynthesis. This enzymatic multistep process starts by consuming fructose-6-phosphate provided by gluconeogenesis and includes four enzymatic steps to convert fructose-6-phosphate to GDP-mannuronic acid which is an activated donor of sugar molecules for the polymerization process. Except for the soluble cytoplasmic proteins AlgA, AlgC and AlgD which are responsible for providing the activated nucleotide sugar precursor, GDP-mannuronic acid, proteins

encoded by the operon are proposed to constitute an envelope-spanning multiprotein complex (92-97).

TABLE 1 The subunits constituting the alginate polymerization/secretion multiprotein complex and their proposed localization and function

Group	Subunits	Localization	Function
Alginate polymerization	Alg8	Membrane proteins	Polymerization
	Alg44	Membrane-anchored protein with a cytoplamic PilZ domain and periplasmic membrane fusion domain	Multiple Function: Co-polymerization and alginate length regulation , spanning periplasm to co-localizing Alg8 and AlgE
Alginate modification	AlgI	Membrane protein	O-acetylation
	AlgJ	Membrane protein	O-acetylation
	AlgF	Periplasmic protein	O-acetylation
	AlgG	Periplasmic protein	Dual function: C5-epimerization and part of scaffold
	AlgX	Periplasmic protein	Part of periplasmic scaffold
Guiding and protecting alginate	AlgK	Periplasmic protein	Part of periplasmic scaffold
	MucD	Periplasmic protein	Part of periplasmic scaffold
	AlgL	Periplasmic protein	Part of periplasmic scaffold
	Alg44	Abovementioned	
	AlgG	Abovementioned	
Alginate secretion	AlgE	Outer membrane protein	Secretion

Alginate biosynthesis/modification/secretion multi-protein complex

Bacterial alginate polymerization, translocation across membrane and secretion are mediated by an envelope-spanning multi-protein complex in *P. aeruginosa* (98). Briefly, this multi-protein complex involves: 1) alginate-polymerizing unit (Alg8-Alg44); 2) a proposed periplasmic protein scaffold (Alg44-AlgG-AlgX-AlgK) responsible for protecting nascent alginate (polyM) against the lyase activity of AlgL and translocating

the polymer across the membrane coincident with modifications (i.e. epimerization (AlgG) /acetylation (AlgX)); and 3) the secretion complex (AlgK-AlgE) that is responsible for completing the translocation of modified alginate across the outer membrane of bacteria (44, 99, 100). Other subunits such as AlgI, AlgJ and AlgF have been proposed as part of the periplasmic scaffold and they are necessary for acetylation events probably by providing acetylation precursors for terminal acetyltransferase AlgX (101) (Figure 3). However, the exact function of AlgI/J/F and their functional and structural relevance to the multi-protein complex have not yet been assigned.

THESIS AIMS:

The overall aims of this thesis are:

- To investigate biofilm formation by *P. syringae* pv. *actinidiae* and major polymeric substances constituting biofilm matrix
- To assess the susceptibility of *P. syringae* pv. *actinidiae* to kasugamycin and chlorine dioxide at different stages of biofilm formation and planktonic mode
- To investigate the functional relationship of proteins constituting the alginate polymerization/modification/secretion machinery complex in *P. aeruginosa*
- To investigate the impact of various alginates on *P. aeruginosa* biofilm architecture
- To understand the molecular mechanism of alginate polymerization mediated by the second messenger c-di-GMP binding to Alg44.
- To investigate the function of Alg44 in alginate polymerization and modification and investigating its quaternary structure
- Assessment of establishing alginate biosynthesis pathway in heterologous hosts

THESIS FINDINGS:

Chapter II of this thesis provide insights into *Pseudomonas syringae* pv. *actinidiae* NZ V-13 biofilm formation with respect to its architecture, matrix composition and susceptibility to kasugamycin and chlorine dioxide. Also, two novel polysaccharides as major polymeric components of the biofilm matrix were identified and characterized.

Chapter III of this thesis provides further insights into the biosynthesis of the alginate in *P. aeruginosa* and the functional relationships of Alg8 (polymerase), Alg44 (co-polymerase), AlgG (epimerase) and AlgX (acetyltransferase). Here, the correlation of alginate polymerization and modifications were unravelled. The production of various alginates via genetic manipulation of the producer was demonstrated and the composition and physicochemical properties of various alginates were characterized. Furthermore, the impact of various alginates on biofilm architecture of *P. aeruginosa* were visualized.

Chapter IV of this thesis presents new insights into the molecular mechanism of activation of alginate polymerization upon c-di-GMP binding to the alginate polymerase unit. Also, the periplasmic domain of Alg44 was probed and its functional and structural role was assigned. Furthermore, Alg44 was found as a stable dimer protein. Also, the subcellular localization and distribution of Alg8 and Alg44 forming the alginate polymerase unit was visualized.

Chapter V of this thesis provides preliminary data on the evaluation of establishing the enzymatic steps required for alginate biosynthesis in non-pathogen heterologous hosts for the ultimate goal of producing tailor-made alginates.

Chapter II

Bactericidal Compounds Controlling Growth of the Plant Pathogen *Pseudomonas syringae* pv. *actinidiae*, Which Forms Biofilms Composed of a Novel Exopolysaccharide

Shirin Ghods[a], Ian M. Sims[b], M. Fata Moradali[a], Bernd H. A. Rehm[a,c]

[a]Institute of Fundamental Sciences, Massey University, Palmerston North, New Zealand; [b]The Ferrier Research Institute, Victoria University of Wellington, Petone, New Zealand; [c]MacDiarmid Institute for Advanced Materials and Nanotechnology, Wellington, New Zealand

Published in: Applied and Environmental Microbiology (AEM) 81: 4026-4036 (2015)

ABSTRACT

Pseudomonas syringae pv. *actinidiae* (*Psa*) is a severe threat for kiwifruit production worldwide as the major cause of bacterial canker. Many aspects of the *Psa* caused disease such as pathogenicity relevant formation of a biofilm composed of extracellular polymeric substances (EPS) are still unknown. Here, a highly virulent strain of *Psa* NZ V-13 was studied with respect to biofilm formation and architecture using a flow cell system combined with confocal laser scanning microscopy. *Psa* NZ V-13 formed a thin cellular base layer with 5 μm in thickness and it was a heterogeneous biofilm composed of microcolonies with irregular structures. The major component of EPS produced by *Psa* NZ V-13 bacteria was isolated and identified as an exopolysaccharide. Extensive compositional and structural analysis showed that rhamnose, fucose and glucose were major constituents present at a ratio of 5:1.5:2. Experimental evidence was provided that *Psa* NZ V-13 produces two polysaccharides, a branched α-D-rhamnan with side-chains of terminal α-D-Fuc*f* and an α-D-1, 4-linked glucan. The susceptibility of cells in biofilms to kasugamycin and chlorine dioxide was assessed. Approximately 64 and 73% of *Psa* NZ V-13 cells in biofilms were killed when kasugamycin and chlorine dioxide were used at 5 and 10 ppm, respectively. Kasugamycin inhibited attachment of *Psa* NZ V-13 to solid surfaces at concentrations of 80 and 100 ppm. Kasugamycin was bacteriostatic against *Psa* NZ V-13 growth in planktonic mode with the minimum inhibitory concentration at 40-60 ppm and bactericidal effect at 100 ppm. Here we studied *Psa* biofilm formation, architecture and composition as well as using the biofilm as a model to assess the efficacy of bactericidal compounds.

INTRODUCTION

Pseudomonas syringae pv. *actinidiae* (*Psa*) is the main cause of kiwifruit canker now a worldwide epidemic (15-17). The *Psa* epidemic in New Zealand has become threatening for the kiwifruit industry which is the second most important horticultural export crop by value. In New Zealand, the highly virulent strain *Psa*-V was reported in 2010 in the Bay of Plenty region causing an estimated 50% loss of vines from "*Hort16A"* kiwifruit variety known as "ZESPRI® GOLD Kiwifruit" (18-20). This bacterial disease can affect all commercial species of kiwifruit (17, 102, 103). The main distinctive symptoms of disease are cankers on the vines and trunks, gummosis, die-back of the canes, wilting and sometimes death of the vines (19).

Similar to other pseudomonads, *P. syringae* pv. *actinidiae* can form cell communities known as biofilms. The formation of biofilms is a physiological response to environmental stresses mediated by the regulation of specific sets of genes including genes encoding virulence factors. Biofilm formation protects cells against host defence mechanisms as well as various chemical agents. Previously, it was shown that the biofilm growth mode of *P. syringae* is involved in plant pathogenicity (11, 24, 25). The *Psa* bacterial communities can be established outside and inside host tissues and are composed of bacterial cells embedded into a dense matrix of extracellular polymeric substances (EPS) often composed of exopolysaccharides, proteins and eDNA. Biofilm formation of *P. syringae* pv. *actinidiae* is involved in different phases of kiwifruit infection both outside and inside the host plant (24). It is likely that plant pathogenic bacteria can complete the pathogenic cycle, spreading and survival on plant surfaces and within tissues by involving cycles of biofilm formation and dispersion (26).

In New Zealand, *P. syringae* pv. *actinidiae* caused disease management programs to implement regular monitoring, the removal of infected plant material, and spraying with streptomycin and/or copper, biological control agents (BCAs) as well as host resistance elicitors. However, lack of effectiveness and toxicity suggest that streptomycin/copper treatments are not viable and sustainable options (19).

In 2013, New Zealand`s Environmental Protection Authority has approved the kasugamycin antibiotic for controlling *Psa* caused kiwifruit canker (http://www.epa.govt.nz). Kasugamycin is an aminoglycosidic antibiotic isolated from *Streptomyces kasugaensis* (28, 30). Also, chlorine dioxide (ClO_2) with high oxidation

capability is thought to be effective against biofilms at low concentrations (32). ClO_2-based formulated products have been reported to be used against *Psa* disease in New Zealand (http://www.kvh.org.nz).

ClO_2 is formulated as Alphasan® as a broad spectrum bactericide, fungicide, virucide and algaecide. It is recommended to be used at low concentrations, as effective in short contact times with WHO approval for application in food industry (http://www.alphaenvironmental.co.nz).

In the present study, we investigated biofilm formation by *Psa* NZ V-13 with respect to its architecture, matrix composition and susceptibility to kasugamycin and chlorine dioxide using a flow cell system, confocal laser scanning microscopy and solid surface attachment. Furthermore, the production and composition of EPS involved in biofilm formation was studied. The EPS was isolated and its composition and structure analysed.

MATERIALS AND METHODS

Bacterial strains, media, growth condition and chemical components.

Pseudomonas syringae pv. *actinidiae* NZ V-13 strain (*Psa* NZ V-13) and *Escherichia coli* JM101 (29) were used in this study. *Psa* NZ V-13 and *E. coli* were cultivated in King`s Broth (104) and Luria Bertani (LB) at 25 °C and 37 °C, respectively. All chemicals were purchased from Sigma-Aldrich and Merck KGaA unless otherwise mentioned. A liquid formulation of kasugamycin named Kasumin® (containing 2.14% active ingredient) was kindly supplied by HOKKO CHEMICHAL INDUSTRY Co. and Alphasan® (liquid formulation containing 1000 ppm active ingredient of chlorine dioxide) was kindly supplied by ALPHA INVIROMENTAL Co.

Continuous-culture flow cell biofilms.

Biofilm architecture analysis and chemical treatments were performed using continuous-culture flow cells (channel dimensions of 4 mm by 40 mm by 1.5 mm) with King`s Broth medium (104) at 22 °C. A 500 µl suspension of cells at early stationary-phase was injected into each channel and kept upside down for 3 hours. Then, flow was started with a mean flow rate of 0.3 ml min^{-1}, corresponding to a laminar flow with a Reynolds number of 5 (105, 106). The flow cells were then incubated at 22 °C for 4 days. Biofilms were stained

utilizing the LIVE/DEAD BacLight bacterial viability kit (Molecular Probes, Inc., Eugene, OR) according to the manufacturer‘s recommendation and visualized using confocal laser scanning microscopy (Leica SP5 DM6000B). After allowing to flow for 15 min, the BacLight Bacterial Viability Kit contains both SYTO9 stain and propidium iodide; use of just SYTO9 stain marks live and dead bacteria. No interference by chlorine dioxide and kasugamycin was found in pretests conducted on biofilm stained with the BacLight Bacterial Viability Kit and observed with a fluorescence microscope (CLSM; Leica SP5 DM6000B microscope). LAS AF software (Leica Application Suite Advanced Fluorescence) (Version 2.7.3.9723 Leica Microsystems 1997-2012 CMS GmbH) was used. For image analysis, metrics were obtained using IMARIS (Bitplane Inc. Version 7.2) software (18, 19). Each test series was repeated twice, and in each replicate, two or three samples were analysed per treatment.

Isolation and purification of the EPS from *Psa* NZ V-13.

Psa NZ V-13 was grown at 25 °C overnight in 50 ml King`s Broth medium and 2 ml of this culture was centrifuged at 13000 rpm for 3 min. Cell sediment was then washed twice in 1 vol. sterile normal saline (0.9% NaCl in Milli-Q water). Two hundred µl of cell suspension was plated on King`s B agar medium supplemented with a range from 200 to 700 mM NaCl and incubated at 25 °C for 120 h. Cell material and EPS were scraped off and washed twice in 25 ml sterile normal saline. Supernatants were retained for EPS purification and cell pellets were freeze-dried to determine cellular dry mass. The EPS from supernatants was precipitated with 1 volume of ice-cold isopropanol, and then EPS was harvested by centrifugation at 5000 rpm for 15 min, then freeze-dried and weighed. For further purification, the precipitated EPS was re-dissolved in 0.05 M Tris-HCl and 10 mM $MgCl_2$ buffer (pH 7.4) to a final concentration of 0.5% (wt/vol), followed by incubation with 15 µg ml^{-1} of DNase I and 15 µg ml^{-1} of RNase A at 37 °C with shaking for 6 h. Then, Pronase E (20 µg ml^{-1}) was added and incubated with shaking for a further 18 h at 37 °C. This mixture was then dialyzed (12 kDa limit) against 5 litres of ultrapure H_2O for 30 h. Purified EPS were harvested by precipitating with 1 volume of ice-cold isopropanol, centrifuging and freeze-dried and weighed (98).

Statistical analysis.

Assessment of EPS yield was conducted using three independent repetitions and data were presented as mean ± standard deviation (SD). The Shapiro-Wilk test was used to evaluate the normality of distribution of the data indicating data were normally distributed (Shapiro-Wilk test: $p < 0.05$). The results were statistically analysed by analysis of variance (ANOVA) followed by *post hoc* Tukey's honestly significant difference (HSD) test for pair-wise comparisons using XLSTAT statistical add-in software for Microsoft Excel©14.0. The letters on the histogram provide a graphical representation for *post hoc* pair-wise comparisons (Tukey's HSD). A p value less than or equal to 0.05 was considered significant in all evaluations.

Uronic acid assay.

Uronic acid content in EPS produced under the stress of 300 mM NaCl was estimated using a method described previously (107) by using alginic acid from brown seaweed (Sigma-Aldrich) as the standard (250, 125, 65.5 and 31.25 mg ml^{-1}). Briefly, the EPS samples were dissolved in 200 µl ultrapure H_2O at concentrations of between 0.25 and 0.05 mg ml^{-1}. The sample was mixed with 1.2 ml tetraborate solution (0.0125 M disodium tetraborate in concentrated sulfuric acid), then it was incubated on ice for 10 min. The mixtures were incubated at 100 °C for 5 min and then cooled down on ice for a further 5 min. 20 µl of m-hydroxybiphenyl reagent (0.15% m-hydroxybiphenyl in 0.125 M NaOH) was added and the reaction mixtures were mixed for 1 min. For each sample or dilution, a negative control was included by using 0.0125 M NaOH instead of the hydroxybiphenyl reagent. The uronic acid concentrations were measured spectrophotometrically at a wavelength of 520 nm (108). This experiment was performed with three replicates for each concentration.

Anthrone assay.

The anthrone-sulfuric acid assay was used to determine soluble carbohydrate concentrations in EPS samples by using anthrone reagent (0.2 g anthrone (UNILAB)), 8 ml ethanol (96% (vol/vol)), 30 ml H_2O, 100 ml H_2So_4 (95 to 97% (vol/vol)) and glucose as the standard (250, 125, 65.5 and 31.25 mg ml^{-1}). Briefly, dilutions of 125 µg ml^{-1} and

250 µg ml^{-1} were used from a 1 mg ml^{-1} stock solution of EPS sample. One hundred µl of EPS samples were mixed with 1 ml of ice-cold anthrone reagent. As a control ultrapure H_2O was also added to another tube in place of sample. For equilibration the sample is cooled on ice for 5 min and heated at 95 °C for 7 min. After cooling down, the soluble carbohydrate concentrations were measured spectrophotometrically at a wavelength of 644 nm. This experiment was performed with three repetitions for each concentration (109).

Protein, DNA and RNA content analysis.

The protein concentrations were determined by Bradford protein assay (110, 111) and bicinchoninic acid (BCA) assay (Pierce, Rockford, IL, USA) using bovine serum albumin (Gibco) as standards. EPS samples were analysed for protein content by sodium dodecyl sulfate-polyacrylamide gel electrophoresis (SDS-PAGE) as described elsewhere (112). Bis-Tris polyacrylamide gels were used which had acrylamide concentrations of 8% and 12% (resolving gel) and 4% (stacking gel). Twelve % gels were stained with 0.1% (wt/vol) Coomassie Brilliant Blue R-250 for at least 20 min and destained overnight and 8% gel stained with silver staining. A Qubit fluorometer (Invitrogen) was used to measure the DNA and RNA content of EPS samples using the Qubit® dsDNA BR (Broad-Range) and Qubit® RNA BR Assay Kits.

Lipid profile analysis.

Analysis of EPS was performed to investigate presence of lipids utilizing gas chromatography-mass spectrometry (GC-MS). The sample was prepared as described previously (112, 113). GC-MS instrument (GCMS/QP5050A quadrupole mass spec coupled with GC17a gas chromatograph) (Shimadzu) was equipped with Restek Rxi-5ms, size 30 m x 0.25 mm ID x 0.25 um film thickness column. Carrier gas helium with a flow rate of 1.0 ml min^{-1} was used. The following temperature gradient program was used: initial temperature was 35°C for 5min, injector and interface temperature were 220 and 250 °C respectively, then followed by an increased from 35 to 100 °C at the rate of 5 °C per min and from 100 to 285 °C at the rate of 15 °C per min, operating in scan mode**.** The 33 *m*/*z* to 500 *m*/*z* peaks representing mass to charge ratio characteristic of the lipid

fractions were compared with those in the mass spectrum library of the corresponding fatty acid.

Constituent sugar analysis.

The constituent sugar composition of purified EPS was determined by high-performance anion-exchange chromatography (HPAEC) after hydrolysis of the polysaccharides present to their component monosaccharides, as described by De Ruiter et al. (114) with modifications (115). Briefly, samples (0.5 mg) were hydrolysed with methanolic HCl (3 N, 0.5 ml, 80 °C, 18 h), followed by aqueous trifluoroacetic acid (TFA; 2.5 M, 0.5 ml, 120 °C, 1 h). Standard sugar mixes were hydrolysed at the same time as the samples. The resulting hydrolysates were dried, re-dissolved in distilled water (0.05 mg ml^{-1}) and aliquots (20 µl) were separated at 30 °C on a CarboPac PA-1 (4 x 250 mm) column equilibrated in 25 mM NaOH and eluted with simultaneous gradients of NaOH and sodium acetate and monitored by pulsed amperometric detection, using the Dionex standard carbohydrate waveform (115). The sugars were identified from their elution times relative to the standard sugars and quantified from response calibration curves at different concentrations of each sugar. Monosaccharide yields are expressed as weight percent anhydro-sugar because this is the form of sugar present in a polysaccharide.

Glycosyl linkage analysis.

EPS samples (0.5 mg in duplicate) were dispersed in dimethylsulfoxide (DMSO; 0.2 mL) and methylated as described by Ciucanu and Kerek (116). After extraction into chloroform, the methylated polysaccharides were hydrolysed with TFA and the products were reduced and acetylated before analysis by GC–MS, as described by Carnachan et al. (117). Identifications were based on peak retention times and by comparison of electron impact mass spectra with the spectra obtained from reference compounds.

NMR spectroscopy.

Purified EPS was exchanged with deuterium by freeze-drying with D_2O (99.9 atom%) three times. Samples were dissolved in D_2O and ^{1}H and ^{13}C spectra were recorded on a Bruker Avance DPX-500 spectrometer at 60 °C. The ^{1}H and ^{13}C chemical shifts were

measured relative to an internal standard of DMSO (^{1}H, 2.70 ppm; ^{13}C, 39.5 ppm) (118). Assignments were made from DEPT-135, ^{1}H–^{1}H COSY, ^{1}H–^{13}C HSQC (uncoupled) and ^{1}H–^{13}C HSQC-TOCSY experiments and by comparing the spectra with published data.

Treatment of EPS with α-amylase.

Purified EPS was dissolved in water (5 mg ml^{-1}) and 15 units of porcine pancreatic α-amylase (Megazyme International Ireland, Bray, Ireland) prepared by dissolving in water (10 mg ml^{-1}) added. The mixture was incubated at 40 °C overnight.

Size-exclusion chromatography.

Purified EPS (5 mg ml^{-1} in water) and amylase treated EPS were centrifuged (14,000 x *g*, 5 min) before injection (50 µl) and eluted with 0.1 M $LiNO_3$ (0.7 ml min^{-1}) from two columns (TSK-Gel G5000$_{PWXL}$ and G4000$_{PWXL}$, 300 x 7.8 mm, Tosoh Corp., Tokyo, Japan) connected in series. The eluent was monitored by refractive index. Molecular weights were estimated by comparison of elution volumes with those of pullulan molecular weight standards (12–830 kDa).

Qualitative and quantitative analysis of biofilms.

For qualitative and quantitative analysis of biofilms IMARIS image analysis software (Bitplane, Inc.) was employed. Biofilm architecture and appearance, biovolume (µm^3), the ratio of biovolume per unit area (µm^3 µm^{-2}), dead-to-live ratio, compactness and thickness of base layers were analysed (106, 119). Dead-to-live ratio correspond to the colocalization scatter graph were used to compare chemical treatments. To obtain volume per unit area (µm^3 µm^{-2}), a ratio between total volume and total area covered by biofilm was calculated. The compactness of the biofilm was assessed as total fluorescence per volume of biofilm. To obtain the ratio between the numbers of dead cells to the number of living cells per biofilm volume, the ratio between red fluorescence and green fluorescence was calculated (106). Live (green) and dead (red) cells of chemically treated and untreated biofilms were counted for 9 independent replicates considered in total area of 1550 µm^2.

Solid surface attachment (SSA) assay.

A bacterial suspension with 0.05 density at OD_{600} was utilized to inoculate sterile flat-bottom polystyrene 96-well microtiter plates. Wells were filled with 100 µl of suspension and incubated at 25 °C for 36 hour. Then microtiter plates were vigorously and repeatedly washed off with running tap water to remove planktonic/non-adherent bacteria. Formed biofilm in SSA assay was analysed by staining each well with 100 µl of 1% (wt/vol) crystal violet solution inoculated for 20 min at room temperature. Residual crystal violet was washed off and wells were filled with 100 µl of dimethyl sulfoxide. Absorbance was measured at OD_{595} nm using an ultra microplate reader (BIO- TEK INSTRUMENTS, INC.). All assays were performed in 8 replicates and repeated three independent times (120).

Chemical treatments of continuous-culture flow cell biofilms and SSA assay.

To treat biofilms with chemicals, chlorine dioxide at 10, 20 and 50 ppm and kasugamycin at 5, 10 and 20 ppm were gently injected into each channel of continuous-culture flow cells containing 4-day-old *Psa* NZ V-13biofilms and incubated for 1 hour without flow. Then medium was flown through chamber to wash off chemical residues and treated biofilms were stained to visualize by confocal laser scanning microscopy. Normal saline-treated biofilms were considered as negative controls. Each treatment was repeated twice and each time with three replicates. Treatment of preformed biofilms in SSA assay with 100 µl of kasugamycin was performed to have final concentrations at 5, 10, 20, 50, 60, 80, 100, 120, 140, 150 and 200 ppm. Treated wells were incubated at 25 °C for an hour. Then chemical solutions was removed from the wells and washed off under sterile normal saline three times. A hundred µl of King`s B medium was added in each treatment and incubated at 25 °C for 24 h in sterile condition and then stained with crystal violet solution 1% (wt/vol).

Bacteriostatic assessment of kasugamycin on *Psa* NZ V-13to determine minimal inhibitory concentration (MIC).

Appropriate aliquots of kasugamycin were added to 15 ml of *Psa* NZ V-13 culture with pre-defined OD_{600}= 0.44 to have final concentrations at 5, 10, 20, 30, 40, 50, 60, 70, 80, 90, 100, 110 and 120 ppm. Cultures were incubated at 25 °C for 24 h. Similarly treated

(100 ppm of kasugamycin) *E. coli* JM101 culture was also prepared as positive control which was incubated at 30 °C for 24 h. Normal saline-treated sample was considered as negative control. Bacteriostatic effect was measured using optical density determination of cultures at 600 nm after treatments and incubation. The lowest concentration of antibiotic preventing bacterial growth was considered as the minimal inhibitory concentration (MIC; the minimal concentration that inhibited growth by ≥ 95%). The more effective a concentration is, the less OD_{600} deviates from initial density. This experiment was performed three times independently and each time with three replicates (121).

Bactericidal assessment of kasugamycin on *Psa* NZ V-13.

Following bacteriostatic assessment, treated and untreated cultures were subsequently prepared at dilutions for plating on King`s B agar or LB agar plates. Plated treated *Psa* NZ V-13and *E. coli* JM101 were incubated at 25 and 30 °C, respectively, for 24 h. Colony forming units (CFU) of treated samples were compared to initial CFUs (before treatment) and normal saline-treated culture`s CFU to determine bactericidal effect (122). This experiment was performed in triplicate with three replicates at each time.

RESULTS

***Psa* NZ V-13 biofilm formation and architecture.**

Here, a continuous-culture flow cell system was employed to assess this pathogen's ability to form three-dimensional biofilms. The CLSM images were converted into three-dimensional (3D) images using IMARIS software which enabled calculation of the biovolume, thickness and compactness of *Psa* NZ V-13 biofilm (Fig. 1). Incubated for 4 days at 22 °C in the flow cell system, *Psa* NZ V-13 established a heterogeneous biofilm consisting of a base multilayer of cells (~5 μm in thickness) scattered across the slide surface with some irregular dome-shaped microcolonies with a maximum biovolume of 2.25 $\mu m^3\ \mu m^{-2}$ (Fig. 1A-E).

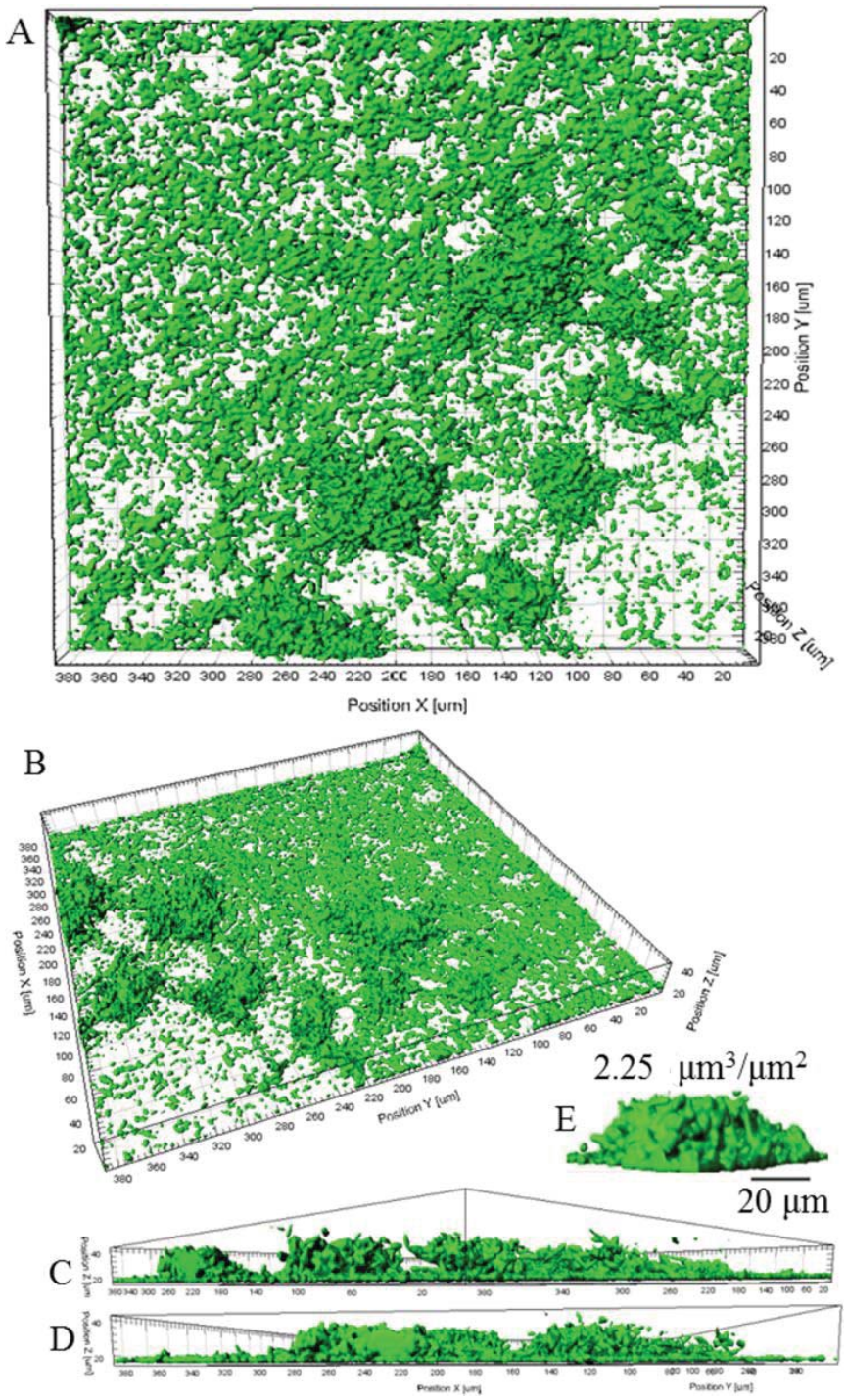

FIG. 1 CLSM images of *Psa* NZ V-13 biofilm architecture in the flow cells system. (A) and (B) top views of structure with a base layer of cells scattering on the surface of cover slide surrounded microcolonies. (C) and (D) side views of highly structured cells. (E) A typical architecture of an irregular dome-shaped microcolony.

Isolation and identification of EPS produced by *Psa* NZ V-13.

Production of EPS constituting the biofilm matrix is drastically influenced by osmolarity. Here, *Psa* NZ V-13 was exposed to increasing concentrations of NaCl on solid media to stimulate EPS production and to evaluate the impact on yield and composition. EPS produced in response to different concentrations of salt was quantified (Fig. 2). The greatest yield of EPS ((0.103 (g)/cell dry mass (CDM) (g)) was obtained in response to 600 mM NaCl which gave 4-fold lower CDM when compared to 300 mM NaCl. On the other hand, 300 mM NaCl produced the greatest dry weight of EPS per culture volume (Fig. 2).

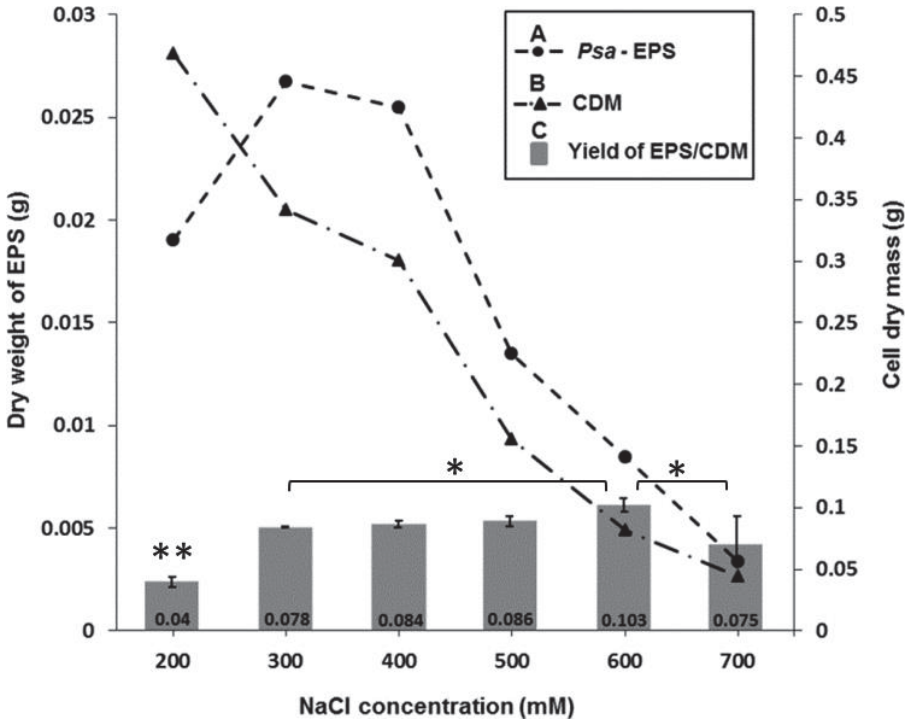

FIG. 2 Assessment of EPS yield by exposing *Psa* NZ V-13 to different concentrations of NaCl (mM) on solid media. (A) Dry weight of EPS (g). (B) Cell dry mass (CDM) (g). (C) Yield of EPS (g)/CDM (g). The data represent the means ± the SDs of three replicates and asterisks indicate pairs of significantly different values (post hoc Tukey HSD Test, *$p<0.05$ and **$p < 0.01$).

Analysis of EPS composition.

Colorimetric analysis showed that the purified EPS contained 21.9% neutral sugars (0.006 g of sugar/CDM (g)) and 9.3% uronic acid (0.0026 g of uronic acid/CDM (g)). The amount of DNA, RNA and protein present in purified EPS were quantified as 0.36, 0.75 and 6.54%, respectively. SDS-PAGE analysis (8% acrylamide gel) followed by staining with Coomassie Brilliant Blue R-250 did not reveal any major bands, apart from that of Pronase E that was added during isolation of the EPS (Fig. S1). A smear observed on a silver-stained gel suggested the presence of traces of lipopolysaccharide (Fig. S1).

The purified EPS revealed the presence of fatty acids mainly including octadecane, 5-methyl ($X_{\text{octadecane, 5-methyl}}$= 0.18), methyl 3-hydroxytetradecanoate ($X_{\text{methyl 3-hydroxytetradecanoate}}$= 0.15), hexadecanoic acid, 2-hydroxy-, methyl ester ($X_{\text{hexadecanoic acid, 2-hydroxy-, methyl ester}}$= 0.11), C12: FAME– Lauric ($X_{\text{C12: FAME – Lauric}}$= 0.9), methyl 3-hydroxydecanoate ($X_{\text{methyl 3-hydroxydecanoate}}$= 0.9) and other kinds of fatty acids included less than X= 0.5 of total lipid content (Fig. S2).

Constituent sugar analysis showed that EPS purified from *Psa* NZ V-13 contained 59.4% carbohydrate, comprised mostly of rhamnose, fucose and glucose with an approximate ratio of 5:1.5:2 (Table 1). Non-carbohydrate fraction of total EPS contained 15% moisture and the remaining part could be phospholipid or lipopolysaccharide derivatives originated from membrane derived fatty acids as indicated by GC-MS analysis.

TABLE 1 Sugar composition of EPS isolated from *Psa* NZ V-13

Type of Sugar	Dry% weight	Normalized% weight
Fuc	9.9	16.7
Rha	32.0	53.8
GalN	0.9	1.5
GlcN	1.9	3.2
Gal	1.3	2.2
Glc	12.3	20.6
Rib	1.2	1.9
Total	59.4	100.0

Data are means of duplicate analyses, but any more than that is probably not possible.

In order to investigate the impact of different salt concentrations on carbohydrate composition, molar ratios and total sugar dry weight of EPS was analysed (Fig. 3). While the composition of the EPS was not affected, the total sugar content of the EPS varied with the largest amount of sugar content obtained at 300 mM NaCl (Fig. 3).

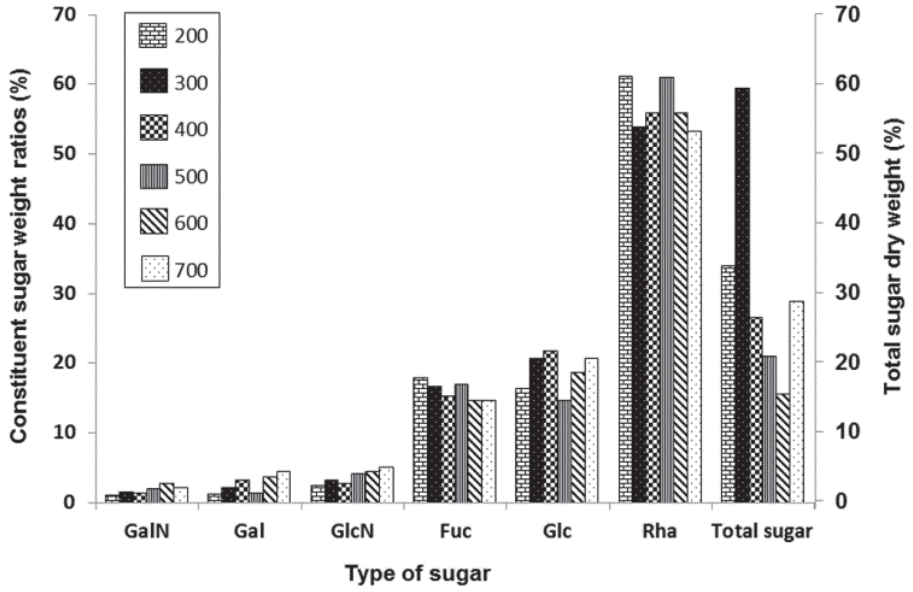

FIG. 3 Analysis of constituent sugar weight ratios and total sugar dry weight of EPS from *Psa* NZ V-13 when cultivated at different concentrations of NaCl (mM) on solid media.

The purified EPS was eluted as a minor peak at the exclusion limit of the columns and a major peak eluting from 20–23 min (Fig. 4). Following treatment of the EPS with α-amylase the early eluting peak was smaller than for the untreated EPS, suggesting that this early eluting peak may be α-glucan. Compared to pullulan standards, the elution of the EPS showed two peaks when analysed by size-exclusion chromatography. The first peak corresponded to the exclusion limit of the column, which is greater than 850 kDa and the second corresponded to a molecular weight of about 200 kDa (Fig. 4).

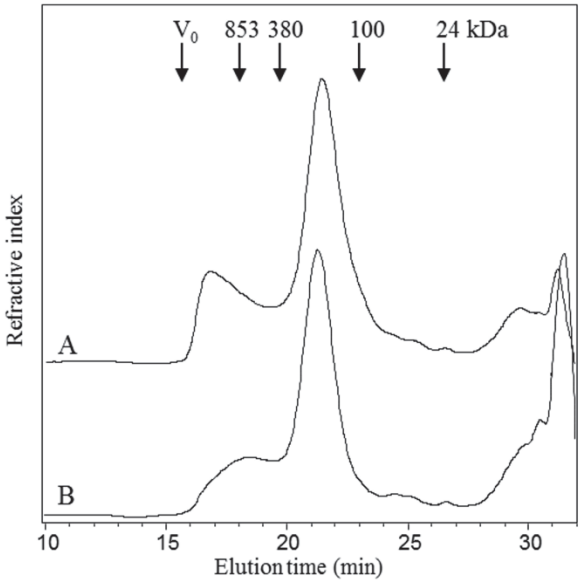

FIG. 4 Chromatogram of size-exclusion of EPS sample before (A) and after (B) treatments with α-amylase.

Glycosyl linkage analysis.

The glycosyl linkage analysis of purified EPS showed mostly 2-, 3- and 3-, 4-linked rhamnopyranosyl residues, together with terminal fucofuranosyl residues (Table 2), consistent with the structure of the *O*-polysaccharides reported for some other *Pseudomonas syringae* strains (123-126). The other major linkage observed was 4-linked glucopyranose; α-1, 4-glucan has been reported as the *O*-polysaccharide chain from certain strains of *Pseudomonas syringae* (123-127) and *Pseudomonas fluorescens* (128).

The ratios of rhamnose, fucose and glucose from the linkage analysis were similar to those determined from the constituent sugar analyses.

The high resolution ^{1}H NMR spectrum (Fig. S3) of the purified EPS showed five major signals in the anomeric region at 4.98–5.36 ppm, in agreement with the five major linkages detected by glycosyl linkage analysis. Signals at 1.2–1.4 ppm were assigned to H-6 (CH_3) of rhamnopyranosyl and fucofuranosyl residues. Similarly, the proton-decoupled ^{13}C NMR spectrum (Fig. S4) showed five signals for anomeric carbons (100.4–103 ppm) and four CH_3 signals assigned to C-6 of the rhamnopyranosyl and fucofuranosyl residues. A DEPT 135 spectrum showed an unsubstituted CH_2OH signal at 61.1 ppm. The ^{1}H and ^{13}C resonances for the sugar residues of the EPS (Table S1) were assigned using a combination of DEPT and 2D NMR (COSY, HSQC, TOCSY) experiments (Fig. S5-8), and comparing the spectra with published data (123-125, 127, 129-133).

TABLE 2 Glycosyl linkage analysis of the EPS composition isolated from *Psa* NZ V-13

Type of sugar	Linkage	Mol%[a]	Molar ratio
Rhamnopyranose	terminal	1.6	0.1
	2-	23.2	1.0
	3-	21.9	0.9
	2,3-	1.2	0.1
	3,4-	14.2	0.6
Fucofuranose	terminal	17.8	0.8
Glucopyranose	terminal	2.2	0.1
	2-	1.2	0.1
	4-	14.7	0.8
	2,4-	0.1	-
	4,6-	0.7	-
Xylitol[b]		1.2	0.1

[a] normalized mol%

[b] detected as non-deuterated pentitol pentacetate

The NMR data were consistent with the presence of the major sugars and glycosyl linkages determined by the constituent sugar and glycosyl linkage analyses (Table 1 and 2). A signal at H-1/C-1 5.36/100.4 ppm was assigned to →4) -α-D-Glc*p*- (1→, with a C-4 signal at 77.7 ppm consistent with O-4 substitution. Signals at H-6/C-6 3.87-3.81/61.1 ppm were also consistent with this residue (Table S1). The four other major anomeric signals were assigned to the deoxysugars, α-D-rhamnose and α-D-fucose, and was consistent with the presence of four CH_3 signals. The anomeric signal at H-1/C-1 5.27/102.0 ppm was assigned to α-D-Fuc*f*- (1→, while the other three were assigned to the three rhamnose linkages (124, 125). A weak signal at C/H 56.6/3/44 ppm indicated the presence of an *O*-methyl group as observed previously for similar molecules (123, 125), but the position of this substituent was not investigated further. Based on the sugar, glycosyl linkage and NMR data Fig. 5 shows possible structures for these two polysaccharides.

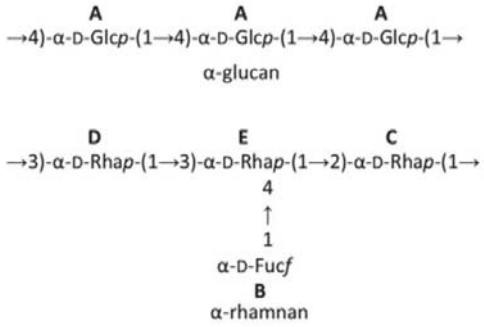

FIG. 5 Proposed repeat unit structures of the polysaccharide identified through EPS analysis.

Effect of antimicrobial agents on viability of biofilm-grown *P. syringae* pv. *actinidiae* NZ V-13.

Generally bacterial biofilms show greater resistance to antibacterial agents than free-living cells. Here the susceptibility of biofilm-grown *Psa* NZ V-13 to commonly used antimicrobial agents was studied. Kasugamycin and chlorine dioxide were applied to *Psa* NZ V-13 biofilms. Biofilms were treated with different concentrations of these compounds and the ratio of live (green) and dead (red) cells was visualized and calculated (Fig. 6).

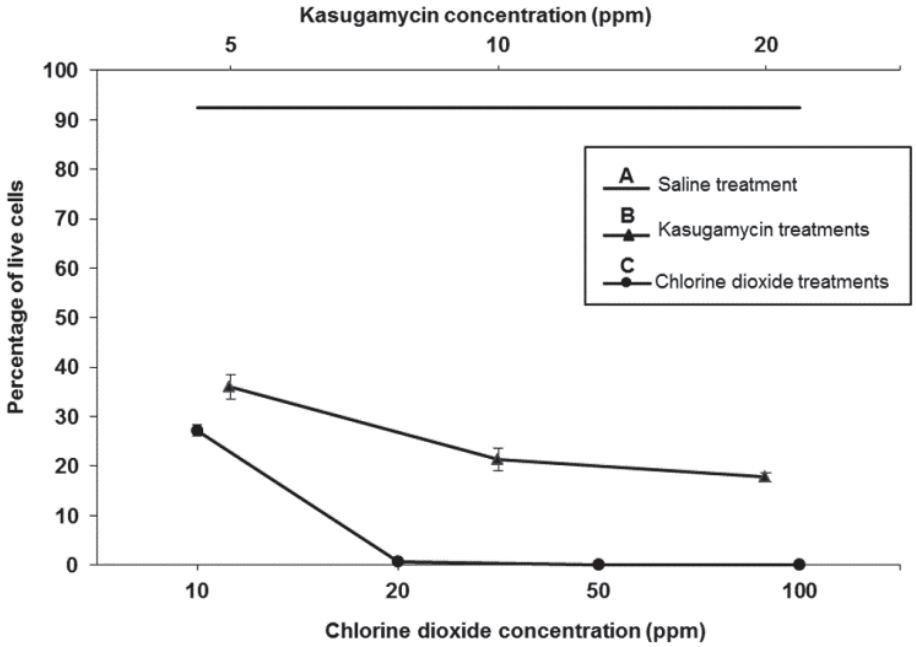

FIG. 6 Live and dead cell ratios of *Psa* NZ V-13 in biofilms treated with different concentrations of chlorine dioxide and kasugamycin grown in a flow cell system. (A) *Psa* NZ V-13 strain treated with normal saline as control. (B) *Psa* NZ V-13 treated with different concentrations of kasugamycin. (C) Different concentrations of chlorine dioxide were used to kill *Psa* NZ V-13 in biofilms. Values and error bars represent averages and standard deviations for 9 independent replicates considering a biofilm grown area of 1550 μm^2.

After staining of treated biofilms with SYTO9/propidium iodide stain different intermediate fluorescent colours such as yellow, orange and brown were visualized and considered as dead cells with impaired membrane integrity due to treatment with the reagent (Fig. 7 and 8) (111). Analysis of images showed cells in biofilms were susceptible to kasugamycin and chlorine dioxide and the percentage of dead cells was directly correlated with increasing concentrations of the respective reagent. Kasugamycin caused ~64% killing at 5 ppm and it increased to ~83% at 20 ppm. Ten ppm of chlorine dioxide showed ~73% killing which increased to >99% at 20 ppm or higher concentrations. Normal saline-treated biofilms served as controls and contained 92.5% living cells (Fig. 6). The two-channel laser confocal images of the biofilm cells treated with kasugamycin and chlorine dioxide are shown in Figures 7 and 8, respectively. Colocalization scatter graphs were obtained for biofilms treated with kasugamycin (Fig. 7) and chlorine dioxide (Fig. 8) using IMARIS software. This graph was developed to analyse the co-distribution and intensity of pixels corresponding to the prevalence of live (green) and dead (red) cells.

Colocalization scatter graphs of kasugamycin-treated biofilms (Fig. 7E-H) showed that the intensity of pixels was arrayed towards the red channel (dead cells) compared to normal saline-treated biofilm which showed more fluorescence intensities towards the green channel (live cells). This array of intensity of pixels towards the red channel was also clearly demonstrated for biofilms treated with different concentrations of chlorine dioxide (Fig. 8F-J). In summary, these data showed the effectiveness of kasugamycin and chlorine dioxide on *Psa* NZ V-13 grown in biofilm growth mode.

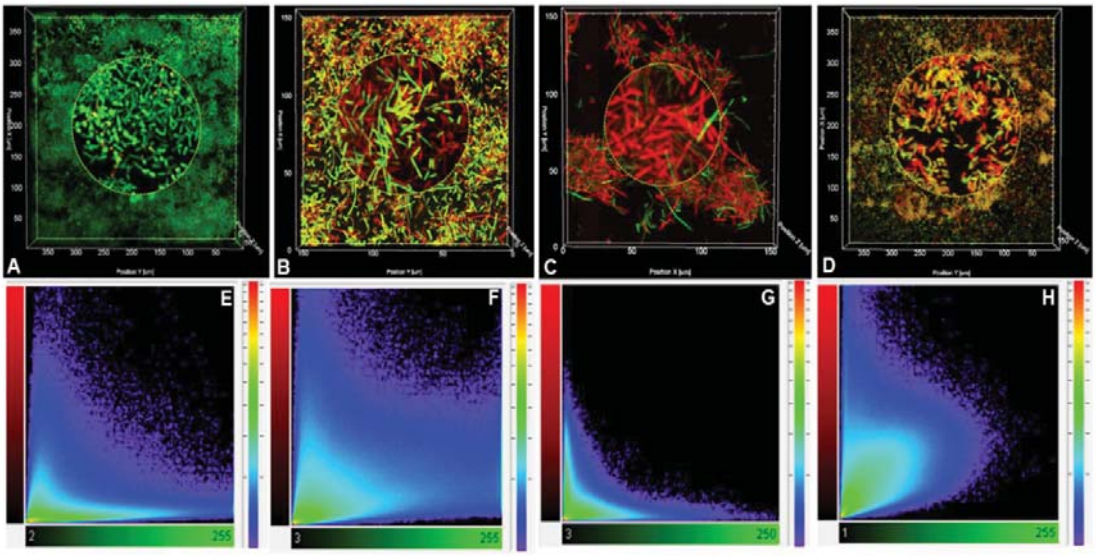

FIG. 7 CLSM images of *Psa* NZ V-13 biofilm treated with different concentrations of kasugamycin and normal saline in a flow cell system. (A) Normal saline-treated biofilm (control). Biofilms treated with 5 ppm (B) 10 ppm (C) and 20 ppm (D) of kasugamycin. (E- H) Colocalization intensity graphs representing green fluorescent channel (horizontal axis) versus red fluorescent channel (vertical axis) corresponding to each frame (A- D). For all frames and colocalization graphs, detected green fluorescent pixels are live cells, red fluorescent are dead cells and intermediate colors , orange or yellow are membrane-damaged cells which are considered dead.

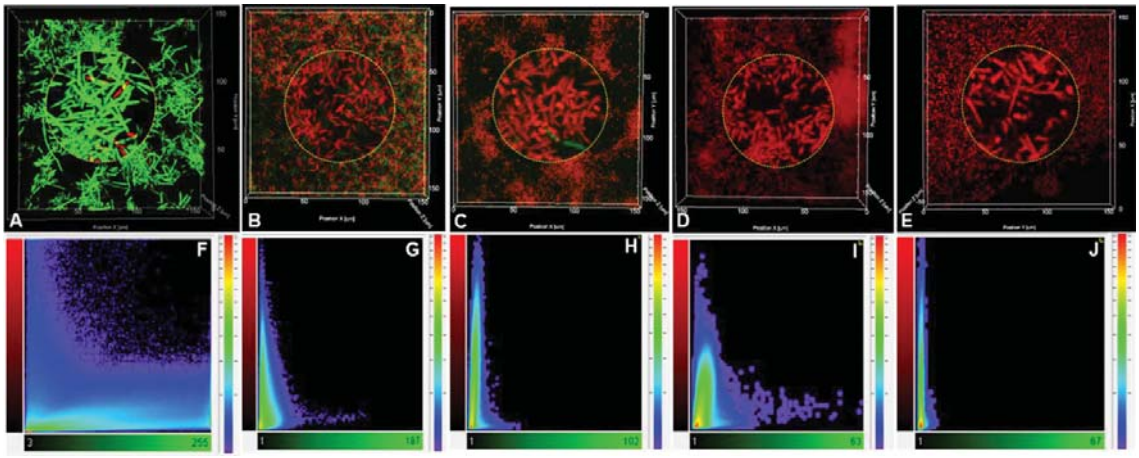

FIG. 8 CLSM images of *Psa* NZ V-13 biofilms treated with different concentrations of chlorine dioxide in flow cell system. (A) Normal saline-treated biofilm (control). Biofilms treated with 10 ppm (B) 20 ppm (C) 50 ppm (D) and (E) 100 ppm of kasugamycin. (F- J) Colocalization intensity graphs representing green fluorescent channel (horizontal axis) versus red fluorescent channel (vertical axis) corresponding to each frame (A- E). For all frames and colocalization graphs, detected green fluorescent pixels are live cells, red fluorescent are dead cells and intermediate colors, orange or yellow are membrane-damaged cells which are considered dead.

Kasugamycin effect on *Psa* NZ V-13 with respect to attachment to solid surfaces.

The first stage of biofilm formation is the attachment of the cells to surfaces. The SSA assay was conducted to evaluate the effect of kasugamycin on the attachment of planktonic *Psa* NZ V-13 to solid surface during initial stages of biofilm development (Fig. 9). Incubation of inoculated microplates with *Psa* NZ V-13 for 24 h provided OD_{595} = 0.054 which was considered as T0 or initial attachment phase before treatment. Treatment of initially attached cells with different concentrations of kasugamycin at 5 to 200 ppm prevented further attachment while normal saline-treated cells continued their growth and attachment to the maximum of OD_{595} = 0.075 (Tmax). The most inhibitive effect of kasugamycin on surface attachment was found at concentrations of 80 and 100 ppm (Fig. 9).

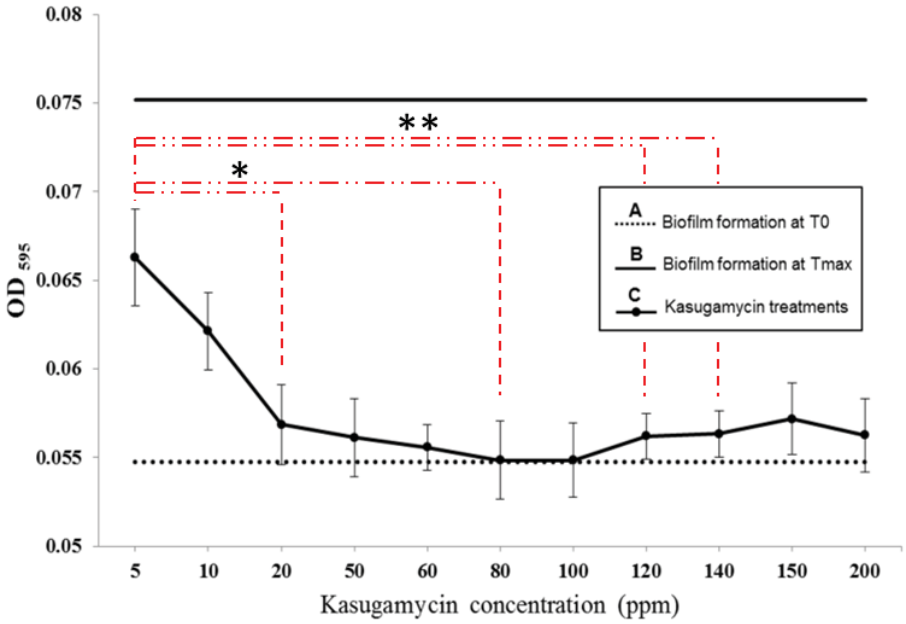

FIG. 9 The effect of different concentrations of kasugamycin on *Psa* NZ V-13 in SSA assay. (A) Biofilm formation-attachment phase (T0); (B) maximum adherent biofilms treated with normal saline (Tmax); (C) biofilm formation affected by different concentrations of kasugamycin. The data represent the means ± the SDs of 24 replicates and asterisks indicate pairs of significantly different values (post hoc Tukey HSD Test, *p<0.05 and **p < 0.01).

Bacteriostatic and bactericidal assay using kasugamycin.

In this study, kasugamycin was found to be effective against *Psa* NZ V-13 grown in biofilm mode and preventive against surface attachment. Here, the bacteriostatic and bactericidal property of kasugamycin using different concentrations ranging from 5 ppm and 10 to 120 ppm in 10 ppm intervals was evaluated. The bacteriostatic effect of kasugamycin was assessed against cells grown in planktonic mode with an initial OD_{600}=0.44 and then cultures were treated with abovementioned concentrations. Compared with the normal saline-treated culture (OD_{600}=1.97), kasugamycin prevented growth of bacteria at all concentrations (Fig. 10). The values for the antibiotic where ≥95% of growth was inhibited (MIC) was 40 ppm with a mean value of OD_{600}=0.47. This analysis was followed by bacteriocidal assessment which was measured by a conventional growth based approach on solid cultures counting colony forming units (CFUs). Figure 11 shows the number of viable *Psa* NZ V-13 (CFU/ml) recovered after application of various kasugamycin concentrations. A hundred ppm of kasugamycin showed a bactericidal effect against *Psa* NZ V-13. In these experiments, *E. coli* was used

as species with known susceptibility to kasugamycin and was considered as a positive control (29).

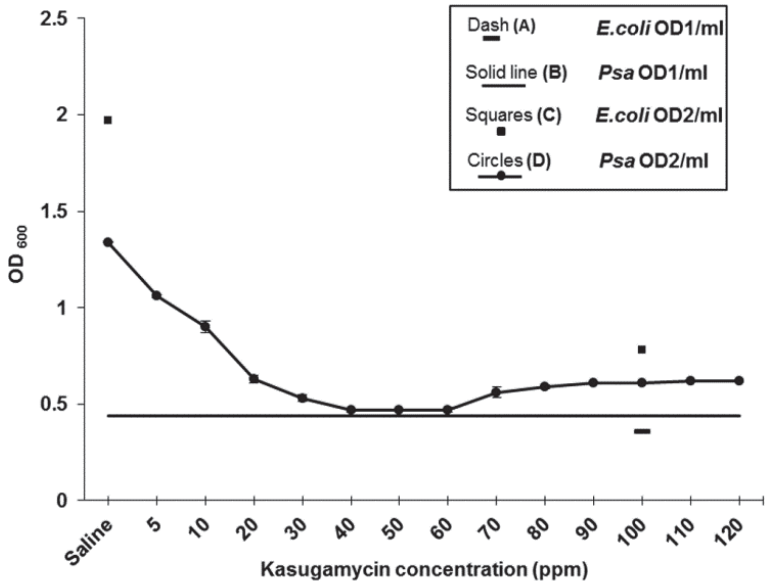

FIG. 10 Assessment of bacteriostatic effect of kasugamycin on *Psa* NZ V-13 grown in planktonic mode and *E. coli* JM101 applied as positive control at 600 nm. (Dash (A)) Initial OD_{600} of untreated *E. coli* (OD1=0.36); (Solid line (B)) Initial OD_{600} of untreated *Psa* NZ V-13 (OD1=0.44); (Squares (C)) Final OD_{600} of treated *E. coli* with 100 ppm of kasugamycin (OD2= 0.78) and normal saline (OD2=1.97); (Circles (D)) Final OD_{600} of treated *Psa* NZ V-13 with different concentrations of kasugamycin and normal saline (OD2=1.34); Values and error bars (<0.03 in all treatments) represent the averages and standard deviations for 3 independent replicates.

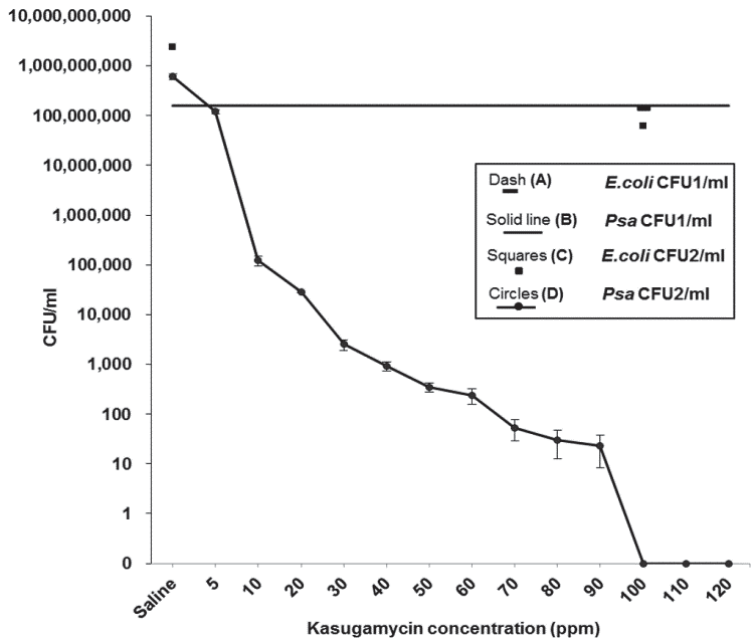

FIG. 11 Assessment of bactericidal effect of kasugamycin on *Psa* NZ V-13 in planktonic mode and *E. coli* JM101 applied as positive control. (Dash (A)) *E. coli* CFU1 ml^{-1} untreated (1.4E+08); (Solid line (B)) Untreated *Psa* NZ V-13 CFU1 ml^{-1} (1.58E+08); (Squares (C)) CFU2 ml^{-1} of treated *E. coli* with 100 ppm of kasugamycin (6.19E+07) and normal saline (2.39E+09); (Circles (D)) CFU2 ml^{-1} of treated *Psa* NZ V-13 with different concentrations of kasugamycin and normal saline (6.10E+08); Values and error bars represent the averages and standard deviations, respectively, for 3 independent replicates.

DISCUSSION

In the present study, the ability of *Psa* NZ V-13 to form structured biofilms was investigated. Here, biofilms formed by *Psa* NZ V-13 were shown to be heterogeneous containing cellular aggregations and microcolonies (Fig. 1). Previous studies showed that some characteristics of plant-associated bacterial biofilms such as cell size, density and exopolymeric matrix were affected by physical parameters, the availability of water and nutrition. Several authors suggested that the biofilm growth mode is critical for plant-microbe interactions (134-139). The type of biofilm and cell aggregation observed here potentially mimics the biofilms formed by the bacteria outside and inside plant tissues i.e. shows the ability of *Psa* to attach to surfaces in an aqueous environment and to form three-dimensional biofilms. Here the ability of *Psa* to form structured biofilms made of

polysaccharides with novel composition was established. Previously, it was reported that *Psa* NZ V-13 can form biofilms on external and internal surfaces of plants which is likely involved in different phases of infection (24).

During biofilm maturation, the expression of sets of genes associated with virulence and production of biofilm matrix cause enhancement of bacterial survival and resistance to antimicrobial compounds, host defence mechanisms, desiccation, UV damage and predation (8, 140-142). The biofilm growth mode and associated cell-density dependent gene regulation was found to be crucial for the plant-pathogenicity of *P. syringae* (22, 23).

Biofilms are composed of cells embedded in a matrix composed EPS (8). The EPS protects embedded cells against plant recognition and defence mechanisms as well as antibacterial treatment (143). In this study, the capability of *Psa* NZ V-13 to produce EPS likely involved in biofilm formation was assessed (Fig. 2). EPS was isolated from *Psa* (Fig. 2), its molecular weight (Fig. 4) and composition (Fig. 5 and Table 1) induced in response to increased osmolarity (300 mM NaCl) was analysed. Our analysis showed that purified EPS was mainly composed of rhamnose, fucose and glucose (Table 1). Although the total amount of sugar content in EPS is significantly affected by changing osmolarity, the structure and composition of constituent sugars were not significantly impacted (Fig. 3).

Further analysis of the EPS revealed that the EPS is likely composed of two polysaccharides, a branched α-D-rhamnan with side-chains of terminal α-D-Fuc*f* and an α-D-1, 4-linked glucan (Fig. 5, Table 2). Similar rhamnose-rich polysaccharides have been reported as *O*-polysaccharide chains of lipopolysaccharides from *P. syringae* pv. *phaseolicola* (124) and *Pseudomonas putida* (129), and from strains of *Xanthomonas campestris* (125) and *Halomonas alkaliantarctica* (132). However, this is the first time that such branched rhamnans have been reported as exopolysaccharides from *Pseudomonas* species. Rhamnose-rich exopolysaccharides have been also reported from *Bifidobacterium animalis* subsp. *lactis* (128) and *Lactococcus lactis* subsp. *cremoris* B39 (143), but in both cases the rhamnose was reported as α-L-rhamnose.α-D-Glucans, similar to those reported here, have been shown to co-extract with lipopolysaccharides from strains of *P. syringae* pv. *morsprunorum* (123, 127).

Here, the effect of two commonly used bacterial growth control reagents, kasugamycin and chlorine dioxide on survival of *Psa* NZ V-13 biofilm cells in view of the need to manage the *Psa* disease caused by the spreading of *Psa* and the treatment of infected plants was studied. Kasugamycin and chlorine dioxide were found to efficiently kill cells grown in biofilm mode at low concentrations (Fig. 6, 7 and 8). Kasugamycin inhibits proliferation of bacteria by targeting the ribosome consequently blocking proper mRNA placement i.e. inhibiting translation (144). It was noted that kasugamycin can be more effective against *Pseudomonas* when compared to various other bacteria (27). This antibiotic was approved by New Zealand`s Environmental Protection Authority for the control of *Psa* NZ V-13 disease in kiwifruit (http://www.epa.govt.nz). In contrast ClO_2 was previously reported to be able to penetrate biofilms causing detachment of biofilm clusters. It is a strongly oxidizing reagent which can inactivate cells. Advantage of this compound is being effective and applicable at low concentrations (32, 35, 145) . Kasugamycin was shown to inhibit attachment of *Psa* NZ V-13 in the SSA assay i.e. interfering with the initial stages of biofilm formation (Fig. 9).

The effect of different concentrations of kasugamycin on *Psa* NZ V-13 growth in planktonic mode was measured and showed that the bactericidal level of kasugamycin was about 2-fold the MIC when compared to various *Pseudomonas* sp. (Fig. 10 and 11) (27).

In this study, *Psa* NZ V-13, a highly virulent strain causing kiwifruit canker, was studied with respect to biofilm formation and EPS composition as well as its susceptibility to chlorine dioxide and kasugamycin. We have provided experimental evidence for the effectiveness of chlorine dioxide and kasugamycin to control *Psa* NZ V-13. Based on EPS compositional analysis and comparing with the literature, the polysaccharide identified in this study can be cautiously stated to be a new polysaccharide. Overall, this study sheds light on *Psa* biofilm formation and composition as well as the control of *Psa* growth aiding the development of a management program to control the spread of *Psa*.

ACKNOWLEDGMENTS

The present research was funded by Massey University research grants to B. Rehm (Institute of Fundamental Sciences, Massey University). Shirin Ghods is funded by a Massey University Doctoral scholarship. We are grateful to M. S. Savoian (Manawatu

Microscopy & Imaging Centre, Institute of Fundamental Sciences, Massey University) for his technical assistance and Dr. Adrian Turner (School of Biological Sciences, University of Auckland) for permission to use the IMARIS software. Mention of trade names or commercial products in this article is solely for the purpose of providing specific information and does not imply recommendation or endorsement by Massey University.

SUPPLEMENTAL FIGURES AND TABLES

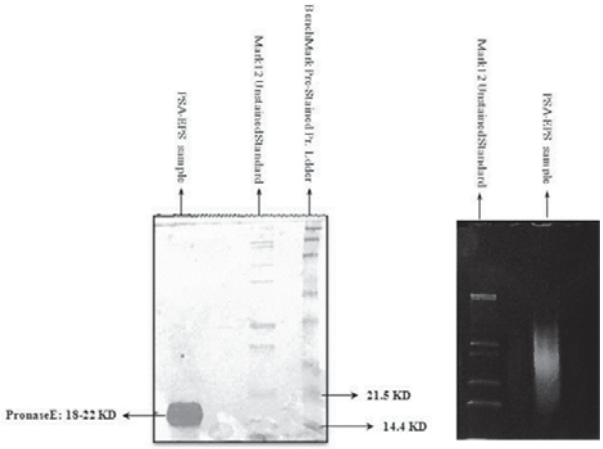

FIG. S1 SDS- PAGE (8% acrylamide) of EPS stained with Coomassie Brilliant Blue R-250 (left) and silver-stained SDS-PAGE (8% acrylamide) of EPS (right).

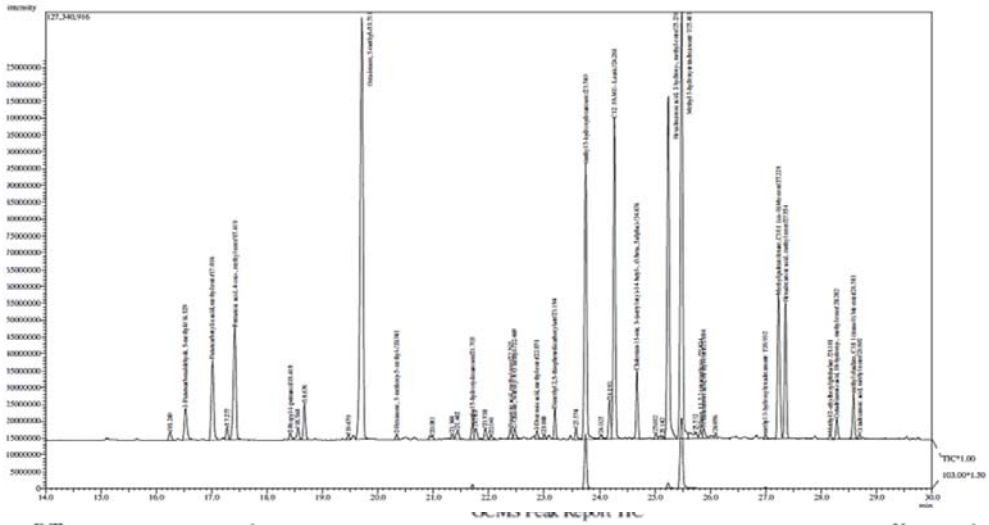

Conti

GC/MS Peak Report TIC

Peak#	R.Time	Area	Name	Area%
1	7.034	32442842	Ethane, 1,1,2-trimethoxy-	1.29
2	7.640	3209375	Ethane, 1,1,2-trimethoxy-	0.13
3	8.900	5181291	2-Furancarboxaldehyde	0.21
4	10.384	5449126	Ethylbenzene	0.22
5	10.525	40505528	Sulfuric acid, dimethyl ester	1.61
6	10.861	21779483	Benzene, 1,2-dimethyl-	0.86
7	12.285	7919916	Benzene, 1,2-dimethyl-	0.31
8	16.249	7503712		0.30
9	16.529	30717337	2-Furancarboxaldehyde, 5-methyl-	1.22
10	17.016	72795021	Furancarboxylic acid, methyl ester	2.89
11	17.277	9684831		0.38
12	17.419	113833982	Pentanoic acid, 4-oxo-, methyl ester	4.52
13	18.418	5780403	2-Propyl-1-pentanol	0.23
14	18.560	10574206		0.42
15	18.676	26796056		1.06
16	19.470	3981213		0.16
17	19.711	461618225	Octadecane, 5-methyl-	18.32
18	20.341	4166092	2-Hexanone, 3-methoxy-5-methyl-	0.17
19	20.981	4755279		0.19
20	21.344	3637879		0.14
21	21.442	8387363		0.33
22	21.705	11584631	methyl 3-hydroxydecanoate	0.46
23	21.762	10272315		0.41
24	21.938	9611419		0.38
25	22.041	3787038		0.15
26	22.397	8675618	Decanoic acid, methyl ester	0.34
27	22.469	8277321	L-Glucose, 6-deoxy-3-O-methyl-	0.33
28	22.871	6593497	2-Decenoic acid, methyl ester	0.26
29	23.000	3699611		0.15
30	23.194	19839738	Dimethyl 2,5-thiophenedicarboxylate	0.79
31	23.574	8286898		0.33
32	23.749	229704737	methyl 3-hydroxydecanoate	9.11
33	24.025	4507784		0.18
34	24.180	30517822		1.21
35	24.268	239095717	C12: FAME - Lauric	9.49
36	24.676	44699399	Cholestan-15-one, 3-(acetyloxy)-14-butyl-, (3.beta.,5.alpha.)-	1.77
37	25.012	4587064		0.18
38	25.142	3548025		0.14
39	25.238	289978755	Hexadecanoic acid, 2-hydroxy-, methyl ester	11.51
40	25.481	390188035	Methyl 3-hydroxytetradecanoate ?	15.48
41	25.732	14477950		0.57
42	25.824	6331957	Ethane, 1,1,2,2-tetramethoxy-	0.25
43	25.884	8178309	Tetradecanoic acid, methyl ester	0.32
44	26.096	5207149		0.21
45	26.992	2876159	methyl 3-hydroxyhexadecanoate ?	0.11
46	27.228	124276484	Methyl palmitolenate, C16:1 (cis-9) Me ester	4.93
47	27.354	95075856	Hexadecanoic acid, methyl ester	3.77
48	28.161	4230986	Methyl 2-ethylhexyl phthalate	0.17
49	28.282	15418871	Octadecanoic acid, 10-hydroxy-, methyl ester	0.61
50	28.581	32785234	methyl elaidate, C18:1 (trans-9) Me ester	1.30
51	28.692	3379566	Octadecanoic acid, methyl ester	0.13

FIG. S2 GC/MS chromatogram performed on EPS sample isolated from *Psa* NZ V-13.

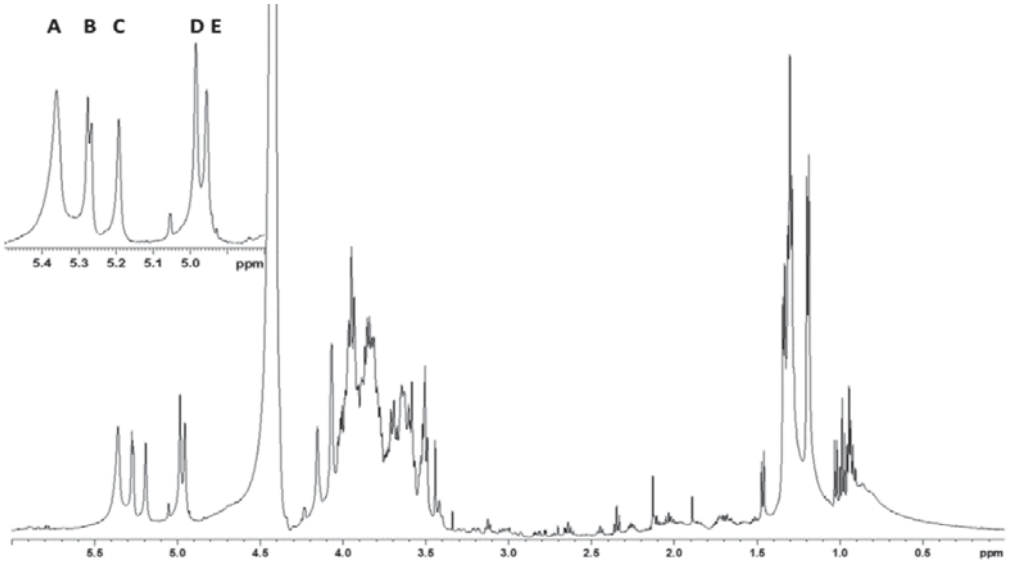

FIG. S3 ^{1}H-NMR spectrum of the EPS dissolved in D_2O recorded at 60°C (500MHz). Insert shows expanded plot of anomeric region. Letters refer to sugar residues shown in Fig. 5.

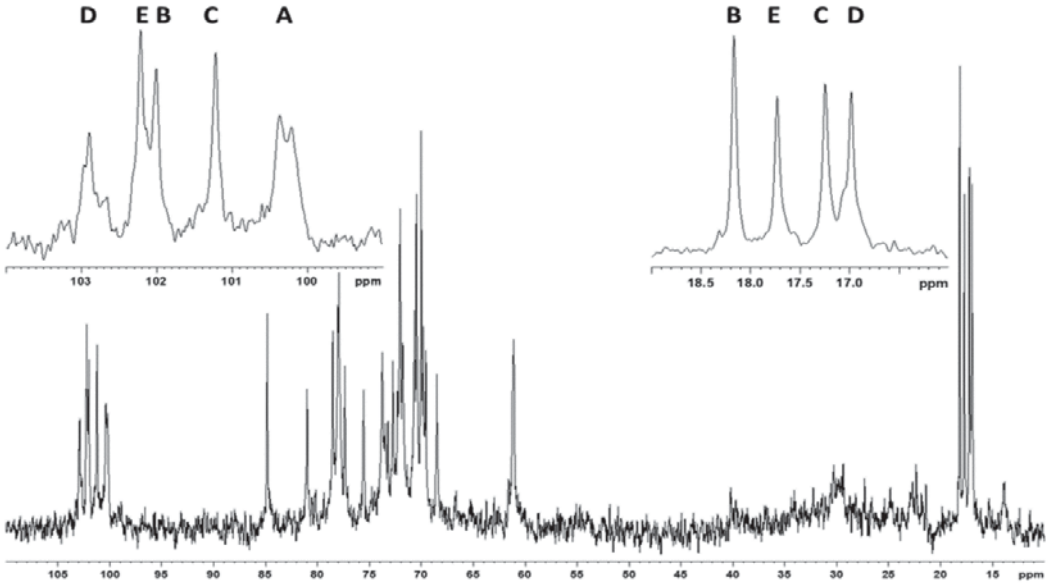

FIG. S4 ^{13}C -NMR spectrum of the EPS dissolved in D_2O recorded at 60°C (500MHz). Inserts show expanded plot of anomeric region (left) and CH3 of C-6 of deoxy sugars (right). Letters refer to sugar residues shown in Fig. 5.

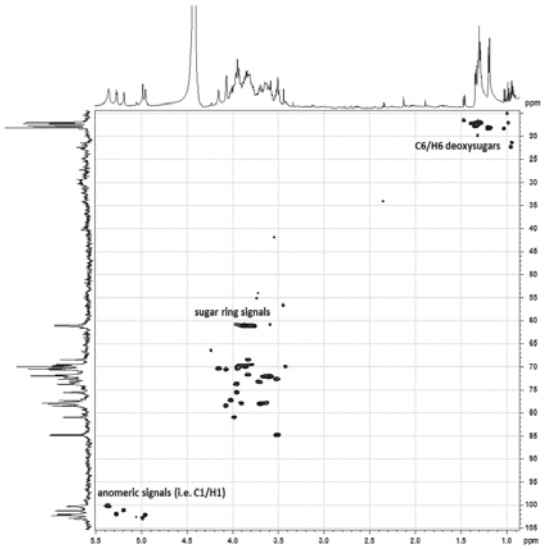

FIG. S5 HSQC spectrum of the *Psa* NZ V-13 - EPS dissolved in D_2O recorded at 60 °C (500MHz).

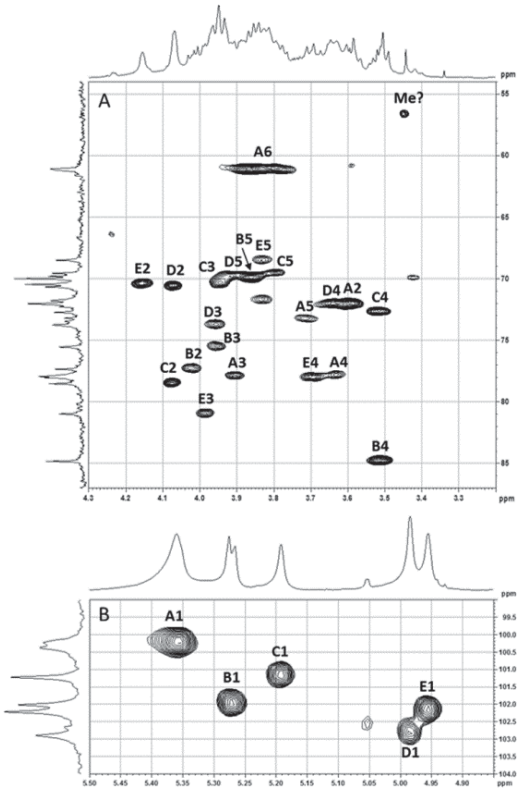

FIG. S6 ^{1}H-^{13}C-HSQC spectrum of the ring sugar (A) and anomeric (B) regions of the *Psa* NZ V-13- EPS dissolved in D_2O recorded at 60 °C (500MHz). Letters refer to sugar residues shown in Fig. 5 and numbers to carbons in sugar rings.

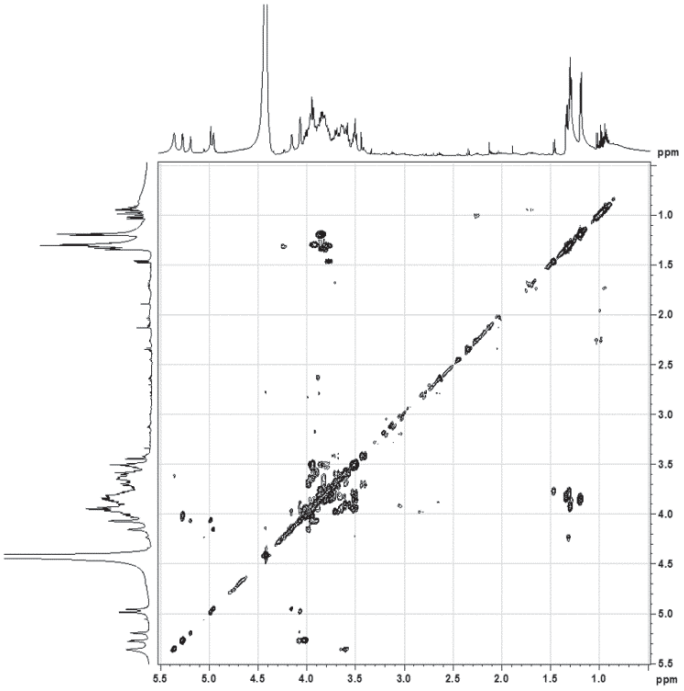

FIG. S7 ^{1}H-^{1}H COSY NMR spectrum of the *Psa* NZ V-13 -EPS dissolved in D_2O recorded at 60 °C (500MHz).

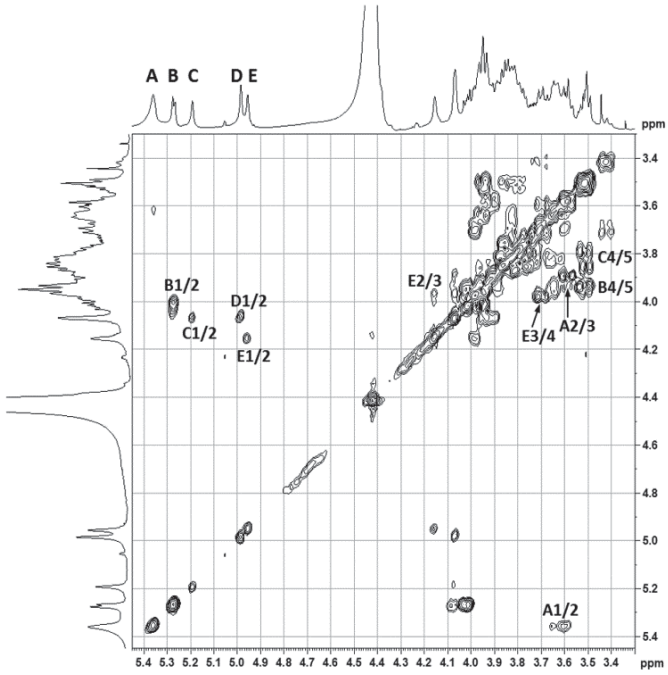

FIG. S8 ^{1}H-^{1}H COSY spectrum of the *Psa* NZ V-13 -EPS dissolved in D_2O recorded at 60 °C (500MHz). Letters refer to sugar residues shown in Fig. 5 and numbers to proton cross-peaks in the sugar rings.

TABLE S1 ^{1}H-NMR and ^{13}C-NMR of the EPS composition

Sugar residue	Nucleus	Chemical shift of proton and carbon (ppm)					
		1	2	3	4	5	6
→4)-α-D-Glc*p*-(1→	^{1}H	5.36	3.60	3.91[b]	3.63[b]	3.72	3.87/3.81
	^{13}C	100.4	72.1	77.9[b]	77.7[b]	73.2	61.1
α-D-Fuc*f*-(1→	^{1}H	5.27	4.02	3.95[d]	3.51	3.86	1.20
	^{13}C	102.0	77.3	75.6[d]	84.8	69.9	18.1
→2)-α-D-Rha*p*-(1→	^{1}H	5.20	4.07	3.94[b]	3.52[b]	3.79	1.31[c]
	^{13}C	101.2	78.5	70.3[b]	72.7[b]	69.5	17.1[c]
→3)-α-D-Rha*p*-(1→	^{1}H	4.99	4.06	3.95[d]	3.64[b]	3.92	1.30[c]
	^{13}C	102.9	70.6	73.7[d]	72.0[b]	69.8	17.0[c]
→3,4)-α-D-Rha*p*-(1→	^{1}H	4.96	4.16	3.99	3.69	3.83	1.34
	^{13}C	102.2	70.4	80.9	77.9	68.5	17.6

[b] assignments are only tentative

[c, d] assignments are interchangeable

MASSEY UNIVERSITY
GRADUATE RESEARCH SCHOOL

STATEMENT OF CONTRIBUTION TO DOCTORAL THESIS CONTAINING PUBLICATIONS

(To appear at the end of each thesis chapter/section/appendix submitted as an article/paper or collected as an appendix at the end of the thesis)

We, the candidate and the candidate's Principal Supervisor, certify that all co-authors have consented to their work being included in the thesis and they have accepted the candidate's contribution as indicated below in the *Statement of Originality*.

Name of Candidate: Shirin Ghods

Name/Title of Principal Supervisor: Professor Bernd H. A. Rehm

Name of Published Research Output and full reference:

Shirin Ghods, Ian M. Sims, M. Fata Moradali, Bernd H. A. Rehm. Bactericidal Compounds Controlling Growth of the Plant Pathogen Pseudomonas syringae pv. actinidiae, Which Forms Biofilms Composed of a Novel Exopolysaccharide. Applied and environmental microbiology 81.12 (2015): 4026-4036

In which Chapter is the Published Work: Chapter II

Please indicate either:

- The percentage of the Published Work that was contributed by the candidate 80%

  and / or

- Describe the contribution that the candidate has made to the Published Work:

  The Design and performance of all experiments with the exception of some

Shirin Ghods Digitally signed by Shirin Ghods Date: 2018.01.08 13:32:19 -05'00'
Candidate's Signature

8/1/2018
Date

Bernd Rehm Digitally signed by Bernd Rehm Date: 2018.01.24 08:15:03 +10'00'
Principal Supervisor's signature

24/1/2018
Date

GRS Version 3– 16 September 2011

Chapter III

Interplay of alginate polymerisation and modifications in *Pseudomonas aeruginosa* and their impact on biofilm formation*

Shirin Ghods [1] **, M. Fata** Moradali [1], Ivan Donati [2], Ian M. Sims [3], Bernd H.A. Rehm [1,4]

[1]Institute of Fundamental Sciences, Massey University, Palmerston North, New Zealand, [2] Department of Life Sciences, University of Trieste, Trieste, Italy, [3] The Ferrier Research Institute, Victoria University of Wellington, Lower Hutt, Wellington, New Zealand,[4] MacDiarmid Institute for Advanced Materials and Nanotechnology, Massey University, Palmerston North, New Zealand

* This study is co-published in: mBio 6 (3):e00453-15 (Appendix)

ABSTRACT

The molecular mechanisms of alginate polymerization/modification/secretion by a proposed envelope spanning multiprotein complex are unknown. Here, the interactive role of Alg8, Alg44, AlgG (epimerase) and AlgX (acetyltransferase) on alginate polymerization and modification was studied by using site-specific deletion mutants, inactive variants and overproduction of subunits. The composition, molecular weight and material properties of resulting novel alginates were analysed. The molecular weight of resulting alginates was reduced by epimerization while it was increased by acetylation. Interestingly, when overproduced, Alg44, AlgG and the non-epimerizing variant AlgG (D324A) increased the degree of acetylation while epimerization was enhanced by AlgX and its non-acetylating variant AlgX (S269A). Biofilm architecture analysis showed that acetyl groups promoted cell aggregation while non-acetylated polymannuronate alginate promoted stigmergy. Overall, this study sheds new light on the functional relationship of alginate polymerisation and modifications as well as their impact on *P. aeruginosa* biofilm development.

INTRODUCTION

Pseudomonas aeruginosa is an opportunistic human pathogen which can become life-threatening in immunocompromised patients. It is the leading cause of morbidity and mortality in cystic fibrosis patients. This is mainly due to its ability to colonize lungs by forming structured biofilms which consist of bacterial cells embedded in a complex matrix predominantly composed of alginate. Bacterial cells in biofilms are protected against the immune system and antibiotics (146, 147). Alginates are anionic exopolysaccharides composed of variable proportions of 1, 4-linked β-D-mannuronic acid (M) and its C5 epimer α-L-guluronic acid (G). The alginate derived from *P. aeruginosa* is naturally acetylated and lacks consecutive G residues (GG-blocks) (148). Alginates exhibit unique gel-forming properties suitable for numerous medical and industrial applications (148, 149). The alginate structure strongly impacts its materials properties. Hence, development of bioengineering approaches to control the alginate structure will enable production of alginates with new material properties towards novel applications.

For many years *P. aeruginosa* has been the model organism to study various aspects of alginate biosynthesis such as e.g. polymerization, epimerization, acetylation, secretion and regulation. Thirteen proteins are directly involved in the biosynthesis of alginate and except for *algC* their encoding genes are clustered in the alginate biosynthesis operon (*algD, alg8, alg44, algK, algE, algG, algX, algL, algI, algJ, algF, algA*) (89, 150). Except for soluble cytoplasmic proteins AlgA, AlgC and AlgD which are responsible for providing the activated nucleotide sugar precursor, GDP-mannuronic acid, proteins encoded by the operon are proposed to constitute an envelope-spanning multiprotein complex. Two interacting cytoplasmic membrane-anchored proteins, the glycosyltransferase, Alg8, and the proposed co-polymerase, Alg44, are necessary for alginate polymerization (95-97, 151). The MucR sensor protein, a diguanylate cyclase (DGC)/phosphodiesterase (PDE) embedded in the cytoplasmic membrane was proposed to provide c-di-GMP for binding to the cytoplasmic PilZ domain of Alg44 by which alginate polymerization is activated (152). Translocation of nascent alginate across the periplasm is coupled with modification processes including O-acetylation and epimerization. O-acetylation is independently catalysed by AlgJ and AlgX (153) while the acetyl group donor is provided by AlgI and AlgF (154, 155). The AlgG epimerase converts M residues to G residues in the nascent alginate chain. AlgG, AlgX and AlgK were suggested to form a periplasmic scaffold for guiding alginate through the periplasm for secretion via the outer membrane protein AlgE (156-161). It was also suggested that if alginate is misguided into the periplasm then degradation would be mediated by the periplasmic AlgL lyase (162). Previous studies on protein-protein interactions and mutual stabilities of proposed subunits of the multiprotein biosynthesis machinery provided evidence of binary protein interactions including Alg8-Alg44, Alg44-AlgK, AlgE-AlgK, AlgX-AlgK, AlgX-MucD (a serine protease), Alg44-AlgX and Alg8-AlgG (98, 151, 163). However, experimental evidence was needed to unravel the functional relationship of these subunits and their impact on biofilm development.

In this study, the role of Alg8, Alg44, AlgG and AlgX with respect to polymerization and modification was studied by analysing the composition and material properties of alginates produced by various strains. We employed a constitutive alginate-producing strain *P. aeruginosa* PDO300 and various isogenic single- and double-gene knockouts of *alg8*, *alg44, algG* and *algX*. This allowed investigation of the role of the respective proteins in alginate polymerization and/or modifications by introducing additional copies

of subunits or their variants *in trans*. The impact of various alginate structures on biofilm formation and architecture was investigated.

MATERIALS AND METHODS

Bacterial strains, plasmids, growth conditions and chemicals.

Strains and plasmids used in this study are summarized in Table 1. *P. aeruginosa* and *Escherichia coli* strains were cultivated in Luria Broth medium supplemented by appropriate antibiotics and were grown at 37 °C. For those assays designed for studying alginate production, compositional and molecular mass analyzes, bacterial phenotype and protein-protein interaction and stability, Difco™ Pseudomonas Isolation Agar (PIA) medium was used which was supplemented by appropriate antibiotics. To rule out the effect of growth condition and media on alginate composition and quantity, all experiments were conducted under the same conditions and using the same batch culture at the same time. All chemicals were purchased from Sigma-Aldrich and Merck KGaA unless otherwise mentioned. All enzymes used for cloning were manufactured by Roche, New England Biolabs GmbH or Invitrogen.

Construction of isogenic single- and double-gene knockout mutants.

Marker-free single- and double-gene knockout mutants in *alg44* and/or *alg8*, *algG* and *algX* were generated in previous studies (151, 164-166). In order to generate PDO300Δ*algX*Δ*algG* and PDO300Δ*alg44*Δ*algG* through two events of homologous recombination, the suicide plasmid pEX100TΔ*algG*ΩGm and background mutants in *algX* and *alg44* were utilized. These suicide plasmid containing knockout genes (only 5' and 3' flanking regions of the respective gene) which were disrupted by the *aacC1* gene (1,100-bp fragment encoding gentamicin acetyltransferase) were flanked by two *FRT* sites (flippase recombinase target) (95). This plasmid was transferred into PDO300Δ*alg44* and PDO300Δ*algX* using *E. coli* S17-1 competent cells as donor. Transconjugants were selected on mineral salt medium (MSM) containing 100 μg ml^{-1} gentamicin and 5% (wt/vol) sucrose (167). Cells emerging from double-crossover events grew on this medium and those cells harboring a suicide plasmid with counter-selectable marker, *sacB*, or undergoing single crossover events did not grow. Gene replacement was

TABLE 1 Strains and plasmids applied in this study

Strains and plasmids	Description	Source or reference
Strains		
P. aeruginosa		
PDO300	*mucA22* isogenic mutant derived from PAO1, Alg^+	(168)
PDO300Δ*alg8*	Isogenic *alg8* deletion mutant derived from PDO300, Alg^-	(95)
PDO300 Δ*alg44*	Isogenic *alg44* deletion mutant derived from PDO300, Alg^-	(169)
PDO300 Δ*alg8*Δ*alg44*	Isogenic *alg8* and *alg44* deletions mutant derived from PDO300, Alg^-	(151)
PDO300 Δ*algG*	Isogenic *algG* deletion mutant derived from PDO300, Alg^-	(151)
PDO300 Δ*algX*	Isogenic *algX* deletion mutant derived from PDO300, Alg^-	(170)
PDO300 Δ*algG*Δ*algX*	Isogenic *algG* and *algX* deletions mutant derived from PDO300, Alg^-	This study
PDO300 Δ*algG*Δ*alg44*	Isogenic *algG* and *alg44* deletions mutant derived from PDO300, Alg^-	This study
PDO300 Δ*algX*Δ*alg44*	Isogenic *algX* and *alg44* deletions mutant derived from PDO300, Alg^-	(151)
E. coli		
Top10	Cloning strain; F^-,*mcr*A, Δ(*mrr-hsdRMS-mcrBC*), φ80*lacZ*ΔM15, Δ*lac*X74,*rec*A1, *ara*D139, Δ(*araleu*)7697 *gal*U,*gal*K, *rps*L (StrR), *end*A1, *nup*G	Invitrogen
S17-1	Donor strain in transconjugation; *thi*-1, *pro*A, *hsd*R17 (r_K^- m_K^+), *rec*A1; tra gene of plasmid RP4 integrated in chromosome	(171)
Plasmids		
pBBR1MCS-5	Gm^r; broad-host-range vector; P_{lac}	(172)
pBBR1MCS-5:*alg8*	*Hind*III-*Pst*I fragment comprising *alg8* inserted into vector pBBR1MCS-5	(95)
pBBR1MCS-5:*alg44*	*Hind*III-*Bam*HI fragment comprising *alg44* inserted into vector pBBR1MCS-5	(169)
pBBR1MCS-5:*algG*	*Bam*HI-*Xba*I fragment comprising *algG* inserted into vector pBBR1MCS-5	(151)
pBBR1MCS-5:*algG*(D324A)	*Bam*HI-*Xba*I fragment comprising *algG* encoding site-directed mutagenesis D324A inserted into vector pBBR1MCS-5; mannuronic acid(M)-epimerase activity$^-$	This study
pBBR1MCS-5:*algX*	*Hind*III-*Bam*HI fragment comprising *algX* inserted into vector pBBR1MCS-5	(166)
pBBR1MCS-5:*algX*(S269A)	*Hind*III-*Bam*HI fragment comprising *algX* encoding site-directed mutagenesis S269A inserted into vector pBBR1MCS-5; Acetyltransferase activity$^-$	This study
pBBR1MCS-5:*algX:algG*	*Hind*III-*Bam*HI fragment comprising *algX* and *Bam*HI-*Xba*I fragment comprising *algG* inserted into vector pBBR1MCS-5	This study
pBBR1MCS-5:*algX*(S269A)*:algG*(D324A)	*Hind*III-*Bam*HI fragment comprising *algX* encoding site-directed mutagenesis S269A and *Bam*HI-*Xba*I fragment comprising *algG* encoding site-directed mutagenesis D324A inserted into vector pBBR1MCS-5; M-epimerase activity$^-$, Acetyltransferase activity$^-$	This study
pBBR1MCS-5:*alg44:algG*	*Cla*I-*Bam*HI fragment comprising *alg44* and *Bam*HI-*Xba*I fragment comprising *algG* inserted into vector pBBR1MCS-5	This study
pBBR1MCS-5:*algX:alg44*	*Cla*I-*Hind*III fragment comprising *algX* and *Hind*III-*Bam*HI fragment comprising *alg44* inserted into vector pBBR1MCS-5	(98)
pEX100T	Ap^r Cb^r, gene replacement vector containing *sacB* gene for counterselection	(173)
pEX100T:Δ*algG*Gm	Ap^r Cb^r, Gm^r, vector pEX100T with SmaI-inserted *algG* deletion construct	This study
pFLP2	Ap^r Cb^r; broad-host-range vector encoding Flp recombinase	(173)
pGEM-T Easy	Cloning vector; Amp^r; T-overhang cloning	Promega
pGEM-T Easy:*algG*	A-tailed fragment encoding C-terminally *algG* inserted into pGEM-T Easy used for sequencing	This study

confirmed after subculture of cells on PIA medium containing 300 µg/ml gentamicin followed by PCR with primers binding to sites outside the flanking regions of the respective target gene. *E. coli* SM10 was used as donor to transfer the flippase recombinase encoding vector pFLP2 into presumable knockout mutants and after 24 h of cultivation on PIA medium containing 5% (wt/vol) sucrose, they were screened based on sensitivity to gentamicin and carbenicillin (173). Gentamicin and carbenicillin-sensitive cells were analyzed by PCR with primers alg44 up/down, algX up/down and algG up/down for successful loss of the *FTR-aacC1-FRT* cassette and to confirm that the target gene was deleted.

In trans-complementation of single- and double-gene knockout mutants.

The sequences of genes of interest were individually amplified by PCR and *P. aeruginosa* PAO1 genome and separately ligated into pGEM-T Easy vector (Promega) for sequencing. The genes *algG*(D324A) and *algX*(S269A) encoding point-mutated non-epimerizing AlgG and non-acetylating AlgX proteins respectively, were synthesized by GenScript. These genes were individually or simultaneously ligated into the corresponding sites of pBBR1MCS-5 (172) (cf. Table 1) resulting in the final constructs pBBR1MCS-5:*algX*:*algG,* pBBR1MCS-5:*alg44*:*algG,* pBBR1MCS-5:*algX*(S269A), pBBR1MCS-5:*algG*(D324A) and pBBR1MCS-5:*algX*(S269A):*algG*(D324A). These constructs were transferred into appropriate single- and double-gene knockout mutants via transconjugation using *E. coli* S17-1 as donor or electroporation. Resultant transformants were selected on PIA medium containing 300 μg ml^{-1} gentamicin and confirmed by selecting cells with mucoid phenotypes followed by plasmid isolation and analysis. Phenotypic characterization of transformants included alginate isolation and quantification. All generated strains are listed in Table 1.

Alginate purification and quantification.

A total of 2 ml of bacterial overnight cultures grown in LB medium supplemented with appropriate antibiotic were harvested and washed twice with saline solution. Then, the harvested cell sediments were re-suspended in 1 ml of saline solution and then normalized to an OD_{600} of 3.0. A 200 μl of cell suspension was plated onto each PIA medium (with three repetitions) containing 300 μg ml^{-1} of gentamicin and incubated at 37 °C for 72 h.

Cells of each plate were scraped off and suspended in saline solution until all alginate materials were completely dissolved. To separate cells from alginate-containing supernatant, the suspensions were pelleted and alginates in supernatants were precipitated with an equal volume of ice-cold isopropanol. Additionally, cellular sediments were freeze-dried and the final weights were determined. The alginate precipitants were freeze-dried and then re-dissolved in 50 mM Tris-HCl pH 7.4, 10 mM $MgCl_2$ to a final concentration of 0.5% (wt/vol), followed by incubation with 15 μg ml^{-1} DNaseI and 15 μg ml^{-1} RNaseI at 37 °C for 6 h. Then, Pronase E was added to a final concentration of 20 μg ml^{-1} and incubated for a further 18 h at 37 °C. Alginate solutions were dialyzed (12-14 kDa MWCO, ZelluTrans/Roth mini dialyzer, Carl Roth GmbH & Co) against 5 l of ultrapure H_2O for 48 h. Finally, alginates were precipitated with an equal volume of ice-cold isopropanol and freeze-dried for uronic acid assay and biochemical analysis.

Following a modified protocol for alginate quantification or uronic acid assay (97) and using purified alginic acid from brown algae (Sigma-Aldrich) as a standard, alginate samples were dissolved in 200 μl of ultrapure water at concentrations between 0.25 and 0.05 mg ml^{-1}. Each sample was mixed with 1.2 ml of tetraborate solution (0.0125 M disodium tetraborate in concentrated sulfuric acid) and incubated on ice for 10 min followed by incubation at 100 °C for 5 min and then cooled down on ice for a further 5 min. By adding 20 µl of 3-phenylphenol reagent (0.15% of 3-phenylphenol in 0.125 M NaOH), reactions were developed within 1 min of vortexing. For each sample and dilution, a negative control was assayed using 0.125 M NaOH instead of the 3-phenylphenol reagent. Uronic acid concentrations were determined spectrophotometrically at a wavelength of 520 nm.

Size exclusion chromatography-multiangle laser light scattering (SEC-MALLS) analysis.

The average molecular weights of the alginates produced were analyzed by SEC-MALLS (Waters 2690 Alliance separations module; Waters 450 variable wavelength detector set at 280 nm; DAWN-EOS multi-angle laser light scattering detector with a laser at 690 nm (Wyatt Technology Corp., Santa Barbara, CA, USA); Waters 2410 refractive index monitor). Purified samples were dissolved in 0.1 M $NaNO_3$ (2 mg ml^{-1}) and allowed to hydrate fully by incubating at room temperature overnight. Immediately prior to analysis,

samples were pre-heated at 80 °C for 5 min, injected (100 μl) and eluted with 0.1 M $NaNO_3$ (0.7 ml min^{-1}, 60 °C) from two columns (TSK-Gel $G5000P_{WXL}$ and $G4000P_{WXL}$, 300×7.8 mm, Tosoh Corp.) connected in series. ASTRA software (version 6.1.1.17, Wyatt Technology Corp.) and dn/dc of 0.150 g ml^{-1} was used for determining weight-average molecular weights ($\overline{M_w}$) and number-average molecular weights ($\overline{M_n}$) and polydispersity index (PI) via the fraction $\overline{Mw}/\overline{Mn}$. In the case of a perfectly monodisperse (homogeneous) polymer PI value equals 1.0.

^{1}H-nuclear magnetic resonance (NMR) spectroscopy analysis.

Compositional analysis of alginate samples was carried out using ^{1}H-NMR. The spectra were recorded at 90 °C with a JEOL 270 NMR spectrometer (6.34 T) operating at 270 MHz for proton. Samples were prepared as described by Grasdalen et al (174). The chemical shifts were expressed in ppm downfield from the signal for 3-(trimethylsilyl) propanesulfonate. The integration of the ^{1}H-NMR signals allowed us to determine the composition of the different deacetylated alginate samples and their acetylation degree (38, 175, 176). For alkaline deacetylation 30 ml of 1% alginates in saline solution were treated with 12 ml of 1M NaOH in 65 °C for 30 min and neutralized with 12 ml of 1M HCl. Treated samples were then dialyzed against 5 l of distilled water for 48 h and then freeze-dried.

Microrheological analysis.

In order to measure viscoelastic properties of the alginates, the mean-square displacement (MSD) of probe particles embedded in the samples and in turn the viscoelastic moduli (G' (elastic) and G'' (viscose)) were measured (177-179). A 2.8 μl aliquot of a 2.5% (wt/vol) suspension of Polybead® polystyrene microspheres (0.5 μm) (Polysciences) was mixed with 250 μl aliquot of 0.1% alginate samples in Milli-Q water. Particle motion was recorded using an inverted microscope (Nikon Eclipse TE2000-U) on an air damped table (Photon Control) equipped with an Andor Neo CMOS camera operated at 204 fps, and a 60x 1.2 NA (Nikon, Plan Apo VC 60x WI) water immersion objective lens. An image series was acquired for approximately four seconds and x-y coordinate data extracted

using polyparticle tracking software (180). An in-house program was used to calculate the MSD with a program to extract the rheological information (181).

Continuous-culture flow cell biofilms and quantitative analysis.

Biofilm architecture analysis was performed for those mutants producing alginates with very distinct composition and properties from each other including PDO300 (pBBR1MCS-5), PDO300Δ*alg8* (pBBR1MCS-5:*alg8*), PDO300Δ*alg44* (pBBR1MCS-5:*alg44*), PDO300Δ*algG* (pBBR1MCS-5:*algG*), PDO300Δ*algG* (pBBR1MCS-5:*algG*(D324A)), PDO300Δ*algX* (pBBR1MCS-5:*algX*), PDO300Δ*algX* (pBBR1MCS-5:*algX*(S269A)) and PDO300Δ*algX*Δ*algG* (pBBR1MCS-5:*algX* (S269A):*algG*(D324A)). Each mutant was grown in continuous-culture flow cells (channel dimensions of 4 mm by 40 mm by 1.5 mm) at 37 °C (182). A 500 μl suspension of cells at early-stationary-phase was injected into each channel and kept upside down for 4 hours. Then, flow was started with a mean flow of 0.3 ml min^{-1}, corresponding to a laminar flow with a Reynolds number of 5(105, 106). The flow cells were then incubated at 37 °C for 24 h. Biofilms were stained utilizing the LIVE/DEAD BacLight bacterial viability kit (Molecular Probes) and visualized using confocal laser scanning microscopy (Leica SP5 DM6000B). For quantitative analysis of biofilms IMARIS image analysis software (Bitplane) was employed. Biofilm architecture and appearance, biovolume (μm^3), the ratio of biovolume per unit area (μm^3 μm^{-2}), dead-to-live ratio, compactness and thickness of base layers were analyzed (106, 119, 183).

RESULTS

Functional relationship of alginate polymerisation and modifications.

Previously, it was shown that Alg8 and Alg44 (mediating alginate polymerisation) constitute a protein complex which itself interacts with AlgG (alginate epimerase) and AlgX (alginate acetylteransferase) (98, 151), but their functional interplay remained unknown. In order to investigate the relationship between alginate polymerization and modifications, single- and double-gene knockout mutants of *P. aeruginosa* PDO300 were generated and followed by individual and combinatorial *in trans* complementation using relevant genes including *alg8*/*alg44* (encoding alginate-polymerizing proteins),

algX/algX (S269A) (encoding alginate-acetylating/non-acetylating AlgX) and *algG/algG* (D324A) (encoding alginate-epimerizing/non-epimerizing AlgG). The generated knockout mutants lost mucoidity while mucoidity was restored upon *in trans* complementation with relevant genes.

In order to shed light on the functional interaction between alginate-polymerizing and modifying subunits, the polymerization degree, epimerization degree and acetylation level of resulting alginates were assessed. The ratio of M to G residues and molar fraction of MM, MG/GM and GG blocks was determined using ^{1}H-NMR analysis as described previously (38, 174). Furthermore, ^{1}H-NMR was employed to analyse the degree of acetylation of alginates via the same approach explained by Pawar et al (176). The degree of polymerisation, which is proportional to molecular weight was determined using SEC-MALLS.

The composition and the molecular weights of the respective alginates are summarized in Table 2. Our analysis showed that additional copies of Alg8 and/or Alg44 had a similar effect on alginate production such as resulting in high molecular weights with reduced epimerization and acetylation when compared to the wild-type control (Fig, 1; Table 2). The same effect of Alg8 and Alg44 on alginate polymerization supported the hypothesis that they are subunits that together constitute the alginate polymerase.

Two alginate-modifying enzymes AlgX and AlgG are neccesory subunits of the alginate biosynthesis multiprotein complex for protecting nascent alginates from being misguided into the periplasm and degraded. Here we used AlgX and AlgG and their catalytically inactive variants of AlgX (S269A) and AlgG (D324A) and the resulting alginates were analysed. When only the inactive AlgX variant was present, the resulting alginate was non-acetylated. Interestingly, additional copies of active AlgX or inactive AlgX resulted in the highest epimerization value of $F_G = 0.36$. Additional copies of both AlgG and AlgX or inactive variants respectively, increased the degree of epimerization of the resulting alginate (Fig. 1, Table 2). Additional copies of both AlgX and AlgG increased the degree of acetylation when compared to additional copies of only AlgX (Fig. 1, Table 2). Interestingly, additional copies of Alg44 enhanced acetylation 2.7-fold when compared to AlgX.

The correlation between the molecular weight of alginate and alginate modification, such as acetylation and epimerization, was assessed (Fig. 1). The molecular weight of the various alginates was determined by SEC-MALLS (Table 2). The highest molecular weight (4653±1.1% kDa corresponding to about 22876 uronic acid residues) was detected

in alginates from strains with additional copies of the catalytically inactive epimerase variant AlgG (D324A). This was about a 70% increase in molecular weight when compared to alginate produced from strains with additional copies of epimerizing AlgG. The lowest molecular weight alginates were produced by strains harbouring additional copies of those subunits contributing the highest levels of epimerization i.e. AlgX (F_G = 0.36), AlgX (S269A) (F_G = 0.36) along with the lowest levels of acetylation (9.8% and 0). Non-acetylated and non-epimerized alginates (F_G = 0, Ac. = 0%) showed the lowest molecular weight (1811±0.9% kDa). Since ^{1}H-NMR spectra of the various alginates did not provide evidence for double bonds (between the C4 and C5 carbons leading to 4-deoxy-L-erythro-hex-4-enopyranosyluronic acid), which are introduced by alginate lyase mediated degradation, the alginate lyase presumably did not influence the degree of polymerization. Additional copies of Alg8 and Alg44 gave rise to increased molecular weights ranging 3000 to 3800 kDa supporting their direct involvement in alginate chain synthesis. These data suggested that the alginate molecular weight is inversely correlated with alginate epimerization but positively correlated with acetylation (Fig. 1). Alginates produced by the various strains showed a narrow molecular weight distribution with a polydispersity index close to 1 (Table 2).

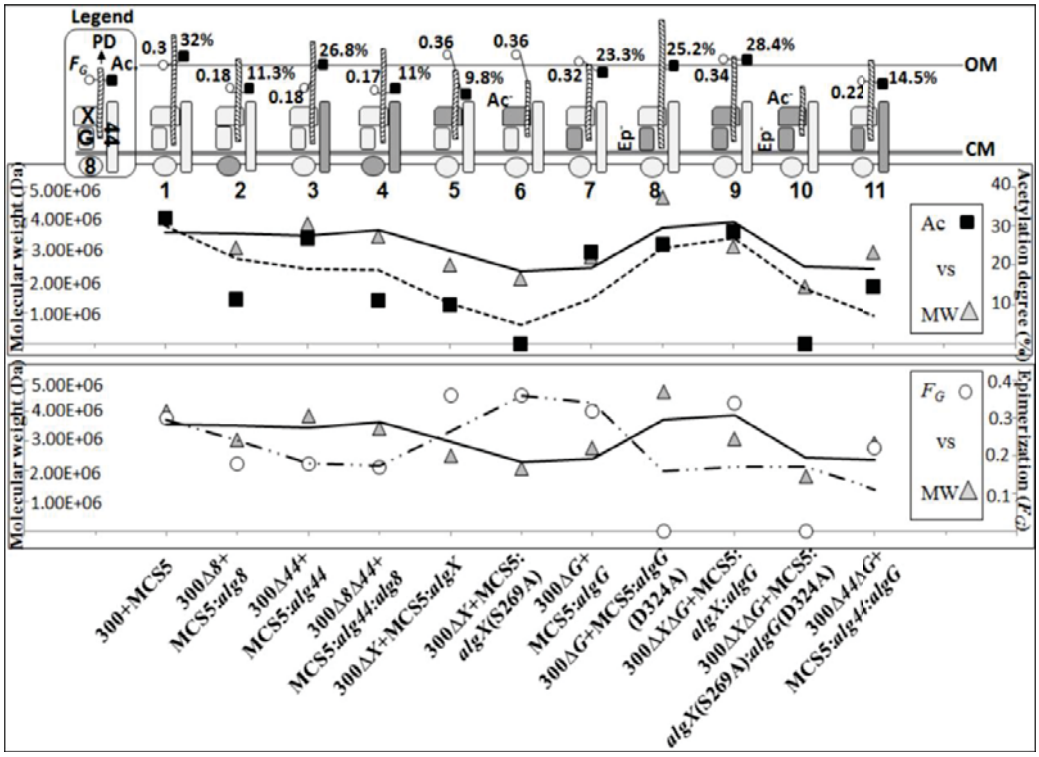

FIG. 1 Correlation between alginate polymerization and modifications. Presumable features (No. 1-11) show protein complexes constituted by Alg8, Alg44, AlgG and AlgX (cf. legend on top left corner of plot). The subunit produced upon *in trans* complementation is shown as darker shape(s). Inactive AlgX (S269A) and AlgG (D324A) are labelled as (Ac^{-}) and (Ep^{-}), respectively. The length of various alginates (PD) with respect to acetylation (Ac.%) and epimerization (F_G) degrees are presented and proportionally illustrated for each feature. 300: PDO300; MCS5: pBBR1MCS-5; PD: polymerization degree; OM: outer membrane; CM: cytoplasmic membrane.

In vivo alginate polymerase activity.

Alginate produced by the various strains was isolated and quantified (Table 2). Although additional copies of the various proteins increased the amount of alginate produced when compared to the reference strain PDO300 (pBBR1MCS-5), a significant variation of alginate productivity, i.e. alginate polymerase activity, was detected. Interestingly, additional copies of non-acetylating AlgX (S269A) and native AlgX mediated production of the largest amounts of alginate while epimerizing and non-epimerizing AlgG mediated the lowest level of production (Table 2). Pairwise comparison of these four strains showed that more alginate is produced in the absence of modification events. The enhancing role of AlgX in alginate production was further supported when additional copies of AlgX together with AlgG led to a strong production of alginate. However, the non-acetylating and non-epimerizing pair resulted in a much lower quantity (Table 2). Furthermore, all attempts to restore alginate production in PDO300Δ*alg44*Δ*algX* with pBBR1MCS-5:*alg44*:*algX* failed. Previously, it was shown that the mucoid phenotype of this double-gene knockout mutant was only restored when one of the introduced complementing genes, either *alg44* or *algX*, were integrated into the genome (*in cis* complementation using mini-CTX) and the other one presented *in trans* resulting in alginate production of 1.9 (g) / CDM (g) (151).

TABLE 2 Composition and molecular weight analyses of alginate produced by different mutants

	Mutant	F_G	F_M	$F_{GM/MG}$	F_{MM}	Ac.%	$\overline{M}_n$ (kDa)	$\overline{M}_w$ (kDa)	PI	Alginate yield (g)/ CDM(g)
1	300 +MCS5	0.3	0.7	0.29	0.41	32	3927 (±0.864%)	3832 (±0.842%)	1.025 (±1.2%)	1.3±0.03
2	300Δ*8*+ MCS5:*alg8*	0.18	0.82	0.17	0.65	11.3	3045 (±0.556%)	3037 (±0.551%)	1.003 (±0.7%)	12.8±1.03
3	300Δ*44*+ MCS5:*alg44*	0.18	0.82	0.18	0.64	26.8	3831 (±0.963%)	3650 (±0.950%)	1.05 (±1.3%)	8.7±0.53
4	300Δ*44*Δ*8*+ MCS5:*alg44*:*alg8*	0.17	0.83	0.17	0.66	11	3369 (±0.839%)	3352 (±0.821%)	1.005 (±1.1%)	41.5±4.9
5	300Δ*X*+ MCS5:*algX*	0.36	0.64	0.36	0.28	9.8	2460 (±0.932%)	2447 (±0.913%)	1.005 (±1.3%)	104.1±5.5
6	300Δ*X*+ MCS5:*algX*(S269A)	0.36	0.64	0.36	0.28	0	2086 (±0.960%)	2065 (±0.944%)	1.010 (±1.3%)	125.8±9.9
7	300Δ*G*+ MCS5:*algG*	0.32	0.68	0.32	0.36	23.3	2755 (±1.041%)	2726 (±0.986%)	1.011 (±1.4%)	2.6±0.04
8	300Δ*G*+ MCS5:*algG*(D324A)	0	1	0	1	25.2	4653 (±1.097%)	4575 (±1.117%)	1.017 (±1.5%)	7.6±0.57
9	300Δ*X*Δ*G*+ MCS5:*algX*:*algG*	0.34	0.66	0.34	0.32	28.4	3076 (±1.051%)	3044 (±1.029%)	1.011 (±1.4%)	67.42±4.8
10	300Δ*X*Δ*G*+ MCS5:*algX*(S269A): *algG*(D324A)	0	1	0	1	0	1811 (±0.884%)	1716 (±0.888%)	1.055 (±1.2%)	8.7±0.42
11	300Δ*44*Δ*G*+ MCS5:*alg44*+*algG*	0.22	0.78	0.22	0.56	14.5	2907 (±0.966%)	2861 (±0.944%)	1.016 (±1.3%)	9.0±0.3

300:PDO300; MCS5: pBBR1MCS-5; F_G: molar fraction of guluronate (G) residue; F_M: molar fraction of mannuronate (M) residue; $F_{GM/MG}$: molar fraction of two consecutive G and M residues; F_{MM}: molar fraction of two consecutive M residues; Ac.: acetylation; $\overline{M}_n$: weight-average molecular weights; $\overline{M}_n$: number-average molecular weights; PI: polydispersity index; CDM: cell dry mass.

Viscoelastic properties of various resulting alginates.

Physicochemical properties of natural polymers are harnessed by various organisms to adapt to environments and impact biofilm development and maturation. Viscoelastic property is a key physical property determined by the chemical structure of biopolymers. Here, particle-tracking microrheology was applied to assess the viscoelastic properties of the various resulting alginates. Our analysis showed that all alginates displayed

viscoelastic properties in which the solid-like elastic modulus G' was greater than the liquid-like viscous modulus G'' ($G'>G''$). The plot of particles mean square displacement (MSD) versus correlation time showed MSD curves of the alginates are distributed in four distinct categories (Fig. 2). In the first category, the alginates produced from PDO300Δ*algG* (pBBR1MCS-5:*algG*(D324A)) and PDO300Δ*alg8* (pBBR1MCS-5:*alg8*), respectively, without G-residues and with the highest molar fraction of MM-blocks, and both with very high molecular weight, showed the highest and quite similar viscoelastic properties (G' = 0.41, G'' = 0.3; G' = 0.40, G'' = 0.28, respectively). Interestingly, the alginates from PDO300Δ*alg44* (pBBR1MCS-5:*alg44*), PDO300Δ*algG* (pBBR1MCS-5:*algG*) and PDO300 (pBBR1MCS-5) dropped into the second category with lower viscoelastic property. In the third category, showing lower viscoelastic properties, those alginates with molecular weight of ≤ 2000 kDa produced by PDO300Δ*algX* (pBBR1MCS-5:*algX*(S269A) and PDO300Δ*algX*Δ*algG* (pBBR1MCS-5:*algX*(S269A): *algG* (D324A) were found. Surprisingly, acetylated alginate from PDO300Δ*algX* (pBBR1MCS-5:*algX*) was the only member of the fourth category with the lowest viscoelastic property amongst all analysed samples. These results suggested that viscoelasticity was positively impacted by the molecular weight combined with high M content, while the presence of G residues and acetyl groups in the alginate chain lowered viscoelasticity. All these polymers showed greater elasticity than viscosity ($G'>G''$) (Fig. 2).

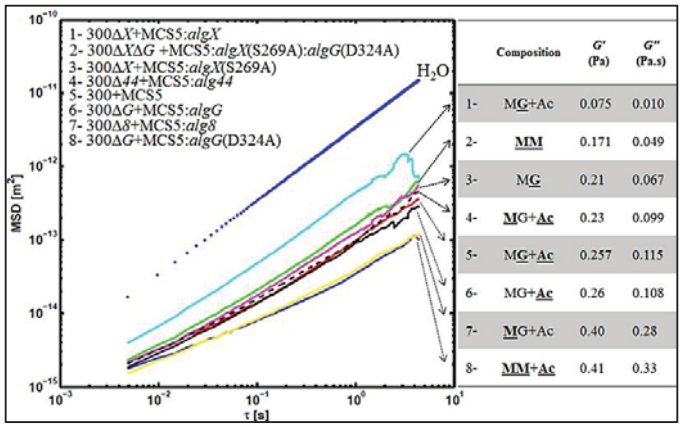

	Composition	G' (Pa)	G'' (Pa.s)
1-	MG+Ac	0.075	0.010
2-	MM	0.171	0.049
3-	MG	0.21	0.067
4-	MG+Ac	0.23	0.099
5-	MG+Ac	0.257	0.115
6-	MG+Ac	0.26	0.108
7-	MG+Ac	0.40	0.28
8-	MM+Ac	0.41	0.33

FIG. 2 Viscoelastic property of alginates was impacted by molecular weight and modifications. The plot of MSD versus time shows distribution of alginate viscoelastic properties in four distinct regions. Alginates composition and viscoelasticity moduli (G': elastic, G'': viscous) are presented next to the plot. Bold and underlined letters indicate the predominance of mannuronate (M)/guluronate (G) molar fraction or acetylation (Ac.) degree among all analysed alginates. 300: PDO300; MCS5: pBBR1MCS-5.

The impact of various alginates on biofilm formation.

P. aeruginosa is capable of forming biofilms on biotic and abiotic surfaces and alginate predominantly constitutes the *P. aeruginosa* biofilm matrix. Overproduction of alginate is characteristic of the mucoid phenotype of most clinical isolates from CF patients. Development of the mucoid phenotype and the formation of highly structured biofilms is the hallmark of chronic infections (9, 184). In this study, we applied various generated mutants of *P. aeruginosa* producing various alginates to investigate the impact of various alginates with different physicochemical properties on biofilm development and architecture.

Confocal laser scanning microscopy images of biofilms formed by mutant PDO300Δ*algX* (pBBR1MCS-5:*algX*) and its non-acetylating counterpart, PDO300Δ*algX* (pBBR1MCS-5:*algX*(S269A)) highlighted the crucial role of acetylation of alginate for developing biofilms and cellular arrangements (Fig. 3). Comparison of the two strains revealed significant differences in elevated structures and the distribution of microcolonies. For example, the structures formed by strains producing acetylated alginates were perfectly shaped and developed with a biovolume of 5.5±1.26 $\mu m^3 \mu m^{-2}$ and a maximum height of 83 μm, while those formed with non-acetylated alginate showed a smaller biovolume of 3.9±0.2 $\mu m^3 \mu m^{-2}$ and a reduced height of 26 μm, with irregular architecture. Interestingly, the strain producing acetylated alginate did not produce a multicellular base-layer and cells were organized in pillar-shaped architectures similar to structures described for the architectures of Psl-overproducing strain (i.e. *P. aeruginosa* WFPA801) (185, 186). In contrast, the strain producing non-acetylated alginate formed a biofilm with disordered and scattered microcolonies (Fig. 3, frame 3). Furthermore, PDO300Δ*algX* (pBBR1MCS-5:*algX*) formed a biofilm with 1.5-fold more compactness and 31% more live cells than the biofilm formed by PDO300Δ*algX* (pBBR1MCS-5:*algX*(S269A)) (Table 3). PDO300Δ*algX* (pBBR1MCS-5) mutant did not form a structured biofilm (Fig. 3, frame 4) but a multicellular layer with a thickness of 6 μm.

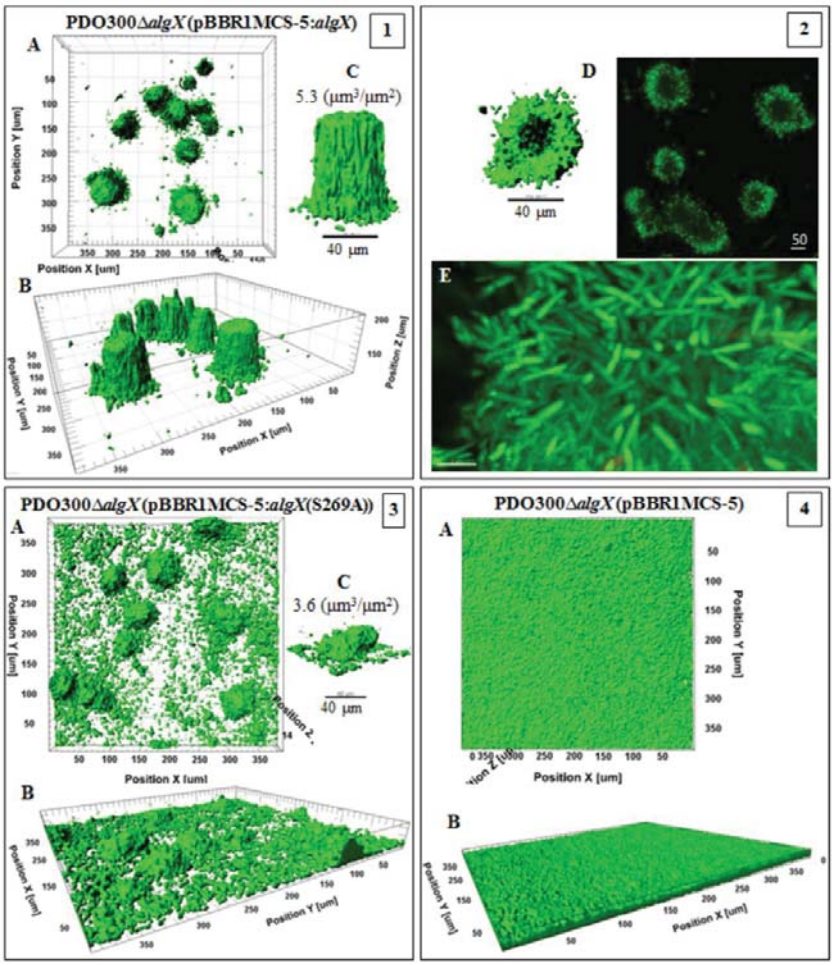

FIG. 3 Biofilm architecture of mutants producing acetylated and non-acetylated alginates. This figure shows biofilm formation and architecture of the mutants PDO300Δ*algX* (pBBR1MCS-5:*algX*) (frames 1, 2), PDO300Δ*algX* (pBBR1MCS-5:*algX*(S269A)) (frame 3) which produce acetylated and non-acetylated alginates, respectively, and PDO300Δ*algX* (pBBR1MCS-5) (frame 4) with no alginate production. In all frames A-C shows top view, side views and a representative of typical highly structured cell community, respectively. The cell community dimensions are provided as $\mu m^3 \mu m^{-2}$.

PDO300Δ*algG* (pBBR1MCS-5:*algG*(D324A) which produced a high molecular-weight, acetylated polymannuronate with strong viscoelasticity acquired the largest biovolume of $6.0 \pm 0.22 \mu m^3 \mu m^{-2}$ (Fig. 4, frame 3). Interestingly, adjacent structures were networked with horizontal appendages, with void spaces and channels formed underneath whole structures, likely to constitute water channels (Fig. 4, frame 4). On the other hand, PDO300Δ*algG* (pBBR1MCS-5:*algG*) which produced lower molecular weight acetylated and G residue-containing alginate formed elevated, but less developed

structures with less biovolume of 4.8±0.22 $\mu m^3 \mu m^{-2}$ (Fig.4, frame 1). The base layers formed by both strains were dense and covered the whole area of the surface. The biofilm of PDO300Δ*algG* (pBBR1MCS-5) was a homogeneous layer of cells (7 μm thickness) without elevated structures (Fig. 4, frame 2).

PDO300Δ*algG*Δ*algX* (pBBR1MCS-5: *algX*(S269A):*algG*(D324A) produced a non-acetylated polymannuronate with a low molecular weight and the respective biofilm was composed of very long and narrowly elevated structures (Fig. 5, frame 1, 2). The biovolume was 1.5±0.2 $\mu m^3 \mu m^{-2}$) which was less than for all the other investigated strains (Table 3).

Strains PDO300Δ*alg8* (pBBR1MCS-5:*alg8*) and PDO300Δ*alg44* (pBBR1MCS-5:*alg44*) established heterogeneous highly structured biofilms (Fig. 6). The former formed a biovolume of 3.95±0.43 $\mu m^3 \mu m^{-2}$ and compactness of 6.09E+02 while the latter generated very dense and large structures with biovolume of 5.8±0.43 $\mu m^3 \mu m^{-2}$ but less compactness (4.43E+02). Both mutants showed higher numbers of dead cells among all applied mutants but less than wild-type (Table 3). Conversely, PDO300Δ*alg8* (pBBR1MCS-5) and PDO300Δ*alg44* (pBBR1MCS-5) generated a homogeneous biofilm without elevated or highly structured architectures. Compactness values and dead/live ratios are summarized in Table 3.

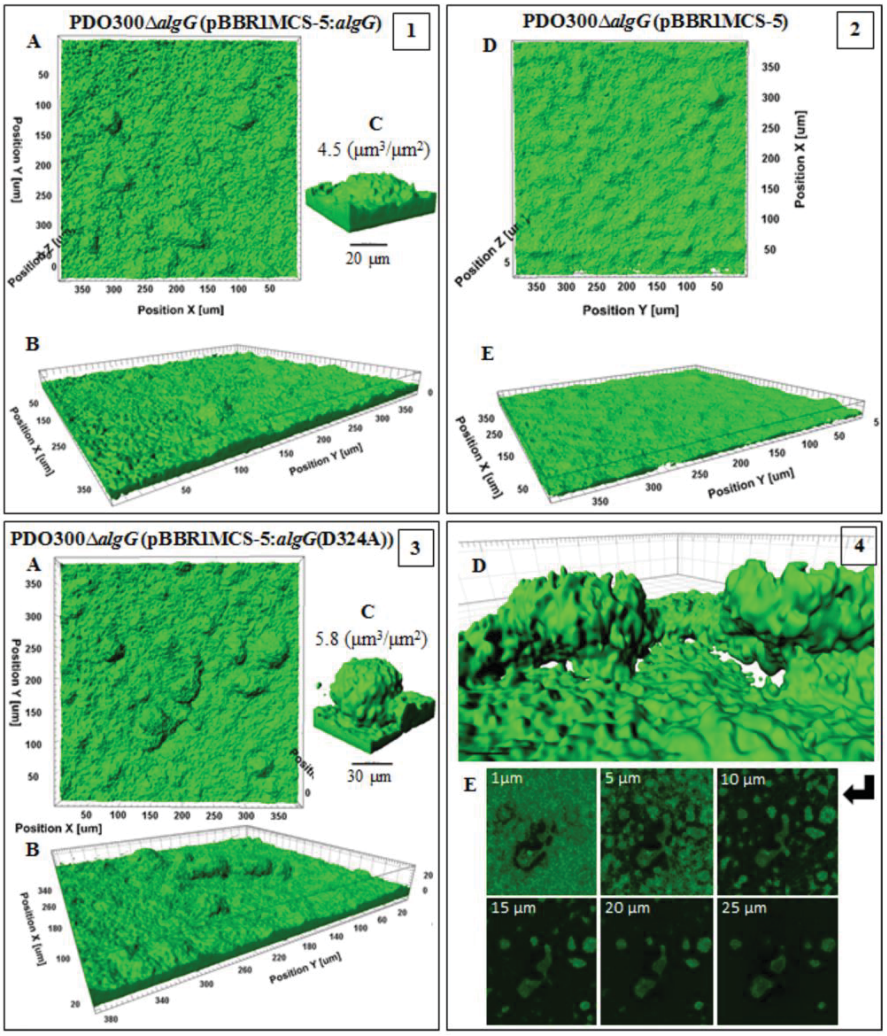

FIG. 4 Biofilm architecture of mutants producing epimerized and non-epimerized alginates. This figure shows biofilm formation and architecture of the mutants PDO300Δ*algG* (pBBR1MCS-5:*algG*) (frame 1), PDO300Δ*algG* (pBBR1MCS-5:*algG*(D324A)) (frames 3 and 4) which produce, respectively, epimerized (poly-MG) and non-epimerized (poly-M) alginates and PDO300Δ*algG* (pBBR1MCS-5)(frame 2) with no alginate production. In all frames A, B and C shows respectively top view, side views and a representative of typical highly structured cell communities for that mutant with biovolume per area ($\mu m^3 \mu m^{-2}$) ratio. In frame 3, poly-M alginate-based biofilm is highly developed than poly-MG alginate-based in frame 1, presenting larger biovolume and biovolume per area ratio. Cells of both mutant covered entire cover slide surface. Frame 4D and E represent the architecture of poly-M alginate-based microcolonies in which two adjacent structures are connected with horizontal appendages and free-cell void cavities channelled underneath of microcolonies. Frame 4E shows 6 different slices of microcolonies with connected structure at the middle of figures surrounded by free-cell and matrix

areas. Frame 2 represents homogenous cell community of non-mucoid mutant without highly structured architecture.

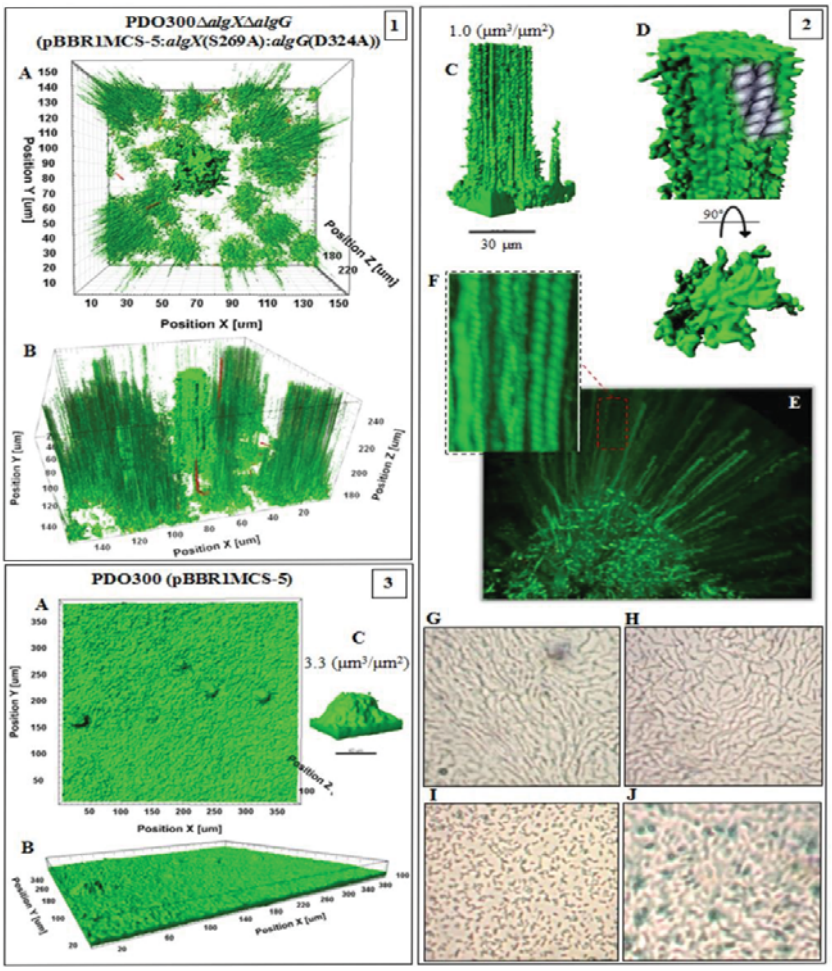

FIG. 5 Biofilm architecture of mutant producing non-epimerized and non-acetylated alginates and wild-type. This figure shows biofilm formation and architecture of the mutants PDO300Δ*algX*Δ*algG* (pBBR1MCS-5:*algX*(S269A):*algG*(D324A)) (frames 1, 2) and PDO300 (pBBR1MCS-5) (frame 3). In all frames A, B and C shows respectively top view, side views and a representative of typical highly structured cell communities for that mutant with biovolume per area ($\mu m^3 \mu m^{-2}$) ratio. Biofilm architecture visualized for mutant producing non-acetylated poly-M alginate (frames 1, 2) was remarkably different from other applied mutants. Affected by alginate properties, emerging biofilm consists of very narrow but long elevated microcolonies representing longitudinal cell trails or strips indicating stigmergic self-organization and adaptation of cells in weak matrices. Frame 2D-Frepresents close side and top views of one of the microcolonies and cell trails and cell-cell interactions in each cell trail are depicted in sketches. Frame 2 G-J shows micrographs (40X magnification) of the edge (H, I) and surface (G, J) of

mucoid colonies of PDO300Δ*algX*Δ*algG* (pBBR1MCS-5:*algX*(S269A):*algG*(D324A)) (G, H) and PDO300 (pBBR1MCS-5) (I, J) forming a thin layer on PIA medium after incubation at 37°C for 18 h. Organization of cells of PDO300Δ*algX*Δ*algG* (pBBR1MCS-5:*algX*(S269A):*algG*(D324A) mutant showed linear filamentous aggregation pattern. Wild-type biofilm architecture is presented in frame 3.

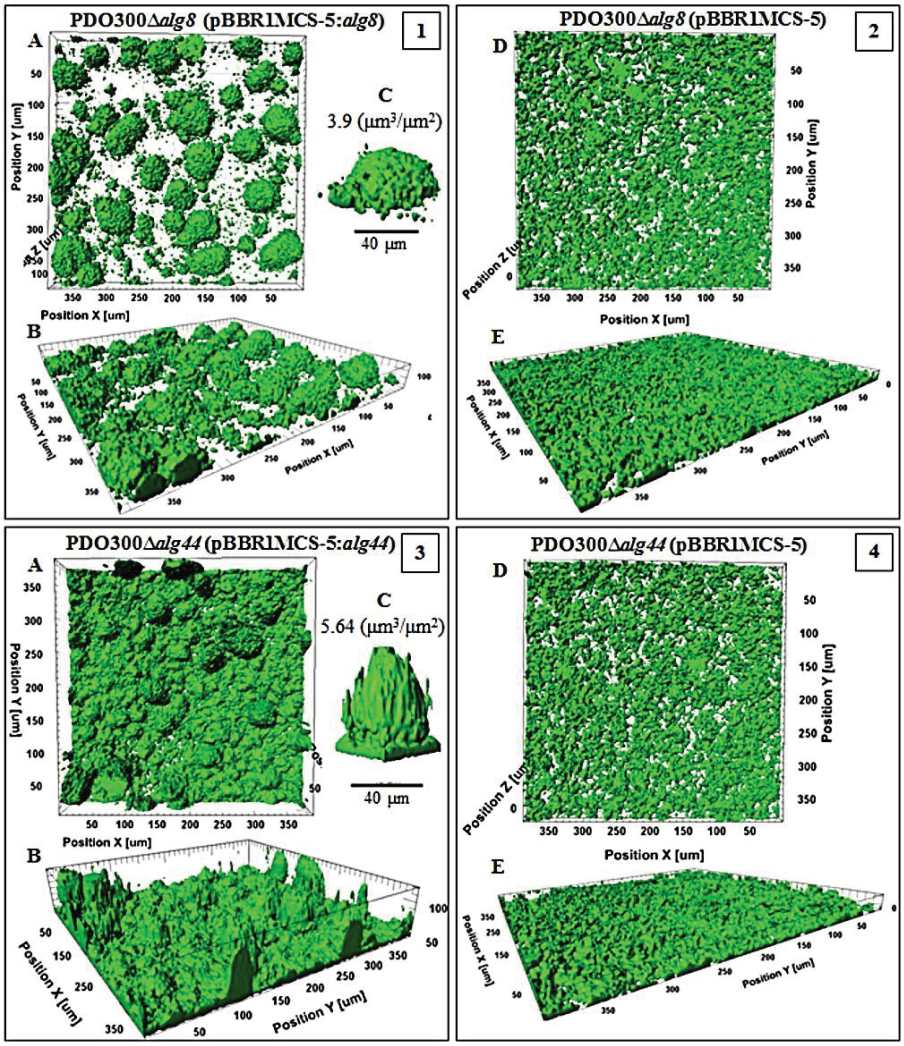

FIG. 6 Biofilm architecture of mutant producing high mannuronate molar fraction and M-block. This figure shows biofilm formation and architecture of the mutants PDO300Δ*alg8* (pBBR1MCS-5:*alg8*) (frame 1) and PDO300Δ*alg44* (pBBR1MCS-5:*alg44*) (frame 3) and non-mucoid mutants (frames 2, 4). In all frames *A-C* shows respectively top view, side views and a representative of typical highly structured cell communities for that mutant with biovolume per area ($\mu m^3 \mu m^{-2}$) ratio. Both mutants produce alginates with highest degree of M-block occurrence

but very different degree of acetylation. PDO300Δ*alg44* (pBBR1MCS-5:*alg44*) (frame 3) which produce highly acetylated alginate established a very dense and highly developed and larger microcolonies than PDO300Δ*alg8* (pBBR1MCS-5:*alg8*) (frame 1). One explanation for this significant difference is the presence of an additional copy of Alg44 which senses c-di-GMP which is a common second messenger in the cells governing the physiological condition of cells during colonization. However, non-mucoid mutants did not establish highly structured biofilm and microcolonies.

TABLE 3 Compactness and dead/live ratio calculated for analyzed biofilms

mutant	Compactness*	Dead/live ratio**
300Δ*8*+MCS5:*alg8*	6.09E+02	1.43±0.10
300Δ*44*+ MCS5:*alg44*	4.43E+02	1.17±0.04
300Δ*G*+ MCS5:*algG*	2.77E+02	0.70±0.06
300Δ*G*+ MCS5:*algG*(D324A)	1.68E+02	0.97±0.04
300Δ*X*+ MCS5:*algX*	3.00E+02	0.42±0.02
300Δ*X*+ MCS5:*algX*(S269A)	2.20E+02	0.55±0.02
300Δ*G*Δ*X*+MCS5: *algG*(D324A): *algX*(S269A)	1.20E+03	0.49±0.03
300+MCS5	4.46E+02	2.40±0.29
300Δ*8*+MCS5	1.39E+02	1.46
300Δ*44*+MCS5	1.42E+02	0.7
300Δ*G*+MCS5	8.90E+01	1.01
300Δ*X*+MCS5	1.16E+02	0.94

300:PDO300; MCS5: pBBR1MCS-5; *Total fluorescence per volume of biofilm; **Ratio between red and green fluorescence shown by each biofilm-forming mutant

DISCUSSION

In this study, we investigated the functional relationship between alginate polymerisation and modification and the impact of various resulting alginates on the *P.aeruginosa* biofilm development and architecture. To this end, a range of alginate compositions and molecular weights exhibiting various material properties were produced by engineering *P. aeruginosa* strains. This study revealed how alginate polymerization (Alg8, Alg44) is aligned with alginate modifications (AlgG, AlgX). As shown in Fig. 1, additional copies of active or inactive AlgX acetyltransferase significantly increased the molar fraction of G residues as well as productivity, which appeared inversely correlated with the alginate molecular weight (Fig. 1; Table 2).

The first experimental evidence that AlgX and AlgG exhibit a mutually auxiliary behavior was obtained, suggesting that the two modification events (acetylation, epimerization) are not competitive, but linked (187). Also, this study suggests a new role of AlgX in epimerization and as a periplasmic scaffold protein playing a key role in efficient translocation of the alginate chain across the periplasm. Interestingly, restoration of alginate production of the AlgG negative mutant by an inactive variant of AlgG led to a significantly increased alginate molecular weight when compared to active AlgG suggesting that AlgG as a scaffold subunit is critical for processivity of alginate polymerization while the actual epimerization event interferes with processivity (Fig. 1). Furthermore, the role of AlgG mediated epimerization on alginate length might be due to AlgG mediated alginate degradation as polysaccharide epimerases show a similar reaction mechanism compared to polysaccharide lyases (187). This finding might also explain why algal alginates with a high molar fraction of G residues introduced by epimerases have very low molecular weights (188). Acetylation was correlated with the molecular weight suggesting that there was no negative impact on processivity of alginate polymerization (Fig. 1). In addition, we propose a new auxiliary role for Alg44 in acetylation besides being necessary for c-di-GMP dependent activation of alginate polymerization (Table 2; Fig. 1).

In general, additional copies of any subunit increased alginate production when compared to the reference strain, indicating that the stoichiometry of the various subunits is less critical for the activity of the multiprotein complex (Table 2).

To shed light on the functional relationships of the various alginates, their viscoelasticity was assessed. The presence of acetyl groups lowered viscoelasticity by possibly interfering with intermolecular alginate chain interactions (Fig. 2). In contrast, increasing molar fractions of MM-blocks and higher molecular weights increased viscoelasticity (Fig. 2). Acetylated alginates gave rise to well-developed and highly organized heterogeneous architectures and promoted cell aggregations (Fig. 3) which was consistent with previous studies (189) but these findings suggested viscoelasticity is not critical for biofilm architecture formation. Fig. 4 shows that non-epimerized alginate (polymannuronate) with a high molecular weight and strong viscoelasticity supported the establishment of these biofilm features and that by controlling the molar fraction of G residues biofilm architecture characteristics could be adapted to various environments. We showed that the lack of G-residues and acetyl groups caused the formation of undeveloped and narrow microcolonies which were supported by specific long trails or

strips of cells emerging from stigmergic self-organization of cells affected by this particular alginate (Fig. 5) (190). The stigmergy concept describes self-organization processes in various organisms occurring via indirect communications that influence the behaviour of other individuals in the cell communities, such as a biofilm (190). This was further evidence for the role of alginate material properties on the formation of particular biofilm architectures and cellular aggregation patterns.

Overall, this study led to the development of strains producing a range of alginates. This enabled the analysis of functional relationships of protein subunits in the alginate biosynthesis multiprotein complex, from a materials property and biological function perspective, such as demonstrating that viscoelasticity of alginate contributed to enhanced cell aggregation during biofilm formation.

ACKNOWLEGMENTS

We are thankful to the Manawatu Microscopy and Imaging Centre (MMIC) of Massey University and especially Matthew Savoian for microscopic technical assistance and Martin A. K. Williams and Bradley W. Mansel assisting us for microrheology analysis. This work was supported by grants from Massey University Research Fund and the MacDiarmid Institute of Advanced Materials and Nanotechnology (New Zealand) to B.H.A.R. M.F.M is funded by a Massey University Doctoral scholarship.

MASSEY UNIVERSITY
GRADUATE RESEARCH SCHOOL

STATEMENT OF CONTRIBUTION TO DOCTORAL THESIS CONTAINING PUBLICATIONS

(To appear at the end of each thesis chapter/section/appendix submitted as an article/paper or collected as an appendix at the end of the thesis)

We, the candidate and the candidate's Principal Supervisor, certify that all co-authors have consented to their work being included in the thesis and they have accepted the candidate's contribution as indicated below in the *Statement of Originality*.

Name of Candidate: Shirin Ghods

Name/Title of Principal Supervisor: Professor Bernd H. A. Rehm

Name of Published Research Output and full reference:

M. Fata Moradali, Ivan Donati, Ian M. Sims, Shirin Ghods, Bernd H. A. Rehm. Alginate Polymerization and Modification Are Linked in Pseudomonas aeruginosa. mBio 6 (3) (2015):e00453-15)

In which Chapter is the Published Work: Chapter III

Please indicate either:

- The percentage of the Published Work that was contributed by the candidate 30%

  and / or

- Describe the contribution that the candidate has made to the Published Work:

  Generation of some mutants and production of various alginates, interpretation of physicochemical properties of alginates, setting up and analysis of biofilms results

Shirin Ghods Digitally signed by Shirin Ghods Date: 2018.01.08 13:32:19 -05'00'
Candidate's Signature

8/1/2018
Date

Bernd Rehm Digitally signed by Bernd Rehm Date: 2018.01.24 08:15:03 +10'00'
Principal Supervisor's signature

24/1/2018
Date

Chapter IV

Activation Mechanism and Cellular Localization of Membrane-Anchored Alginate Polymerase in *Pseudomonas aeruginosa*

M. Fata Moradali[1], **Shirin Ghods[1]**, Bernd H. A. Rehm[1]

[1]Institute of Fundamental Sciences, Massey University, Private Bag 11222, Palmerston North, New Zealand

Applied and Environmental Microbiology 83.9 (2017): e03499-16

ABSTRACT

The exopolysaccharide, alginate, produced by the opportunistic human pathogen *Pseudomonas aeruginosa* represents a survival advantage by contributing to formation of characteristic biofilms during infection. Membrane anchored proteins Alg8 (catalytic subunit) and Alg44 (co-polymerase) constitute the alginate polymerase which is activated by the second messenger molecule c-di-GMP, but the mechanism of activation remains elusive. To shed light on the c-di-GMP mediated activation of alginate polymerization *in vivo*, an *in silico* structural model of Alg8 fused to the c-di-GMP binding PilZ domain informed by the structure of cellulose synthase, BcsA, was developed. This structural model was probed by site-specific mutagenesis and different cellular levels of c-di-GMP. Results suggested that c-di-GMP-mediated activation of alginate polymerization involves amino acids residing at two loops including H323 (loop A), T457 and E460 (loop B) surrounding the catalytic site in the predicted model. Activity of respective Alg8 variants suggested that c-di-GMP-mediated control of substrate access to the catalytic site of Alg8 is dissimilar to the known activation mechanism of BcsA. Alg8 variants responded differently to various c-di-GMP levels while MucR imparted c-di-GMP for activation of alginate polymerase. Furthermore, we showed that Alg44 co-polymerase constituted a stable dimer, with its periplasmic domains required for protein localization, alginate polymerization and modification. Super folder GFP fusions of Alg8 and Alg44 showed a non-uniform, punctuate and patchy arrangement of both proteins surrounding the cell. Overall, this study provides insights into the c-di-GMP mediated activation of alginate polymerization while assigning functional roles to Alg8 and Alg44 including their subcellular localization and distribution.

IMPORTANCE

The exopolysaccharide, alginate, is an important biofilm component of the opportunistic human pathogen *P. aeruginosa* and the principle cause of the mucoid phenotype which is the hallmark towards chronic infections of cystic fibrosis patients. Production of alginate is mediated by interacting membrane proteins Alg8 and Alg44 while their activity is post translationally regulated by the second messenger c-di-GMP, a well-known regulator of the synthesis of a range of other exopolysaccharides in bacteria. This study provides new insights into the unknown activation mechanism of alginate polymerization by c-di-GMP. Experimental evidence was provided that the activation of alginate polymerization requires the engagement of specific amino acid residues residing at the catalytic domain of Alg8 glycosyltransferase and they are proposed to exert an allosteric effect on the $PilZ_{Alg44}$ domain upon c-di-GMP binding. This mechanism is dissimilar to the proposed mechanism of the autoinhibition and the c-di-GMP activated cellulose polymerization. On the other hand, conserved amino acid residues in the periplasmic domain of Alg44 were found to be involved in alginate polymerization as well as modification events i.e. acetylation and epimerization. Due to the critical role of c-di-GMP in regulation of many biological processes particularly the motility-sessility switch and also the emergence of persisting mucoid phenotypes, these results aid to a better understanding of biofilm-associated regulatory networks and c-di-GMP signalling as well as might assist the development of inhibitory drugs.

INTRODUCTION

Alginate is a secreted anionic exopolysaccharide composed of variable proportions of 1,4-linked β-$_D$-mannuronic acid (M) and its C-5 epimer α-$_L$-guluronic acid (G) which is naturally produced by some bacteria and brown seaweeds (191). Understanding alginate biosynthesis has been of significant importance for the scientific community due to its role in bacterial pathogenesis as well as the possibility of producing tailor-made alginates exhibiting material properties suitable for various medical and industrial applications. In the context of pathogenesis, *P. aeruginosa* is the leading cause of chronic bronchopulmonary infection in cystic fibrosis patients and many nosocomial infections ,associated with an extraordinary capability to form multicellular aggregates embedded

in extracellular polymeric substances (EPS) known as biofilms. In bacteria, the secretion of EPS leads to the formation of a developed biofilm, protecting embedded bacteria from environmental stresses as well as the immune system and antibiotic treatment (192). Alginate production by *P. aeruginosa* creates a survival advantage as it mediates formation of persistent biofilms during chronic infections (191, 193-195). It reduces diffusion of antibiotics, scavenges free radicals released by triggered mechanisms in the immune system and interferes with cell-mediated killing of *P. aeruginosa* (40-42). For many years, alginate biosynthesis has been studied in *P. aeruginosa* as a model organism. Briefly, bacterial alginate is synthesized by an envelope-spanning multiprotein complex consisting of proteins Alg8 andAlg44 (polymerization), AlgG (epimerization), AlgX (acetylation), AlgK and AlgE (secretion) with the possible involvement of AlgI-AlgJ-AlgF (acetylation) and AlgL (alginate degradation) (98, 151, 196). These proteins are responsible for processive polymerization of alginate, translocation of nascent polymer (poly-M) across the periplasm, modification events in the periplasm (i.e. epimerization of M to G residues and acetylation) and secretion of modified alginate (poly-MG) through the outer membrane (98, 151, 196).

However, alginate biosynthesis is under the control of the second messenger bis-(3',5')-cyclic dimeric guanosine monophosphate (c-di-GMP). C-di-GMP signaling is very complex and almost ubiquitous in bacteria, controlling various biological processes including a motility-sessility switch and biofilm formation (197). Adjustment of cellular levels of c-di-GMP are critical for binding to specific receptor/effector proteins mainly via the PilZ domain in order to reach a desired physiological output such as exopolysaccharide production (36, 198). In this regard, the molecular mechanism of posttranslational activation of alginate polymerization by c-di-GMP is still unknown. The interacting cytoplasmic membrane-anchored proteins Alg8 and Alg44 constitute the catalytic unit of the alginate polymerase which is activated by binding of a dimeric form of c-di-GMP to the Alg44 PilZ domain in the cytoplasm (151, 199).

In this study, we investigated the molecular mechanism of the c-di-GMP mediated activation of alginate polymerization by applying an *in silico* model of Alg8 and $PilZ_{Alg44}$ domain to mimic the structure of BcsA protein (cellulose synthase). BcsA was chosen because it has the c-di-GMP sensing PilZ domain mediating the activation of the polymerization of cellulose exopolysaccharide in *Rhodobacter sphaeroides* which is controlled by a proposed autoinhibition mechanism (200). This mechanism is referred to

the steric hindrance by salt bridge formation in proximity to the catalytic site of BcsA, which is formed between the first arginine of the PilZ domain's R580XXXR584 motif and E371 preceding the RW motif (a signature of the glycosyltransferase family 2). Consequently, the BcsA gating loop adopts a resting state and blocks the catalytic site. This steric hindrance was proposed to be eliminated upon c-di-GMP binding to R580, opening up the gate for substrate to enter into the catalytic site (200, 201). To this end, various site-specific mutagenesis assays were performed informed by predicted models. The impact of respective Alg8 variants on alginate production was tested in PDO300 with either single or double deletions of *alg8* and *alg44,* respectively, at high and low cellular levels of c-di-GMP mediated by the activity of c-di-GMP metabolizing enzymes MucR and RocR. Furthermore, the role of Alg44 proposed as alginate co-polymerase was assessed through site-specific mutagenesis with respect to *in vivo* alginate polymerase activity, alginate modification (i.e. acetylation and epimerization), and protein localization. Subcellular localization of Alg8 and Alg44 was visualized by generating translational fusions with a super folding derivative of GFP (sfGFP) and confocal laser scanning microscopy.

MATERIALS AND METHODS

Bacterial strains, plasmids, and growth condition.

P. aeruginosa and *Escherichia coli* strains (Table 1) were cultivated in Luria Broth Lennox medium (enzymatic digest of casein (10 g/l), yeast extract (5 g/l), sodium chloride (5 g/l), pH 7.3 ± 0.2) (Acumedia; Neogen Corporation) supplemented by appropriate antibiotics. Depending on the selection marker on the plasmid, 300 µg/ml of gentamicin (AppliChem) (for *P. aeruginosa*) and 10 µg/ml of gentamicin or 100 µg/ml of ampicillin (AppliChem) (for *E. coli*) were used. Cultivated cultures were grown at 37 °C overnight unless otherwise stated. Alginate production and phenotypic assessments were performed using Difco™ Pseudomonas Isolation Agar (PIA) medium supplemented by 300 µg/ml of gentamicin. *E. coli* strains including C41 (DE3), C43 (DE3), BL21(DE3), Origami™ (DE3), ClearColi BL21(DE3) and Rosetta™ strains applied for heterologous production of protein were purchased from Lucigen or Novagen (Table 1). Large-scale cell culture preparations were performed in Luria Broth medium. All chemicals were purchased from Sigma-Aldrich unless otherwise

mentioned. All restriction enzymes used for cloning were manufactured by New England Biolabs GmbH. Enzymes for PCR and gene sequencing were purchased from Invitrogen. Alginate powder (from brown algae; Sigma-A2158) was purchased from Sigma-Aldrich.

Construction of isogenic mutants with knockout of *alg8/alg44* and *mucR/alg8* genes.

The *P. aeruginosa* PDO300 was used to generate isogenic single-and double-gene knockout mutants in *alg8* and/or *alg44* and *mucR* and/or *alg8* genes as described previously (105, 164). Briefly, this was performed through two events of homologous recombination using suicide plasmid pEX100T. This plasmid contained knockout genes which were disrupted by the *aacC1* gene (encoding gentamicin acetyltransferase) flanked by two *FRT* sites. Removing the *FTR-aacC1-FRT* cassette was performed by transfer the flippase recombinase-encoding vector pFLP2 (173) into presumable knockout mutants resulting in *P. aeruginosa* PDO300Δ*alg8,* PDO300Δ*alg44*, PDO300Δ*alg8*Δ*alg44,* PDO300Δ*mucR and* PDO300Δ*mucR*Δ*alg8* mutants which were confirmed using antibiotic-sensitivity screening and PCR with *alg8* up/down, *alg44* up/down and *mucR* up/down primers (164, 165, 167).

***In trans* and *in cis* complementation of knockout mutant in *alg8* and/or *alg44* and *mucR* and/or *alg8* genes and *E. coli* strains transformation.**

The genes encoding Alg8/Alg44 or Alg44-6His and MucR/Alg8 were transferred into generated mutants using pBBR1MCS-5(172) plasmid. For incorporation into the genome, mini-CTX-*lacZ* plasmid was used(202) as described previously in detail (98, 151, 164). The vector pETDuet-1 (Novagen) was applied to construct pETDuet-1:*alg44*-12His for heterologous production of Alg44-12His (Table 1). Relevant encoding genes (i.e. *alg8*, *alg8*-12His, *alg44*, and *alg44*-12His) for heterologous production were optimized based on *E. coli* codon usage and synthesized by GenScript.

Site-specific mutations of *alg8* and *alg44* genes.

Site-specific mutagenesis of Alg8 was performed by amplifying the fragments of *alg8* by PCR using genomic DNA of POA1 strain and the primers carrying point mutations (Table 1). Amplified fragments were ligated into pBBR1MCS-5:*alg8* at *Aat*II/*Xmn*I or *Bgl*II/*Pst*I sites resulting in pBBR1MCS-5:*alg8*(T320A), pBBR1MCS-5:*alg8*(H323A), pBBR1MCS-5:*alg8*(P324A), pBBR1MCS-5:*alg8*(P325A), pBBR1MCS-

5:*alg8*(T453A), pBBR1MCS-5:*alg8*(R454A), pBBR1MCS-5:*alg8*(T457A), pBBR1MCS-5:*alg8*(E460A), pBBR1MCS-5:*alg8*(H323E), pBBR1MCS-5:*alg8*(E322A), pBBR1MCS-5:*alg8*(E322A/H323E), pBBR1MCS-5:*alg8*(T453A/T457A), pBBR1MCS-5:*alg8*(R454A/T457A). Resultant constructs were confirmed by sequencing at Massey Genome Service, Massey University. Also, pBBR1MCS-5:*alg8*(P325A)*: alg44*(R17A), pBBR1MCS-5:*alg8*(P325A): *alg44*(R21A), pBBR1MCS-5:*alg8*(T457A): *alg44*(R17A), pBBR1MCS-5:*alg8*(T457A): *alg44*(R21A), pBBR1MCS-5:*alg8*(E460A): *alg44*(R17A), pBBR1MCS-5:*alg8*(E460A): *alg44*(R21A), pBBR1MCS-5:*alg8*(H323E): *alg44*(R17A), pBBR1MCS-5:*alg8*(H323E): *alg44*(R21A) were generated. Combinations of all constructs with *rocR* (PA3947) were also provided (Table 1).

For site-specific mutagenesis of Alg44, each residue of the clusters QMK (residues 258-260) and TSPCDC (residues 264-269) were mutated to alanine using DNA synthesis (GenScript) and ligated into corresponding region on *alg44* using *Sap*I and *Bam*HI sites. The resultant plasmids were pBBR1MCS-5:*alg44*(Q258A)-6His, pBBR1MCS-5:*alg44*(M259A)-6His, pBBR1MCS-5:*alg44*(K260A)-6His, pBBR1MCS-5:*alg44*(T264A)-6His, pBBR1MCS-5:*alg44*(S265A)-6His, pBBR1MCS-5:*alg44*(P266A)-6His, pBBR1MCS-5:*alg44*(C267A)-6His, pBBR1MCS-5:*alg44*(D268A)-6His, pBBR1MCS-5:*alg44*(C269A)-6His, pBBR1MCS-5:*alg44*(C267A/C269A)-6His.

Protein localization assessment in the envelop fraction of the cells.

Transformants of *P. aeruginosa* were grown in LB supplemented with Gentamicin 300 µg/ml overnight at 37 °C as inoculum. Each PIA plate supplemented with antibiotic were inoculated with 200 µl of washed inoculum and incubated for 36 h at 37 °C. Grown bacteria on plates were scraped off and washed twice with buffer W (HEPES 10 mM, NaCl 150mM, pH 7.4). Pelleted cells were lysed in buffer L (HEPES 10 mM, NaCl 150mM, glycerol 10%, EDTA 10 mM, lysozyme 0.5 mg/ml, Roche complete protease inhibitor EDTA-free, pH 7.4) for 20 min and were subjected to sonication for disruption. Unbroken cells were separated by centrifugation at 8000 × *g* for 30 min at 4 °C. Supernatants were subjected to ultracentrifugation at 100,000 × *g* for 90 min at 4 °C to isolate the envelope fraction. Pellets were solubilized in SDS containing loading buffer supplemented with 0.2% triton X-100 and incubated for 1 h at 4 °C. Before protein

analysis, protein concentration of samples was assessed via densitometry using various concentrations of bovine serum albumin.

Alginate purification and quantification and free uronic acid assay.

Two ml of bacterial overnight culture grown in LB medium supplemented with the appropriate antibiotic were sedimented and cells washed twice with saline solution. Cells were suspended in 1 ml of saline solution and 200 µl of cell suspension (OD_{600} 3.0) was plated onto a thick layer of PIA medium (40 ml in each plate) containing 300 µg/ml of gentamicin and then incubated at 37 °C for 72 h which time point was previously described and found to be optimal for cell growth and alginate quantification avoiding nutrient deprivation and desiccation stress (11). Grown cells were scraped off agar plates and suspended in saline solution until homogenous suspension was formed. Then suspensions were pelleted and supernatants containing alginate were precipitated with an equal volume of ice-cold isopropanol. The alginate precipitates were freeze-dried and then re-dissolved in 50 mM Tris-HCl pH 7.4, 10 mM $MgCl_2$ to a final concentration of 0.5% (wt/vol), followed by incubation with 15 µg/mL DNaseI and 15 µg/mL RNaseI at 37 °C for 6 h. Then, Pronase E was added to a final concentration of 20 µg/ml and incubated at 37 °C for further 18 h. Alginate solutions were dialyzed (12-14 kDa MWCO, ZelluTrans/Roth mini dialyzer, Carl Roth GmbH & Co) against 5 liters of ultrapure H_2O for 48 h. Finally, alginates were precipitated with an equal volume of ice-cold isopropanol and freeze-dried for uronic acid assay and biochemical analysis which was previously described in detail (98, 151, 203).

Assessment of free uronic acids was performed using 2 ml of overnight liquid culture. Cells were pelleted and supernatants were filtered through a Vivaspin-500 (GE Healthcare) filter device with a molecular mass cutoff of 10 kDa. The uronic acids in the flow through which consist of free uronic acids and short alginate degradation products and total sample were measured according to previously described procedure (108).

The analysis of composition of the alginates.

Compositional analysis of alginate samples was carried out using ^{1}H-NMR for two different sets of original and deacetylated samples. Preparation of samples was done according to previously described method (38, 151, 175). A ten milligram partially hydrolyzed samples were dissolved in 2 ml of D_2O (99.96%) with shaking for 2 h and

lyophilized. This deuteriation step was repeated twice. The deuterium-exchanged alginates (6 mg) were dissolved in 0.7 mL of D_2O. ^{1}H-NMR spectra were recorded at 85 °C using 500 MHz BrukerAvance spectrometers. Spectra were interpreted as previously described by Grasdalen et al (151, 174).

Protein production, cell disruption and preparation of membrane fractions.

The strains of *E. coli* with pETDuet-1:*alg44*-12His were grown overnight. The main cultures of LB media supplemented with 70 µg/ml of ampicillin were inoculated with 1% (vol/vol) of overnight cultures and incubated at 37 °C until OD_{600} reached 0.5-0.6. Then cultures were induced with isopropyl β-D-1-thiogalactopyranoside (IPTG) to a final concentration of 1 mM and subsequently grown at 25 °C. In *cis*-complemented PDO300Δ*alg44* with *alg44*-6His was grown at 37 °C overnight for mass production of cells.

Cells were harvested and washed twice with sodium phosphate buffer. After disruption using sonication or microfluidizer, unbroken cells and cellular debris were removed using centrifugation at 8,000 × *g* for 45 min at 4 °C. Supernatants were subjected to ultracentrifugation at 100,000 × *g* for 90 min at 4 °C to isolate the envelope fraction. Pelleted membrane fractions were dissolved at 4 °C for 2 h with buffer A (800 mM NaCl, 50 mM NaH_2PO_4, 10% glycerol, 5 mM EDTA, 1.5% Triton X-100, 5 mM imidazole and Roche complete protease inhibitor EDTA-free, pH 7.7). Insoluble part was pelleted again at 100,000 × *g* for 30 min at 4 °C. Supernatants were subjected to protein purification and analysis.

Protein purification and analysis.

The His-spin protein miniprep kit (Zymo Research) was employed for preliminary purification assessment. Roche cOmplete His-tag purification resin (EDTA-compatible) was employed for large-scale purification of His-tagged protein. The solubilized membrane fraction was mixed with five ml of pre-equilibrated resin with buffer A and incubated at 4 °C for 6 h with gentle shaking. The mixture was packed into columns by gravity flow and washed with 10 column volumes (cv) of buffer A. Elution was performed with 5 cv of buffer B (similar to buffer A with 500 mM imidazole, pH 7.7). A 250 µl of eluent was loaded on to a Superdex 200 Increase 10/300 GL column. Two column volumes of buffer C (300 mM NaCl, 50 mM NaH_2PO_4, 10% glycerol, 5 mM EDTA,

0.02% Triton X-100, pH 7.8) was passed through the column at 0.6 ml min^{-1} and the absorbance at 280 nm was monitored.

A standard curve of retention volume (Rv) vs. apparent molecular weight was applied via measuring the elution volume for low and high molecular weight protein standards (Sigma). The plot was obtained for log [MW] vs. Rv where MW is the known apparent molecular weight of the standard including: 1) ferritin (~440 kDa), 2) alcohol dehydrogenase (~150 kDa), 3) bovine serum albumin (~66 kDa) and 4) carbonic anhydrase (~29 kDa). The curve was approximately linear at R^2=0.9891 over the range of standards from MW = 29-440 kDa. This curve is presented in supplemental material.

Fractions were collected in 0.5 ml steps and subsequently assessed by SDS-PAGE (8% acrylamide gels) either with staining with Coomassie Brilliant Blue solution or immunoblotting. Immunoblotting was performed using an iBlot dry-blotting system (Invitrogen) as described previously (98). For the detection of His-tagged protein, a HisProbe-HRP kit (Thermoscientific) was used according to the manufacturer's instruction. For detection of Alg8, anti-Alg8 (2:5,000) in 2% bovine serum albumin-fraction V (Gibco/Invitrogen) was used. Immunoblots were processed with SuperSignal West Pico chemiluminescent substrate (Thermoscientific) and developing on X-ray film (Kodak, Rochester). Protein sequencing was performed by The Centre for Protein Research (CPR) of Otago University.

Imaging of fluorescent proteins and analysis.

The sequences encoding GFP and sfGFP were synthesized (GenScript) and ligated at the C-terminal end of *alg8*, *alg44 and pilN* genes (without a stop codon) using *XbaI* and *SacI* sites resulting in pBBR1MCS-5:*alg8:gfp*, pBBR1MCS-5:*alg8:sfgfp*, pBBR1MCS-5:*alg44:gfp*, pBBR1MCS-5:*alg44:sfgfp,* pBBR1MCS-5:*pilN:gfp*, pBBR1MCS-5:*pilN:sfgfp*. Constructs were introduced into PDO300, PDO300Δ*alg8* and PDO300Δ*alg44* by electroporation. Complemented and mucoid colonies were selected for alginate quantification. Microscopic analysis was performed using the cells grown on solid media within 24 hours (mucoid colony), followed by analysis of a variable number of optical sections (Z-stack series), each of which were separated by 0.13 μm, using confocal laser scanning microscopy (Leica SP5 DM6000B). This experiment was repeated three times to analyze the cells. Images were analyzed using IMARIS image analysis software (Bitplane).

Statistical analysis.

Alginate quantification and uronic acid assays were conducted using four independent repetitions and data were presented as mean ± standard deviation (SD). Shapiro-Wilk test was used to evaluate the normality of distribution of the data indicating data were normally distributed (Shapiro-Wilk test: $p < 0.05$). The results were statistically analysed by analysis of variance (ANOVA) followed by *post hoc*Tukey's honestly significant difference (HSD) test for pair-wise comparisons using XLSTAT statistical add-in software for Microsoft Excel©14.0. The *Letters* on the histogram provide a graphical representation for *post hoc* pair-wise comparisons (Tukey's HSD). A p value less than or equal to 0.05 was considered significant in all evaluations.

RESULTS

How is alginate polymerization regulated by a c-di-GMP-dependent mechanism? The second messenger c-di-GMP is required for alginate production via interaction with the PilZ domain of membrane-anchored Alg44 which itself interacts with Alg8 glycosyltransferase (alginate polymerase) (98, 151). Previously, it was shown that alteration of intracellular levels of c-di-GMP is critical for engaging c-di-GMP receptor/effector proteins to trigger specific outputs (198, 204). In the regulation of alginate biosynthesis, RocR (a phosphodiesterase degrading c-di-GMP) and MucR (a diguanylatecyclase synthesizing c-di-GMP) are important in c-di-GMP turnover and they negatively and positively regulate alginate biosynthesis, respectively (105). However, the activation mechanism of alginate polymerization via Alg8 glycosyltransferase as a target in response to different c-di-GMP levels remains unknown.

C-di-GMP mediated activation of cellulose synthesis via the BcsA protein in *R. sphaeroides* provides currently the best understood mechanistic model (200). Furthermore, bioinformatic analysis showed that Alg8 (PA3541) and BcsA (Accession: 5EIY_A; *Rhodobacter sphaeroides* 2.4.1) both belong to the glycosyltransferase family 2 (GT-2), and they share the same conserved signature motifs and residues (13.7% identity and 23.6% similarity) which were experimentally shown as critical for production of alginate and cellulose, respectively (151, 201).

This experiment aimed at unraveling the molecular mechanism of c-di-GMP mediated activation of alginate polymerization in comparison to the c-di-GMP dependent activation of cellulose synthesis while also considering the importance of different levels of c-di-GMP. Informed by the BcsA structure, an *in silico* structural model of Alg8 (1-494 aa) C-terminally fused to the $PilZ_{Alg44}$ domain (1-122 aa of Alg44) was developed by using the Phyre2 Protein Fold Recognition Server (205). Phyre2 server relies on the key principle that protein structure is more conserved in evolution than protein sequence (206). Hence, this prediction server enables reliable prediction of the three-dimensional structure of a given protein by using a library of well-known protein structures and advanced remote homology detection (206).

The overall Phyre2 output was a structural model homologous to BcsA (confidence, 100%; coverage, 84%) with the C-terminal part aligned with the crystal structure of the PilZ domain from Alg44 (199) (Fig.1a, Fig. S1). This model showed the full incorporation of the PilZ domain into the last C-terminal transmembrane helix domain of Alg8 (TM4) through a linker and a two-stranded β-sheet formation with one strand located at the C-terminal end of a long loop of Alg8 running across the catalytic pocket (Fig.1a, Fig. S1). This loop, designated here as loop B comprising residues I441-G462, was homologous to the gating loop (residues R499-I517) in the BcsA structure which also contained BcsA`s T511 residue conferring the autoinhibition mechanism found in cellulose synthesis. This loop is also critical for relocating precursor of cellulose into the catalytic site at open-rest transition (200). Another predicted loop of Alg8-$PilZ_{Alg44}$, designated here as loop A comprising residues T320-E326, was homologous to BcsA`s loop harboring E371 of the glycosyltransferase domain which further stabilizes the autoinhibition mechanism by salt bridge formation (200). Based on this model, we hypothesized that the amino acid residues located within predicted loops A and B surrounding the Alg8 catalytic site potentially impact on the response of Alg8 to c-di-GMP binding at its different cellular levels, resulting in the alteration of the alginate production. To test this hypothesis, alanine substitution of cytoplasmic amino acid residues surrounding the catalytic site of Alg8 were conducted. This included T320, E322, H323, P324 and P325 from loop A and T453, R454, T457 and E460 from loop B (Fig. 1a, Fig. S1). In addition, the mutations H323E (for the effect of opposite charge substitution), and combinational mutations including E322A/H323E, P324A/P325A, T453A/T457A, R454A/T457A were introduced and analyzed. Then, all the above

mentioned site-specific *alg8* mutants were expressed *in trans*, i.e. using respective pBBR1MCS-5 derivatives, in PDO300Δ*alg8* to assess alginate production in the absence or presence of overproduced c-di-GMP-degrading RocR, providing permissive (high level of c-di-GMP) and non-permissive (low level of c-di-GMP) conditions, respectively.

Alginate quantification data (Fig. 1b, Fig S2) showed the following: 1) Alanine substitutions of Alg8 amino acid residues T320, E322, P324 (on loop A), and T453, R454 (on loop B) abolished alginate polymerization independent of the c-di-GMP level i.e. the presence or absence of overproduced RocR; 2) Alanine substitutions of H323, P325 (on loop A), and T457, E460 (on loop B) resulted in either abolished or significantly reduced alginate production in the absence of RocR (i.e. permissive levels of c-di-GMP), but they were positively responsive to the presence of RocR (i.e. lower non-permissive levels of c-di-GMP) as shown by increased alginate production. Remarkably, the point mutation E460A on loop B abolished alginate production while it restored alginate production upon the presence of RocR overproduction to a similar level as obtained for the non-mutated control strain PDO300Δ*alg8* (pBBR1MCS-5:*alg8*:*rocR*) (Fig. 1b, Fig S2).

Interestingly, the replacement of H323 with negatively charged glutamic acid (PDO300Δ*alg8* (pBBR1MCS-5:*alg8*(H323E)) abolished alginate production in the absence of RocR overproduction, while alginate production was restored to 60% of the non-mutated strain PDO300Δ*alg8* (pBBR1MCS-5:*alg8*:*rocR*) and to 86% of the H323A mutant in the presence of RocR overproduction (Fig.1b, Fig S2).

We also applied the c-di-GMP non-binding variant of Alg44 (i.e. R17A and R21A) in combination with the responsive group of Alg8 variants (i.e. H323A, H323E, P325A, T457A and E460A) (Table 1) to assess the possibility of alginate production independent of c-di-GMP in PDO300Δ*alg8*Δ*alg44* mutant (Table 1). None of these Alg8 variants could restore alginate production (data not shown) indicating that binding of c-di-GMP to the PilZ domain of Alg44 is required for activation of alginate production, presumably via conformational change of the $PilZ_{Alg44}$ domain as observed by Whitney and coworkers (199).

To assess whether the resulting different levels of alginate production obtained from various Alg8 variants were due to impaired function of Alg8 rather than impaired protein localization or protein production level, the strains producing the respective Alg8 variants were subjected to protein analysis. The envelope fractions of the cells were isolated and

assessed via immunoblotting using anti-Alg8 antibodies. The results showed that corresponding protein bands were detected for all Alg8 variants exhibiting similar intensity when compared with the positive control (i.e. PDO300Δ*alg8* (pBBR1MCS-5:*alg8*)) (Fig. 1c). This result indicated that the replacement of any of the amino acid residues tested did not impact on the overall structure of Alg8 suggesting a role in Alg8 function.

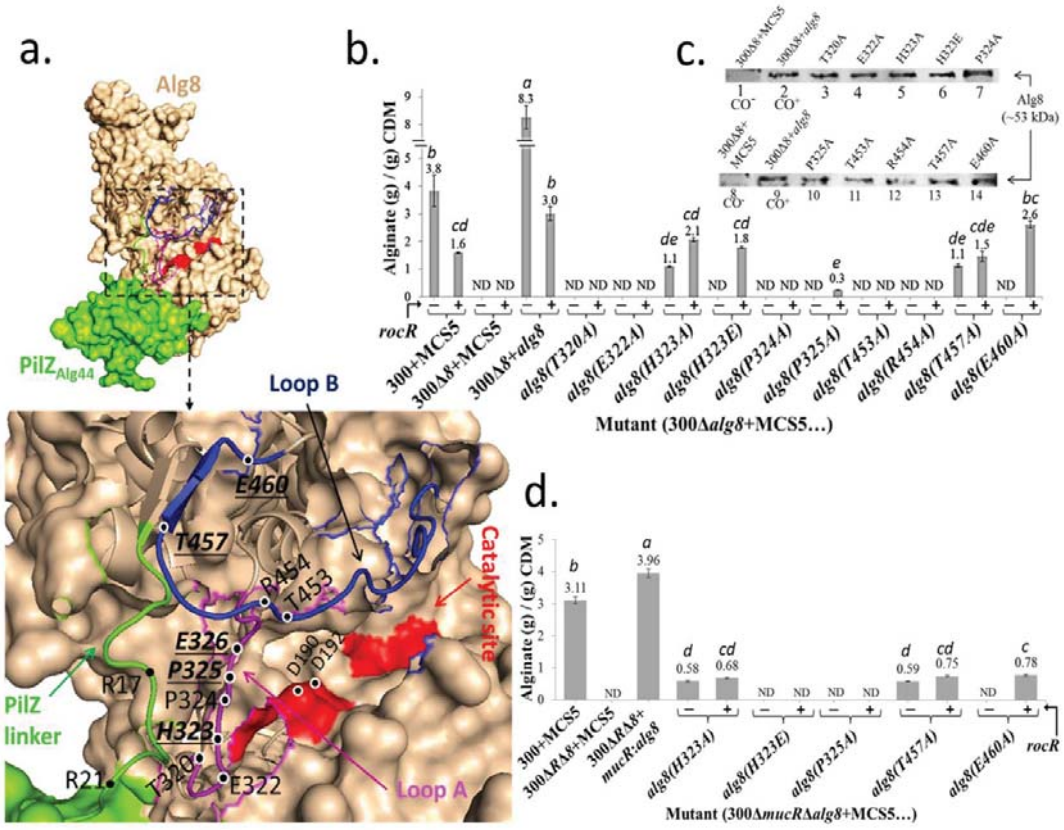

FIG. 1 Highly conserved amino acids of Alg8 are involved in c-di-GMP dependent regulation of alginate polymerization. (**a**) The *in silico* fusion of Alg8-PilZ$_{Alg44}$ was emboldened using the Phyre2 server. Residues selected for site-specific mutagenesis were shown on loop A (magenta), loop B (blue) and PilZ domain (green). Mutations of emboldened and underlined residues were responsive to the absence and presence of RocR overproduction (i.e. reduced levels of c-di-GMP) while for other shown residues alginate production was abolished independent of RocR. (**b**) Alginate quantification of PDO300Δ*alg8*transformants harboring various plasmids containing respective site-specific mutants of *alg8* with (+) and without (-) the *rocR* gene. (**c**) Immunoblot analysis of envelope fractions developed using an anti-Alg8 antibody showed that none of

mutations impacted on Alg8 localization to the envelope fraction (lanes 3-7 and lanes 10-14). Lanes 1-8 and 2-9 represents negative and positive controls, respectively. For estimating relative protein amounts, the protein band intensity was analyzed by the ImageJ software. The protein band based on genomic expression derived from 300Δ*8*+*alg8* (lanes 2 and 9) was assumed as 1.0 in density and relative densities of other bands were calculated as follows: lane 3 (1.14), lane 4 (0.937), lane 5 (1.06), lane 6 (1.03), lane 7 (1.48), lane 10 (0.9), lane 11 (0.848), lane 12 (0.817), lane 13 (0.985), and lane 14 (0.987). (**d**) Highly conserved amino acids of Alg8 whose replacement with alanine decoupled alginate polymerization from c-di-GMP-dependent and MucR-dependent regulation. Alginate quantification was performed for PDO300Δ*mucR*Δ*alg8* transformants with plasmids harboring respective site-specific mutants of *alg8* with (+) and without (-) the *rocR* gene. The data in histograms (**b**) and (**d**) represent the means ± the SDs of four independent repetitions and treatments with different *letters* are significantly different (*post hoc*Tukey HSD Test, $p < 0.05$). CDM, cell dry mass; 300, PDO300; ND, not detectable; MCS5, pBBR1MCS-5.

Overall, these results indicated that predicted loop A and B of Alg8 and amino acid residues H323, P325, T457 and E460 surrounding the catalytic site might be involved in the c-di-GMP mediated activation of alginate polymerization.

Furthermore, the replacement of the catalytic domain (residues 71-381), loop A and B of *P. aeruginosa* Alg8 with the algal (*Ectocarpus siliculosus*) homologous sequences did not restore alginate production with and without RocR overproduction (Fig. S1c (underlined sequences). In addition, hybrid genes encoding various fusion proteins of Alg8-Alg44-PilZ$_{Alg44}$ could not restore alginate production in the PDO300Δ*alg8*Δ*alg44* mutant (Fig. S3). However, it cannot be excluded that the lack of functionality is due to instability or impaired localization of the fusion proteins.

Decoupling alginate polymerization from MucR-dependent regulation.

The GGDEF-EAL motif present in MucR was proposed to specifically regulate alginate synthesis by imparting a localized c-di-GMP pool for the PilZ domain$_{Alg44}$-mediated activation of alginate polymerization in response to environmental stimuli (105, 207). We hypothesized that the c-di-GMP-responsive group of Alg8 variants (i.e. H323A, H323E, P325A, T457A and E460A) might also respond to the absence of MucR and the associated elimination of the proposed c-di-GMP pool. Therefore, the impact of these

variants on alginate production was analyzed in non-mucoid mutant PDO300Δ*mucR*Δ*alg8* with and without RocR overproduction (Fig.1d).

The variants H323E and P325A with RocR overproduction could not restore alginate production in PDO300Δ*mucR*Δ*alg8* to a detectable level, while they did in PDO300Δ*alg8* as described above (i.e. when MucR was present) (Fig. 1b and d, Fig S2 and S4). However, the variants H323A, T457A and E460A could restore alginate production in the absence of MucR in PDO300Δ*mucR*Δ*alg8*, but interestingly; the respective alginate production levels were not significantly different to each other. On the other hand, when compared with their activity in PDO300Δ*alg8* (i.e. in the presence of MucR), they were significantly reduced by up to 3.4-fold (Fig. 1b and d, Fig. S2 and S4).

These results confirmed that MucR specifically regulates alginate polymerization and alanine substitution of H323, T457 and E460 of Alg8 decoupled activation of alginate polymerization from c-di-GMP. However, the analysis of other existing c-di-GMP synthesizing and degrading enzymes in *P. aeruginosa* and their impact on c-di-GMP levels could provide further insight into conditions required for c-di-GMP mediated activation of alginate production.

Schematic representation of mutual and combinational effects of Alg8 variants, MucR and RocR on alginate polymerization is provided in Fig.S3. This model shows the various Alg8 variants interplay with the various levels of c-di-GMP in view of activation of alginate polymerization. Remarkably, high c-di-GMP levels caused inhibition in H323E and E460A variants (Fig. S5, row a), while RocR-mediated reduction of c-di-GMP levels favored the activation of alginate polymerization (Fig. S5, row b). Interestingly, H323A, T457A and E460A variants retained functionality independent from c-di-GMP depletion due to the absence of MucR and the presence of RocR overproduction (Fig. S5, row d).

Periplasmic domain of Alg44 co-polymerase is important for alginate polymerization and modification events.

Alg44 is essential for alginate polymerization through its interaction with Alg8 and binding to c-di-GMP (151). Alg44 has been proposed as alginate co-polymerase which consists of three distinct domains including the c-di-GMP-binding cytoplasmic PilZ domain, a transmembrane domain and a periplasmic domain (Fig. 2a) (164, 208). The periplasmic domain has been proposed to contribute to the periplasmic scaffold bridging

between inner and outer membrane, but its functional role in alginate biosynthesis remains unexplored.

Bioinformatic analysis using the Universal Protein Resource (UniProt) server showed highly conserved clustered residues 258QMKGTLTSPCDC269 in the periplasmic domain of Alg44 of alginate-producing *Pseudomonas* and *Azotobacter* species (Fig.2a). Therefore, these amino acid residues were subjected to site-specific mutagenesis to assess their impact on alginate polymerization, Alg44 production and localization in PDO300Δ*alg44* mutant (Table 1).

Site-specific mutagenesis of these residues with alanine either abolished or significantly reduced alginate production compared to wild-type and PDO300Δ*alg44* (pBBR1MCS-5:*alg44*-6His) (Fig.2a, Fig. S6). Except for variant D268A, which produced small amounts of alginate, alanine substitution of each residue in the PCDC (residues 266-269) cluster abolished alginate production. Additionally, alanine substitution of M259 resulted in significant decrease in alginate production (Fig.2a, Fig. S6).

We hypothesized that if polymerization occurs, but the alginate is misguided into the periplasm, it must be secreted as uronic acid as a consequence of periplasmic alginate lyase, AlgL, mediated degradation (209). To test this hypothesis, an alginate oligomers/uronic acid detection assay was used. Statistical analyzes did not show a significant difference between the total uronic acid amount (i.e. high and low molecular mass alginate) and the low molecular weight fraction (filtrate (10 kDa cutoff) for all variants, except for S265A ($p< 0.05$), which suggested that the reduction in alginate production was due to impaired polymerization (Fig. 2b). For P266A, C267A and C269A the total uronic acid amount and the low molecular weight fraction were equal indicating alginate polymerization was completely abolished (Fig. 2b). The ratio of high to low molecular mass alginate produced by the wild-type strain and PDO300Δ*alg44* (pBBR1MCS-5:*alg44*) was significantly ($p< 0.001$) different when compared to PDO300Δ*alg44* producing Alg44 variants (Fig. 2b). Furthermore, the impact of amino acid replacements on protein localization was analyzed. Immunoblotting using anti-His-tag antibodies showed that no Alg44 variant harboring alanine substitution of P266, C267 and C269, respectively, could be detected (Fig. 2c). However, Alg44 variants M259A and D268A, which mediated very low alginate yields on solid culture, were not detectable by immunoblotting (Fig. 2a and c). These results indicated that these amino acids contribute

to the integrity of the proposed periplasmic scaffold which is necessary for accomplishment of polymerization.

Furthermore, the possibility that the two cysteine residues (residues 267 and 269) mediate disulfide bond formation for localization of protein or inter- and intramolecular interactions was investigated. Immublotting analysis of DTT-treated and untreated membrane fractions of PDO300Δ*alg44* complemented with *alg44*-6His either *in cis* or *in trans* expression showed a higher molecular weight band (~70 kDa) when Alg44 was encoded *in cis* and in the absence of DTT, while it was missing when treated with DTT i.e. under reducing conditions (Fig. S7). This difference equals to ~25 kDa and the identity of this interacting partner could not be confirmed as protein quantities were too low. This band was not detected when Alg44 was encoded on the respective plasmids *in trans* (Fig. S7). The lack of Alg44 in samples corresponding to alanine substitution of cysteine residues re-confirmed their role in localization of Alg44 (Fig. S7).

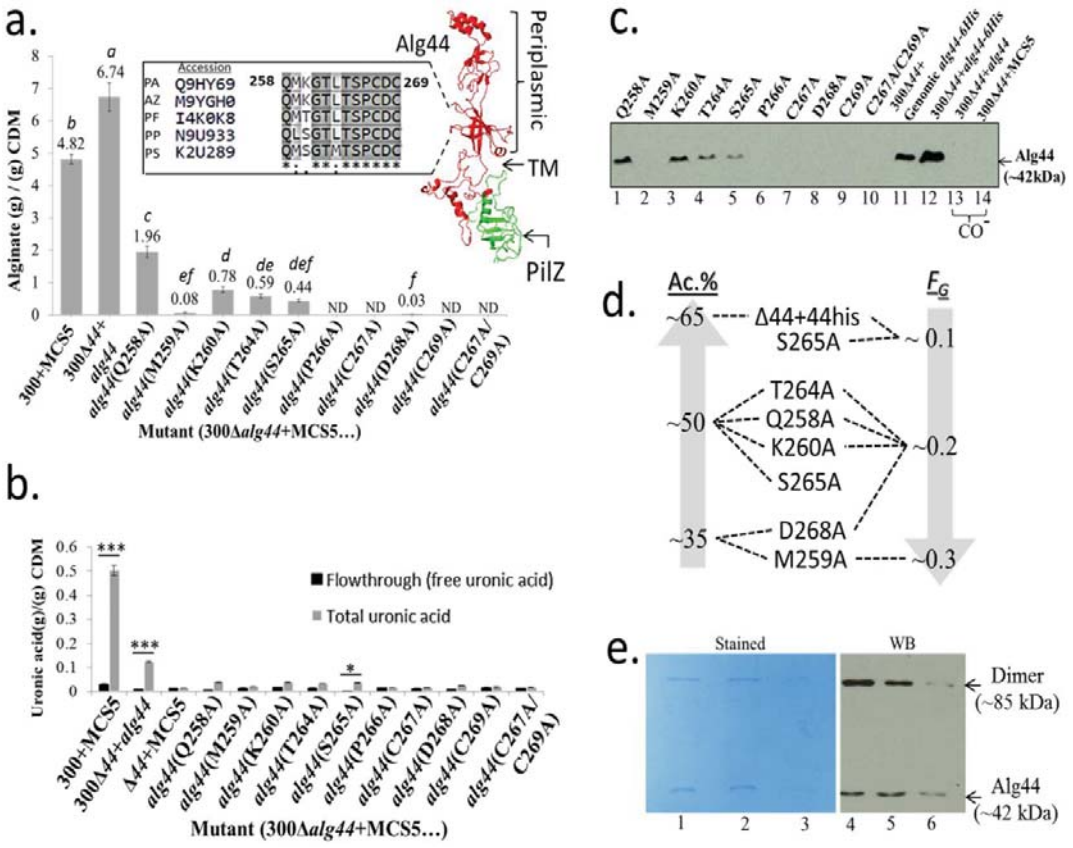

FIG. 2 Role of conserved amino acid residues of Alg44 proposed to be localized to the periplasmic domain in alginate biosynthesis and purification of the Alg44 dimer produced by recombinant *P. aeruginosa*. (**a**) Uniprot analysis of the periplasmic domain of Alg44 showed the

alignment of highly conserved regions among different alginate-producing species. PA (*P. aeruginosa*), AZ (*Azotobacter vinelandii*), PF (*P. fluorescens*), PP (*P. putida*) and PS (*P. syringae*). Dashed lines show the position of these highly conserved regions in the Alg44 model predicted by the Phyre2 server. Alginate quantification showed P266A, C267A and/or C269A completely abolished alginate production and for other residues it was significantly reduced. The data represent the means ± the SDs of four replicates and treatments with different *letters* are significantly different (*post hoc*Tukey HSD Test, $p<0.05$). (**b**) This figure shows the production of free uronic acids in liquid culture mediated by variants of Alg44 (flow-through samples were obtained using filters with 10 kDa cutoff), indicating alginate polymerization was impaired by site-specific mutagenesis of highly conserved periplasmic amino acid residues of Alg44. The data represent the means ± the SDs of four repetitions and asterisks indicate pairs of significantly different values (*post hoc*Tukey HSD Test, $*p<0.05$ and $***p < 0.001$).(**c**) Immunoblot analysis of envelope fractions developed using anti-His-tag antibodies showed that mutations M259A, P266A, C267A, D268A and C269A completely disrupted Alg44 localization to the envelope fraction (lanes 2 and lanes 6-10). The intensity of other protein bands was consistent with the amount of alginate produced by complemented mutants (lanes 1, 3-5 and 12). For estimating relative protein amount, the protein band intensity was analyzed using ImageJ software. The band of genomic expression of *alg44*-6His (lane 11) was assumed as 1.0 in density and relative densities of other bands were calculated as follows: lane 1 (0.76), lane 3 (0.76), lane 4 (0.29), lane 5 (0.13) and lane 12 (2.1). Lanes 13 and 14 represent negative controls. (**d**) Composition of alginates impacted by various Alg44 variants (see also Supplementary Tables S2 and S3). (**e**) Purification of the Alg44 dimer. SDS-PAGE gel (stained with Coomassie Brilliant Blue) (lanes 1-3) and immunoblot (lanes 4-6) of peak I (Fig. S10) showed a very stable dimer plus the monomer bands of Alg44. TM: transmembrane domain; CDM: cell dry mass; 300:PDO300; MCS5: pBBR1MCS-5; ND: Not detectable.

Alg44 regulates modification of alginate through its periplasmic domain. Previously, our *in vivo* assessment had shown that alginate polymerization is linked with modification events including acetylation and epimerization (151). Alg44 overproduction was shown to impact on alginate composition via affecting modification events while it structurally interacts with Alg8 (alginate polymerase) and the periplasmic subunits (i.e. AlgX and AlgK) to constitute the proposed periplasmic scaffold of the multiprotein complex (98, 151). We hypothesized that impaired polymerization of alginates observed in previous experiments must impact modification events too. As a result, compositional analysis of alginates produced by Alg44 variants grown on solid media showed that the replacement of respective residues with alanine (i.e. Q258A, M259A, K260A, T264A, S265A and

D268A) decreased the acetylation degree to 34%-52% when compared to wild-type Alg44 (acetylation = 64%) (Fig. 2d, see also Supplementary Tables S2 and S3). Among them, M259A and D268A, which also showed impaired localization, revealed the highest impact on degree of acetylation with 38% and 34%, respectively (Fig. 2d, see also Supplementary Tables S2 and S3).

Additional copies of Alg44 contributed to a lower molar fraction of G residues (F_G) = 0.14 which was consistent with previous results (151). Interestingly, S265A, whose impact on polymerization was less than for the other variants, did not change the molar fraction of G residues while other amino acid residue substitutions increased the molar fraction of G residues to 0.2-0.23 (Fig. 2d, see also Supplementary Tables S2 and S3). M259A showed the highest epimerization degree (F_G) = 0.3 (Fig. 2d, see also Supplementary Tables S2 and S3). These data demonstrated that the periplasmic domain of Alg44 has a regulatory impact on alginate modification events. Additional copies of Alg44 increased acetylation and lowered epimerization (Supplementary Tables S2 and S3), while alanine substitution of periplasmic residues impaired this regulatory effect with regard to both modification events.

Alg44 forms a homodimer in *P. aeruginosa*.

In order to analyze the quaternary structure of Alg44, both heterologous and homologous production of the full length *alg44*-12His gene were assessed. Briefly, due to weak production and significant truncation of Alg44 in *E. coli* strains, heterologous production was found to be not suitable (Fig. S8). However, homologous overproduction of Alg44 in *P. aeruginosa* was continued using the mutant PDO300Δ*alg44* complemented with the integration of *alg44*-6His into the genome. Importantly, initial protein analysis using immunoblotting showed that the presence of 5 mM EDTA could significantly reduce proteolytic truncation of Alg44 (Fig. S9). This suggested that metallo proteases might have mediated degradation. Membrane fractions of disrupted cells were subjected to affinity chromatography purification in the presence of a cocktail of the protease inhibitors, 5 mM EDTA and DTT. Interestingly, two distinct bands corresponding to the molecular mass of monomer and dimer of Alg44 were detected using immunoblotting (Fig. S9).

To further purify Alg44, size exclusion chromatography was employed. The chromatogram showed two major peaks (Fig. S10). Interestingly, when protein samples

were treated with 0.2% alginate solution and DTT, impurities were dissociated from the two major peaks when compared with untreated samples (Fig. S10a and b). Protein analysis showed that the first major peak (I) with coverage of Rv (retention volume):11-13 ml corresponded to an apparent MW of ~160-370 kDa (Fig. S10a and b) indicating either the presence of high oligomeric states of Alg44 or detergent. However, under denaturing conditions using SDS-PAGE analysis and subsequent immunoblotting a protein band corresponding to an apparent MW of ~85 kDa was detected in peak (I) fractions, which suggested the presence of a stable Alg44 dimer (Fig. 2e). No peak belonging to an Alg44 monomer was detectable. On the other hand, when Triton X-100 was replaced with n-Dodecyl β-$_{D}$-maltoside (DDM), a distinct peak at Rv: 14.5 ml was detected which was calculated to exhibit an apparent MW of 83.7 kDa corresponding to the Alg44 dimer (Fig. S10c). This peak was further analyzed by immunblotting which suggested the presence of the stable Alg44 dimer with an apparent MW of ~85 kDa (Fig. S11). Interestingly, replacement of Triton X-100 with DDM detergent caused loss of the stability of the dimer along with protein truncation (Fig. S11). Protein sequencing of the corresponding purified protein band confirmed the identity of Alg44 (coverage 67.61%; unique peptides: 24) along with the presence of the proposed signal peptide sequence (Fig. S10d). Besides achieving full-length Alg44 purification, these experiments suggest that this protein forms at least a very stable dimer. These results suggested that Alg44 dimerization is not dependent on disulfide bond formation because treatment with DDT did not disrupt the dimer. This result was consistent with previous findings suggesting Alg44 dimerization which were based on *in vivo* chemical crosslinking (151) as well as the purified $PilZ_{Alg44}$ domain existing in dimer form after crystallization (199).

The Alg8-Alg44 complex appears in a non-uniform, punctuate and patchy arrangement in the envelope surrounding the *P. aeruginosa* cell.

In previous studies, it was shown that interacting proteins Alg8 and Alg44 localize to the cytoplasmic membrane of *P. aeruginosa*, while the C-termini of both proteins was proposed to be exposed to the periplasm (165, 208, 210). How the proposed alginate biosynthesis multiprotein complex localizes and distributes in the cells remains elusive. Here, membrane-anchored Alg8 and Alg44 forming alginate polymerase were selected to visualize cellular localization and distribution. Due to the presence of the N-terminal signal peptides and localization of the C-terminal part of these proteins in the oxidizing environment of the periplasm, a super folding derivative of GFP (sfGFP) (211-213) was

translationally fused to the C-terminus of Alg8 and Alg44, respectively. Genes encoding these fusion proteins were transferred into respective negative mutants resulting in recombinant strains PDO300Δ*alg8* (pBBR1MCS-5:*alg8*:*sfgfp*) and PDO300Δ*alg44* (pBBR1MCS-5:*alg44*:*sfgfp*). As regular GFP is not fluorescent in the oxidizing environment of the periplasm, strains PDO300Δ*alg8* (pBBR1MCS-5:*alg8*:*gfp*) and PDO300Δ*alg44* (pBBR1MCS-5:*alg44*:*gfp*) were used as negative controls to further confirm the periplasmic localization of the C-termini of both proteins (data not shown). Furthermore, PDO300 (pBBR1MCS-5:*pilN*:*sfgfp*) was used as an additional control to rule out technical artifacts. PilN protein is part of a multiprotein complex responsible for the biogenesis of type IV pili in *P. aeruginosa*. PilN is anchored in the cytoplasmic membrane with its C-terminal domain exposed to the periplasm (214). All strains were grown under the same conditions on PIA media to rule out the effect of cultivation conditions on the level of gene expression and the experiments were repeated three times.

Initially, functional protein localization of sfGFP fusion proteins was assessed by confirming restoration of alginate production in the respective isogenic knockout mutants. The mucoid phenotype and alginate quantification showed PDO300Δ*alg8* (pBBR1MCS-5:*alg8*:*sfgfp*) and PDO300Δ*alg44* (pBBR1MCS-5:*alg44*:*sfgfp*) were complemented and produced alginate (respectively 5.16±0.1 and 1.1±0.02 (g) /CDM (g)).

The sfGFP fusion protein and alginate producing *P. aeruginosa* cells were observed using Confocal Laser Scanning Microscopy (CLSM). By employing IMARIS image analysis software (Bitplane), respective images of bacteria included the cells which appeared with co-planar orientation based on fluorescent distribution were analyzed by including variable numbers of optical sections (Z-stack series), each of which separated by 0.13 µm. As expected, PDO300Δ*alg8* (pBBR1MCS-5:*alg8*:*gfp*) and PDO300Δ*alg44* (pBBR1MCS-5:*alg44*:*gfp*) were not fluorescent while both Alg8-sfGFP and Alg44-sfGFP led to fluorescent cells with punctuate fluorescent foci which were distributed surrounding the cells in non-uniform and patchy patterns (Fig. 3, columns a-c and columns d-f). Analysis of Z-stack series showed that the intensity and arrangement of distributed fluorescent foci were different between optical sections (Fig. 3, columns a-c and columns d-f).

These results were compared with a translational fusion of PilN (PA5043) with sfGFP (PDO300 (pBBR1MCS-5:*pilN*:*sfgfp*)) in order to rule out artifacts that might be mediated

by sfGFP or the microscopic technique. No punctate and particular arrangement could be observed between optical sections for PilN-sfGFP distribution by Z-stack series analysis and fluorescent foci were uniformly distributed (Fig. 3, columns g-i). This result further supported that Alg8 and Alg44 are distributed in specific and non-uniform arrangements around the cell. However, to visualize this distribution at higher resolution, alternative techniques such as STED (stimulated emission depletion) microscopy and immunoelectron microscopy might be employed for further analysis.

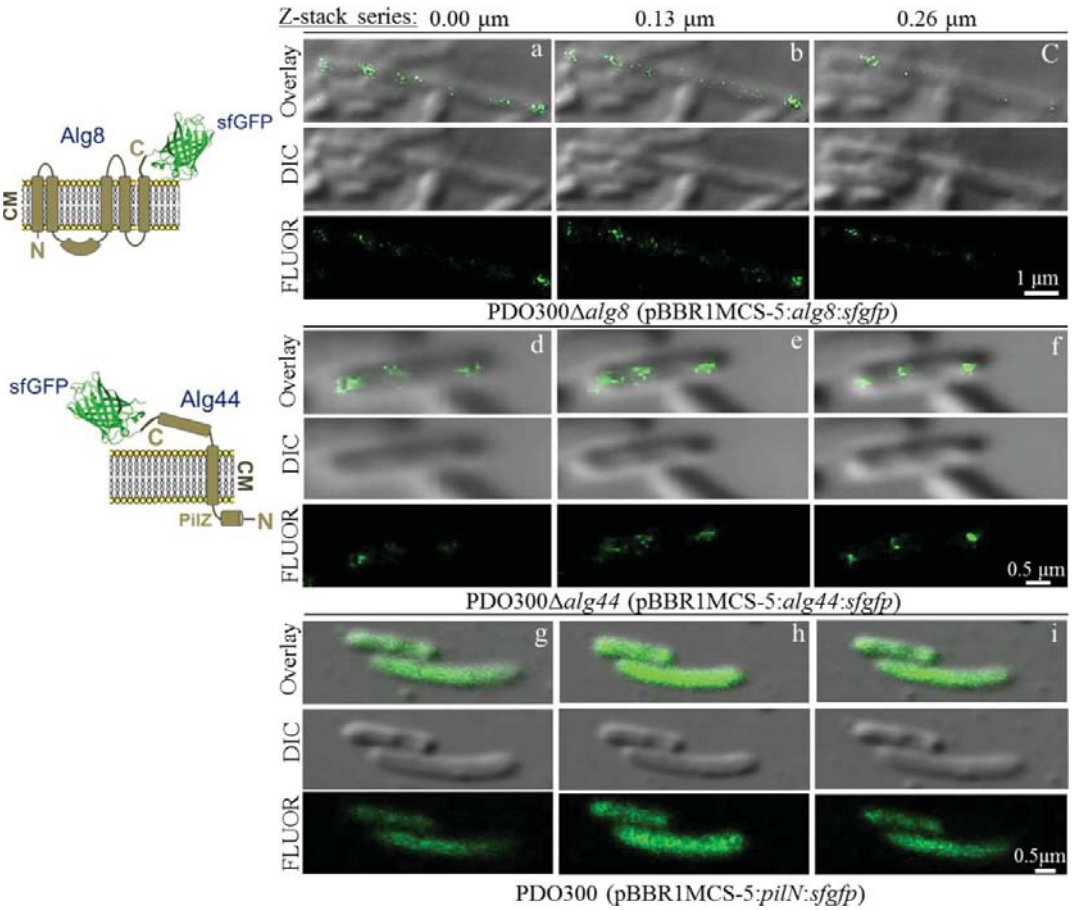

FIG. 3 Alg8 and Alg44 proteins appear localized and distributed in a non-uniform, punctuate and patchy arrangement in the cell envelope of *P. aeruginosa*. Schematic membrane models of the C-terminal fusions of Alg8 and Alg44 with sfGFP protein are represented at left side of the images. In addition to the C-terminal fusion of PilN with sfGFP protein, all respective images of bacteria which appeared with co-planar orientation based on fluorescent distribution were visualized using CLSM and analysed using IMARIS image analysis software (Bitplane), each in

three independent times. Analysis of a variable numbers of optical sections (Z-stack series), each of which were separated by 0.13 µm,showed fluorescent foci of PDO300Δ*alg8* (pBBR1MCS-5:*alg8*:*sfgfp*) (columns **a-c**) and PDO300Δ*alg44* (pBBR1MCS-5:*alg44*:*sfgfp*) (columns **d-f**) are arrayed in a particular puncta and patchy patterns around the cells while fluorescent foci in PDO300 (pBBR1MCS-5:*pilN*:*sfgfp*) (columns **g-i**) were uniformly distributed, not in particular pattern, which ruled out the possible technical artifacts. FLUOR: fluorescent, DIC: differential interference contrast.

DISCUSSION

C-di-GMP signaling in bacteria is one of the most complex signaling systems which regulates many physiological activities of bacteria leading to adaptation and fitness in varying environments. Molecular mechanisms of effector proteins for c-di-GMP signaling are still poorly understood. Until now, the number of molecular mechanisms which have been profoundly analyzed for a specific output is limited to membrane anchored BcsA-BcsB complex (cellulose synthase) and the cytosolic FleQ protein regulating the expression of flagellar and exopolysaccharide biosynthesis genes, both in response to c-di-GMP (200, 215).

Indeed, the response threshold of c-di-GMP receptor/effector proteins is dependent on their binding affinity to c-di-GMP i.e. at different cellular levels of c-di-GMP, particular c-di-GMP receptor/effector proteins such as Alg44 will be engaged to mediate a well-orchestrated physiological response (204). The c-di-GMP levels are tightly regulated by c-di-GMP synthesizing and degrading proteins (i.e. PDE/DCG proteins) in response to environmental stimuli (198). For example, it was recently shown that the membrane anchored MucR is a nitrate sensing protein with PDE/DCG activity involved in regulation of alginate polymerization (105). Here, the underlying molecular mechanism of c-di-GMP mediated activation of alginate polymerization was studied. We developed a structural model of Alg8 *in silico* fused to the c-di-GMP binding PilZ domain of Alg44 in resemblance to the cellulose synthase, BcsA (Fig.1, Fig. S1). This structural model and recent findings unraveling the molecular mechanism of c-di-GMP mediated activation of cellulose synthesis informed the identification of amino acid residues involved in activation of alginate polymerization. Amino acid residues of Alg8 predicted to interact

with c-di-GMP receptor/effector $PilZ_{Alg44}$ domain were subjected to site-specific mutagenesis.

Critical amino acid residues of Alg8 were identified whose replacement with alanine impacted on the c-di-GMP level required for activation of alginate polymerization, while H323A, T457A and E460A resulted in decoupling of alginate synthesis from both general (RocR controlled) and localized (MucR mediated) levels of c-di-GMP (Fig. 1, Fig. S1 and S5).

These residues were distributed in loops A and B of Alg8 which were modeled by the Phyre2 server according to BcsA structure and homology to those loops of BcsA involved in activation of cellulose polymerization by c-di-GMP (Fig. 1, Fig. S1). Here, we provided experimental evidence that H323 and P325 from loop A and T457 and E460 from loop B are involved in the c-di-GMP-dependent mechanism that regulates alginate polymerization (Fig.1). Since, not all of these critical Alg8 residues align with conserved amino acid residues of BcsA, we propose that the molecular mechanism of alginate polymerization activation is different from the autoinhibition mechanism as described for activation of cellulose polymerization.

In the Phyre2 structural model (Fig.1, Fig. S1), T457 and E460 flank two-β-sheet strands which are formed by loop B (homologous to the gating loop of BcsA) and the N-terminal end of $PilZ_{Alg44}$ as previously discussed by Whitney and coworkers (2015) (199). This segment was not structurally elucidated and it remained disordered in solution, while it became ordered upon binding to c-di-GMP (199). These results suggested that this region of Alg8 which comprises T457 and E460 adds another interface with the N-terminal end of $PilZ_{Alg44}$.The region comprising H323 was previously proposed to interface with the PilZ domain (151)and was found to be critical for regulation of alginate polymerization upon binding to c-di-GMP (Fig.1). Alanine replacement of P325, E460 and H323E abolished alginate production in the presence of c-di-GMP, strongly inducing alginate production in the control strains (PDO300 (pBBR1MCS-5) and PDO300Δ*alg8* (pBBR1MCS-5:*alg8*), while E460A and H323E restored alginate production to about wild-type level when c-di-GMP levels were decreased by overproduction of the c-di-GMP degrading enzyme RocR (Fig.1). Alignment of loops A and B with homologous counterparts of Alg8 from various bacteria showed that these loops are highly conserved, while E460 is less conserved (Fig. S12). Interestingly, H322, which is highly conserved

among alginate-producing *Gammaproteobacteria*, is replaced with a negatively charged glutamic or aspartic acid in several representatives from *Alphaproteobacteria* (belonging to the *Rhizobiaceae* family) and *Epsilonproteobacteria* (Fig. S12c). No bacteria from the latter group have been reported to produce alginate, while bacteria belonging to *Rhizobiaceae* are well-known cellulose producers.

Although the cytosolic PilZ domain of Alg44 which binds c-di-GMP had been well characterized, the full-length Alg44 was not purified and the role of its periplasmic domain was not studied. Alanine substitutions of highly conserved periplasmic residues caused a significant reduction or abolishment of alginate production (Fig.2a) by impacting on the polymerization process or Alg44 localization to the membrane (Fig.2b and c). These residues comprise a region homologous to biotinyl-lipoyl-domains of biotin/lipoyl attachment proteins with carboxylase/decarboxylase and acyltransferase activity (216). Furthermore, the cluster of PCDC (residues 266-269) was identified for being critical for Alg44 localization (Fig.2c). The role of the CXC motif on localization of other proteins has been reported, such as the outer membrane lipoprotein CsgG exposed to the periplasm, copper chaperones in the mitochondrial intermembrane space as well as its functional importance for copper trafficking by CopC protein across the bacterial periplasm (217-219). In Alg44, both cysteine residues were required for protein localization. The role of these residues for intra- and intermolecular interactions is still not clear. However, here experimental evidence was obtained that disulfide bond formation might be involved in protein-protein interactions (Fig. S7). This was only observed when Alg44 was produced from a single gene integrated into the genome, i.e. at physiological copy number suggesting that the stoichiometry of Alg44 and interacting proteins is important for this function (Fig.S7).

Consistent with previous results which showed Alg44 increases acetylation of alginate (151), replacement of periplasmic amino acid residues impaired the this effect on acetylation while causing a higher level of epimerization (Fig. 2d, see also Supplementary Table S1 and S2). These data suggested that Alg44 plays a role in alginate modifications through its periplasmic domain, possibly by linking polymerization with modification events.

For further biochemical characterization, full-length Alg44 was produced in *P. aeruginosa* containing the *alg44*-6His gene integrated into the genome. Alg44 was

purified as a stable dimer (Fig. 2e, Fig. S9-11). These results suggested that Alg44 forms at least a stable dimer as had been suggested on the basis of *in vivo* crosslinking experiments (151). In addition, the dimer of only the cytoplasmic $PilZ_{Alg44}$ domain had been demonstrated (199).

Bioinformatic prediction using the PRED-TAT server (220) showed that protein subunits constituting alginate biosynthesis/modification/secretion multiprotein complex comprise Sec-dependent signal peptides for secretion and localization. In this secretion pathway, unfolded proteins are secreted across the membrane through a protein-conducting channel (220, 221). Alg8 and Alg44 are both membrane-anchored and interact with each other constituting the alginate polymerizing component of the multiprotein complex. In order to assess the cell surface localization and distribution of the alginate synthesis complex, we employed translational fusions of Alg8 or Alg44 to the sfGFP. In contrast to GFP, the sfGFP properly folds in the oxidative environment such as the periplasm, particularly when the Sec-dependent pathway mediates secretion and localization (211, 212). Alg8 and Alg44 fused to the N-terminus of either GFP or sfGFP, respectively, were functional as they restored alginate production in respective isogenic knockout mutants. CLSM analysis revealed that sfGFP fusions were fluorescent, but GFP fusions not. This confirmed localization of both C termini to the periplasm. In addition, CLSM analysis indicated that both Alg8 and Alg44 sfGFP fusion proteins were localized as non-uniform and patchy distribution of fluorescent foci surrounding the *P. aeruginosa* cell (Fig. 3). As both proteins had been shown to interact with each other plus Alg44 interacts with AlgX and AlgK (periplasmic subunits of the multiprotein complex) as well as interacting with the outer membrane pore AlgE, visualization of the distribution of these proteins presumably indicates the cell surface arrangement of the entire alginate producing multiprotein complex (98, 151, 196). Using an immunogold labeling approach, a recent study showed that AlgE was not randomly distributed over the entire outer membrane, but co-localized with the proposed multiprotein complex (222). Previously, it was shown that the Psl polysaccharide which is produced by *P. aeruginosa* at initial stages of biofilm development is helically attached to the cell surface (185). It was suggested that this helical distribution of Psl may promote the formation and stabilization of a polysaccharide matrix and in turn enhances cell-cell interactions which are critical for biofilm development (185). However, our result did not show a typical helical distribution for alginate polymerase but its possibility cannot be ruled out due to limitations of the

imaging techniques used in this study. Nevertheless, the observed non-uniform and patchy distribution might provide some insights into a possible link between the distribution of the alginate biosynthesis multiprotein complex and the proposed asymmetrical and spatial distribution of c-di-GMP pools essential for activation of specific proteins such as alginate polymerase (105, 223). Asymmetrical, but non-stochastic, distribution of c-di-GMP in *P. aeruginosa* was previously observed upon cell division mediated by the activity of c-di-GMP metabolizing enzymes for regulating the activity of c-di-GMP-binding proteins (223, 224). At least 40 proteins directly synthesize and/or degrade c-di-GMP in *P. aeruginosa* which controls cellular level of this molecule in response to perceived stimuli. However, due to spatial distributions of this molecule for specific outputs, cognate receptor/effector proteins variably respond to c-di-GMP cellular levels mainly via the PilZ domain (225). Therefore, non-uniform and patchy distribution of alginate polymerase (Fig. 3) might be a non-stochastic event and might link to spatial distribution of c-di-GMP metabolizing enzymes for controlling c-di-GMP turnover when alginate overproduction is required as a specific output. To test this hypothesis, we suggest applying a similar approach to visualize the distribution of the c-di-GMP providers for alginate polymerase such as MucR.

Overall, this study provided experimental evidence towards elucidating the molecular mechanism of c-di-GMP mediated activation of alginate polymerization, Alg44 role in alginate polymerization and modifications as well as the cell surface distribution of the respective alginate synthesis multiprotein complex.

ACKNOWLEDGMENTS

We are thankful to Bio-NMR facility of Massey University and Dr. Patrick Edwards, the Manawatu Microscopy and Imaging Centre (MMIC) of Massey University and especially Dr. Matthew Savoian for assistance using microscopic techniques.

FUNDING INFORMATION

This work was supported by grants from the Massey University Research Fund (New Zealand) to B.H.A.R., M.F.M. and S.G. are funded by a Massey University doctoral scholarship.

SUPPLEMENTAL MATERIAL

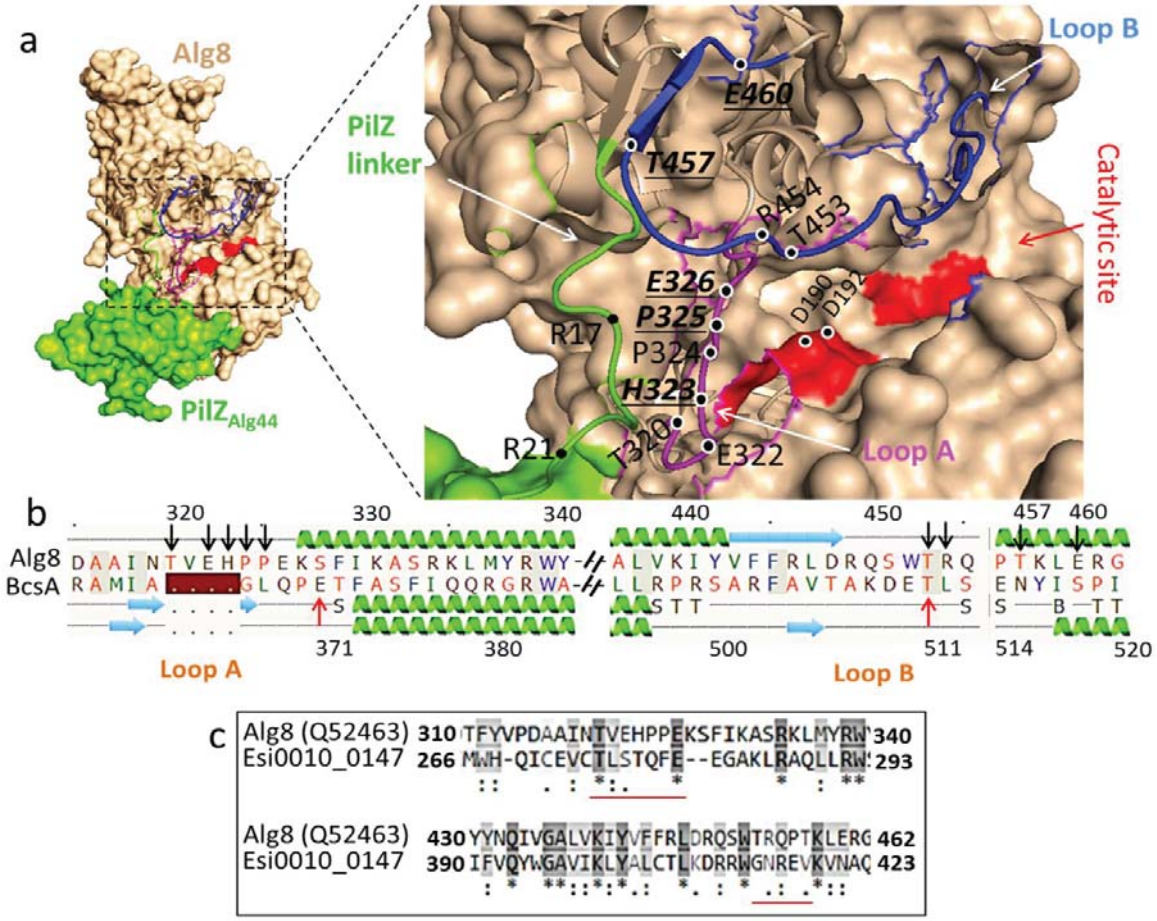

FIG. S1 Highly conserved loops and residues of the *in silico* model of Alg8-PilZ$_{Alg44}$ proposed to be involved in c-di-GMP dependent regulation of alginate polymerization. (**a**) The *in silico* fusion of Alg8-PilZ$_{Alg44}$ was modeled using the Phyre2 server. Residues selected for site-specific mutagenesis were shown on loop A (magenta), loop B (blue) and PilZ domain (green). Mutations of bolded and underlined residues were responsive to the absence and presence of RocR overproduction (i.e. reduced levels of c-di-GMP) while for other shown residues alginate production was abolished independent of RocR. (**b**) Pairwise alignments of Alg8 with BcsA (cellulose synthase) shows highly conserved residues (black arrows) on loop A and loop B (of Alg8) to those of BcsA which could form a salt bridge (residues are marked with red arrows) with R residues of PilZ domain. (**c**) Pairwise alignment of Alg8 of *P. aeruginosa* with homologous protein found in the seaweed *Ectocarpus siliculosus* (Esi0010_0147). Underlined segments of Alg8 were replaced with algal homologous segments to assess the functionality of protein in *P. aeruginosa* PDO300Δ*alg8*.

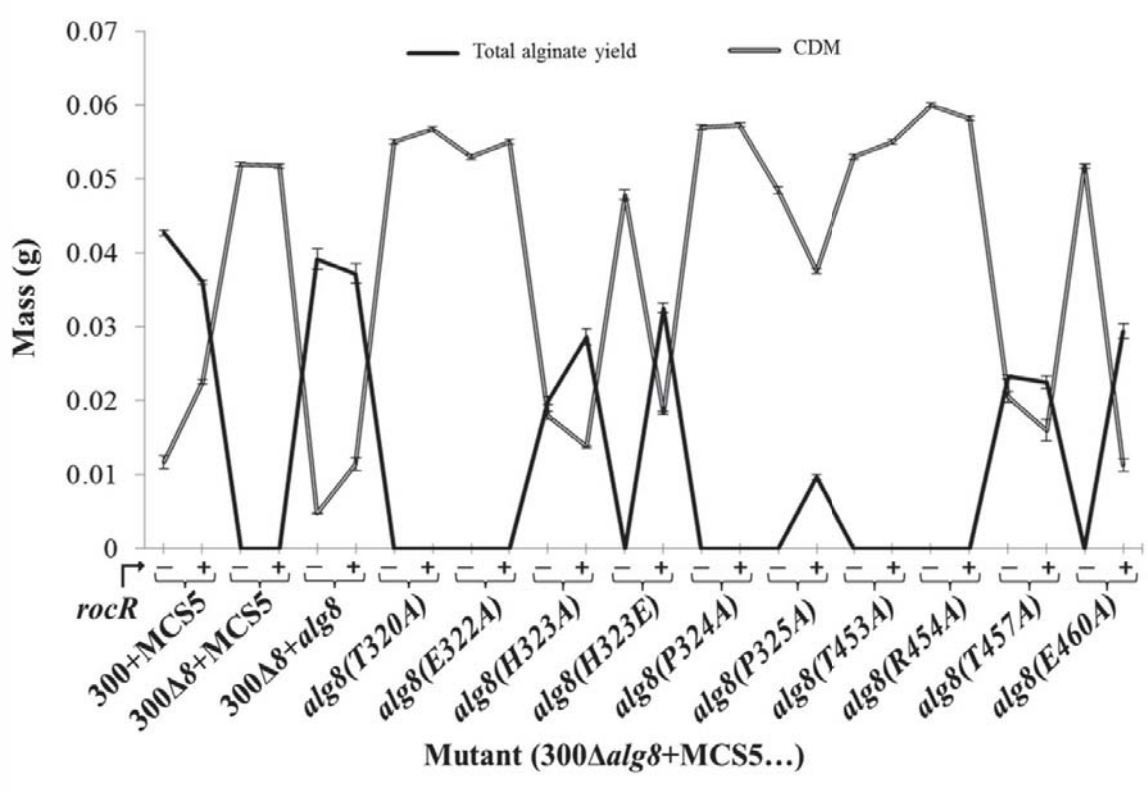

FIG. S2 Correlation of dry cell mass (CDM) and total alginate yield produced by PDO300Δ*alg8* transformants harboring various plasmids containing respective site-specific mutagenesis variants of *alg8* with (+) and without (-) the *rocR* gene. These quantifications are based on incubation of cells at 37 °C for 72 h grown on PIA medium (solid culture) containing 300 µg/ml of gentamicin. Data are means ± standard deviations of four independent repetitions.300, PDO300; MCS5, pBBR1MCS-5.

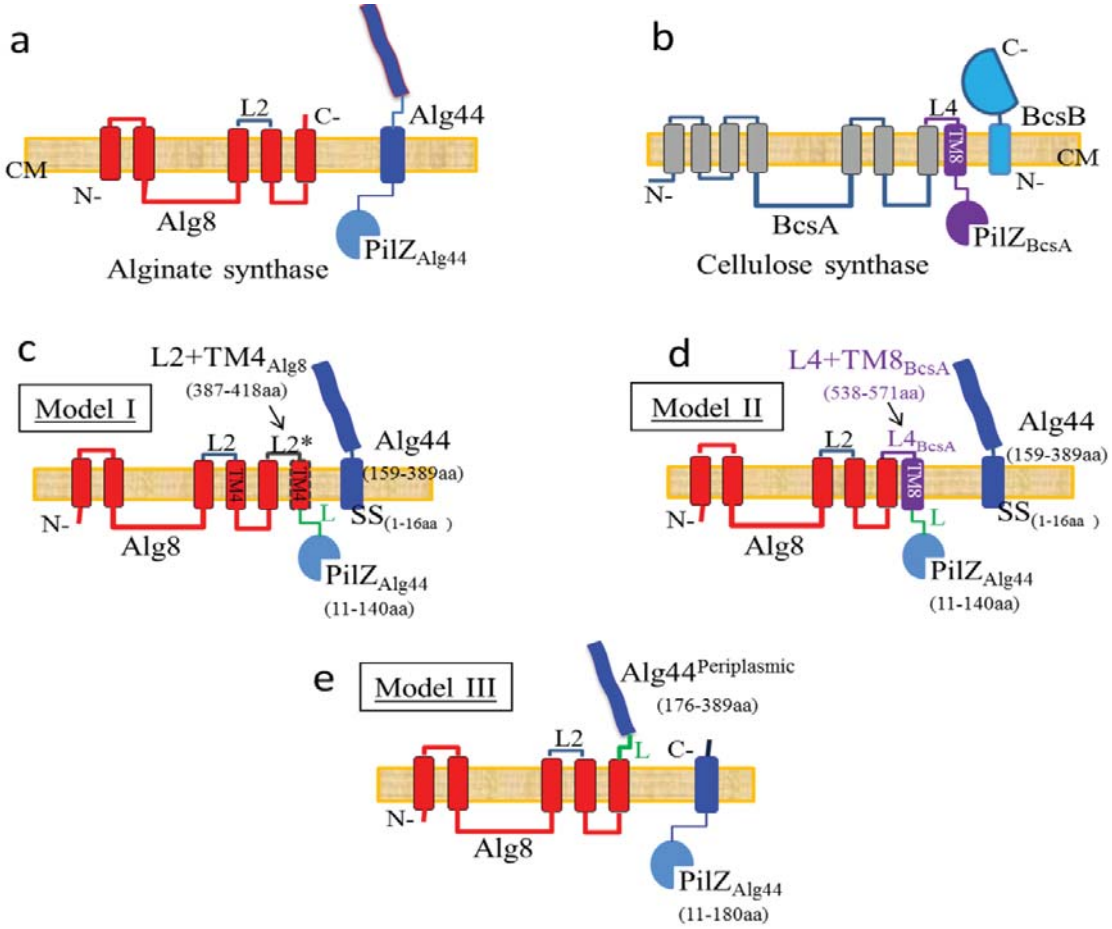

FIG. S3 Schematic fusion models of Alg8-Alg44-PilZ$_{Alg44}$ and BcsA were analysed *in vivo*. (**a**) Model of alginate synthase complex consisting of Alg8-Alg44 and (**b**) cellulose synthase complex including BcsA-BcsB proteins.One of the major structural differences between two complexes lies on the position of c-di-GMP sensing domain i.e. PilZ domain and the number and orientation of transmembrane domains. The C-terminal part of BcsA contains a transmembrane domain (TM) which extends into the cytoplam leading to the PilZ domain while the C-terimnal part of Alg8 is exposed to the periplasm and the PilZ domain is located at the N-terminal part of Alg44 in the cytoplam. (**c**) the C-terminal fusion of Alg8 with a similar sequence of loop2 (L2$_{Alg8;}$ labled with star) and TM4$_{Alg8}$ was linked to PilZ$_{Alg44}$ domain via a five glycine linker (L). This was in combination with Alg44 without the N-terminal PilZ domain, but with signal sequence for localization into the cytoplasmic membrane. (**d**) the C-terminal fusion of Alg8 with a homologous sequence of L4$_{BcsA}$ and TM8$_{BcsA}$ was linked to PilZ$_{Alg44}$ domain via similar linker. This was in combination with Alg44 without the N-terminal PilZ domain, but with signal sequence for localization. (**e**) the C-terminal fusion of Alg8 was linked to the periplasmic domain of Alg44 via similar linker while it was combined with Alg44 without periplasmic domain. N-: N-terminal; C-: C-terminal; L2: loop 2; L4: loop 4; L: linker; aa: amino acid; SS: signal sequence; TM: transmembrane domain; CM: cytoplasmic membrane.

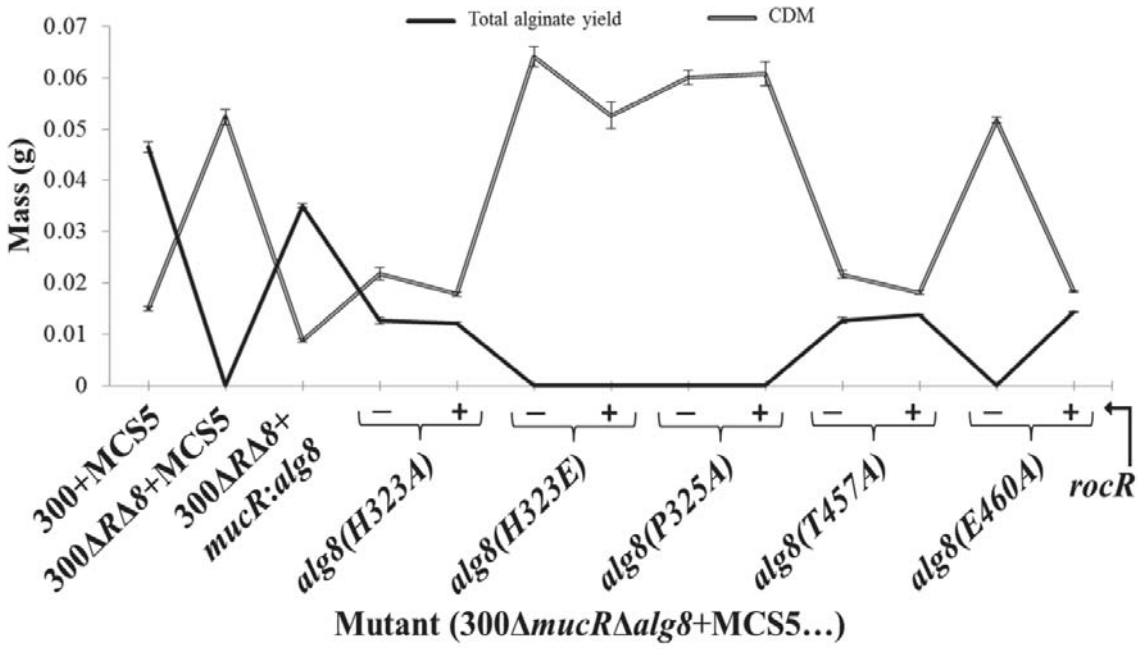

FIG. S4 Correlation of dry cell mass (CDM) and total alginate yield produced by PDO300Δ*mucR*Δ*alg8* transformants harboring various plasmids containing respective site-specific mutagenesis variants of*alg8* with (+) and without (-) the *rocR* gene. These quantifications are based on incubation of cells at 37 °C for 72 h grown on PIA medium (solid culture) containing 300 µg/ml of gentamicin. Data are means plus standard deviations of four independent repetitions. 300, PDO300; MCS5, pBBR1MCS-5.

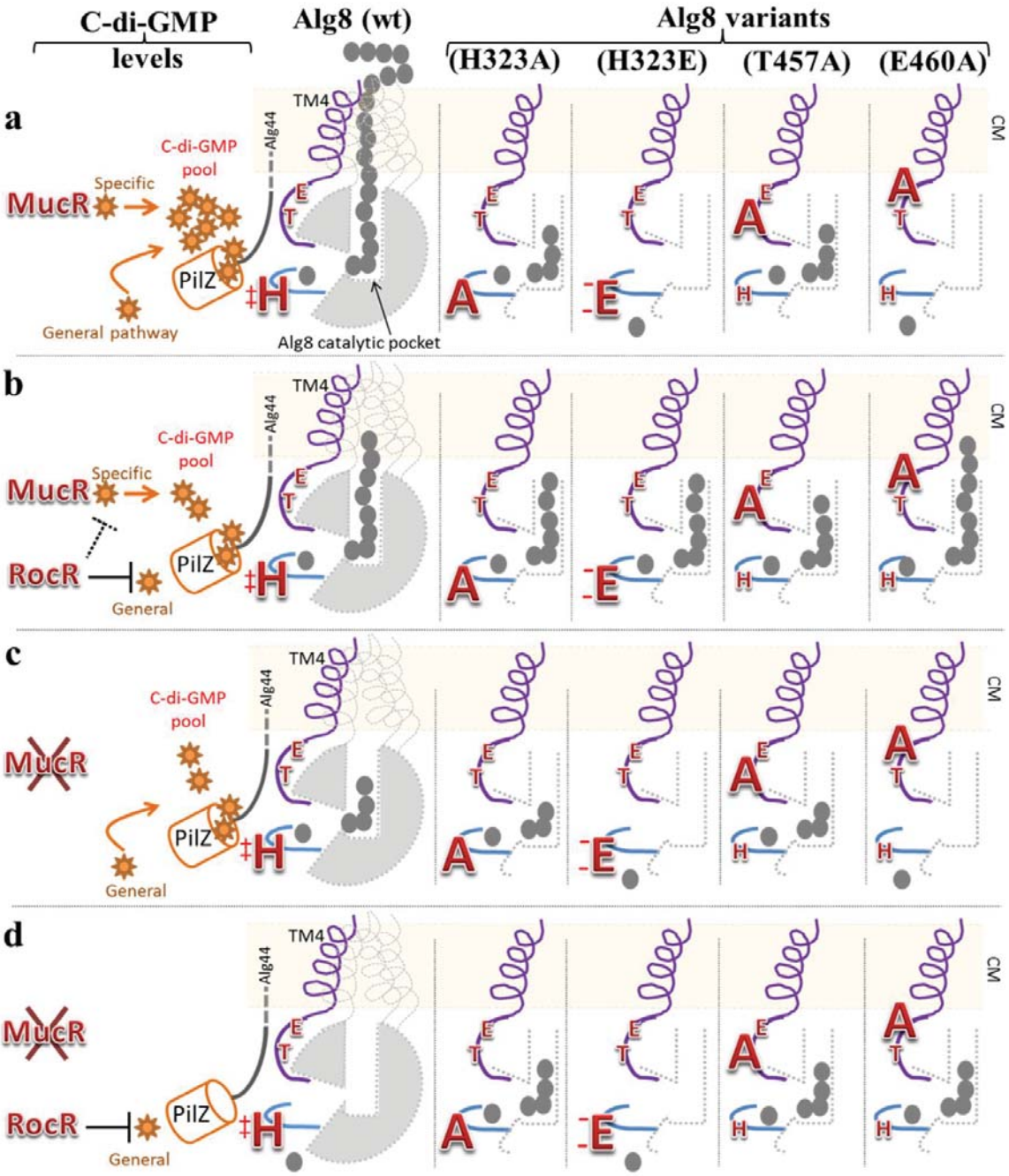

FIG. S5 Proposed schematic representation of mutual and combinational effects of point-mutation of Alg8 residues including H323, T457 and E460 (red letters in wild-type (wt) column) and c-di-GMP levels (orange stars) (impacted by RocR and/or MucR) on activation of alginate polymerization. Alginate synthesis is positively regulated by elevated levels of c-di-GMP in the cytosol (RocR degrades c-di-GMP in the cytosol) or specifically by MucR proposed to generate a localized pool of c-di-GMP in proximity to $PilZ_{Alg44}$. Informed by the *in silico* model of Alg8-$PilZ_{Alg44}$, three residues including H323 (on loop A), T457 and E460 (on loop B) were proposed as critical for c-di-GMP dependent activation of Alg8. The various levels of c-di-GMP and their

impact on activation of alginate polymerization based on Alg8 variants were illustrated in rows **a-d** (enlarged bold letters represent replaced residues). Remarkably, high c-di-GMP levels caused inhibition in H323E and E460A variants (row **a**), while RocR mediated reduction of c-di-GMP levels mediated activation of alginate polymerization (row **b**). The H323E variant was not active in the MucR knockout mutant (row **c** and **d**), while H323A, T457A and E460A variants retained functionality independent from c-di-GMP depletion due to the absence of MucR and the presence of RocR overproduction (row **d**). Gray circles represent monomeric units (mannuronic acid); TM4, transmembrane domain 4; CM, cytoplasmic membrane.

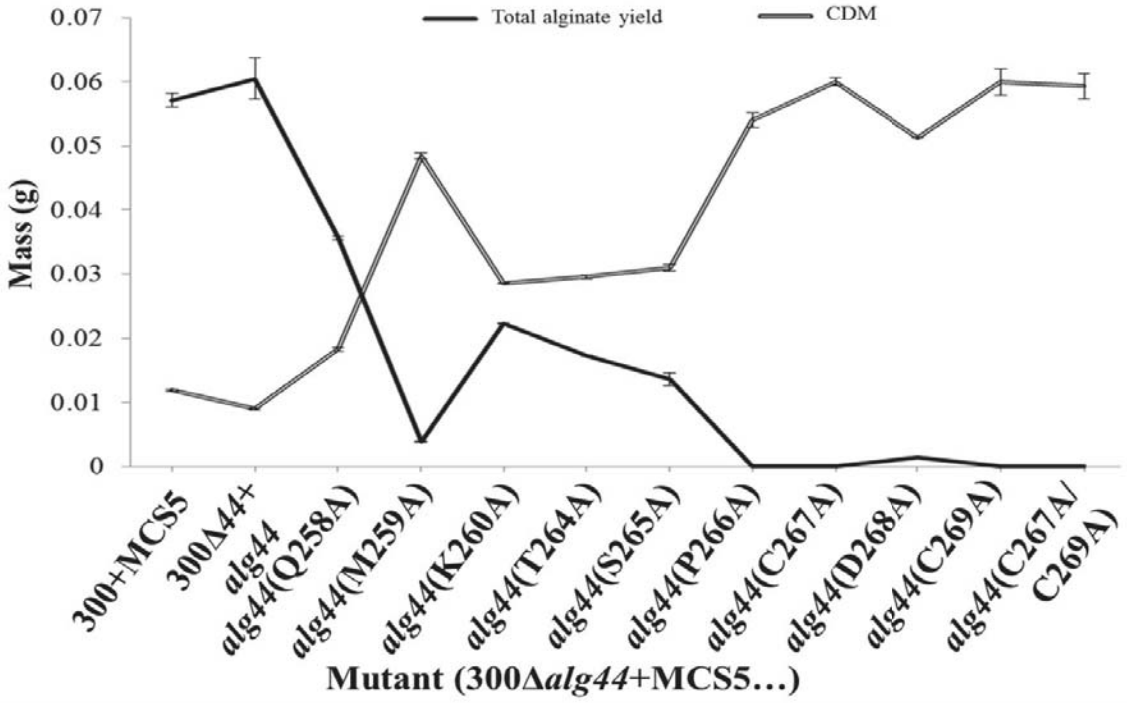

FIG. S6 Correlation of dry cell mass (CDM) and total alginate yield produced by PDO300Δ*alg44* transformants harboring various plasmids containing respective site-specific mutagenesis variants of *alg44* gene. These quantifications are based on incubation of cells at 37 °C for 72 h grown on PIA medium (solid culture) containing 300 µg/ml of gentamicin. Data are means plus standard deviations of four independent repetitions.300, PDO300; MCS5, pBBR1MCS-5.

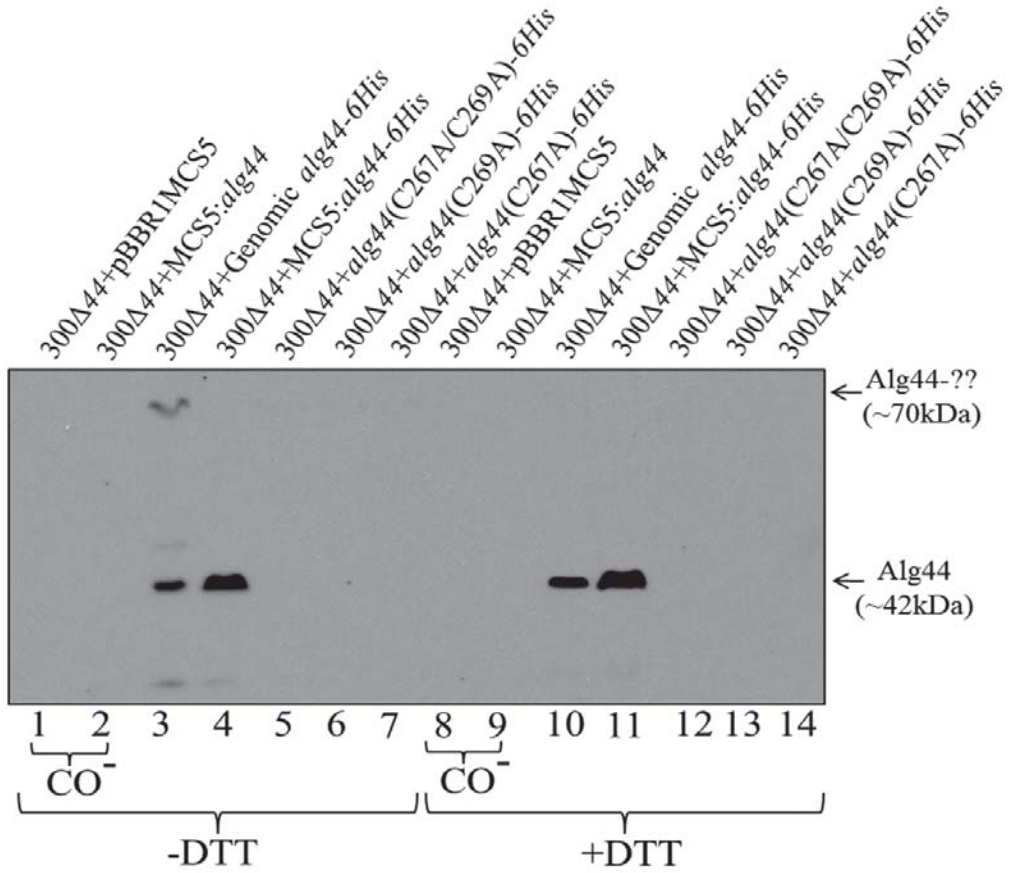

FIG. S7 Disulfide bond formation in Alg44 and impact on dimerization/protein-protein interactions. Immunoblot analysis of envelope fractions developed using anti-His-tag antibodies showed that a protein band with greater apparent molecular weight (~70 kDa) was detected without DTT treatment (lane 3) while it was missing after addition of DTT (lane 10) or when protein was produced encoded from plasmid (lanes 4 and 11). Immunoblot analysis confirmed Alg44 is missing when cysteine residues were replaced with alanine (lanes 5-7 and 12-14). Lanes 1-2 and 8-9 represent negative controls. 300: PDO300; MCS5: pBBR1MCS-5; Co^-: negative control.

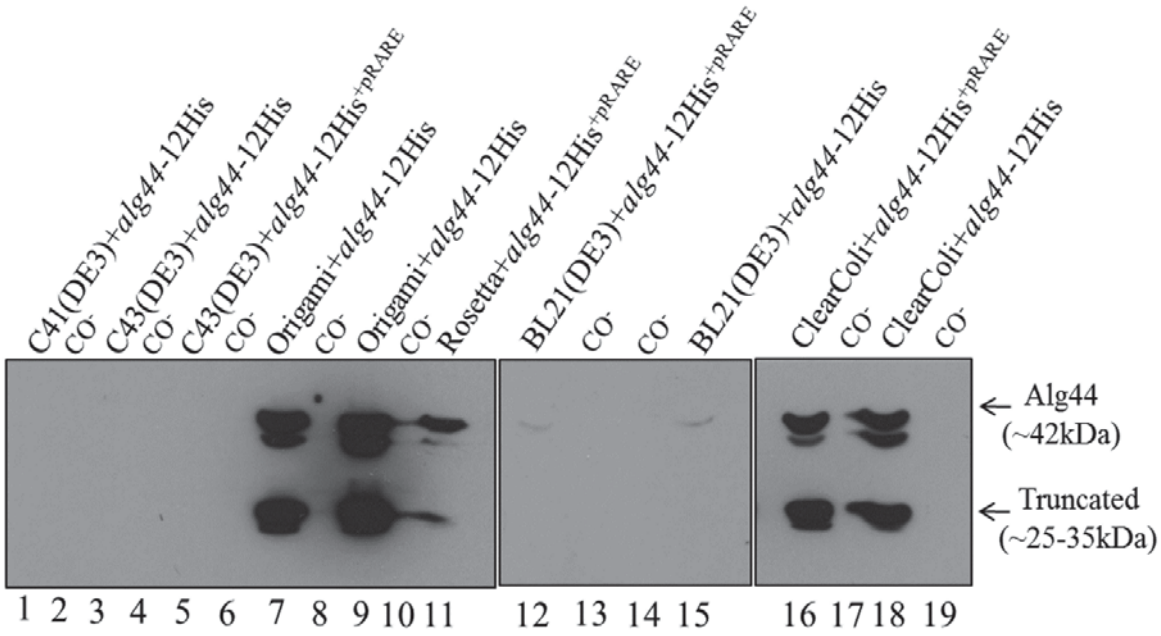

FIG. S8 Assessment of heterologous production of Alg44 using immunoblotting and anti-His-tag antibodies. In order to analyse the quaternary structure of Alg44 and to assess the heterologous production of this protein for purification and *in vitro* functional/structural analyses, we screened different strains of *E. coli* for the expression of the full length *alg44*-12His gene. Briefly, strains C41(DE3) and C43 (DE3) (lanes 1, 3 and 5) did not show any detectable protein production and BL21(DE3) (lanes 12 and 15) showed only weak production while Origami™ (DE3)(lanes 7 and 9), ClearColi BL21(DE3)(lanes 16 and 18) and Rosetta™ strains (lane 11) gave rise to higher protein production levels of the *alg44*-12His gene when compared with the other strains (Fig. S5). However, a significant fraction of protein was subjected to proteolytic truncation during membrane isolation even in the presence of protease inhibitors (Fig. S5). However, in all cases recombinant Alg44 was truncated. All genes were inserted into pETDuet-1 vector. Negative controls harbored empty plasmids. Co^-: negative control.

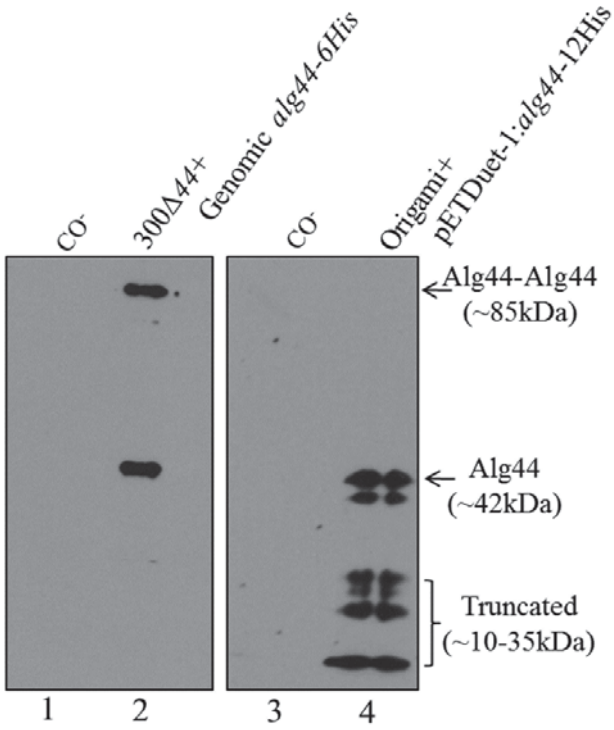

FIG. S9 His-affinity chromatography purification of Alg44 produced by homologous *P. aeruginosa* (left) and heterologous *E. coli* (right) hosts**.** Immunoblot analysis using anti-His-tag antibodies showed when EDTA was added, the presence of two distinct bands corresponding to the molecular weight of Alg44 monomer and dimer (lane 2) while heterologous Alg44 was truncated (lane 4). Negative controls harbored empty plasmids. 300: PDO300; MCS5: Co^-: negative control i.e. *P. aeruginosa* PDO300 or *E. coli* Origami (pETDuet-1).

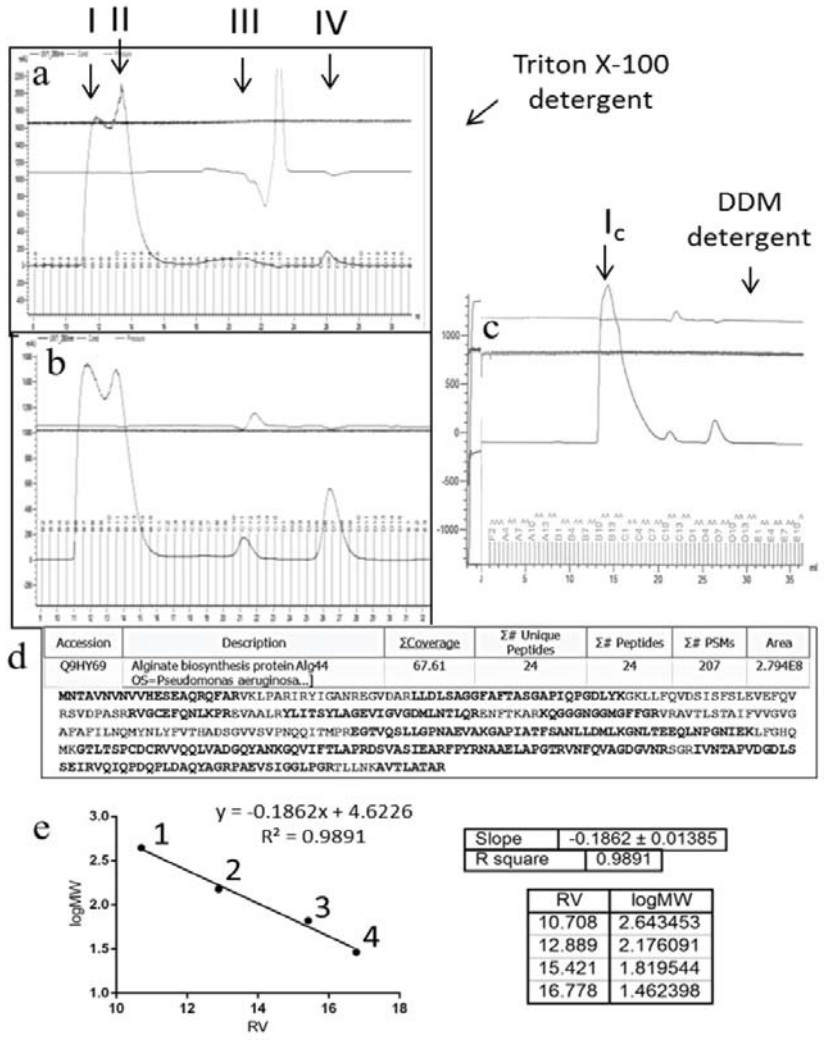

Accession	Description	ΣCoverage	Σ# Unique Peptides	Σ# Peptides	Σ# PSMs	Area
Q9HY69	Alginate biosynthesis protein Alg44 OS=Pseudomonas aeruginosa...	67.61	24	24	207	2.794E8

MNTAVNVNVVHESEAQRQFARVKLPARIRYIGANREGVDAR**LLDLSAGGFAFTASGAPIQFGDLYK**GKLLFQVDSISFSLEVEFQV
RSVDPASR**RVGCEFQNLKPR**EVAALR**YLITSYLAGEVIGVGDMLNTLQR**ENFTKAR**KQGGGNGGMGFFGR**VRAVTLSTAIFVVGVG
AFAFILNQMYNLYFVTHADSGVVSVPNQQITMPR**EGTVQSLLGPNAEVAKGAPIATFSANLLDMLKGNLTEEQLNPGNIEK**LFGHQ
MK**GTLTSPCDCRVVQQLVADGQYANKGQVIFTLAPRDSVASIEARFFYRNAAELAPGTRVNFQVAGDGVNR**SGR**IVNTAPVDGDLS**
SEIRVQIQPDQFLDAQYAGRPAEVSIGGLPGRTLLNK**AVTLATAR**

Slope	-0.1862 ± 0.01385
R square	0.9891

RV	logMW
10.708	2.643453
12.889	2.176091
15.421	1.819544
16.778	1.462398

FIG. S10 Gel filtration chromatogram showing purification of the Alg44 dimer. (**a-b**) Chromatograms belong to purification of Alg44-6His from a partially purified sample (provided using His-tag affinity chromatography), before (**a**) and after (**b**) treatment with triton X-100, alginate solution and DTT. Two major peaks I and II were separated in panels **a** and **b**. Presumable impurities associated with these peaks were removed after treatment of protein sample with 0.2% (wt/vol) alginate solution and 50 mM DTT and resulted in peaks III and IV appearance (**b**). Protein analysis using immunoblotting showed peak I which was collected in three 500-μL fractions (at K_{av}: 11-13) containing oligomeric states of Alg44 which was detected as Alg44 dimer under denaturing condition using SDS-PAGE and immunoblotting. Protein concentration in each fraction of peak I was quantified as 2.88-2.99 mg/mL. Peak II was not detectable and identifiable using SDS-PAGE or immunoblotting. (**c**) Replacement of triton X-100 by DDM resulted in resolving one peak corresponding to an apparent MW of 83.7 kDa indicating the presence of the Alg44 dimer. Similarly a band corresponding to stable Alg44 dimer was detected by immunoblotting. (**d**) Protein sequence of the purified protein showed the existence of Alg44 with

its signal peptide. Bold letters indicate identified peptides by mass spectrometry. (**e**) Molecular weight standard curve was applied to calculate protein molecular weights (for detail of calculation see materials and methods).

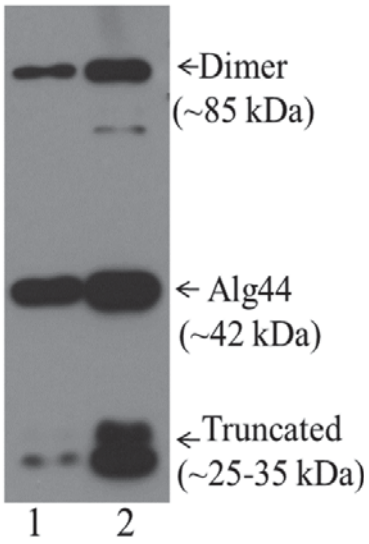

FIG. S11 Immunoblot analysis (lanes 1 and 2) showed that treatment of the sample with n-Dodecyl β-$_{D}$-maltoside (DDM) during purification of Alg44 resulted in reduction of Alg44 dimer stability and more truncations. Immunoblots were developed using anti-His-tag antibodies.

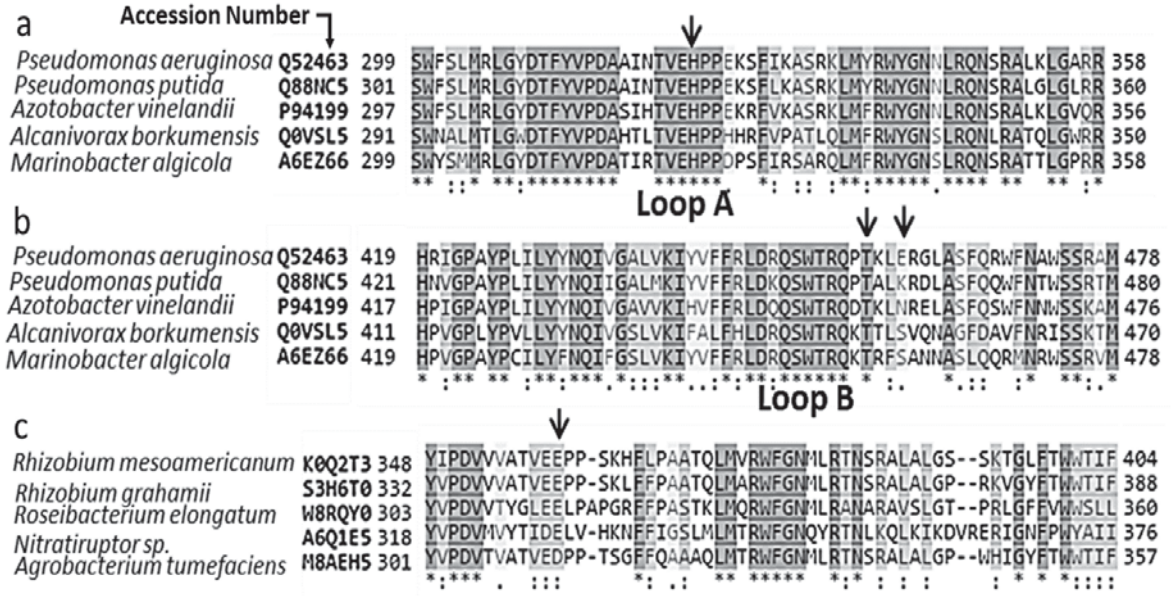

FIG. S12 Loops A and B of Alg8 are highly conserved among alginate-producing bacteria and others with Alg8 homologous counterparts. Multiple alignments of loop A (**a**) and loop B (**b**) among *Gammaproteobacteria* which produce alginate show highly conserved sequences. Arrows show respectively H323 (**a**), T457 and E460 (**b**) of *P. aeruginosa* which are respectively highly and less conserved, but their mutations identified with the most significant effect on regulation of alginate production. (**c**) Multiple alignments of the loops homologues to loop A of Alg8, but originating from *Alphaproteobacteria* and *Epsilonproteobacteria* show H323 of Alg8 is replaced with a negatively charged amino acid.

TABLE 1 Strains, plasmids and primers applied in this study

Strains and plasmids	Description	Source or reference
P. aeruginosa		
PDO300	*mucA22* isogenic mutant derived from PAO1, Alg^+	(168)
PDO300Δ*alg8*	Isogenic *alg8* deletion mutant derived from PDO300, Alg^-	(165)
PDO300 Δ*alg44*	Isogenic *alg44* deletion mutant derived from PDO300, Alg^-	(164)
PDO300 Δ*alg8*Δ*alg44*	Isogenic *alg8* and *alg44* deletions mutant derived from PDO300, Alg^-	(151)
PDO300Δ*mucR*	Isogenic *mucR* deletion mutant derived from PDO300	(105)
PDO300 Δ*mucR*Δ*alg8*	Isogenic *mucR*and *alg8* deletions mutant derived from PDO300, Alg^-	This study
E. coli		
Top10	Cloning strain; F^-,*mcr*A, Δ(*mrr-hsdRMS-mcrBC*), φ80*lacZ*ΔM15, Δ*lac*X74,*rec*A1, *ara*D139, Δ(*araleu*)7697 *gal*U,*gal*K, *rps*L (StrR), *end*A1, *nup*G	Invitrogen
XL1 Blue	Cloning strain; *ec*A1, *end*A1,*gyr*A96, *thi-1, hsd*R17, (r_K^-,m_K^+),*sup*E44, *rel*A1, Δ(*lac-pro*AB) [F',*pro*AB, *lac*I^q,*lacZ*ΔM15, Tn*10(tet^r)*]	(226)
S17-1	Donor strain in transconjugation; *thi*-1*, pro*A*, hsd*R17 ($r_K^-m_K^+$), *rec*A1; tra gene of plasmid RP4 integrated in chromosome	(171)
SM10	Donor strain for pFLP2 plasmid; *thi*-1*, thr*-1*, leu*B6*, sup*E44*, ton*A21*, lac*Y1*, recA*::RP4-2-Tc::*Mu Km^r*	(171)
BL21(DE3)	F^- *omp*T *hsd*SB(rB–, mB–) *gal dcm* (DE3)	Novagen
C41(DE3)	F^- *ompThsdSB (rB- mB-) gal dcm* (DE3)	Lucigen
C43(DE3)	F^- *ompThsdSB (rB- mB-) gal dcm* (DE3)	Lucigen
Origami™ (DE3)	F^- *ompThsd*S_B(r_B^- m_B^-) *gal dcm lacY1 ahpC* (DE3) *gor522*:: Tn*10 trxB* (Kan^R, Tet^R)	Novagen
ClearColi®	F– *ompThsdSB (rB- mB-) gal dcmlon* λ(DE3 [*lacI lac*UV5-T7 gene 1 *ind1 sam7 nin5*]) *msbA148* Δ*gutQ*Δ*kdsD*Δ*lpxL*Δ*lpxM*Δ*pagP*Δ*lpx P*Δ*eptA*	Lucigen
Rosetta™	F^- *ompThsd*S_B(r_B^- m_B^-) *gal dcm* pRARE (Cam^R)	Novagen
Plasmids		
pETDuet-1	Amp^r; co-expression of two target genes; carries the pBR322-derived ColE1 replicon, *lacI* gene,P_{T7}	Novagen

pETDuet-1:*alg44*-12His	*Nco*I-*Bam*HI fragment comprising *alg44*-12xhistidine tag fusion and , the *E. coli* codon-optimized	This study
pBBR1MCS-5	Gm^r; broad-host-range vector; P_{lac}	(172)
pBBR1MCS-5:*alg8*	*Hind*III-*Pst*I fragment comprising *alg8* inserted into vector pBBR1MCS-5	(165)
pBBR1MCS-5:*alg44*	*Hind*III-*Bam*HI fragment comprising *alg44* inserted into vector pBBR1MCS-5	(164)
pBBR1MCS-5:*alg44*-6his	Translational *alg44*-hexahistidine tag fusion, inserted into vector pBBR1MCS-5	(164)
pBBR1MCS-5:*mucR*	*Kpn*I-*Cla*I fragment comprising *mucR* inserted into vector pBBR1MCS-5	(105)
pBBR1MCS-5:*mucR:alg8*	*Kpn*I-*Cla*I fragment comprising *mucR* and *Hind*III-*Bam*HI fragment comprising *alg8* inserted into vector pBBR1MCS-5	This study
pBBR1MCS-5:*pilN*	*Hind*III-*Eco*RI fragment comprising *pilN*inserted into vector pBBR1MCS-5	This study
pBBR1MCS-5:*alg8(Δstop):gfp*	*Hind*III-*Eco*RI fragment comprising *alg8* without stop codon and *Pst*I-*Xba*I fragment comprising *gfp* inserted into vector pBBR1MCS-5	This study
pBBR1MCS-5:*alg8(Δstop):sfgfp*	*Hind*III-*Eco*RI fragment comprising *alg8* without stop codon and *Pst*I-*Xba*I fragment comprising *sfgfp* inserted into vector pBBR1MCS-5	This study
pBBR1MCS-5:*alg44(Δstop):gfp*	*Hind*III-*Eco*RI fragment comprising *alg44* without stop codon and *Pst*I-*Xba*I fragment comprising *gfp* inserted into vector pBBR1MCS-5	This study
pBBR1MCS-5:*alg44(Δstop)*:*sfgfp*	*Hind*III-*Eco*RI fragment comprising *alg44* without stop codon and *Pst*I-*Xba*I fragment comprising *sfgfp* inserted into vector pBBR1MCS-5	This study
pBBR1MCS-5:*pilN(Δstop):sfgfp*	*Hind*III-*Eco*RI fragment comprising *pilN* without stop codon and *Pst*I-*Xba*I fragment comprising *sfgfp* inserted into vector pBBR1MCS-5	This study
pBBR1MCS-5:*alg8*(T320A)	*Hind*III-*Pst*I fragment comprising *alg8* encoding site-directed mutagenesis T320A inserted into vector pBBR1MCS-5	This study
pBBR1MCS-5:*alg8*(T320A):*rocR*	*Hind*III-*Pst*I fragment comprising *alg8* encoding site-directed mutagenesis T320A and *Xba*I-*Sac*I fragment comprising *rocR*(PA3947) inserted into vector pBBR1MCS-5	This study
pBBR1MCS-5:*alg8*(H323A)	*Hind*III-*Pst*I fragment comprising *alg8* encoding site-directed mutagenesis H323A inserted into vector pBBR1MCS-5	This study
pBBR1MCS-5:*alg8*(H323A):*rocR*	*Hind*III-*Pst*I fragment comprising *alg8* encoding site-directed mutagenesis H323A and *Xba*I-*Sac*I fragment comprising *rocR*(PA3947) inserted into vector pBBR1MCS-5	This study
pBBR1MCS-5:*alg8*(P324A)	*Hind*III-*Pst*I fragment comprising *alg8* encoding site-directed mutagenesis P324A inserted into vector pBBR1MCS-5	This study
pBBR1MCS-5:*alg8*(P324A):*rocR*	*Hind*III-*Pst*I fragment comprising *alg8* encoding site-directed mutagenesis P324A and *Xba*I-*Sac*I fragment comprising *rocR*(PA3947) inserted into vector pBBR1MCS-5	This study

pBBR1MCS-5:*alg8*(P325A)	*Hind*III-*Pst*I fragment comprising *alg8* encoding site-directed mutagenesis P325A inserted into vector pBBR1MCS-5	This study
pBBR1MCS-5:*alg8*(P325A):*rocR*	*Hind*III-*Pst*I fragment comprising *alg8* encoding site-directed mutagenesis P325A and *Xba*I-*Sac*I fragment comprising *rocR*(PA3947) inserted into vector pBBR1MCS-5	This study
pBBR1MCS-5:*alg8*(P325A):*alg44*(R17A)	*Hind*III-*Pst*I fragment comprising *alg8* encoding site-directed mutagenesis P325A and *Cla*I-*Hind*III fragment comprising *alg44* encoding site-directed mutagenesis R17A inserted into vector pBBR1MCS-5	This study
pBBR1MCS-5*:alg8*(P325A):*alg44*(R17A):*rocR*	*Hind*III-*Pst*I fragment comprising *alg8* encoding site-directed mutagenesis P325A and *Cla*I-*Hind*III fragment comprising *alg44* encoding site-directed mutagenesis R17A and *Xba*I-*Sac*I fragment encoding RocR (PA3947) inserted into vector pBBR1MCS-5	This study
pBBR1MCS-5:*alg8*(P325A):*alg44*(R21A)	*Hind*III-*Pst*I fragment comprising *alg8* encoding site-directed mutagenesis P325A and *Cla*I-*Hind*III fragment comprising *alg44* encoding site-directed mutagenesis R21A inserted into vector pBBR1MCS-5	This study
pBBR1MCS-5:*alg8*(P325A):*alg44*(R21A):*rocR*	*Hind*III-*Pst*I fragment comprising *alg8* encoding site-directed mutagenesis P325A and *Cla*I-*Hind*III fragment comprising *alg44* encoding site-directed mutagenesis R21A and *Xba*I-*Sac*I fragment encoding RocR (PA3947) inserted into vector pBBR1MCS-5	This study
pBBR1MCS-5:*alg8*(T453A)	*Hind*III-*Pst*I fragment comprising *alg8* encoding site-directed mutagenesis T453A inserted into vector pBBR1MCS-5	This study
pBBR1MCS-5:*alg8*(T453A):*rocR*	*Hind*III-*Pst*I fragment comprising *alg8* encoding site-directed mutagenesis T453A and *Xba*I-*Sac*I fragment comprising *rocR*(PA3947) inserted into vector pBBR1MCS-5	This study
pBBR1MCS-5:*alg8*(R454A)	*Hind*III-*Pst*I fragment comprising *alg8* encoding site-directed mutagenesis R454A inserted into vector pBBR1MCS-5	This study
pBBR1MCS-5:*alg8*(R454A):*rocR*	*Hind*III-*Pst*I fragment comprising *alg8* encoding site-directed mutagenesis R454A and *Xba*I-*Sac*I fragment comprising *rocR*(PA3947) inserted into vector pBBR1MCS-5	This study
pBBR1MCS-5:*alg8*(T457A)	*Hind*III-*Pst*I fragment comprising *alg8* encoding site-directed mutagenesis T457A inserted into vector pBBR1MCS-5	This study
pBBR1MCS-5:*alg8*(T457A):*rocR*	*Hind*III-*Pst*I fragment comprising *alg8* encoding site-directed mutagenesis T457A and *Xba*I-*Sac*I fragment comprising *rocR*(PA3947) inserted into vector pBBR1MCS-5	This study
pBBR1MCS-5:*alg8*(T457A):*alg44*(R17A)	*Hind*III-*Pst*I fragment comprising *alg8* encoding site-directed mutagenesis T457A and *Cla*I-*Hind*III fragment comprising *alg44* encoding site-directed mutagenesis R17A inserted into vector pBBR1MCS-5	This study
pBBR1MCS-5*:alg8*(T457A):*alg44*(R17A):*rocR*	*Hind*III-*Pst*I fragment comprising *alg8* encoding site-directed mutagenesis T457A and *Cla*I-*Hind*III fragment comprising *alg44* encoding site-directed mutagenesis R17A inserted into vector pBBR1MCS-5 and *Xba*I-*Sac*I fragment encoding RocR (PA3947) inserted into vector pBBR1MCS-5	This study
pBBR1MCS-5:*alg8*(T457A):*alg44*(R21A)	*Hind*III-*Pst*I fragment comprising *alg8* encoding site-directed mutagenesis T457A and *Cla*I-*Hind*III	This study

	fragment comprising *alg44* encoding site-directed mutagenesis R21A inserted into vector pBBR1MCS-5	
pBBR1MCS-5:*alg8*(T457A):*alg44*(R21A):*rocR*	*Hind*III-*Pst*I fragment comprising *alg8* encoding site-directed mutagenesis T457A and *Cla*I-*Hind*III fragment comprising *alg44* encoding site-directed mutagenesis R21A inserted into vector pBBR1MCS-5 and *Xba*I-*Sac*I fragment encoding RocR (PA3947) inserted into vector pBBR1MCS-5	This study
pBBR1MCS-5:*alg8*(E460A)	*Hind*III-*Pst*I fragment comprising *alg8* encoding site-directed mutagenesis E460A inserted into vector pBBR1MCS-5	This study
pBBR1MCS-5:*alg8*(E460A):*rocR*	*Hind*III-*Pst*I fragment comprising *alg8* encoding site-directed mutagenesis E460A and *Xba*I-*Sac*I fragment comprising *rocR*(PA3947) inserted into vector pBBR1MCS-5	This study
pBBR1MCS-5:*alg8*(E460A):*alg44*(R17A)	*Hind*III-*Pst*I fragment comprising *alg8* encoding site-directed mutagenesis E460A and *Cla*I-*Hind*III fragment comprising *alg44* encoding site-directed mutagenesis R17A inserted into vector pBBR1MCS-5	This study
pBBR1MCS-5:*alg8*(E460A):*alg44*(R17A):*rocR*	*Hind*III-*Pst*I fragment comprising *alg8* encoding site-directed mutagenesis E460A and *Cla*I-*Hind*III fragment comprising *alg44* encoding site-directed mutagenesis R17A inserted into vector pBBR1MCS-5 and *Xba*I-*Sac*I fragment encoding RocR (PA3947) inserted into vector pBBR1MCS-5	This study
pBBR1MCS-5:*alg8*(E460A):*alg44*(R21A)	*Hind*III-*Pst*I fragment comprising *alg8* encoding site-directed mutagenesis E460A and *Cla*I-*Hind*III fragment comprising *alg44* encoding site-directed mutagenesis R21A inserted into vector pBBR1MCS-5	This study
pBBR1MCS-5:*alg8*(E460A):*alg44*(R21A):*rocR*	*Hind*III-*Pst*I fragment comprising *alg8* encoding site-directed mutagenesis E460A and *Cla*I-*Hind*III fragment comprising *alg44* encoding site-directed mutagenesis R21A inserted into vector pBBR1MCS-5 and *Xba*I-*Sac*I fragment encoding RocR (PA3947) inserted into vector pBBR1MCS-5	This study
pBBR1MCS-5:*alg8*(H323E)	*Hind*III-*Pst*I fragment comprising *alg8* encoding site-directed mutagenesis H323E inserted into vector pBBR1MCS-5	This study
pBBR1MCS-5:*alg8*(H323E):*rocR*	*Hind*III-*Pst*I fragment comprising *alg8* encoding site-directed mutagenesis H323E and *Xba*I-*Sac*I fragment comprising *rocR*(PA3947) inserted into vector pBBR1MCS-5	This study
pBBR1MCS-5:*alg8*(H323E):*alg44*(R17A)	*Hind*III-*Pst*I fragment comprising *alg8* encoding site-directed mutagenesis H323E and *Cla*I-*Hind*III fragment comprising *alg44* encoding site-directed mutagenesis R17A inserted into vector pBBR1MCS-5	This study
pBBR1MCS-5:*alg8*(H323E):*alg44*(R17A):*rocR*	*Hind*III-*Pst*I fragment comprising *alg8* encoding site-directed mutagenesis H323E and *Cla*I-*Hind*III fragment comprising *alg44* encoding site-directed mutagenesis R17A inserted into vector pBBR1MCS-5 and *Xba*I-*Sac*I fragment encoding RocR (PA3947) inserted into vector pBBR1MCS-5	This study
pBBR1MCS-5:*alg8*(H323E):*alg44*(R21A)	*Hind*III-*Pst*I fragment comprising *alg8* encoding site-directed mutagenesis H323E and *Cla*I-*Hind*III fragment comprising *alg44* encoding site-directed mutagenesis R21A inserted into vector pBBR1MCS-5	This study
pBBR1MCS-5:*alg8*(H323E):*alg44*(R21A):*rocR*	*Hind*III-*Pst*I fragment comprising *alg8* encoding site-directed mutagenesis H323E and *Cla*I-*Hind*III fragment comprising *alg44* encoding site-directed mutagenesis R21A inserted into vector pBBR1MCS-5	This study

	and *Xba*I-*Sac*I fragment encoding RocR (PA3947) inserted into vector pBBR1MCS-5	
pBBR1MCS-5:*alg8*(E322A)	*Hind*III-*Pst*I fragment comprising *alg8* encoding site-directed mutagenesis E322A inserted into vector pBBR1MCS-5	This study
pBBR1MCS-5:*alg8*(E322A):*rocR*	*Hind*III-*Pst*I fragment comprising *alg8* encoding site-directed mutagenesis E322A and *Xba*I-*Sac*I fragment comprising *rocR*(PA3947) inserted into vector pBBR1MCS-5	This study
pBBR1MCS-5:*alg8*(E322A/H323E)	*Hind*III-*Pst*I fragment comprising *alg8* encoding site-directed mutagenesis E322A and H323E inserted into vector pBBR1MCS-5	This study
pBBR1MCS-5:*alg8*(E322A/H323E):*rocR*	*Hind*III-*Pst*I fragment comprising *alg8* encoding site-directed mutagenesis E322A and H323E and *Xba*I-*Sac*I fragment comprising *rocR*(PA3947) inserted into vector pBBR1MCS-5	This study
pBBR1MCS-5:*alg8*(T453A/T457A)	*Hind*III-*Pst*I fragment comprising *alg8* encoding site-directed mutagenesis T453A and T457A inserted into vector pBBR1MCS-5	This study
pBBR1MCS-5:*alg8*(T453A/T457A):*rocR*	*Hind*III-*Pst*I fragment comprising *alg8* encoding site-directed mutagenesis T453A and T457A and *Xba*I-*Sac*I fragment comprising *rocR*(PA3947) inserted into vector pBBR1MCS-5	This study
pBBR1MCS-5:*alg8*(R454A/T457A)	*Hind*III-*Pst*I fragment comprising *alg8* encoding site-directed mutagenesis R454A and T457A inserted into vector pBBR1MCS-5	This study
pBBR1MCS-5:*alg8*(R454A/T457A):*rocR*	*Hind*III-*Pst*I fragment comprising *alg8* encoding site-directed mutagenesis R454A and T457A and *Xba*I-*Sac*I fragment comprising *rocR*(PA3947) inserted into vector pBBR1MCS-5	This study
pBBR1MCS-5:*alg44*(Q258A)-6his	*Hind*III-*Bam*HI fragment comprising *alg44* encoding translational *Alg44*-hexahistidine tag fusion with site-directed mutagenesis Q258A inserted into vector pBBR1MCS-5	This study
pBBR1MCS-5:*alg44*(M259A)-6His	*Hind*III-*Bam*HI fragment comprising *alg44* encoding translational *Alg44*-hexahistidine tag fusion with site-directed mutagenesis M259A inserted into vector pBBR1MCS-5	This study
pBBR1MCS-5:*alg44*(K260A)-6His	*Hind*III-*Bam*HI fragment comprising *alg44* encoding translational *Alg44*-hexahistidine tag fusion with site-directed mutagenesis K260A inserted into vector pBBR1MCS-5	This study
pBBR1MCS-5:*alg44*(T264A)-6His	*Hind*III-*Bam*HI fragment comprising *alg44* encoding translational *Alg44*-hexahistidine tag fusion with site-directed mutagenesis T264A inserted into vector pBBR1MCS-5	This study
pBBR1MCS-5:*alg44*(S265A)-6His	*Hind*III-*Bam*HI fragment comprising *alg44* encoding translational *Alg44*-hexahistidine tag fusion with site-directed mutagenesis S265A inserted into vector pBBR1MCS-5	This study
pBBR1MCS-5:*alg44*(P266A)-6His	*Hind*III-*Bam*HI fragment comprising *alg44* encoding translational *Alg44*-hexahistidine tag fusion with site-directed mutagenesis P266A inserted into vector pBBR1MCS-5	This study
pBBR1MCS-5:*alg44*(C267A)-6His	*Hind*III-*Bam*HI fragment comprising *alg44* encoding translational *Alg44*-hexahistidine tag fusion with site-directed mutagenesis C267A inserted into vector pBBR1MCS-5	This study

pBBR1MCS-5:*alg44*(D268A)-6His	*Hind*III-*Bam*HI fragment comprising *alg44* encoding translational *Alg44*-hexahistidine tag fusion with site-directed mutagenesis D268A inserted into vector pBBR1MCS-5	This study
pBBR1MCS-5:*alg44*(C269A)-6His	*Hind*III-*Bam*HI fragment comprising *alg44* encoding translational *Alg44*-hexahistidine tag fusion with site-directed mutagenesis C269A inserted into vector pBBR1MCS-5	This study
pBBR1MCS-5:*alg44*(C267A/C269A)-6His	*Hind*III-*Bam*HI fragment comprising *alg44* encoding translational *Alg44*-hexahistidine tag fusion with site-directed mutagenesis C267A and C269A inserted into vector pBBR1MCS-5	This study
Mini-CTX-lacZ	Chromosomal integration vector at the CTX phage *att* site on the *P. aeruginosa* chromosome, Tc^r	(227)
Mini-CTX:P*alg44*-6his	*Pst*I-*Hind*III fragment encoding alginate operon promoter (P*algD*) and *Hind*III-*Bam*HI fragment encoding C-terminally hexahistidine-tagged *Alg44* inserted into vector Mini-CTX-lacZ	(151)
Primers		
Alg8Fw(T453A)	aagcaagaagatctacgtgttcttccgcctcgaccggcagtcctggGCGcgccagccgaccaagctggagcgcggcctggcca	This study
Alg8Fw(T457A)	aagcaagaagatctacgtgttcttccgcctcgaccggcagtcctggacccgccagccgGCGaagctggagcgcggcctggcca	This study
Alg8Fw(T453A-T457A)	aagcaagaagatctacgtgttcttccgcctcgaccggcagtcctggGCGcgccagccgGCGaagctggagcgcggcctggcca	This study
Alg8Fw(R454A)	aagcaagaagatctacgtgttcttccgcctcgaccggcagtcctggaccGCgcagccgaccaagctggagcgcggcctggcca	This study
Alg8Fw(R454A-T457A)	aagcaagaagatctacgtgttcttccgcctcgaccggcagtcctggaccGCgcagccgGCGaagctggagcgcggcctggcca	This study
Alg8Fw(E460A)	aagcaagaagatctacgtgttcttccgcctcgaccggcagtcctggacccgccagccgaccaagctgGCGcgcggcctggccagcttccagcgctggtt	This study
Alg8Rev-Alg8End	aagcaagactgcagaaatcatacgatggtcagcagcacggcgacgaagatgctggcgg	This study
AlgFw-AatII	aagcaagagacgtcgagaacgaccacctggagcactggcgcctgggtcgct	This study
Alg8Rv(P324A)	aagcaagagaagctcttctccggCGCgtgctcgaccgtgttgatcgccgcgtcgggcacgtagaaggt	This study
Alg8Rv(P325A)	aagcaagagaagctcttctcCGCcgggtgctcgaccgtgttgatcgccgcgtcgggcacgtagaaggt	This study
Alg8Rv(P324A-P325A)	aagcaagagaagctcttctcCGCCGCgtgctcgaccgtgttgatcgccgcgtcgggcacgtagaaggt	This study
Alg8Rv(H323E)	aagcaagagaagctcttctccggcggCTCctcgaccgtgttgatcgccgcgtcgggcacgtagaaggt	This study

Alg8Rv(E322H+H323E)	aagcaagagaagctcttctccggcggCTCGTGgaccgtgttgatcgccgcgtcgggcacgtagaaggt	This study
Alg8Rv(T320A)	aagcaagagaagctcttctccggcgggtgctcgacCGCgttgatcgccgcgtcgggcacgtagaaggt	This study
Alg8Rv(T320A+E322A)	aagcaagagaagctcttctccggcgggtgCGCgacCGCgttgatcgccgcgtcgggcacgtagaaggt	This study

TABLE S1 Composition of alginates produced by different variants of Alg44

Mutants	Ac%	F_M	F_G	$F_{MG/GM}$	F_{MM}
300+MCS5	52	0.6	0.4	0.4	0.2
Δ44+44his	64	0.86	0.14	0.14	0.72
Q258A	50	0.8	0.2	0.2	0.6
M259A	38	0.7	0.3	0.3	0.4
K260A	49	0.8	0.2	0.2	0.6
T264A	52	0.78	0.22	0.22	0.56
S265A	49	0.86	0.14	0.14	0.72
D268A	34	0.77	0.23	0.23	0.54

300:PDO300; MCS5: pBBR1MCS-5; F_G: molar fraction of guluronate (G) residue; F_M: molar fraction of mannuronate (M) residue; $F_{GM/MG}$: molar fraction of two consecutive G and M residues; F_{MM}: molar fraction of two consecutive M residues; Ac.: acetylation

TABLE S2 Composition of alginates produced by various *P. aeruginosa* strains and impacted by Alg44 variants (values arranged in descending order)

Mutant	F_G	Mutant	Ac%	Mutant	F_{MM}
300+MCS5	0.4	Δ44+44his	64	Δ44+44his	0.72
M259A	0.3			S265A	0.72
D268A	0.23	300+MCS5	52	Q258A	0.6
T264A	0.22	T264A	52	K260A	0.6
Q258A	0.2	Q258A	50	T264A	0.56
K260A	0.2	K260A	49	D268A	0.54
		S265A	49		
Δ44+44his	0.14	M259A	38	M259A	0.4
S265A	0.14	D268A	34	300+MCS5	0.2

300:PDO300; MCS5: pBBR1MCS-5; F_G: molar fraction of guluronate (G) residue; F_{MM}: molar fraction of two consecutive M residues; Ac.: acetylation

MASSEY UNIVERSITY
GRADUATE RESEARCH SCHOOL

STATEMENT OF CONTRIBUTION TO DOCTORAL THESIS CONTAINING PUBLICATIONS

(To appear at the end of each thesis chapter/section/appendix submitted as an article/paper or collected as an appendix at the end of the thesis)

We, the candidate and the candidate's Principal Supervisor, certify that all co-authors have consented to their work being included in the thesis and they have accepted the candidate's contribution as indicated below in the *Statement of Originality*.

Name of Candidate: Shirin Ghods

Name/Title of Principal Supervisor: Professor Bernd H. A. Rehm

Name of Published Research Output and full reference:

M. Fata Moradali, Shirin Ghods, Bernd H. A. Rehm. Activation Mechanism and Cellular Localization of Membrane-Anchored Alginate Polymerase in Pseudomonas aeruginosa. Applied and Environmental Microbiology 83.9 (2017): e03499-16

In which Chapter is the Published Work: Chapter IV

Please indicate either:

- The percentage of the Published Work that was contributed by the candidate 45%

  and / or

- Describe the contribution that the candidate has made to the Published Work:

  Generation of double-gene knockout mutants, complementation, biofilm assessment, alginate quantification and imaging.

Shirin Ghods Digitally signed by Shirin Ghods Date: 2018.01.08 13:32:19 -05'00'
Candidate's Signature

8/1/2018
Date

Bernd Rehm Digitally signed by Bernd Rehm Date: 2018.01.24 08:15:03 +10'00'
Principal Supervisor's signature

24/1/2018
Date

Chapter V

Preliminary assessment of the establishment of the alginate biosynthesis pathway in non-pathogenic heterologous hosts

Shirin Ghods[1], Bernd H. A. Rehm[1]

[1] Institute of Fundamental Sciences, Massey University, Private Bag 11222, Palmerston North, New Zealand.

Drafted manuscript (2017)

ABSTRACT

Alginates are exopolysaccharides produced by seaweeds and bacteria belonging to the genera *Pseudomonas* and *Azotobacter*. Traditionally, these polymers have been harvested from seaweeds for commercial production and industrial applications due to their unique properties. Algal alginates display different chemical composition from bacterial alginates reflecting their different properties. While algal alginates have been widely applied for industrial applications, our knowledge about the alginate biosynthesis pathway and the underlying molecular mechanisms is based on bacterial alginate production mainly by *P. aeruginosa*. However, while *P. aeruginosa* is a potent alginate producer, it may not be an ideal source for production of alginates due to its pathogenicity; particularly when their application for high value purposes is the ultimate goal. In this study, we aimed to assess establishment of alginate biosynthesis in non-pathogenic and biotechnologically accepted heterologous hosts including *Escherichia coli* and *Bacillus megaterium* strains. To this end, our strategy was the production of minimal protein requirements essential for alginate precursor production, alginate polymerization and secretion. The genes encoding these proteins were transferred into the cells using a two-plasmid system and protein production and localization were assessed using immunoblotting. Our analysis showed that some strains of *E. coli* could be decent hosts for production of these proteins. Furthermore, our results showed that heterologous hosts are effective in hosting AlgD activity that catalyzes the last step of alginate precursor production. However, at polymerization level, our assessment showed Alg8 and Alg44 were produced and localized in the cytoplasmic membrane of some heterologous hosts, but polymerization events could not be detected properly. However, this does not rule out the possibility of polymerization occurring using these experimental settings. Overall, this study provided preliminary assessment for the establishment of alginate biosynthesis in heterologous hosts.

INTRODUCTION

Alginate is a natural unique anionic polysaccharide composed of variable proportions of 1, 4-linked β-D-mannuronic acid (M) and its C5 epimer α-L-guluronic acid (G) produced by brown algae and the bacterial genera *Pseudomonas* and *Azotobacter*. The alginate derived from *P. aeruginosa* is naturally acetylated and lacks consecutive G residues (GG-blocks) (37, 38, 228). Due to the unique composition and physical properties of alginates such as water holding, gelling, thickening, viscoelasticity and stabilizing, they have been widely applied for various industrial purposes such as in food, agricultural, cosmetic, pharmaceutical and biomedical industries (148, 149).

In the last two decades, they have found their way into advanced pharmaceutical and biomedical engineering, owing to their biocompatibility and non-toxicity as well as versatility in modifications. So far, algal alginates have been the sole commercialized products which have been applied for various purposes, while bacterial alginates have been still remained unharnessed. Importantly, algal and bacterial alginates differ substantially from each other with respect to their composition, modifications, molecular mass, viscoelastic properties and polydispersity while bacterial alginates may meet current needs for advanced pharmaceutical and biomedical purposes.

Pseudomonas aeruginosa has been considered as a main model organism for studying alginate biosynthesis, because, on one hand, it is important in bacterial pathogenesis, and on the other hand, it helps us in establishing tailor-made alginate production by non-pathogenic heterologous hosts. Hence, *P. aeruginosa* has been extensively studied with regard to characterization of different steps of alginate biosynthesis, unraveling protein-protein interactions involved in the alginate biosynthesis/modification/secretion machinery complex, and associated regulatory mechanisms. Establishment of an alginate biosynthesis pathway in non-pathogenic bacteria and controlling alginate production using bioengineering approaches will enable the production of the alginates with novel material properties for novel applications. Currently, brown seaweeds are the only cheap resources for alginate extraction, but the quality of alginate, the composition and unwanted contamination with other molecules during separation have limited alginate applications for specific applications such as for biomedical purposes which require highly qualified and pre-defined polymers (9). In the present study, we aimed at establishing alginate biosynthesis in an easy-to-handle, but non-pathogenic, heterologous host. To this end, we relied on existing knowledge about genes encoding various proteins

mediating various events including the biosynthesis of alginate precursors, alginate polymerization/modifications/secretion by constituting an envelope spanning multi-protein complex, and post-translational regulation. Except for *algC,* other selected alginate genes to express in heterologous hosts are co-clustered in one operon in *P. aeruginosa*. The proteins encoded by these genes are briefly discussed here. AlgA, AlgC, and AlgD catalyze four enzymatic steps to convert fructose 6-phosphate to GDP-mannuronic acid as an active sugar donor during polymerization. Two membrane-anchored proteins Alg8 glycosyltransferase and Alg44 constitute the alginate synthase unit by direct interaction where Alg44 senses the second messenger c-di-GMP (151) for activating polymerization. Furthermore, the periplasmic domain of Alg44 interacts with other protein subunits proposed to constitute a periplasmic scaffold which mediates the translocation of nascent alginate across the periplasm for secretion. Secretion of alginate through the outer membrane is mediated by AlgE which is a porin protein localized in the outer membrane. MucR protein was also chosen as it is involved in regulation of alginate production in *P. aeruginosa*. This protein positively regulates alginate polymerization presumably by specifically providing a c-di-GMP pool in the vicinity of the protein complex. Alginate-producing bacteria have the core genetic elements involved in alginate biosynthesis in common. Therefore, these genes were preferably selected from the non-pathogenic alginate producing bacterium *A. vinelandii* to establish their expression in heterlogous hosts. Hence, *algA*, *algC*, *algD*, *alg8*, *alg44* and *algE* (also called *algJ* from *Azotobacter vinelandii*) originated from *A. vinelandii*. However, *mucR* originated from *P. aeruginosa* because its role in providing the c-di-GMP pool in *P. aeruginosa* was considered (105, 229). These genes were transferred into heterlogous hosts using two compatible plasmid systems and protein production was assessed using immunoblotting. Functionality of produced proteins was assessed via enzymatic assessments or enzyme-linked immunosorbent assays (ELISA). Overall, this study took the first steps in establishing the alginate biosynthesis pathway in non-pathogenic and heterologous hosts. This will aid the production of tailor-made alginates with novel properties and harnessing all the benefits lacking in algal alginates for high value purposes (10).

MATERIALS AND METHODS

Bacterial strains, plasmids, growth conditions and chemicals

Strains and plasmids used in this study are summarized in Table S1 and S2 and the map of generated constructs are showed in Figure S1 and Table 3. *Bacillus megaterium, Pseudomonas aeruginosa* and *Escherichia coli* were grown in Luria-Bertani (LB) medium supplemented with appropriate antibiotics at 37 °C. For cultivating *P. aeruginosa* on solid medium, Difco™ Pseudomonas Isolation Agar supplemented with appropriate antibiotics was applied and incubated at 37 °C. All chemicals were purchased from Sigma-Aldrich and Merck KGaA unless otherwise mentioned. All enzymes used for cloning were manufactured by Roche, New England Biolabs GmbH or Invitrogen.

Cloning of minimal, but essential, genetic element requirements for alginate production in heterologous hosts

For recombinant production of proteins as minimal, but essential, requirements for alginate production in heterologous hosts, the *algD* gene (encoding GDP-mannose dehydrogenase (GMD)) was selected from *Azotobacter vinelandii* ATCC9046 which is required to catalyse the last step of precursor preparation i.e. GDP-mannuronic acid. However, for *in vitro* enzymatic assessments on AlgD activity, the *algD* gene was chosen from *Pseudomonas aeruginosa* PAO1 and a Histidine (His)-tagged fusion variant of it was generated resulting in *algD*-10XHis. *algA* and *algC* genes were selected from *A. vinelandii* CA6 and *algJ* (homologous to *algE* gene from *P. aeruginosa*) originated from *A. vinelandii* E. However, since alginate polymerization and post-translational regulation are key parts of this pathway and they were well-known in *P. aeruginosa*, cognate genes mediating these events including *alg8, alg44 and mucR* were selected from *P. aeruginosa* PAO1. Furthermore, 6XHis-tagged variants of these genes were also generated.

Isolation of cytoplasmic proteins

To confirm the localization and functionality of AlgA, AlgC and AlgD in the cytoplasmic fraction of *E. coli* and *B. megaterium* strains, the cytoplasmic fractions were assessed. Overnight culture of *E. coli* and *B. megaterium* transformants (Figure S1 and Table S3)

harbouring the generated recombinant constructs and empty vectors were subcultured in 100 ml of LB media and incubated at 37 °C until reaching an optical density (OD_{600}) of 0.6. Then cultures were induced by the addition of 1 mM IPTG (final concentration) for 18 h at 30 °C. Cells were harvested by centrifugation at 8,000 × *g* at 4 °C for 20 min. Ten mM HEPES buffer (pH 7.5) was used for washing two times and sediments were subjected to enzymatic lysis by suspending in 10 mM HEPES buffer (pH 7.5) containing 150 mM NaCl, 1 mg ml^{-1} DNase I, 1 mg ml^{-1} RNase A, 1 mg ml^{-1} lysozyme and cOmplete™ EDTA-free Protease Inhibitor Cocktail. They were incubated on ice for 30 min followed by sonication to complete cell disruption. Cell debris were removed by centrifugation and supernatants containing cytoplasmic proteins were analyzed using sodium dodecyl sulfate-polyacrylamide gel electrophoresis (SDS-PAGE) (8% acrylamide gel) and immunoblotting.

Expression and purification of recombinant AlgD (GMD)

The expression vector pET-14b: (10xHis) *algD* was transferred into *E. coli* BL21 (DE3). A 400 ml of *E. coli* transformant culture was grown at 37 °C until reaching an OD_{600} = 0.4. Then it was cooled down to 25 °C followed by being induced by the addition of 0.5 mM IPTG (final concentration) and grown at 30 °C for 18 h. Ten-His-AlgD purification was performed under native (non-denaturing) condition. Cells were collected by centrifugation at 8,000 × *g* at 4 °C for 20 min. Cells were washed twice with washing buffer A containing 50 mM NaH_2PO_4, 300 mM NaCl, 1 mM EDTA, 1mM DTT, 10% Glycerol, 5 mM imidazole (pH 7.5). After centrifugation, sediments were subjected to enzymatic cell lysis by suspending in buffer A containing1 mg ml^{-1} DNase I, 1 mg ml^{-1} RNase A, 1 mg ml^{-1} lysozyme and cOmplete™ EDTA-free Protease Inhibitor Cocktail. They were incubated on ice for 30 min followed by sonication. Cell debris was removed by centrifugation at 15,000 × *g* for 20 min at 4 °C. Supernatant was mixed with cOmplete™ His-Tag Purification Resin (Roche). Buffer A was applied for washing two times and then bound proteins were eluted using elution buffer containing 20 mM Tris-HCl, 50 mM KCl, 1 mM DTT, 1mM EDTA, 20% Glycerol, 250 mM imidazole. NAD^+ (Nicotinamide adenine dinucleotide) to a final concentration of 200 µM was added to all buffers applied in purification of AlgD to retain the active form of enzyme. All purification procedures were performed at 4 ºC in the cold room. Aliquots of purified enzyme were snap frozen in liquid nitrogen and stored at -80 °C. (Aliquots retained their

activity over several months under these conditions). The protein concentrations were determined by the Bradford protein assay (110, 111) and the bicinchoninic acid assay (BCA) (Pierce, Rockford, IL, USA) and bovine serum albumin (Gibco) was utilized as the standard. Eluents were analysed by SDS-PAGE (8% acrylamide gel)as described elsewhere (112) followed by immunoblotting using HisProbe-HRP antibody (Thermo Fisher Scientific).

In vitro enzymatic assessment of purified AlgD

Before enzymatic assessment, purified 10His-AlgD was subjected to further purification by removing imidazole through replacing with buffer without imidazol using Vivaspin columns, 30 kDa MWCO (GE Healthcare UK limited). Enzymatic assessments were performed as described by Tenhaken et al. (230) with some modifications. To this end, the increase of NADH concentration, as measured by the change of absorbance at 340 nm, was an indication of the GDP-mannose content where two moles of NAD^+ are reduced per mole of GDP-mannose. This experiment was performed in microtiter plates. The standard assay buffer consisted of 50 mM Tricine buffer (pH 8.75), 1 mM NAD^+ and 0.5 mM GDP-mannose. Purified 10His-AlgD (~30 µg) was applied in assay buffer. The enzymatic reaction was performed at room temperature for 5 min. The absorbance (OD_{340}) corresponding to the increase in NADH concentration was measured using an Ultra Microplate Reader (Bio-Tek Instruments, Inc.). Reading the absorbance was carried out at 2 min intervals for 120 min. All assays were performed in triplicate and repeated twice. To fully stop the reaction, samples were incubated at 45 °C for 15 min.

Analysis of the product of *in vitro* enzymatic activity of AlgD

Samples obtained from *in vitro* enzymatic assessment were cleared by centrifugation for 5 min at 15,000 × *g* before applying in High Performance Liquid Chromatography (HPLC). HPLC was performed using PhenoSphere^{TM} 5 µm SAX 80 A˚, LC Column 250 × 4.6 mm. Running buffers included buffers A and B containing 10 mM NaH_2PO_4 (pH 3.0) and 750 mM NaH_2PO_4 (pH 3.7), respectively. Flow rate was 0.75 ml min^{-1} and the buffered system was set as $t_{0\ min}$ 3% B; t_{25min} 40% B; $t_{33\ min}$ 75% B; $t_{35\ min}$ 75% B; $t_{36\ min}$ 3% B. The enzymatic assay was stopped by applying 100 mM NaH_2PO_4 (pH 3). A UV

absorbance at 254 nm was recorded with a photodiode array (Thermo Scientific Dionex Ultimate 3000) and analysed with the Chromeleon v6.80 Software.

Furthermore, mass spectrometry (MS) was performed to detect the product of enzymatic activity of AlgD i.e. GDP-mannuronic acid. To prepare samples for MS analysis, the salt was removed from sample presumably containing GDP-mannuronic acid by using a Solid Extraction Column (SPE) (Thermo Scientific^{TM} HyperSep^{TM} Hypercarb^{TM}). This cartridge was manufactured as 200 mg/ 3 ml with 30 µm spherical particles of 100 % porous graphitic carbon (PGC). The following steps were used for desalting and separation of the sample: Continuing step; 1 ml of 80% acetonitrile and 0.1% TFA, Equilibrating step; 3 ml of MQ water, Loading Step; 2 ml of sample, washing step; 2 ml of MQ Water, Elution step; 2 ml of 50 % acetonitrile. A 3 µL sample was injected into an Agilent 1200 liquid chromatography system on bypass mode coupled to an Agilent 6520 quadrupole time of flight (Q-TOF) mass spectrometer with dual ESI source and internal calibration ions (Agilent Technologies, Germany). The sample was delivered in 0.1% formic acid/50% MeCN/water @ 0.2 ml/ min. The optimized ESI source parameters were: nitrogen flow of 6.0 L/min, a gas temperature of 300 °C, a neubulizer spray pressure of 30 psi, positive polarity, a capillary voltage of 3.3 kV, a fragmentator voltage of 155 V and a skimmer voltage of 55V. Ions generated by ESI were recorded in profile mode over a mass-to charge range of 100-1,000 *m/z* and analysed using Agilent MassHunter Workstation Qualitative Analysis software version B.06.00 SP1 with Bioconfirm add-on (Agilent Technologies, Germany).

In vivo assessment of enzymatic activity of AlgD

To assess AlgD activity *in vivo*, whole cells lysates of transformants were prepared similarly to the procedure used for isolation of cytoplasmic protein (above). The protein concentrations were determined by the Bradford protein assay (110, 111). The assay was performed in 96-well microtiter plates. The reaction buffer consisted of 50 mM Tricine buffer (pH 8.75), 0.5 mM GDP-mannose and whole cell lysate of samples after protein content had been determined. After 10 min at room temperature, the reaction was measured at OD_{340} using an Ultra microplate reader (Bio-Tek Instruments, Inc.) to find initial absorbance. Then, 2 mM NAD^+ which was absent in blanks was added to initiate reactions followed by reading the absorbance at 10 min intervals for 170 min. All assays were performed in triplicate and repeated twice.

Isolation of membrane proteins

To confirm the localization of Alg8 and Alg44 in the membrane of *E. coli* and *B. megaterium* strains, the cytoplasmic membrane fraction was isolated as described previously with some modifications (231). Overnight LB liquid culture of *E. coli* and *B. megaterium* transformants (Figure S1 and Table S3) harbouring the generated constructs or empty vector were subcultured in 500 ml of LB media. Cells were harvested by centrifugation at 8,000 × *g* at 4 °C for 20 min. Cells were washed twice within 10 mM HEPES (pH 7.4) and sediments were subjected to enzymatic lysis by suspending in cold lysis buffer (20% cell) containing 10 mM HEPES, 150 mM NaCl (pH 7.4), 0.5 mg ml^{-1} DNase I, 0.5 mg ml^{-1} RNase A, 0.5 mg ml^{-1} lysozyme and cOmplete™ EDTA-free Protease Inhibitor Cocktail. Cell lysis was carried out on ice for 30 min followed by sonication on ice for 12 cycles (15 s on/off intervals). Cell debris were removed and supernatants were then ultra-centrifuged at 60,000 × *g* at 4 °C for 1 h. Supernatants containing the cytoplasmic fraction were discarded immediately. Sediments containing the envelope fraction (inner membrane, outer membrane, and associated proteins) were used immediately or stored at 80 °C for future analysis. To purify inner and outer membrane proteins, envelope pellet was suspended in the same buffer with 0.7% (w/v) *N*-lauroylsarcosine and was incubated on a horizontal shaker with gentle agitation for 1.5 h at 4 ˚C in order to selectively solubilize the cytoplasmic membrane fraction. The mixture was then ultra-centrifuged under the same condition used previously. The outer membrane sediment was expected to be clear, and if the sediment was still red/brown (cytoplasmic membrane contamination) a second solubilization step was applied. Aliquots of the remaining supernatant containing the cytoplasmic membrane fraction were prepared and stored at -80 ˚C. The resulting outer membrane protein sediment was suspended in 50-100 µl HEPES buffer (10mM, pH 7.4). Proteins were analyzed using SDS-PAGE (10% acrylamide gels) and immunoblotting utilizing anti-his tag antibody.

Alginate purification and quantification

A total of 2 ml of bacterial overnight cultures grown in LB medium supplemented with appropriate antibiotic were harvested and washed twice with saline solution. Harvested cell pellets were re-suspended in 1 ml of saline solution and then normalized to OD_{600} = 3.0. A 200 μl aliquot of cell suspension was plated onto each PIA medium (with three

replicates) containing 300 μg ml^{-1} of gentamicin and incubated at 37 °C for 72 h (this is an optimum incubation time to avoid nutritional stress on alginate production). The cells on each plate were scraped off and suspended and agitated in saline solution until all alginate materials were completely dissolved. Centrifugation at 8,000 × *g* at 4 °C for 20 min was applied to separate cells from alginate-containing supernatant. Solubilized alginates in supernatants were precipitated with an equal volume of ice-cold isopropanol. Additionally, cellular sediments were freeze-dried and the final weights were determined. The alginate precipitants were freeze-dried and weighed. Then they were re-dissolved to a final concentration of 0.5% (wt/vol) in 50 mM Tris-HCl (pH 7.4) containing 10 mM $MgCl_2$ followed by incubation with 15 μg ml^{-1} DNaseI and 15 μg ml^{-1} RNaseI at 37 °C for 6 hrs. Then, Pronase E was added to a final concentration of 20 μg ml^{-1} and incubated for a further 18 h at 37 °C. Alginate solutions were dialyzed (12-14 kDa MWCO, ZelluTrans/Roth mini dialyzer, Carl Roth GmbH & Co) against 5 l of ultrapure H_2O for 48 h. Finally, alginates were precipitated with an equal volume of ice-cold isopropanol and freeze-dried and weighed for uronic acid assay and biochemical analysis.

Alginate quantification was performed via uronic acid assay (97) and purified alginic acid from brown algae (Sigma-Aldrich) was used as a standard. Briefly, alginate samples were dissolved in 200 μl of ultrapure water at concentrations between 0.25 and 0.05 mg ml^{-1}. Each sample was mixed with 1.2 ml of tetraborate solution (0.0125 M disodium tetraborate in concentrated sulfuric acid) and incubated on ice for 10 min followed by incubation at 100 °C for 5 min and then cooled down on ice for further 5 min. By adding 20 μl of 3-phenylphenol reagent (0.15% of 3-phenylphenol in 0.125 M NaOH), reactions were developed within 1 min of vortexing. For each sample and dilution a negative control was assayed using 0.125 M NaOH instead of the 3-phenylphenol reagent. Uronic acid concentrations were determined spectrophotometrically at a wavelength of 520 nm.

Osmotic shock to prepare periplasmic fractions.

In all treatments, cells were grown on LB solid medium at 37 °C with appropriate antibiotic and supplemented with 3% D-Mannose, 3% D-fructose and 1 mM IPTG and culture was grown at 37 °C for 4 days. The cells on each plate were scraped off and suspended in 20 mM Tris-HCl (pH 7.5) and incubated on a rocker at room temperature for 30 min. Centrifugation at 4,000 × *g* was performed at 4 °C for 10 min. Extracellular supernatants were taken as a sample to use in ELISA. Cells were washed three times with

20 mM Tris-HCl (pH 7.5). The cell pellet was gently resuspended in 1 ml TSE buffer containing 20% w/v sucrose, 20 mM Tris-HCl (pH 7.5) and 0.5 mM EDTA and then incubated on ice for 10 min. After centrifugation at 12,000 × *g* at 4 ºC for 10 min, cell pellets were resuspended by pipetting in a 500 µl to 1000 µl of TSE buffer and were incubated on ice for an additional 10 min followed by centrifugation under the same conditions. The supernatant from the last step contained the periplasmic fraction (232).

Enzyme-linked immunosorbent assay (ELISA) reagents and procedure.

We used periplasmic fractions in TSE buffer and extracellular supernatants in 20 mM Tris buffer to assess alginate production. Two series of samples were used for performing this experiment. One series was used in uncoated medium binding ELISA plates and another series was used in Poly-L-Lysine (Sigma) coated plates. Stock solution was prepared by dissolving 100 mg of Poly-L-Lysine in 100 ml water and filter sterilized through a 0.22 micron filter. One part of stock solution was mixed with 19 parts water to prepare 50 µg ml^{-1} working solution equilibrated at room temperature before application (18-26 °C). ELISA plates were filled with working solution and were incubated for 1 h at 37 °C, and then Poly-L-Lysine solution was removed and rinsed three times with PBS buffer or sterile water.

A 200 µl aliquot of each sample containing proteins from transformants was added to the ELISA plates which were then incubated at 4 °C overnight. The plates were washed with 0.04 M phosphate buffer with 0.05% Tween 20 three times. A 1:100 dilution of affinity-purified rabbit antibody raised against alginate (233) was added and incubated at 37 °C for 3 h and washed under the same conditions. A 1:3,000 dilution (200 µl) of goat anti-rabbit IgG was used for each well. Incubation was performed at 37 °C for 2 h. The ELISA plates were washed with washing buffer and 200 µl of OPD Peroxidase Substrate (SIGMA*FAST* OPD) was added. Absorbance was measured at 492 nm after 60 min by adding 0.5 M H_2SO_4. Then, the average optical density for samples with three replicates was analysed (234).

Enzymatic *in vitro* alginate synthesis (Assessment of Alg8 and Alg44 activity *in vitro* alginate synthesis).

Crude extracts, envelope fractions and inner membrane fractions were used as sources of alginate polymerase activity. These fractions were obtained as described previously from liquid (*E. coli* cells was grown at 37 °C for 6 h and *P. aeruginosa* cells was grown at 37 °C for 18 h) and solid media (culture was grown at 37 °C for 4 days) separately. *E. coli* cells were grown on LB medium at 37 °C with appropriate antibiotic and supplemented with 3% D-Mannose, 3% D-fructose and induction was done by 1 mM IPTG.

To confirm the activity of Alg8 and Alg44 leading to *in vitro* alginate polymerization, whole cell lysate, envelope fraction and inner membrane of transformants were prepared. A 200 µl aliquot (final volume) of reaction buffer contained 2.5 mg of crude protein for each sample (in 50 mM Tris-HCl buffer (pH 8.0), Roche cOmplete protease inhibitor EDTA-free, 0.1% (vol/vol) Triton X-100 and 2 mM dithiothereitol), 70 µg alginate oligomers (n: 4) (were obtained by acid hydrolysis as previously described (235)), 130 pmol c-di-GMP. To start the polymerization process, in one series of enzymatic steps was established by adding 0.5 mM GDP-mannose, AlgD (31 µg/µL), 2 mM NAD^+, 50 mM Tris-HCl (pH 8), 10 µM $MgCl_2$ to generate GDP- mannuronic acid. In another series, GDP-mannuronic acid (1 µg for 200 µl reaction buffer) purified by HPLC was added to uncoated ELISA plates. The reaction was left for 2 h at 30 °C. Strains harbouring empty vectors were used as negative controls. The ELISA procedure was then carried out as above mentioned.

RESULTS

Production of the recombinant proteins required for establishing alginate biosynthesis in heterologous hosts

Our strategy for establishing the enzymatic steps required for alginate biosynthesis in heterologous hosts relied on two plasmid systems compatible with *E. coli* and *B. megaterium.* In order to establish the cytoplasmic enzymatic steps leading to GDP-mannuronic acid production (precursor) (Figure 1), the genes encoding AlgA (phosphomannose isomerase (PMI)/Guanosine diphosphate (GDP)-mannose pyrophosphorylase (GMP/GDP-MP)), AlgC (phosphomannomutase (PMM)), and AlgD (GDP-mannose 4, 6-dehydrogenase (GMD)) were carried on pMCS69 or pT7 plasmids (Figure 3A and 4A). As expected, proteins produced from plasmids catalyze conversion

of fructose-6-phosphate to GDP-mannuronic acid through four enzymatic steps where the activity of AlgD at the last step (Figure 1) irreversibly leads to precursor production. Our analysis using available databases showed that the production of fructose-6-phosphate naturally occurs in *E. coli* and *B. megaterium* derived from TCA cycle.

Alginate polymerization is mediated by two membrane anchored and interacting proteins Alg8 (polymerase) and Alg44 (co-polymerase) where binding c-di-GMP to the cytoplasmic PilZ domain of Alg44 is required for activation of polymerization (Figure 2). Therefore, genes encoding Alg8 and Alg44 were transferred into the cells using pET-14b or pPT7 plasmids (Figure 3B, 3C and 4B, 4C). Previous studies proved that membrane anchored MucR (c-di-GMP synthesizing) positively regulated alginate production presumably by generating a c-di-GMP pool in the proximity of alginate polymerase (Figure 2). Therefore, *mucR* was co-inserted with the other genes into pMCS69 or pT7 plasmids (Figure 3A and 4A). Establishment of alginate production in Gram-negative heterologous hosts (i.e. *E.coli* strains) were thought to require alginate-secreting protein AlgJ originating from *A. vinelandii* (homologous to AlgE in *P. aeruginosa*) (Figure 2). Therefore, the gene encoding *algJ* was co-inserted with other genes into pMCS69 (Figure 3A). These genes in a two-plasmid system were transferred into various strains of *E. coli* and *B. megaterium* and induction of gene expression was performed (see Materials and Methods).

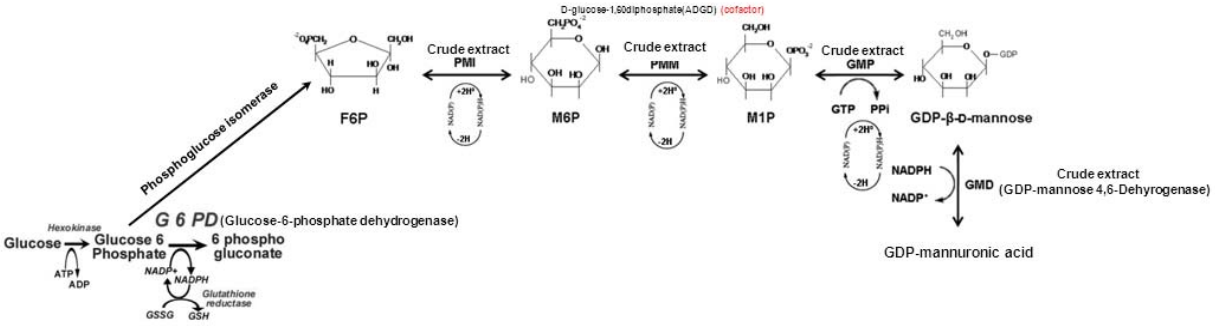

FIG. 1 Schematic enzymatic pathway leading to alginate precursor production

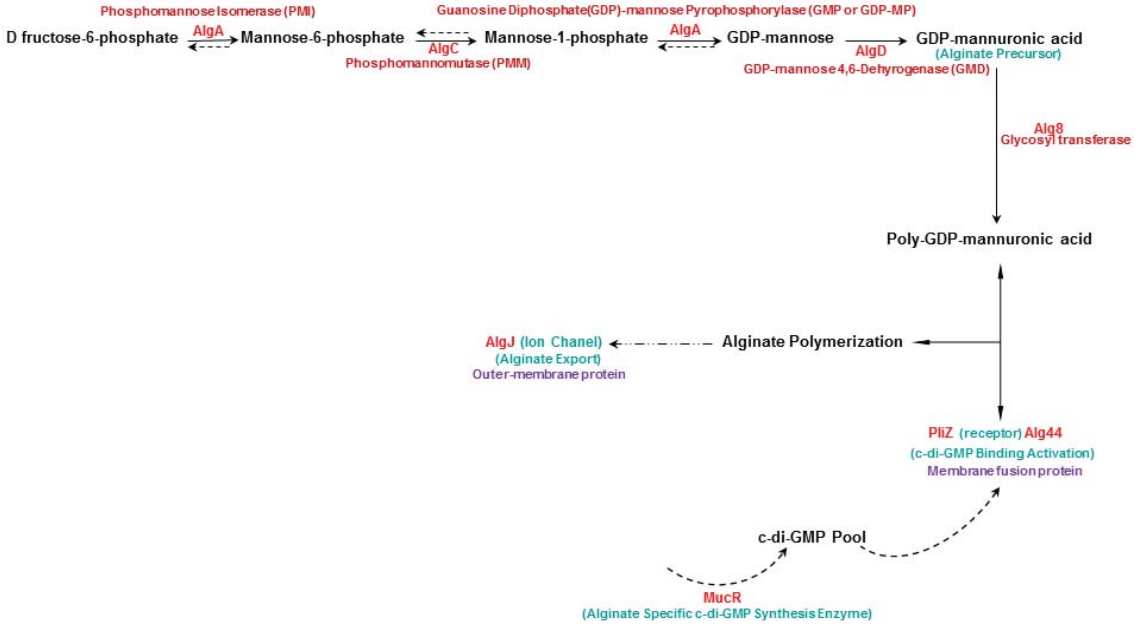

FIG. 2 Schematic minimal requirements for establishing alginate biosynthesis pathway in heterologous hosts

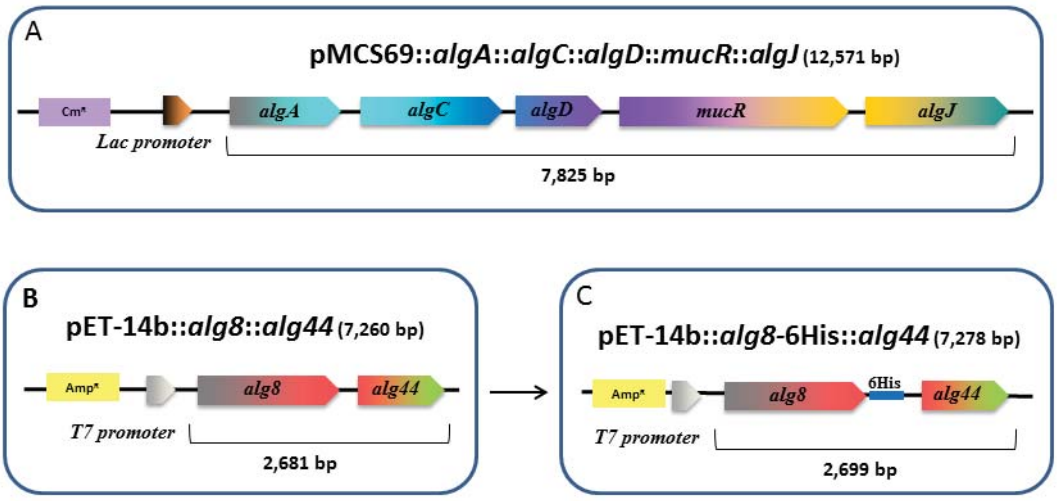

FIG. 3 Two-plasmid system for tailor-made production of alginate polysaccharide in *E. coli* strains. Two-plasmid system consisted of co-expression of pMCS69::*algA*::*algC*::*alg*::*mucR*::*algJ* (A), pET-14b::*alg8*::*alg44* (B). (C) pET-14b::*alg8*-6His::*alg44* was generated and applied to detect Alg8 transcriptionally fused with hexahistidine-tag at the C-terminal. Promoters and antibiotic resistance cassettes are labelled.

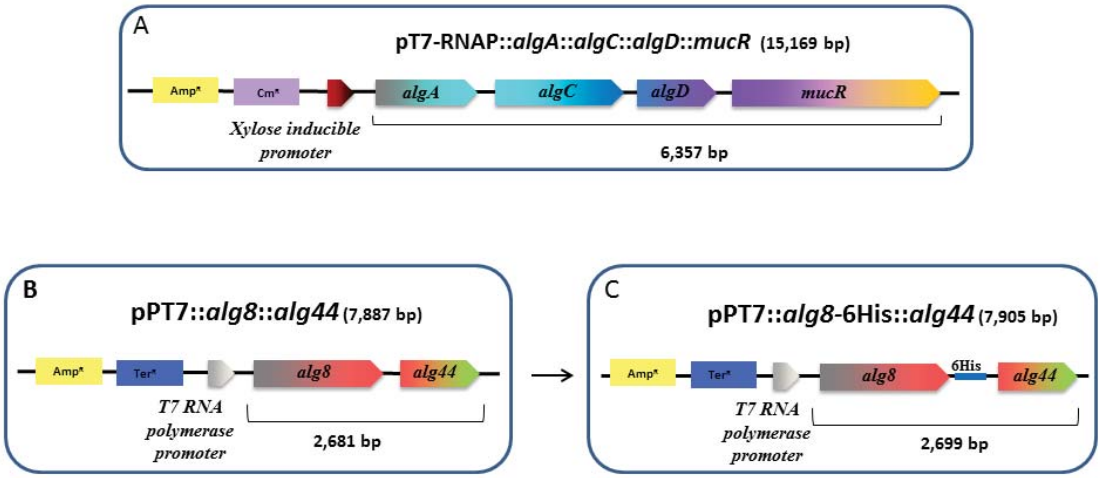

FIG. 4 Two-plasmid system for tailor-made production of alginate polysaccharide in *B. megaterium.* Two-plasmid system consisted of co-expression of pT7-RNAP::*algA*::*algC*::*algD*::*mucR* (A), pPT7::*alg8*::*alg44* (B). (C) pPT7::*alg8*-6His::*alg44*was generated and applied to detectAlg8 transcriptionally fused with hexahistidine-tag at the C-terminal. Promoters and antibiotic resistance cassettes are labelled.

Production of proteins and their localization in the cytoplasmic or membrane fractions of various strains as analyzed using immunoblotting. According to theoretical molecular weights and comparison with applied negative controls, our results showed that AlgA and AlgD were produced in *E. coli* Rosetta 2 and ClearColi®BL21 (DE3) harbouring pET-14b::*alg8*::*alg44* and pMC569::*algA*::*algC*::*algD*::*mucR*::*algJ* (Figure 5 and 6). However, production of AlgC was confirmed in *E. coli* ClearColi®BL21 (DE3) (pET-14b::*alg8*::*alg44* and pMC569::*algA*::*algC*::*algD*::*mucR*::*algJ*) (Figure 7), while its detection in *E. coli* Rosetta 2 was uncertain due to masking by unspecific bands on immunoblots; therefore the possibility of its production in this strain cannot be ruled out.

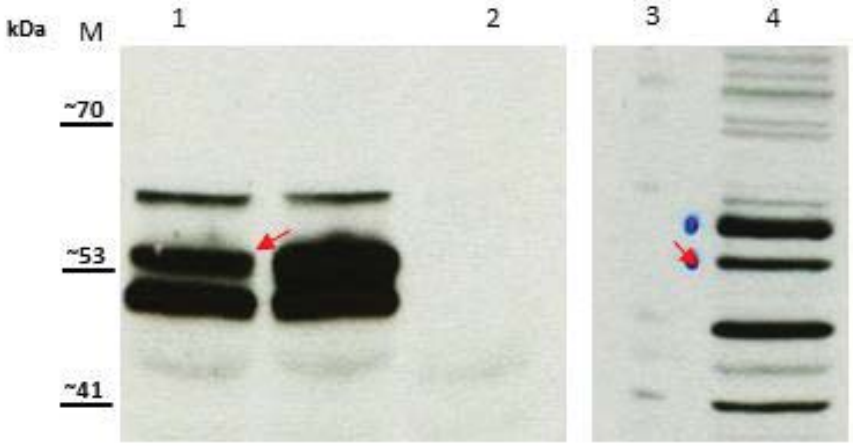

FIG. 5 Western blot analysis to assess production of AlgA protein (55.7 kDa) in a heterologous host. Immunoblotting using anti-AlgA antibody was applied to detect AlgA protein in the cytoplasmic fraction of *E. coli* Rosetta 2 or ClearColi®BL21 (DE3) harbouring pET-14b::*alg8*::*alg44* and pMC569::*algA*::*algC*::*algD*::*mucR*::*algJ*. The processed immunoblots showed a band corresponding to molecular weight of AlgA produced by *E. coli* Rosetta 2 fraction (lane 1) and ClearColi®BL21 (DE3) (lane 4). These bands were not detected in negative controls i.e. *E. coli* Rosetta 2 (pET-14band pMC569) (lane 2) and ClearColi®BL21 (DE3) (pET-14band pMC569) (lane 3). M, molecular weight (GangNam-STAIN™ Prestaine, iNtRON Biothechnology).

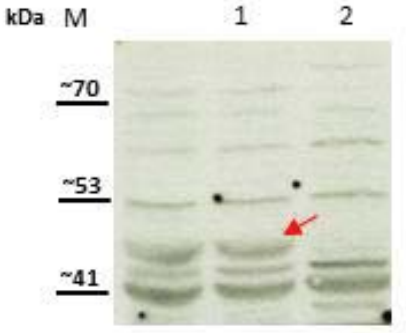

FIG. 6 Western blot analysis to assess production of AlgD protein (50.5 kDa) in a heterologous host. Immunoblotting using anti-AlgD antibody was applied to detect AlgD protein in the cytoplasmic fraction of *E. coli* Rosetta 2 harbouring pET-14b::*alg8*::*alg44* and pMC569::*algA*::*algC*::*algD*::*mucR*::*algJ*. Processed immunoblots showed a band corresponding to the molecular weight of AlgD produced by *E. coli* Rosetta 2 (lane 1) which was not detected in the negative control i.e.*E. coli* ClearColi®BL21 (DE3) (pET-14band pMC569) (lane 2). M, molecular weight (GangNam-STAIN™ Prestaine, iNtRON Biothechnology).

FIG. 7 Western blot analysis to assess production of AlgC protein (55.5 kDa) in a heterologous host. Immunoblotting using anti-AlgC antibody was applied to detect AlgC protein in the cytoplasmic fraction of *E. coli* ClearColi®BL21 (DE3) harbouring pET-14b::*alg8*::*alg44* and pMC569::*algA*::*algC*::*algD*::*mucR*::*algJ*. Processed immunoblots showed a band corresponding to molecular weight of AlgC produced by *E. coli* ClearColi®BL21 (DE3) (lane 1). This band was not detected in the negative control i.e. *E. coli* ClearColi®BL21 (DE3) (pET-14band pMC569) (lane 2). M, molecular weight (GangNam-STAIN™ Prestaine, iNtRON Biothechnology).

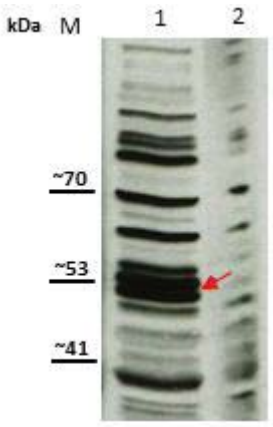

In vitro enzymatic assessment of AlgD activity for production of GDP-mannuronic acid.

Irreversible production of GDP-mannuronic acid as the alginate precursor by AlgD is the last product of the cytoplasmic enzymatic steps essential for establishment of alginate production in a heterologous host. We thought that detection of GDP-mannuronic acid in heterologous strains harboring recombinant constructs was an appropriate indicator for verifying the activity of AlgD and other preceding enzymes i.e. AlgA and AlgC as well as establishment of alginate precursor production. To this end, we attempted purifying

AlgD and establishing *in vitro* synthesis of GDP-mannuronic acid. Recombinant 10His-AlgD produced in *E. coli* BL21 (DE3) (pET-14b::10His-*algD*) was purified under native (non-denaturing) conditions using His-affinity chromatography (Figure 8).

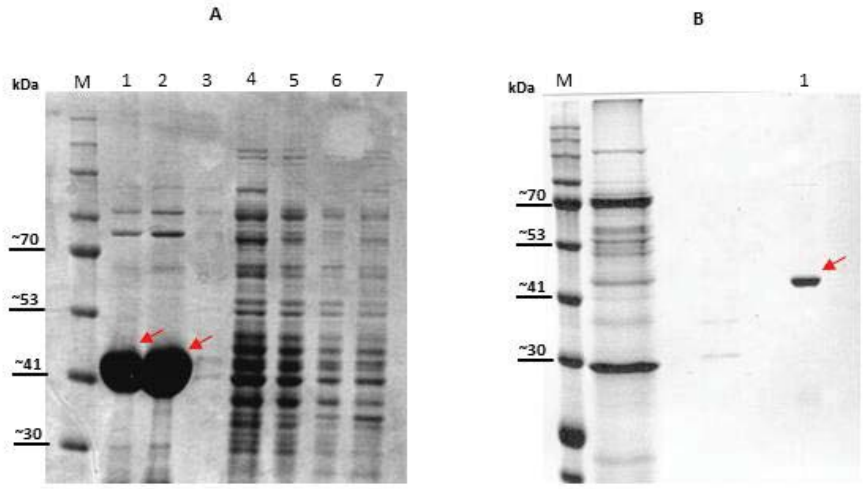

FIG. 8 Recombinant production and purification of AlgD. A, SDS- PAGE (10 % acrylamide gel) stained with Coomassie Brilliant Blue R250 showed protein profiles belonging to various fractions obtained through different steps of purification of 10His-AlgD under native conditions. This protein was produced in *E. coli* BL21 (DE3) harbouring pET-14b::10His-*algD.*; Lanes 1and 2 show the presence of partially purified 10His-AlgD (48.9 kDa) (93 µg and 155 µg of purified sample were loaded in lanes 1 and 2 respectively); other lanes include: second wash step (Lane 3), first wash step (Lane 4); first flow through after loading sample (Lane 5), whole cells lysate of *E. coli* BL21 (DE3) (pET-14b::*10His-algD*) (Lane 6)*;* whole cells lysate of *E. coli* BL21 (DE3)(pET-14b) (lane 7); B, Lane 1, 3 µl of purified his-tagged AlgD (48.9 kDa). M, molecular weight standard (GangNam-STAIN™ Prestaine, iNtRON Biothechnology).

For monitoring enzymatic activity of AlgD, the procedure described by Tenhaken et al was followed (230) with some modifications. In this procedure, catalytic activity of AlgD to convert irreversibly GDP-mannose to GDP-mannuronic acid coincides with generation of NADH by reducing NAD^+. Therefore, increasing NADH concentration during enzymatic reaction corresponds to the progression of enzymatic activity of AlgD that is measurable at 340 nm (Figure 9).

Figure 9 show the kinetics of AlgD activity, with A_2 and A_3 displaying an increase in NADH concentration over 100 min corresponding respectively to the addition of different concentrations of 10His-AlgD to the reaction buffer. Applying 108.5 µg of 10His-AlgD resulted in an approximately three-fold increase in the absorbance compared to the

addition of 38.7 µg of this protein. Over time, using GDP-mannose in an irreversible reaction, the absorbance increased slowly.

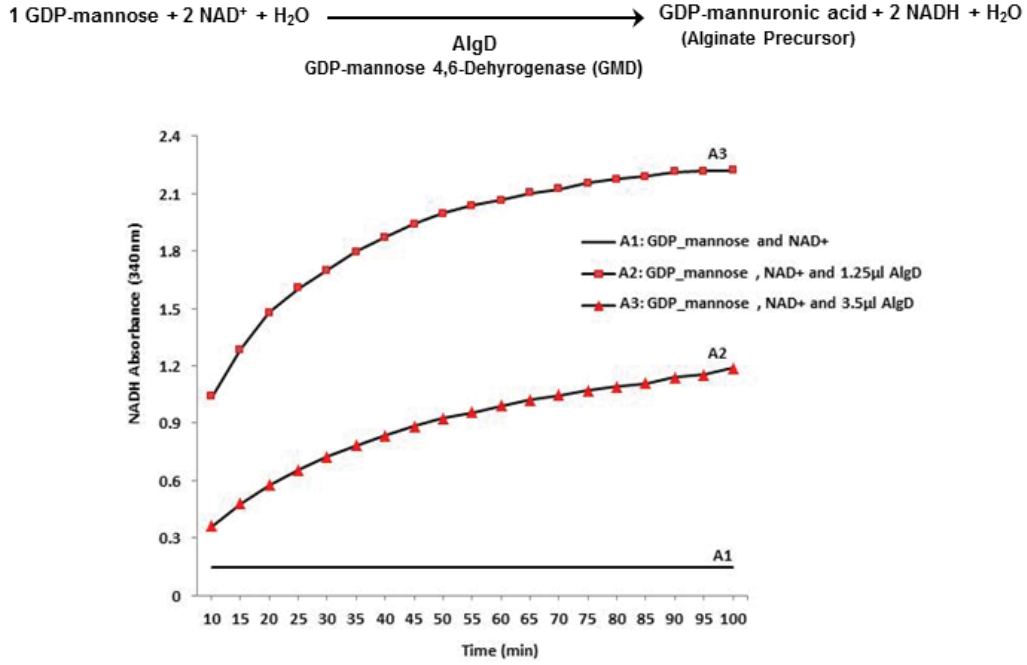

FIG. 9 *In vitro* enzymatic assessment of 10His-AlgD.Top side of figure explains enzymatic activity of AlgD and required elements for synthesis of GDP-mannuronic acid. Graph shows kinetics of purified 10His-AlgD activity *in vitro*. Absorbance at 340 nm corresponds to concentration of NADH produced from reducing NAD required for conversion of GDP-mannose to GDP-mannuronic acid catalysed by AlgD. A1 sample contained NAD+, GDP-mannose and NAD^+; A2 sample included GDP-mannose, NAD^+ and 38.7 µg of AlgD; and A3 sample contained GDP-mannose, NAD^+ and 108.5 µg of 10His-AlgD.

Furthermore, *in vitro* enzymatic activity of 10His-AlgD and production of GDP-mannuronic acid were verified using HPLC (Figure 10). Initially, samples containing commercial GDP-mannose and/or NAD^+ were injected into HPLC column and corresponding peaks were detected respectively at 23 min and 8 min (Figure 10). A 10His-AlgD-containing sample was incubated for 120 min followed by deactivating the enzymatic reaction at 45 ˚C for 15 min. The chromatogram of this assay showed detection of two new peaks belonging to generation of NADH (at 22.5 min) and GDP-mannuronic acid (at 36.2 min) as the products of AlgD activity (Figure 10 C).

Verification of GDP-mannuronic acid production was further pursued by performing purification based on solid phase extraction on surfaced conditioned porous graphitic carbon. The salt-free extract was then analyzed by HPLC as mentioned above. This

analysis showed that GDP-mannuronic acid purified via this method underwent a shift in retention time detected at 28.2 min. This retention time shift was probably due to the influence of reducing and oxidizing agent on the carbon surface of cartridges. The increase of retention time following acid or oxidative treatment may be explained by the exposure or generation of charged groups (236-238). The concentration of GDP-mannuronic acid was calculated as 0.708 mM.

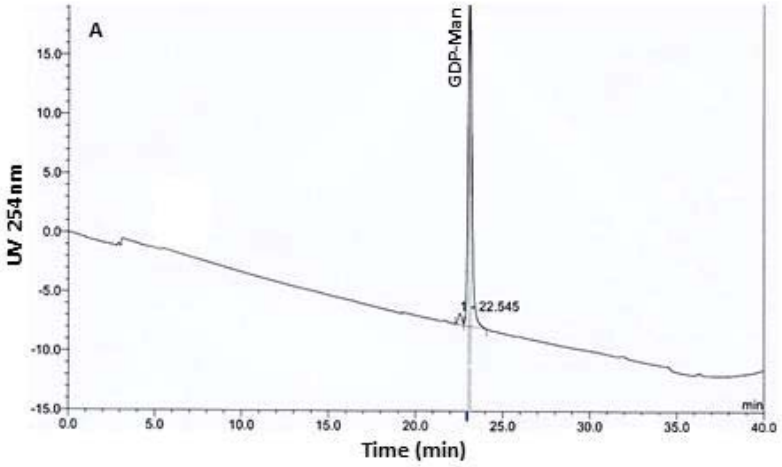

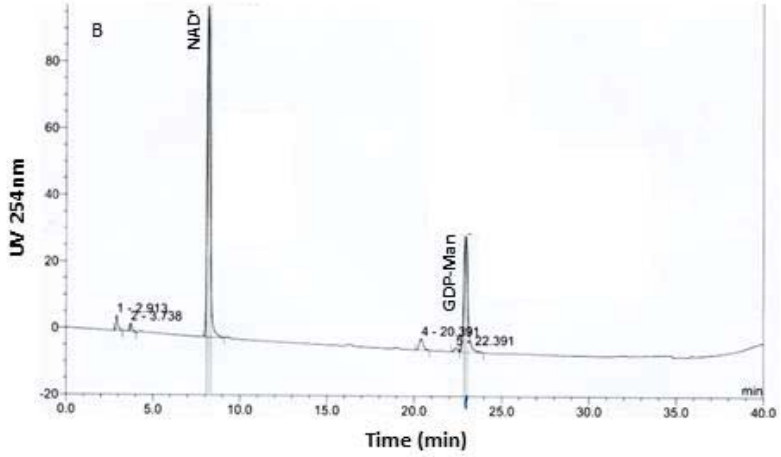

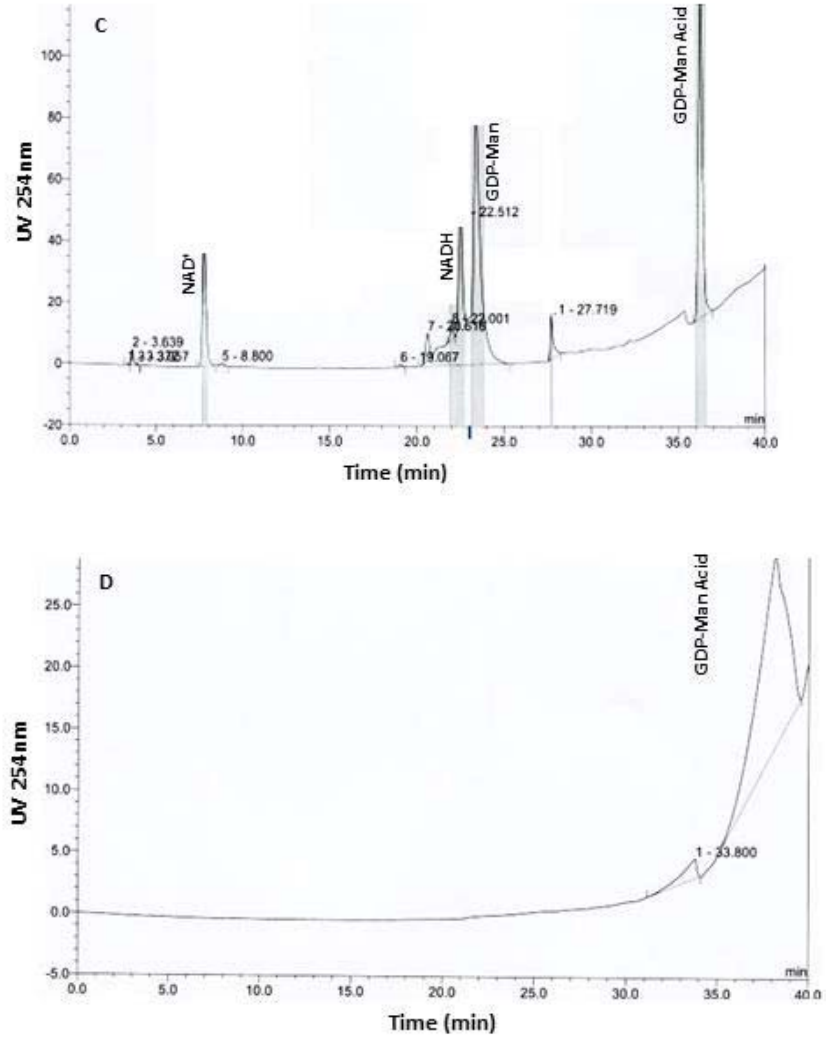

FIG. 10 HPLC based-verification of *in vitro* activity of 10His-AlgD and GDP-mannuronic acid production. A, Peak detected at 23 min represents GDP-mannose (0.5 mM)); B, the mixture of NAD^+ (1 mM) and GDP-Mannose (0.5 mM) was analyzed and respective peaks were respectively detected at 8 and 23 min; C, The chromatogram shows HPLC analysis of a sample containing AlgD, GDP-Mannose (0.5 mM), NAD^+ (1 mM) (incubated for 120 min followed by deactivating enzymatic reaction); D, The chromatogram of purified GDP-mannorunic acid after desalting using SPE cartridges.

Mass spectrometry

As described in the previous step, the HPLC fractions containing GDP-mannuronic acid and desalted via solid phase extraction (on graphic column) were subjected to mass spectrometry to detect peaks corresponding to GDP-mannuronic acid (Figure 11). The peaks representing the molecular mass of GDP-mannuronic acid molecule and GDP-mannuronic acid molecule with sodium salt were identified (Figure 11).

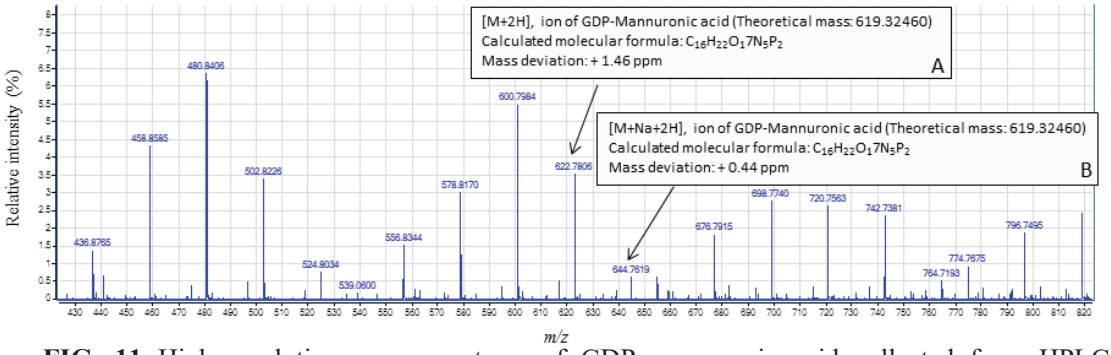

FIG. 11 High resolution mass spectrum of GDP-mannuronic acid collected from HPLC fractionation followed by desalting using solid-phase column. Analysis was performed in a mass range of *m/z* 400-850, applying positive ionization.

Enzymatic assessment of AlgD activity in whole cell lysates

In this experiment the activity of AlgD produced in heterologous hosts was assessed. Heterologous hosts with two-plasmid systems included various strains of *E. coli* harbouring pMCS69::*algA*::*algC*::*algD*::*mucR*::*algJ* and pET-14b::*alg8*::*alg44* and *B. megaterium* YYBm1 harbouring pT7-RNAP::*algA*::*algC*::*algD*::*mucR* and pPT7::*alg8*::*alg44*. Also, the same strains with empty vectors were used as negative controls. All transformants were subjected to IPTG induction and preparation of whole cell lysates (see Materials and Methods). Also, whole cell lysate of *E. coli* BL21 (DE3) (pET-14b::10His-*algD*) and *E. coli* BL21 (DE3) (pET-14b) were used respectively as positive and negative controls because the activity of 10His-AlgD purified from *E. coli* BL21 (DE3) (pET-14b::10His-*algD*) had been confirmed in previous experiments (Fig. 10). An additional control for this experiment (or blank) was to exclude NAD^+ from samples.

Whole cell lysates that had been quantified for protein (see figure legends) were added to reaction buffers and absorbance (340 nm) of samples was measured corresponding to the

concentration of NADH as an indicator for the conversion of GDP-mannose to GDP-mannuronic acid by reducing NAD^+.

Addition of whole cell lysate of ClearColi®BL21 (DE3) (pMCS69::*algA*::*algC*::*algD*::*mucR*::*algJ* and pET-14b::*alg8*::*alg44*) to reaction buffer containing GDP-mannose (0.5 mM) and NAD^+ resulted in increasing NADH concentration over 170 min (measured at 10 min intervals), while excluding NAD^+ from these samples and including whole cell lysates of cells with empty vectors did not result in increasing absorbance, indicating AlgD displayed activity when produced in such a heterologous host (Figure 13).

Similar results were obtained during assessing the activity of AlgD produced in *E. coli* Rosetta 2 (DE3) using the above mentioned two-plasmid system where the absorbance of NADH showed an increasing trend over time, indicating the conversion of GDP-mannose to GDP-mannuronic acid mediated by the catalytic activity of AlgD (Figure 14). Enzymatic assessment of whole cell lysates of *E. coli* Origami B (DE3) (pMCS69::*algA*::*algC*::*algD*::*mucR*::*algJ* and pET-14b::*alg8*::*alg44*) and *B. megaterium* YYBm1(pMCS69::*algA*::*algC*::*algD*::*mucR*::*algJ* and pET-14b::*alg8*::*alg44*) showed steadily increasing trend in absorbance of NADH compared to negative controls (Figures 15 and 16). However, when the Origami B (DE3) sample was compared with Rosetta 2 (DE3) sample (both containing 2.0 µg $µl^{-1}$ of protein content) AlgD activity originating from Origami B (DE3) displayed much lower efficacy as maximum absorbance (340 nm) at 170 min (T170) was < 0.45.

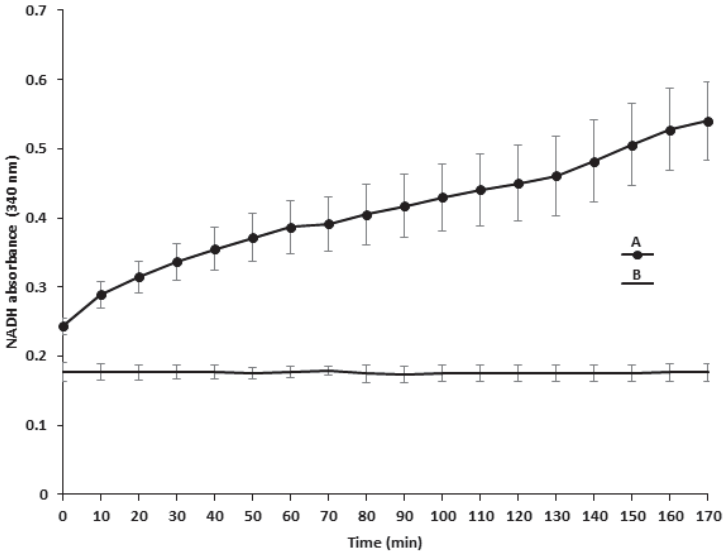

FIG. 12 Enzymatic assessment of AlgD activity in whole cell lysates of *E. coli* BL21 (DE3) (pET-14b::10His-*algD*). Time 0 (T0) corresponds to the first absorbance (340 nm) of NADH that was measured 10 min after mixing reaction buffer. Reaction buffer contained 50 mM Tricine, 0.5 mM GDP-mannose, and 0.5 µg μl^{-1} of protein content of whole cell lysates, incubated at room temperature. A, Measured absorbances of NADH over time after adding NAD^+ to the samples. B, Measured absorbances of NADH over time in samples without NAD^+. The absorbance was measured at 10 min intervals over 170 min. Values and error bars represent the averages and standard deviations from two independent experiments, each with three replicates.

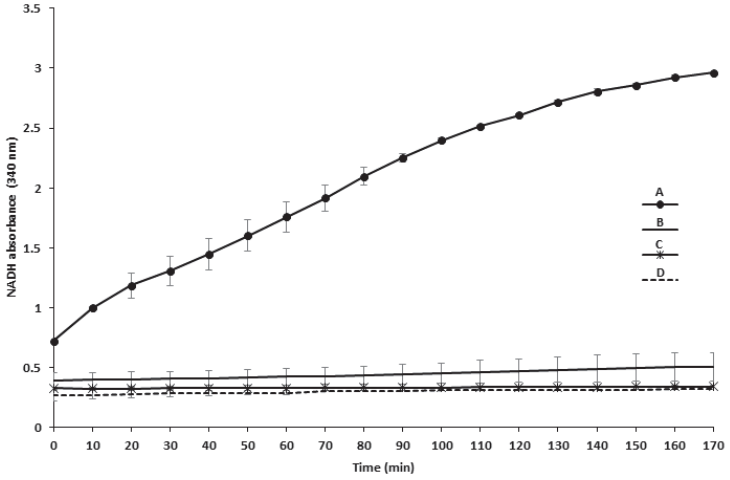

FIG. 13 Enzymatic assessment of AlgD activity in whole cell lysate of *E coli* ClearColi®BL21 (DE3) (pMCS69::*algA*::*algC*::*algD*::*mucR*::*algJ* and pET-14b::*alg8*::*alg44*). Time 0 (T0) corresponds to the first absorbance (340 nm) of NADH that was measured 10 min after mixing reaction buffer. Reaction buffer contained 50 mM Tricin, 0.5 mM GDP-mannose, and 3.0 µg μl^{-1} of protein content of whole cell lysates, incubated at room temperature. A, Measured absorbances of NADH over time after adding NAD^+ to the samples containing whole cells lysate of ClearColi®BL21 (DE3) harbouring two-plasmid system. B, Measured absorbances of NADH over time without NAD^+ in samples containing whole cells lysate of ClearColi®BL21 (DE3) harbouring two-plasmid system. C, Measured absorbances of NADH over time after adding NAD^+ in samples containing whole cells lysate of ClearColi®BL21 (DE3) harbouring empty vectors. D, Measured absorbances of NADH over time without NAD^+ in samples containing whole cells lysate of ClearColi®BL21 (DE3) harbouring empty vectors. The absorbance was measured at 10 min intervals for 170 min. Values and error bars represent the averages and standard deviations from two independent experiments, each with three replicates.

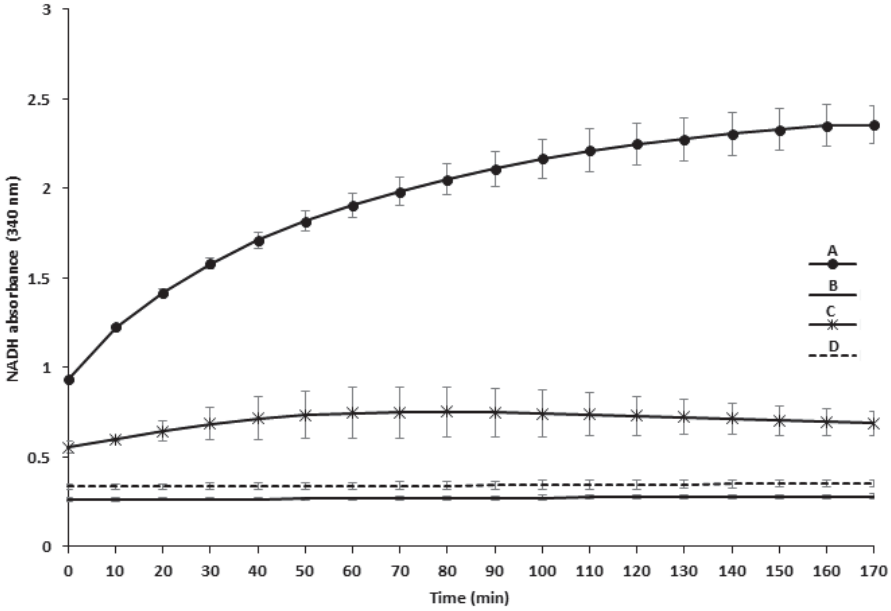

FIG. 14 Enzymatic assessment of AlgD activity in whole cell lysate of *E. coli* Rosetta2 (DE3) (pMCS69::*algA*::*algC*::*algD*::*mucR*::*algJ* and pET-14b::*alg8*::*alg44*). Time 0 (T0) corresponds to the first absorbance (340 nm) of NADH that was measured 10 min after mixing reaction buffer. Reaction buffer contained 50mM Tricine, 0.5 mM GDP-mannose, and 2.0 μg μl^{-1} of protein content of whole cell lysates, incubated at room temperature. A, Measured absorbances of NADH over time after adding NAD^+ in the samples containing whole cells lysate of Rosetta 2 (DE3) harbouring two-plasmid system. B, Measured absorbances of NADH over time without NAD^+ in samples containing whole cells lysate of Rosetta 2 (DE3) harbouring two-plasmid system. C, Measured absorbances of NADH over time after adding NAD^+ in samples containing whole cells lysate of Rosetta 2 (DE3) harbouring empty vectors. D, Measured absorbances of NADH over time without NAD^+ in samples containing whole cells lysate of Rosetta2 (DE3) harbouring empty vectors. The absorbance was measured at 10 min intervals for 170 min. Values and error bars represent the averages and standard deviations from two independent experiments, each with three replicates.

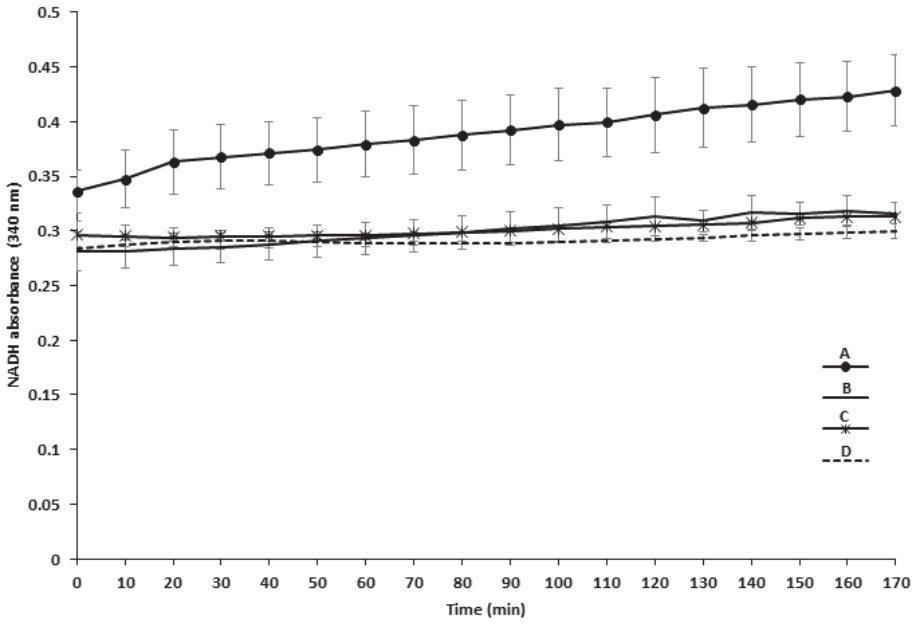

FIG. 15 Enzymatic assessment of AlgD activity in whole cell lysate of *E. coli* Origami B (DE3) (pMCS69::*algA*::*algC*::*algD*::*mucR*::*algJ* and pET-14b::*alg8*::*alg44*). Time 0 (T0) corresponds to the first absorbance (340 nm) of NADH that was measured 10 min after mixing reaction buffer. Reaction buffer contained 50 mM Tricin, 0.5 mM GDP-mannose, and 2.0 μg μl^{-1} of protein content of whole cell lysates, incubated at room temperature. A, Measured absorbances of NADH over time after adding NAD^+ in samples containing whole cells lysate of Origami B (DE3) harbouring two-plasmid system. B, Measured absorbances of NADH over time without NAD^+ in samples containing whole cells lysate of Origami B (DE3) harbouring two-plasmid system. C, Measured absorbances of NADH over time after adding NAD^+ to sample containing whole cells lysate of Origami B (DE3) harbouring empty vectors. D, Measured absorbances of NADH over time without NAD^+ in samples containing whole cells lysate of Origami B (DE3) harbouring empty vectors. The absorbance was measured at 10 min intervals for170 min. Values and error bars represent the averages and standard deviations from two independent experiments, each with three replicates.

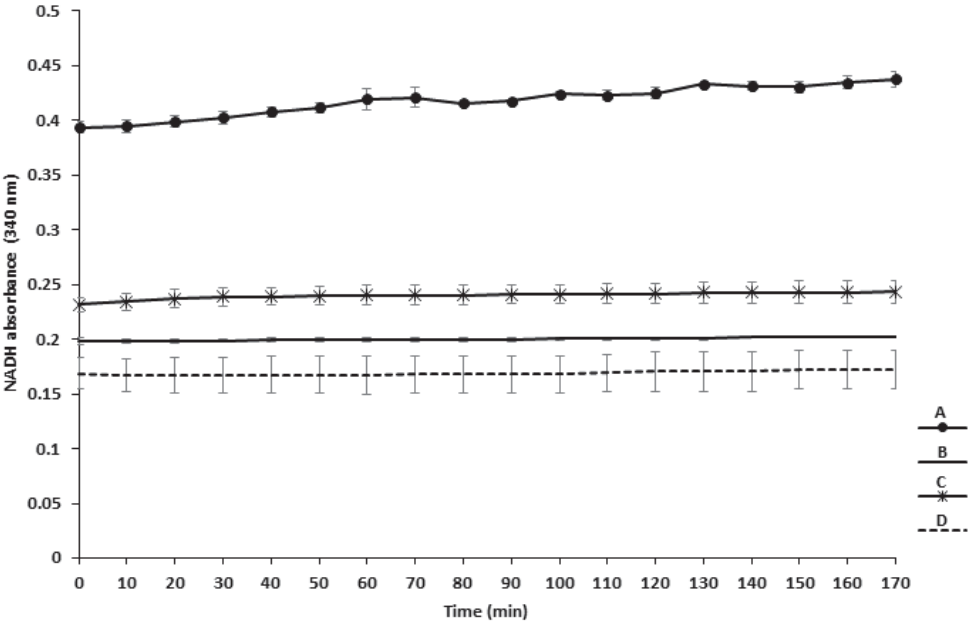

FIG. 16 Enzymatic assessment of AlgD activity in whole cell lysate of *B. megaterium* YYBm1 (pMCS69::*algA*::*algC*::*algD*::*mucR*::*algJ* and pET-14b::*alg8*::*alg44*). Time 0 (T0) corresponds to the first absorbance (340 nm) of NADH that was measured 10 min after mixing reaction buffer. Reaction buffer contained 50mM Tricin, 0.5 mM GDP-mannose, and 0.5 µg μl^{-1} of protein content of whole cell lysates, incubated at room temperature. A, Measured absorbances of NADH over time after adding NAD^+ in samples containing whole cells lysate of *B. megaterium* YYBm1 harbouring two-plasmid system. B, Measured absorbances of NADH over time without NAD^+ in samples containing whole cells lysate of *B. megaterium* YYBm1 harbouring two-plasmid system. C, Measured absorbances of NADH over time after adding NAD^+ in samples containing whole cells lysate of *B. megaterium* YYBm1 harbouring empty vectors. D, Measured absorbance of NADH over time without NAD^+ in samples containing whole cells lysate of *B. megaterium* YYBm1 harbouring empty vectors. The absorbance was measured at 10 min intervals for 170 min. Values and error bars represent the averages and standard deviations from two independent experiments, each with three replicates.

Establishing the production of alginate polymerase complex in heterologous hosts. In *P. aeruginosa*, the alginate polymerase complex consists of the Alg8 glycosyltransferase and its interacting partner Alg44, both of which are cytoplasmic membrane anchored. Alg44 contains a cytoplasmic PilZ domain sensing c-di-GMP for activation of polymerization and a transmembrane domain extending into a periplasmic part interacting with other periplasmic subunits and essential for polymerization while

modulating acetylation (151, 229). Previous findings showed that the production of these two proteins i.e. Alg8 and Alg44 in *E. coli* strains was challenging. In this study, we attempted the production of these two proteins using different approaches from those previously described (229).

All *E. coli* and *B. megaterium* strains harboring two-plasmid system that were initially assessed for AlgD activity were assessed for the production of Alg8 and Alg44 (Table S3). Immunoblotting using anti-Alg8 and anti-Alg44 antibody did not detect any bands corresponding to molecular weight of Alg8 (~54/~57kDa, theoretical masses respectively for Alg8 without and with signal peptide) and Alg44 (~ 41.5 kDa). We thought that this failure in detection of Alg8 and Alg44 in these transformants was due to inefficacy of applied antibodies. Therefore, the C-terminal fusion of *alg8* with hexahistidine tag was generated, and transferred into a heterologous host (Table S3). Membrane fractions of the generated transformants were subjected to immunoblotting using HisProbe-HRP antibody. Immunoblotting showed that only in the membrane fraction of ClearColi®BL21 (DE3) (pMCS69::*algA*::*algC*::*algD*::*mucR*::*algJ* and pET-14b::*alg8*-6His::*alg44*), two bands were developed, but not corresponding to the theoretical molecular mass of Alg8-6His (Figure 17).

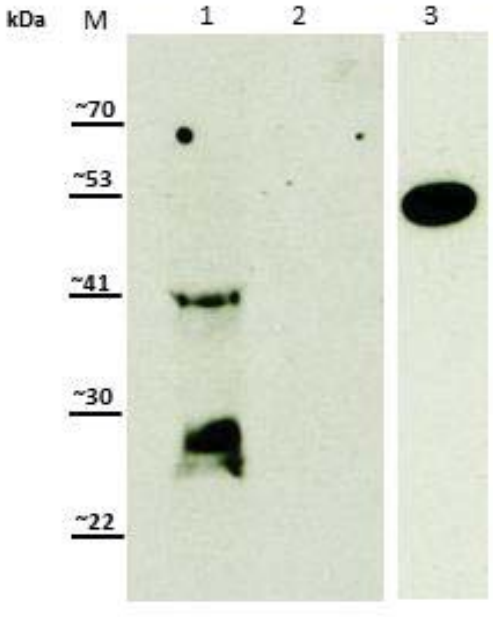

FIG. 17 Assessment of Alg8 production by immunoblotting of envelope fraction of ClearColi®BL21 (DE3) harbouring pMCS69::*algA*::*algC*::*algD*::*mucR*::*algJ* and pET-14b::*alg8*-6His::*alg44*. Immunoblots were developed using HisProbe-HRP antibody. Two bands were detected (lane 1), but not corresponding to theoretical molecular mass of Alg8-6His (61.3 kDa). Envelope fraction of ClearColi®BL21 (DE3) harbouring pMCS69 and pET-14b was used as negative control (lane 2). Also Lane 3, purified 10His-AlgD (48.9 kDa) was used as positive control for antibody specificity and efficacy (lane 3). M, molecular weight standard (GangNam-STAIN™ Prestaine,iNtRON Biothechnology).

This result encouraged us to assess a newly generated construct pKNT25::*alg8*-6His::*alg44* transferred into *E. coli* SHuffle for detection of Alg8-6His. Immunoblotting

analysis of membrane fraction of this transformant showed the presence of one band corresponding to the molecular mass of Alg8 (Figure 18A). This band was also detected in immunoblotting of the inner membrane fraction of this transformant (Figure 18B).

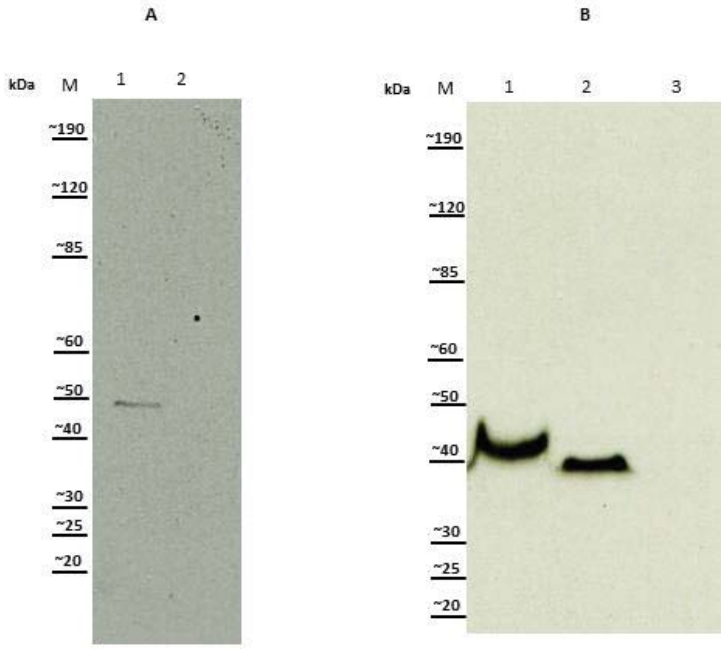

FIG. 18 Assessment of Alg8 production by immunoblotting of envelope and inner membrane fractions of *E. coli* SHuffle with pKNT25::*alg8*-6His. Immunoblots were developed using HisProbe-HRP antibody. One band was detected corresponding to Alg8 molecular mass (~54/~57 kDa) in envelope fraction (blot A, lane 1) and inner membrane fraction (blot B, lanes 1 and 2). Membrane fraction of *E. Coli* SHuffle with pKNT25 was used as negative control (blot A/B, lane 2/3).

Detection of Alg44-12His was attempted by immunoblotting of envelope and inner membrane fractions of *E. coli* BL21 Star (DE3) One Shot (pETDuet-1::*alg8*::*alg44*-12His) (Figure 19) and *E. coli* SHuffle (pKNT25::*alg8*::*alg44*-6His) (Figure 20). Immunoblotting using HisProbe-HRP antibody showed a band corresponding to Alg44-12His molecular mass (43 kDa) was developed. This result confirmed the localization of Alg44protein in the cytoplasmic membrane of *E. coli* Shuffle. However, production of Alg8 and Alg44 in other heterologous transformants (Table S3) were not detected, but the possibility of their production in such transformants cannot be fully ruled out when using other approaches and conditions. Table 1 summarises the results for assessing the production of proteins and their localizations in heterologous hosts.

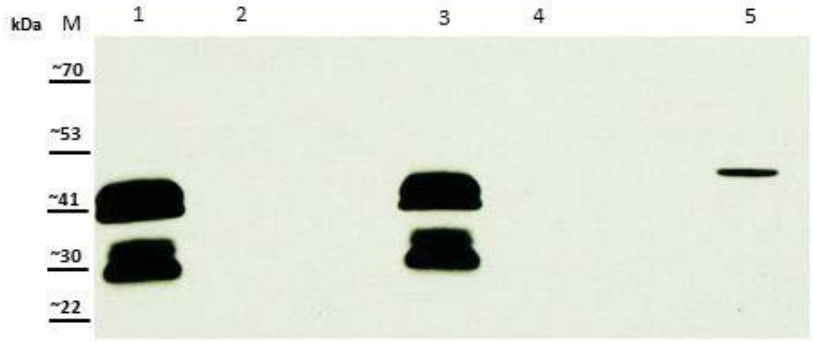

FIG. 19 Assessment of Alg44 production by immunoblotting of envelope fractions of *E. coli* BL21 Star (DE3) One Shot *(*pETDuet-1::*alg8*::*alg44*-12His*)*. Immunoblots were developed using HisProbe-HRP antibody. The band at about 43 kDa corresponds to the molecular mass of Alg44-12His present in the envelope fraction (lanes 1 and 3). A membrane fraction of *E. coli* BL21 Star (DE3) One Shot (pETDuet-1) was used as negative control (lanes 2 and 4). Also lane 5, purified 10His-AlgD (48.9 kDa) was used as positive control for antibody specificity and efficacy (lane 3). M, molecular weight standard (GangNam-STAIN™ Prestaine, iNtRON Biothechnology).

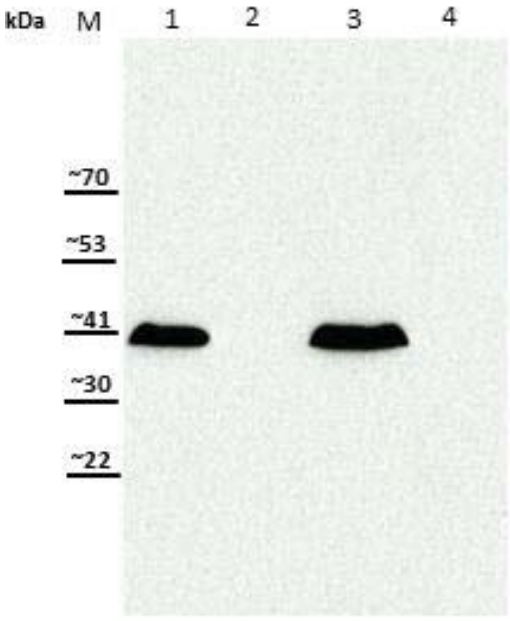

FIG. 20 Assessment of Alg44 production by immunoblotting of envelope and inner membrane fractions of *E. coli* SHuffle (pKNT25::*alg8::alg44*-6His). Immunoblots were developed using HisProbe-HRP antibody. The band at about 41 kDa was detected corresponding to the molecular mass of Alg44-6His present in the envelope fraction (lanes 1) and inner membrane fraction (lane 3). The envelope fraction (lane 2) and inner membrane fraction (lane 4) of *E. coli* SHuffle (pKNT25) was used as a negative control. M, molecular weight standard (GangNam-STAIN™ Prestaine, iNtRON Biothechnology).

TABLE 1 Summarizes the results from SDS-PAGE and immunoblotting analyses of assessing protein production and localization in various heterologous hosts.

Transformants	AlgA	AlgC	AlgD	Alg8	Alg44
E. coli Rosetta 2 (DE3) with pMCS69::*algA*::*algC*::*algD*::*mucR*::*algJ* and pET-14b::*alg8*::*alg44*	✓	?	✓	Not detected	
E. coli Origami B (DE3) with pMCS69::*algA*::*algC*::*algD*::*mucR*::*algJ* and pET-14b::*alg8*::*alg44*	✓	?	?	Not detected	
ClearColi®BL21 (DE3) with pMCS69::*algA*::*algC*::*algD*::*mucR*::*algJ* and pET-14b::*alg8*::*alg44*	✓	✓	?	Not detected	
ClearColi®BL21 (DE3) with pMCS69::*algA*::*algC*::*algD*::*mucR*::*algJ* and pET-14b::*alg8-6His*::*alg44*	Not assessed			†	Not assessed
E. coli BL21 Star (DE3) One Shot with pETDuet-1::*alg8*::*alg44*-12His	-				✓
E. coli SHuffle with pKNT25::*alg8*-6His::*alg44*	-			✓	Not assessed
E. coli SHuffle with pKNT25::*alg8*::*alg44*-6His	-				✓

Question marks (?) indicate uncertain protein detection due to high non-specific background on immunoblots; † indicates detection of one band on immunoblot, but not corresponding to the expected molecular mass of the relevant protein.

Assessment of alginate production.

Initially, we analysed transformants growing on solid or in liquid cultures for detection of possible alginate production by performing uronic acid assays. Our analysis did not reveal significant differences between transformants` samples and negative controls harbouring empty vectors. However, we assumed that this assay might not provide enough sensitivity for detection of a low level of alginate. Therefore, we applied ELISA using an anti-alginate antibody as an alternative method, but with much more sensitivity to assess alginate production. As we had a limited amount of this antibody, only the

transformant *E. coli* SHuffle (pKNT25::*alg8*::*alg44* and pMCS69::*algA*::*algC*::*algD*::*mucR*::*algJ*) was chosen for this experiment because this transformant was found to be producing alginate polymerase proteins. A periplasmic fraction and the extracellular supernatant of this transformant were separately assessed. Similarly, these fractions from *E. coli* SHuffle (pKNT25 and pMCS69) were obtained and assessed as negative controls. Furthermore, commercial alginic acid (2, 1, 0.5, 0.1, 0.05 and 0.025 µg/ml) was applied as a positive control as well as for preparation of standard curves (Figure S2). The ELISA assay showed that purified *P. aeruginosa* alginate was detectable in a concentration dependent manner, while no significant differences were observed between isolated fractions from transformants and negative controls. However, at this stage we cannot confirm if this assay was performed under optimal conditions with respect to sample preparation and sensitivity of the secondary antibody used.

Likewise, *in vitro* activity of Alg8 and Alg44 produced from this transformant was assessed using an ELISA assay using the above mentioned procedure. Crude extracts, envelope fraction and cytoplasmic fractions were obtained separately from solid phase and liquid cultures. *E.coli* SHuffle (pMCS69) and *P. aeruginosa (*PBBR1MCS-5::*alg44*::*alg8)* were applied as negative and positive controls, respectively. In addition, separate sets of samples and controls supplemented with 1.0 and 0.5 µg/ml of purified alginate from *P. aeruginosa* PDO300 were applied as extra controls to make a precise comparison among treatments. Purified *P. aeruginosa* PDO300 alginate at different concentrations (4, 2, 1, 0.5 and 0.1 µg/ml) was used to construct a standard cure.

Our ELISA assay result did not show significant differences between the absorbances of treatments and controls. We should note that this experiment might suffer from a secondary antibody effect as an immediate and very strong colour change was observed upon addition of the OPD Peroxidase Substrate.

DISCUSSION

In the present study, we aimed at establishing the alginate biosynthesis pathway in heterologous hosts. Due to their unique physicochemical properties, alginates have wide industrial applications mainly as gelling and viscosity increasing agent. Alginates produced by seaweeds are currently the only ones that have been commercialized, while bacterial alginates have remained largely unharnessed. Bacterial alginates have different advantages over algal alginates because they have different compositions bringing new properties. For example, bacterial alginates are acetylated, much greater in molecular mass and monodisperse. These parameters are unique to bacterial alginates which may meet some criteria required for their use in high value applications such as in biomedical and pharmaceutical engineering. Another important advantage of bacterial alginates is the possibility to produce them from bacteria in laboratory conditions either as raw polymers or tailor-made. In contrast to algal alginates, the biosynthesis pathway of alginate in bacteria has been extensively studied and many underlying molecular mechanisms at genomic and proteomic levels have been unraveled. Furthermore, previous studies demonstrated the possibility of producing various alginates displaying novel properties from bacteria, mainly *P. aeruginosa*, via genetic manipulation. However, bacterial tailor-made alginate production is still in its early stages. So far, many findings about alginate biosynthesis in bacteria have been based on studying *P. aeruginosa* which is an opportunistic human pathogen. Although studying this model organism has paved our path to understand many aspects of bacterial alginate production, application of alginates produced by *P. aeruginosa* and its mutants is impossible. This is because these alginates more likely suffer from contamination by unwanted potentially pathogenic cells or various virulence factors and molecules that are largely immunogenic agents such as LPS (lipopolysaccharide), fimbriae, pili and toxins. Different approaches can be followed for tackling these potential problems inherently associated with *P. aeruginosa* alginates including production of alginates from non-pathogenic bacteria such as *A. vinelandii* and other non-pathogenic *Pseudomonas* species, generation of avirulent variants of *P. aeruginosa*, and alginate production from heterologous hosts such as *E. coli* strains as easy- and fast-to-grow bacteria for biotechnological applications.

In this study, we tried to assess the possibility of establishing the alginate biosynthesis pathway in heterologous hosts including various strains of *E. coli* and *B. megaterium*.

In modern biotechnology, various strains of *E. coli* have been generated via genetic engineering; each conferring specific genotypic advantage (s) for particular applications. Examples used in this study are ClearColi®BL21 (free of endotoxin or LPS), Rosetta 2 (DE3) (enhancing the expression of eukaryotic proteins), SHuffle (enhancing correct protein folding via disulfide bonds in the cytoplasm), Origami B (DE3) (Enhancing disulfide bond formation in cytoplasm), and BL21 Star (DE3) One Shot (promoting high mRNA stability and protein yield; reducing degradation of heterologous proteins).
A Gram-positive bacterium used in this study was *B. megaterium* strain YYBm1 that is biotechnologically suited for extracellular protein production as it has 1.5 % of the wild-type extracellular protease activity (239).

By taking *P. aeruginosa* alginate biosynthesis into account, we assumed that three cytoplasmic proteins including AlgA, AlgC and AlgD constitute the minimal protein requirements, but more likely sufficient to produce the alginate precursor GDP-mannuroic acid from fructose-6-phosphate in heterologous hosts. Furthermore, membrane proteins Alg8 and Alg44, constituting the minimal requirements for alginate polymerization in *P. aeruginosa,* were considered for establishing this event in heterologous hosts. Furthermore, the MucR protein, as a specific c-di-GMP provider for alginate production in *P. aeruginosa*, was thought to be required for activation of alginate polymerization by providing a presumable c-di-GMP pool in close proximity to the alginate polymerase complex. The final but not the least consideration in alginate production from heterologous Gram-negative strains was the utilization of the alginate secreting outer membrane protein AlgJ (homologous to AlgE in *P. aeruginosa*). The codon-optimized genes encoding these proteins were designed and inserted into different two-plasmid systems compatible for expression in various strains of *E. coli* and *B. megaterium*.

Our first objective was to assess production and appropriate localization of these proteins in heterologous hosts followed by assessing the production of GDP-mannuronic acid and then polymerized alginates. Preliminarily assessments using immunoblotting with polyclonal antibodies showed that AlgA, AlgC, and AlgD were produced in various strains of *E. coli* and the endotoxin-free strain ClearColi®BL21 was a promising strain for producing these proteins. The activity of AlgD as the last crucial step for alginate precursor production in heterologous hosts was further assessed *in vitro* using purified 10His-AlgD and whole cell lysates of heterologous transformants. To this end, we

measured the absorbance (340 nm) of NADH concentration that was generated by reduction of NAD^+ during the conversion of GDP-mannose to GDP-mannuronic acid by AlgD. Our results demonstrate catalytic activity of AlgD produced in heterologous hosts, indicating AlgD activity was correctly folded and was not negatively impacted by the protein production machinery of heterologous hosts or possible post-translational modifications.

Assessment of production and localization of two membrane-anchored proteins Alg8 and Alg44 showed that production of these proteins is a common challenge when the same heterologous hosts producing AlgA, AlgC and AlgD were used. These results were consistent with previous studies describing the same difficulty. In this regard, possible explanations were instability of produced transcripts of these genes or improper folding for localization resulted in failure of protein detection. To test such explained effects, two strains of *E. coli* including Shuffle and BL21 Star (DE3) One Shot were used to assess Alg8 and Alg44 production. The former strain enhances correct protein folding via disulfide bonds while the latter promotes high mRNA stability and protein yield and displays reduction in degradation of heterologous proteins. Our results using immunoblotting and a HisProbe-HRP antibody showed that Alg8 and alg44 were produced in these two strains, indicating production of alginate polymerase complex in heterologous hosts requires extra biotechnological and molecular considerations. In a final step, using an ELISA assay we tried to assess alginate production in heterologous hosts and *in vitro* activity of Alg8 and Alg44. The results of this assessment did not show significant differences among absorbance of treatments and controls probably because nonoptimal conditions were used for the secondary antibody. This experiment needs to be repeated under optimal conditions.

ACKNOWLEGEMENTS

The present research was funded by Massey University research grants to B. H. A. Rehm (Institute of Fundamental Sciences, Massey University). Shirin Ghods is funded by a Massey University Doctoral scholarship.

SUPLEMENTAL MATERIALS

FIG. S1 The maps of made constructs applied in this study (the details of origin of genes in Table S2)

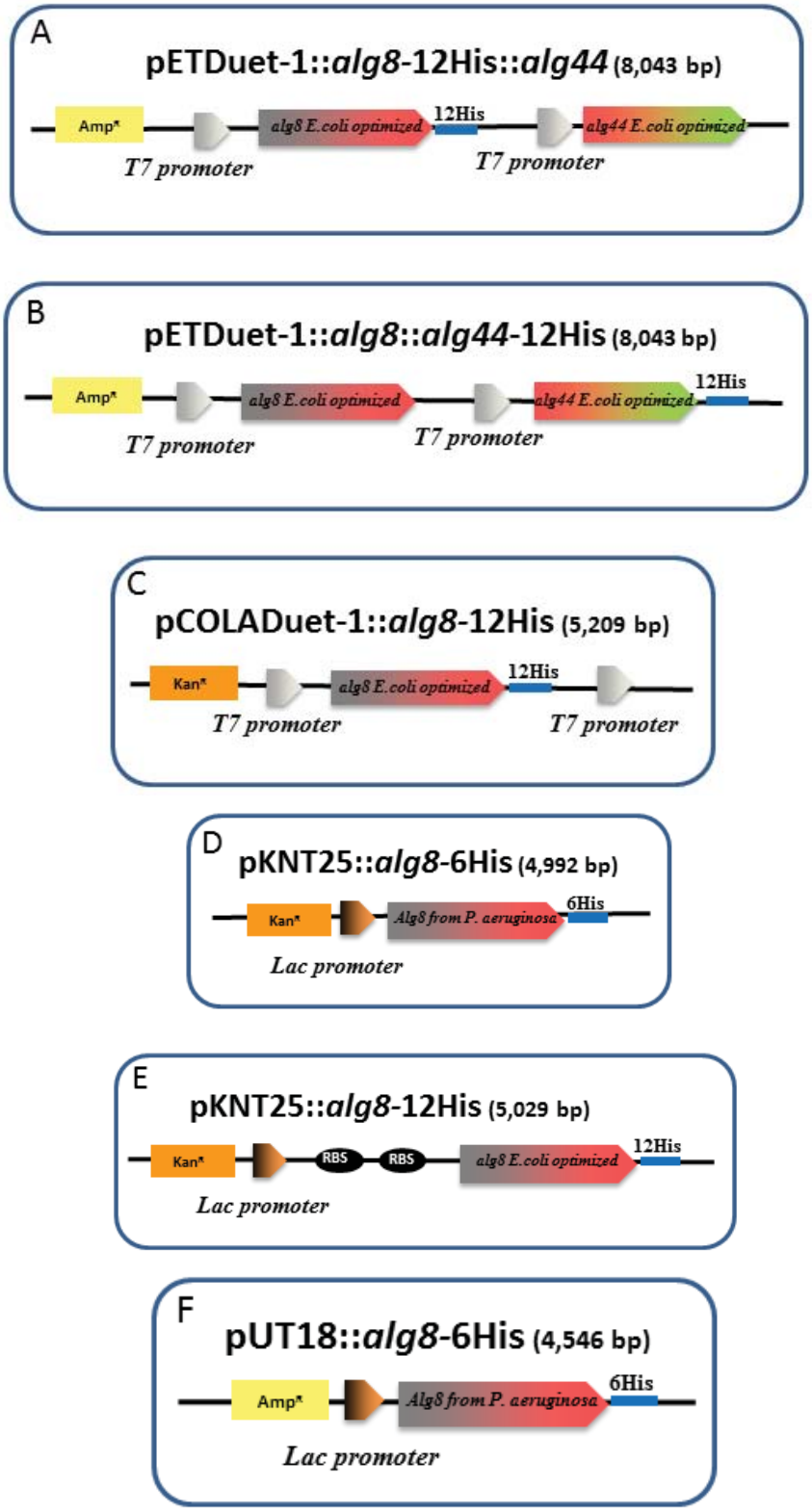

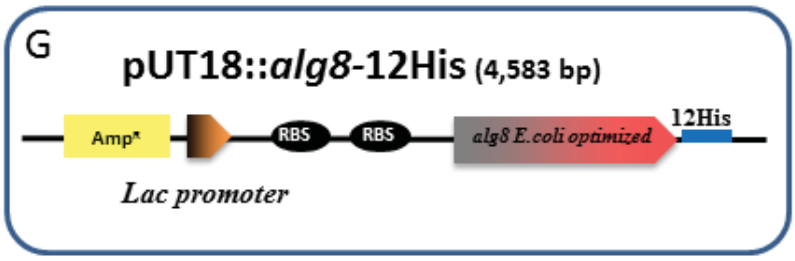
G
pUT18::alg8-12His (4,583 bp)
Amp^R
RBS
RBS
alg8 E.coli optimized
12His
Lac promoter

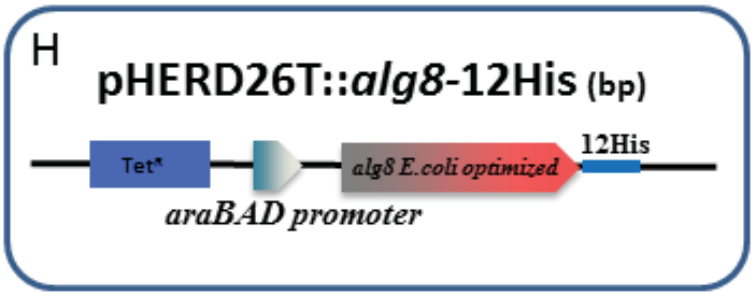
H
pHERD26T::alg8-12His (bp)
Tet^R
alg8 E.coli optimized
12His
araBAD promoter

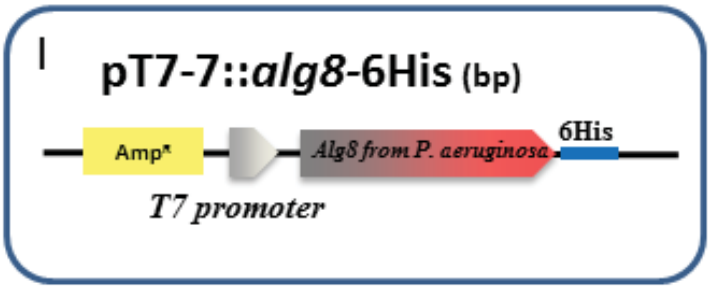
I
pT7-7::alg8-6His (bp)
Amp^R
Alg8 from P. aeruginosa
6His
T7 promoter

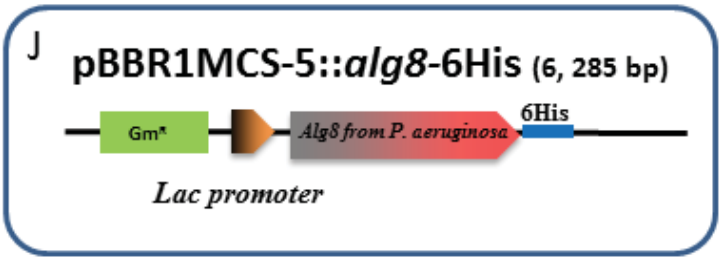
J
pBBR1MCS-5::alg8-6His (6, 285 bp)
Gm^R
Alg8 from P. aeruginosa
6His
Lac promoter

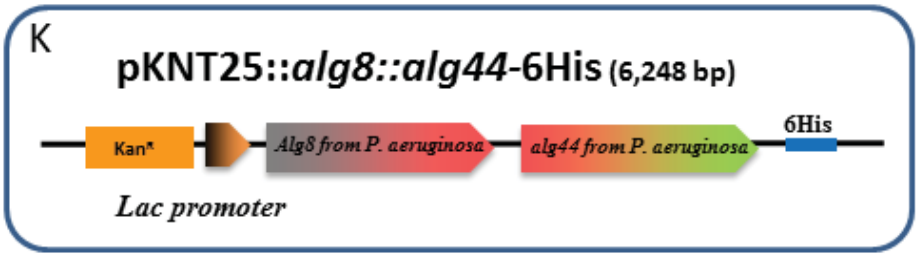
K
pKNT25::alg8::alg44-6His (6,248 bp)
Kan^R
Alg8 from P. aeruginosa
alg44 from P. aeruginosa
6His
Lac promoter

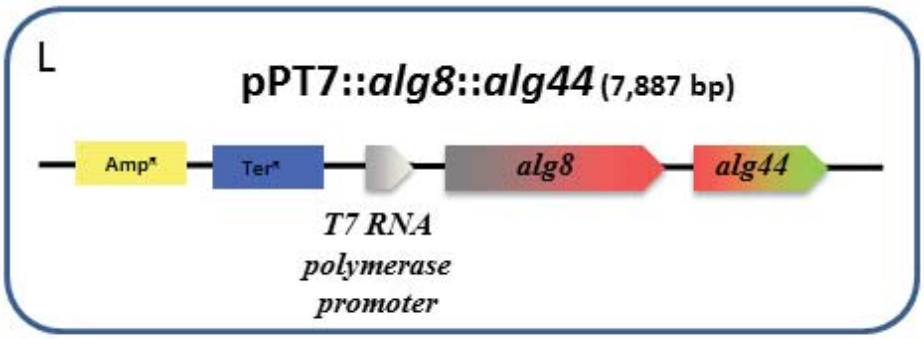
L
pPT7::alg8::alg44 (7,887 bp)
Amp*
Ter*
alg8
alg44
T7 RNA
polymerase
promoter

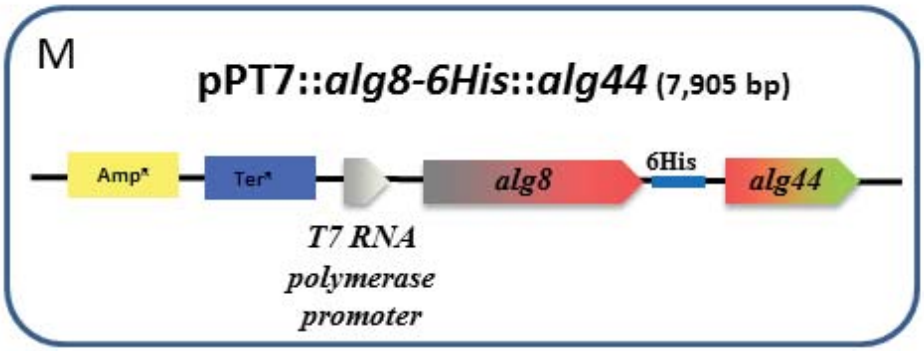
M
pPT7::alg8-6His::alg44 (7,905 bp)
Amp*
Ter*
alg8
6His
alg44
T7 RNA
polymerase
promoter

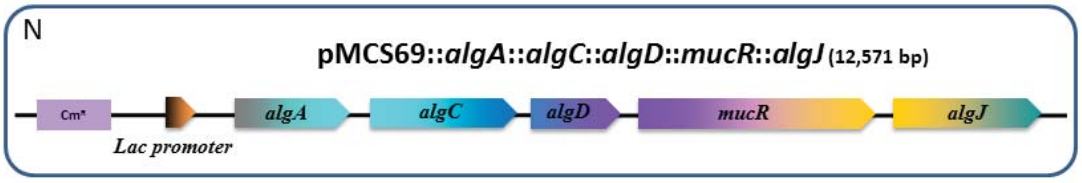
N
pMCS69::algA::algC::algD::mucR::algJ (12,571 bp)
Cm*
algA
algC
algD
mucR
algJ
Lac promoter

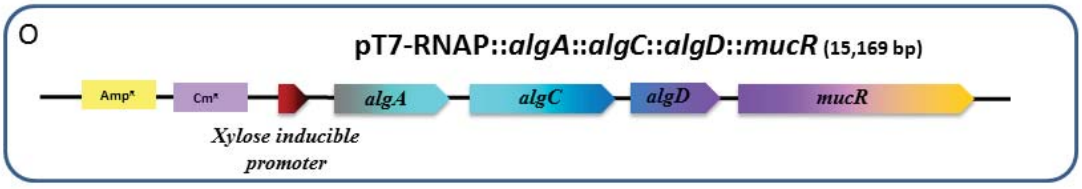
O
pT7-RNAP::algA::algC::algD::mucR (15,169 bp)
Amp*
Cm*
algA
algC
algD
mucR
Xylose inducible
promoter

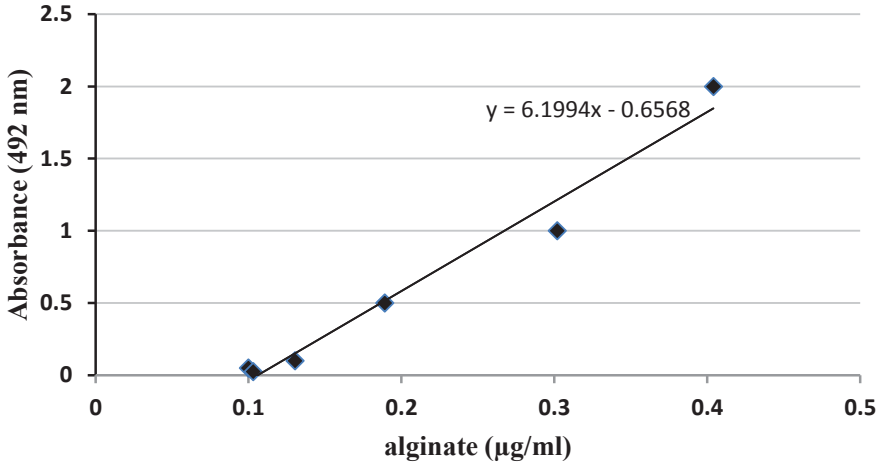

FIG. S2 ELISA assay standard curve created based on various concentrations of purified *P. aeruginosa* PDO300 alginate (4, 2, 1, 0.5 and 0.1 µg/ ml).

TABLE S1 Strains applied in this study

Strains	Characteristics	Source
Escherichia coli		
TOP10	*E. coli* cloning strain	Invitrogen
XL Blue1	*E. coli* cloning strain	Invitrogen
BL21 (DE3)	T7 polymerase in DE3 region	
C43 (DE3)	Parent Strain: *E. coli* BL21 (DE3) Mutagenic Agent directed: mutagenesis Altered Genotype: F – ompT hsdSB (rB- mB-) gal dcm (DE3)	
C41 (DE3)	Parent Strain: *E. coli* BL21 (DE3) Mutagenic Agent : directed mutagenesis Altered Genotype: F – ompT hsdSB (rB- mB-) gal dcm (DE3)	
BL21 Star™ (DE3)	Parent Strain: *E. coli* BL21 (DE3) Mutagenic: Agent directed mutagenesis Altered Genotype: F- ompT hsdSB (rB-mB-) gal dcm rne131	
ClearColi BL21 (DE3)	Genetically modified LPS does not trigger endotoxic response in human	
Rosetta 2 (DE3)	Chloramphenicol resistant (34ug/ml) are designed to enhance the expression of eukaryotic proteins that contain codons rarely used in *E. coli* supply tRNAs for seven rare codons (AUA, AGG, AGA, CUA, CCC, CGG, and GGA) on a compatible plasmid	
Origami B (DE3)	BL21 *lacY* deletion, *trxB*/*gor* mutant. Origami B combines the characteristics of BL21, Tuner and Origami hosts. The *trxB* and *gor* mutations are selectable on kanamycin and tetracycline, respectively. In addition, Origami B (DE3) bears the T7 RNA polymerase g	
SHuffle T7 Express	Engineered *E. coli* B strain to promote disulfide bond formation in the cytoplasm. Expresses constitutively a chromosomal copy of the disufide bond isomerase *DsbC*. Δ*gor* Δ*trxB* (like Origami). Expresses a chromosomal copy of T7 RNAP	

Bacillus megateruim		
YYBm1	Parent Strain: *Bacillus megaterium* MS941 Mutagenic: Agent directed mutagenesis Altered Genotype: delta *xylA*, delta *nprM* Altered Phenotype: mutant of MS941 (protease deficient) that does not utilize xylose	
Pseudomonas aeruginosa		
PDO300	mucA22 isogenic mutant derived from PAO1, Alg+	(132)
PDO300 Δ*alg8*Δ*alg44*	Isogenic *alg8* and *alg44* deletions mutant derived from PDO300, Alg^-	**(151)**

TABLE S2 Plasmids applied in this study

Plasmids	**Characteristics**	**Source**
pBBR1MCS-5	Gm^r; broad-host-range vector; P_{lac}	(172)
pBBR1MCS-5:alg44:alg8	ClaI-HindIII fragment comprising alg44 and HindIII-PstI fragment comprising alg8 inserted into vector pBBR1MCS-5	
pMCS69::*algA*::*algC*::*algD* ::*mucR*::*algJ*	Cm^r; *BamHI-NheI* fragment comprising *algA* (CP005095.1) encoding translational AlgA; *NheI-AsiSI* fragment comprising *algC* (CP005095.1) encoding translational AlgC; *AsiSI-BmtI* fragment comprising *algD* (U11240.1) encoding translational AlgD; *BmtI-MluI/BamHI* fragment comprising *mucR* (AE004091.2) encoding translational mucR; *MluI/BamHI-XmaI* fragment comprising *algJ* (X86533.1) encoding translational AlgJ; The codon usages are optimized for protein production in *E. coli* and inserted into vector pMCS69	This study
pET-14b::*alg8*::*alg44*	Amp^r; *SpeI-XhoI* fragment comprising *alg8* (U11240.1) encoding translational Alg8; *XhoI- BamHI*/*HindIII* fragment comprising alg44 (U11240.1) encoding translational Alg44; The codon usages are optimized for protein production in *E. coli* and inserted into vector pET-14b	This study
pET-14b::*alg8-6*His::*alg44*	Amp^r; *SpeI-XhoI* fragment comprising *alg8* (U11240.1) encoding translational Alg8 with C-terminal hexahistidine tag fusion;*XhoI- BamHI*/*HindIII* fragment comprising alg44 (U11240.1) encoding translational Alg44; The codon usages are optimized for protein production in *E. coli* and inserted into vector pET-14b	This study

pT7-RNAP::*algA*::*algC*::*algD*::*mucR*	Amp^r; Cm^r; *BamHI-NheI* fragment comprising *algA* (CP005095.1) encoding translational AlgA; *NheI-AsiSI* fragment comprising *algC* (CP005095.1) encoding translational AlgC; *AsiSI-BmtI* fragment comprising *algD* (U11240.1) encoding translational AlgD; *BmtI-MluI/BamHI* fragment comprising *mucR* (AE004091.2) encoding translational *mucR*; The codon usages are optimized for protein production in *E. coli* and inserted into vector pT7-RNAP	This study
pPT7::*alg8*::*alg44*	Amp^r; Tet^r; *SpeI-XhoI* fragment comprising *alg8* (U11240.1) encoding translational Alg8;*XhoI- BamHI*/*HindIII* fragment comprising *alg44* (U11240.1) encoding translational Alg44; The codon usages are optimized for protein production in *E. coli* and inserted into vector pPT7	This study
pPT7::*alg8*-6His::*alg44*	Amp^r; Tet^r; *SpeI-XhoI* fragment comprising *alg8* (U11240.1) encoding translational Alg8 with C-terminal hexahistidine tag fusion;*XhoI- BamHI*/*HindIII* fragment comprising *alg44* (U11240.1) encoding translational Alg44; The codon usages are optimized for protein production in *E. coli* and inserted into vector pPT7	This study
pET-14b::10His-*algD*	Amp^r; *NheI-BamHI* fragment comprising *algD* (AE004091.2) encoding translational AlgD with N-terminal 10-histidine tag fusion; The codon usages are optimized for protein production in *E. coli* and inserted into vector pET-14b	This study
pETDuet-1::*alg8*-12His::*alg44*	Amp^r; *NcoI-BamHI* fragment comprising *alg8* (PA3541) encoding translational Alg8 with C-terminal 12-histidine tag fusion;*BglII-KpnI* fragment comprising *alg44* (PA3542) encoding translational Alg44; The codon usages are optimized for protein production in *E. coli* and inserted into vector pETDuet-1	(229)
pETDuet-1::*alg8*::*alg44*-12His	Ampr; NcoI-BamHI fragment comprising *alg8* (PA3541) encoding translational Alg8; BglII-KpnI fragment comprising *alg44* (PA3542) encoding translational Alg44 with C-terminal 12-histidine tag fusion; The codon usages are optimized for protein production in E. *coli* and inserted into vector pETDuet-1	(229)
pCOLADuet-1::*alg8*-12His	Kan^r; *NcoI-BamHI* fragment comprising *alg8* (PA3541) encoding translational Alg8 with C-terminal 12-histidine tag	(229)

	fusion; The codon usages are optimized for protein production in *E. coli* and inserted into vector pCOLADuet-1	
pKNT25::*alg8*-6His	Kan^r; *HindIII-PstI* fragment comprising *alg8* (PA3541) encoding translational Alg8 with C-terminal hexahistidine tag fusion and was inserted into vector pKNT25	This study
pKNT25::*alg8*-12His	Kan^r; *NcoI -BamHI* fragment comprising *alg8* (PA3541) encoding translational Alg8 with C-terminal 12-histidine tag fusion; The codon usages are optimized for protein production in *E. coli* and inserted into vector pKNT25	This study
pUT18::*alg8*-6His	Amp^r; *HindIII-PstI* fragment comprising *alg8* (PA3541) encoding translational Alg8 with C-terminal hexahistidine tag fusion and was inserted into vector pUT18	This study
pUT18::*alg8*-12His	Amp^r; *NcoI -BamHI* fragment comprising *alg8* (PA3541) encoding translational Alg8 with C-terminal 12-histidine tag fusion; The codon usages are optimized for protein production in *E. coli* and inserted into vector pUT18	This study
pBBR1MCS-5::*alg8*-6His	Gm^r; *NdeI-PstI* fragment comprising *alg8* (PA3541) encoding translational Alg8 with C-terminal hexahistidine tag fusion and was inserted into vector pBBR1MCS5	(229)
pHERD26T::*alg8*-12His	Tet^r; *NcoI-PstI* fragment comprising *alg8* (PA3541) encoding translational Alg8 with C-terminal 12-histidine tag fusion; The codon usages are optimized for protein production in *E.* coli and inserted into vector pHERD26T	(229)
pT7-7::*alg8*-6His	Amp^r; *NdeI-PstI* fragment comprising *alg8* (PA3541) encoding translational Alg8 with C-terminal hexahistidine tag fusion and was inserted into vector pT7-7	(229)
pKNT25::*alg8*::*alg44*-6His	Kan^r; *NdeI-PstI* fragment comprising *alg8* (PA3541) encoding translational Alg8; *NdeI-BamHI* fragment comprising *alg44* (PA3542) encoding translational Alg44 with C-terminal hexahistidine tag fusion and was inserted into vector pKNT25	This study
pKNT25::*alg8*::*alg44*	Kan^r; *NdeI-PstI* fragment comprising *alg8* (PA3541) encoding translational Alg8; *NheI-BamHI*/Spe*I* fragment comprising *alg44* (PA3542) encoding translational Alg44 and was inserted into vector pKNT25	This study

TABLE S3 Made transformants applied in this study

Transformants	**Source**
P. aeruginosa PDO300 with pBBR1MCS-5	(151)
P. aeruginosa PDO300 Δ*alg8*Δ*alg44* with pBBR1MCS-5:*alg44*:*alg8*	(151)
E. coli Top10 pUC57-simple:C-ter.*alg8*-6His	This study
E. coli Top10 pUC57-simple:*algD*-6His	This study
E. coli Top10 pUC57:*alg8:alg44*	This study
E. coli Top10 pUC57:*algA*:*algC*::*algD*::*mucR*::*algJ*	This study
E. coli Top10 with pMCS69::*algA*::*algC*::*algD*::*mucR*::*algJ*	This study
E. coli Top10 with pET-14b::*alg8*::*alg44*	This study
E. coli Top10 with pET-14b::*alg8*-6His::*alg44*	This study
E. coli Rosetta 2 (DE3) with pMCS69::*algA*::*algC*::*algD*::*mucR*::*algJ* and pET-14b::*alg8*::*alg44*	This study
E. coli Rosetta 2 (DE3) with pMCS69::*algA*::*algC*::*algD*::*mucR*::*algJ* and pET-14b::*alg8*-6His::*alg44*	This study
E. coli Rosetta 2 (DE3) with pMCS69 and pET-14b	This study
E. coli Origami B (DE3) with pMCS69::*algA*::*algC*::*algD*::*mucR*::*algJ* and pET-14b::*alg8*::*alg44*	This study
E. coli Origami B (DE3) with pMCS69::*algA*::*algC*::*algD*::*mucR*::*algJ* and pET-14b::*alg8*-6His::*alg44*	This study
E. coli Origami B (DE3) with pMCS69 and pET-14b	This study
ClearColi®BL21 (DE3) with pMCS69::*algA*::*algC*::*algD*::*mucR*::*algJ* and pET-14b::*alg8*::*alg44*	This study
ClearColi®BL21 (DE3) with pMCS69::*algA*::*algC*::*algD*::*mucR*::*algJ* and pET-14b::*alg8*-6His::*alg44*	This study
ClearColi®BL21 with pMCS69 and pET-14b	This study
E. coli EPI400 with pT7-RNAP::*algA*::*algC*::*algD*::*mucR*	This study
E. coli Top10 with pPT7::*alg8*::*alg44*	This study
E. coli Top10 with pPT7::*alg8*-6His::*alg44*	This study
B. megaterium YYBm1 with pT7-RNAP::*algA*::*algC*::*algD*::*mucR* and pPT7::*alg8*::*alg44*	This study
B. megaterium YYBm1 with pT7-RNAP::*algA*::*algC*::*algD*::*mucR* and pPT7::*alg8*-6His::*alg44*	This study
B. megaterium YYBm1 with pT7-RNAP and pPT7	This study

E. coli Top10 with pET-14b::10His-*algD*	This study
E. coli BL21 (DE3) with pET-14b::10His-*algD*	This study
E. coli BL21 (DE3) with pET-14b	This study
E. coli BL21 Star (DE3) One Shot with pET-14b::*alg8* -6His::*alg44*	This study
E. coli BL21 Star (DE3) One Shot with pET-14b	This study
E. coli BL21Star (DE3) One Shot with pETDuet-1*::alg8::alg44*-12His	This study
E. coli BL21 Star (DE3) One Shot with pETDuet-1::*alg8* -12His::*alg44*	This study
E. coli BL21 Star (DE3) One Shot with pETDuet-1	This study
ClearColi®BL21 with pETDuet-1::*alg8*-12His::*alg44*	(229)
ClearColi®BL21 with pETDuet-1::*alg8* -12His	
E. coli BL21 (DE3) with pETDuet-1::*alg8* -12His::*alg44*	(229)
E. coli BL21 (DE3) with pETDuet-1::*alg8*-12His	
E. coli Origami B (DE3) with pETDuet-1::*alg8*- 12His::*alg44*	(229)
E. coli Origami B (DE3) with pETDuet-1::*alg8* -12His	
E. coli SHuffle with pETDuet-1::*alg8*- 12His*::alg44*	This study
E. coli C43 (DE3) with pETDuet-1::*alg8*-12His::*alg44*	(229)
E. coli BL21 Star (DE3) One Shot with pCOLADuet-1::*alg8*-12His	This study
E. coli BL21 Star (DE3) One Shot with pCOLADuet-1	This study
E. coli SHuffle with pCOLADuet-1::*alg8*-12His	This study
ClearColi®BL21 with pCOLADuet-1::*alg8*-12His	(229)
E. coli Top10 with pKNT25::*alg8*-6His	This study
E. coli BL21 Star (DE3) One Shot with pKNT25::*alg8*-6His	This study
ClearColi®BL21 with pKNT25::*alg8*-6His	This study
E. coli SHuffle with pKNT25::*alg8*-6His	This study
E. coli Top10 with pKNT25::*alg8*-12His	This study
E. coli BL21 Star (DE3) One Shot with pKNT25::*alg8*-12His	This study
E. coli BL21 Star (DE3) One Shot with pKNT25	This study
ClearColi®BL21 with pKNT25::*alg8*-12His	This study
ClearColi®BL21 with pKNT25	This study

E. coli SHuffle with pKNT25::*alg8*-12His	This study
E. coli SHuffle with pKNT25	This study
E. coli Top10 with pUT18::*alg8*-6His	This study
E. coli BL21 Star (DE3) One Shot with pUT18::*alg8*-6His	This study
ClearColi®BL21 with pUT18::*alg8*-6His	This study
E. coli SHuffle with pUT18::*alg8*-6His	This study
E. coli Top10 with pUT18::*alg8*-12His	This study
E. coli BL21 Star (DE3) One Shot with pUT18::*alg8*-12His	This study
ClearColi®BL21 with pUT18::*alg8*-12His	This study
E. coli SHuffle with pUT18::*alg8*-12His	This study
E. coli SHuffle with pUT18	This study
ClearColi®BL21 with pBBR1MCS5::*alg8*-6His *E. coli* Origami B (DE3) with pBBR1MCS5::*alg8*-6His	(229)
E. coli BL21 Star (DE3) One Shot with pBBR1MCS5::*alg8*- 6His	This study
E. coli SHuffle with pBBR1MCS5::*alg8*-6His	This study
ClearColi®BL21 with pHerd 26T::*alg8*-12His	(229)
E. coli BL21 Star (DE3) One Shot with pherd 26T::*alg8*-12His	This study
E. coli SHuffle with pherd 26T::*alg8*-12His	This study
E. coli C41 (DE3) with pT7-7::*alg8*-6His *E. coli* C43 (DE3) with pT7-7::*alg8*-6His ClearColi®BL21 with pT7-7::*alg8*-6His *E. coli* Origami B (DE3) with pT7-7::*alg8*-6His	(229)
E. coli BL21 Star (DE3) One Shot with pT7-7::*alg8*-6His	This study
E .coli SHuffle with pT7-7::*alg8*-6His	This study
E. coli SHuffle with pKNT25::*alg8*::*alg44*-6His	This study
E. coli SHuffle with pKNT25::*alg8*::*alg44*	This study
E. coli SHuffle with pKNT25	This study
E. coli SHuffle with pKNT25::*alg8*::*alg44* and pMCS69::*algA*::*algC*::*algD*::*mucR*::*algJ*	This study
E. coli SHuffle with pKNT25 and pMCS69	This study

Final Discussion and outlook

FINAL DISCUSION

Bacterial polysaccharides are among the most diverse biopolymers produced. Polysaccharides are biologically important for bacteria and notably they are a major part of the biofilm matrix. Biofilms are defined as cell aggregates embedded in complex extracellular polymeric substances (EPS) mainly composed of exopolysaccharides, proteins, extracellular DNA (eDNA), etc. Biofilm formation is a survival advantage for bacteria under harsh conditions in all environments protecting them from physical and chemical stresses, nutritional stresses, antibiotic treatments and the immune system (200, 240).

There is a wide range of bacterial exopolysaccharides with different chemical compositions. The composition of polysaccharides determines polymer properties and their biological function relevant to the producer. Likewise, humans have discovered the usefulness of polysaccharides and harnessed their properties for a long time. Cellulose, alginate, xanthan, dextran and complex capsular polysaccharides are well-known bacterial exopolysaccharides (2, 4).

Understanding the biosynthesis of polysaccharides is tremendously important. In the context of pathogenesis, these studies would inform the development of drugs for eradication of biofilms causing persistent infections, while they also inform biopolymer sciences and engineering for harnessing natural and unique properties of polysaccharides (2). As an example, studying alginate biosynthesis in *P. aeruginosa* as a model organism, but opportunistic pathogen, has expanded our knowledge in both contexts.

This thesis mainly aimed at studying the biosynthesis of polysaccharides involved in the development of biofilm structure of two pathogenic bacteria in plant and human including *Pseudomonas syringae* pv. *actinidiae* and *P. aeruginosa*. Furthermore, the possibility of harnessing bacterial polysaccharide via known biosynthetic pathways and biotechnological production methods were assessed.

Chapter I focused on understanding biofilm formation of a plant-pathogenic bacterium *Pseudomonas syringae* pv. *actinidiae* (*Psa*) NZ V-13. This is a highly virulent strain threatening Kiwifruit industry in New Zealand. We investigated the capability of *Psa* NZ V-13 in biofilm formation and we analysed polymeric substances that dominantly constitute the biofilm matrix. We found that two different polysaccharides are the major polymers contributing to the formation of the biofilm matrix in this *Pseudomonas* species. Furthermore, we analyzed the chemical composition of these polysaccharides and the

identity of constituting monomers were unravelled. Biofilm formation is a survival advantage for many bacteria. Due to the complex polymeric matrix of biofilms surrounding cells, biofilm cells are largely protected from toxic materials and antibiotics. In this study, we attempted to evaluate anti-biofilm activity of two commercial compounds including kasugamycin and chlorine dioxide at various stages of biofilm formation. These results provided insights into biofilm formation of *Psa* NZ V-13 threatening kiwifruit orchards and we provided experimental evidence for the effectiveness of chlorine dioxide and kasugamycin to control *Psa* NZ V-13.

Chapters II and III focused on studying alginate biosynthesis in *P. aeruginosa*. This bacterium is an opportunistic human pathogen affecting immune compromised patients. It is known as the leading cause of morbidity and mortality in cystic fibrosis (CF) patients and as one of the leading causes of nosocomial infections (9). *P. aeruginosa* strains are well-known alginate producers. In particular, alginate overproduction is characteristic for the mucoid phenotype of most clinical isolates from CF patients and the hallmark of chronic infections. Alginate is overproduced during adaptation to the CF lung environment, and predominantly constitutes the matrix of mature biofilms conferring a slimy or mucoid phenotype. Indeed, it is greatly important in biofilm maturation, structural stability and protection as well as persistence by embedding *P. aeruginosa* cells against opsonophagocytosis, free radicals released from immune cells, and antibiotics used for treatment (9).

For many years various genes and proteins involved in alginate biosynthesis have been investigated (36). It was proposed that a multiprotein complex spanning the envelope of bacteria is responsible for alginate polymerization, modifications, translocation and secretion (98). Despite these valuable findings, the molecular mechanism of alginate biosynthesis has remained largely unknown.

Despite the understanding of alginate modifying enzymes (AlgG and AlgX) in constituting the proposed multiprotein complex, interactive functional relationships of these protein subunits with alginate polymerizing unit (Alg8-Alg44) were elusive. In chapter III, by using various mutants complemented with relevant genes and their catalytically inactive variants, we could unravel interactive functional relationships of these protein subunits in the multiprotein complex. Hence, the correlation of alginate polymerization with modification mechanisms was understood. This information could provide clear answers for different questions trying to explain the relationship of acetylation and epimerization events. These experiments resulted in the production of

various alginates from *P. aeruginosa* and demonstrated tailor-made alginate production via genetic manipulation of bacteria. Generation of various mutants producing different alginates enabled us to assess the impact of various compositions of the alginates on biofilm development and cell-to-cell interactions. Our results showed how biofilm architecture is impacted by the composition of alginates and addition of modifications such as acetylation is biologically important for cell-cell interactions (Chapter III).

In chapter IV, we mainly focused on understanding the molecular mechanisms of alginate polymerization with the involvement of two interacting proteins Alg8 and Alg44 and the second messenger c-di-GMP binding to Alg44 for the activation of alginate polymerization. The result of this chapter is of particular importance because c-di-GMP is an almost ubiquitous molecule in bacteria and c-di-GMP signalling controls motility-sessility (biofilm) transition by impacting many biological processes in bacterial cells. C-di-GMP signalling is an intricate regulatory mechanism during pathogenesis of *P. aeruginosa* and many other pathogens. The synthesis of several biofilm associated exopolysaccharides such as alginate, cellulose and poly-N-acetylglucosamine (PNAG) is post-translationally regulated by this small molecule, but the mechanism of c-di-GMP signalling is largely unknown yet (36, 200, 241, 242). Before this study, the mechanism of cellulose synthesis (200) was the only well understood model that could explain the possible activation of polysaccharide polymerization upon c-di-GMP binding. This model was based on crystallographic approaches and *in vitro* assessments. However, how c-di-GMP binding regulates polysaccharide polymerization in physiological conditions was still unknown. Indeed, in living organisms the cellular level of c-di-GMP is a key determinant for a desired physiological output displaying as an inhibitory or activating mechanism (198). This is why an army of c-di-GMP metabolizing proteins mediate turnover of this molecule during various stages of the bacterial lifestyle (9). By taking all of this valuable information into account, we designed our experiments in chapter IV to unravel the activation mechanism of alginate polymerization upon c-di-GMP binding in *P. aeruginosa*. We could show that, while similar to cellulose synthesis, the c-di-GMP binding targets the catalytic site of glycosyltransferase via inducing conformational changes, but this mechanism for activating alginate polymerization is different from activation of cellulose polymerization (Chapter IV).

Furthermore, this study shed light on the regulation of alginate production that is determined by various levels of c-di-GMP in the cell and it would be an appropriate example for other c-di-GMP controlled cellular processes. Alg44 is another essential

subunit for polymerization of alginate (243). Although its role in binding to c-di-GMP and polymerization had been studied, the function of the periplasmic domain of this protein was elusive. Therefore, we probed the periplasmic domain of Alg44 and we could show the critical role of this domain not only in polymerization but also in the regulation of periplasmic modification events (Chapter IV). In this chapter, we also could visualize the cellular localization and distribution of the alginate polymerase complex surrounding the cells.

In chapter V, we evaluated the establishment of alginate biosynthesis in heterologous hosts which are fast-and easy-to-grow, biotechnologically accepted and non-pathogenic. Alginate from seaweeds are the only commercially available ones and widely used for a various of purposes (244). However, due to the heterogeneity of algal alginates, polydispersity, non-acetylated, low molecular mass, and unwanted contaminations they may not meet some criteria for high value purposes such as in pharmaceutical and biomedical engineering. Therefore there is a need for developing new alginates displaying new properties for high value applications. To these demands, bacterial production of alginate is an advantage as the whole biosynthesis pathway of alginate is understood in bacteria mainly in *P. aeruginosa* and previously we showed that they are valuable tools for tailoring alginates via genetic manipulation (151). However, *P. aeruginisa* is an opportunistic pathogen, unsuitable for applying its alginate products for high value purposes (9). However, in chapter V, the known alginate biosynthesis pathway in *P. aeruginosa* could help us in designing a set of experiments for production of alginate from non-pathogenic heterologous hosts. As production and localization of a whole set of proteins involved in alginate biosynthesis in heterologous hosts such as *E. coli* strains might be challenging process, we aimed to establish essential steps including precursor production, polymerization and secretion by using minimal, but critical, protein requirements. This study evaluated the potential of various *E. coli* and *B. megaterium* strains for producing these heterologous proteins. This study will be a foundation for further investigation of alginate production from heterologous hosts.

In chapter V, we showed that production and localization of proteins as minimal requirements for alginate production in some strains of *E. coli* is achievable. However, there are some considerations to complete this goal. We would suggest that the next step must focus on confirming the production of the precursor of alginate GDP-mannuronic acid in a heterologous host where production of proteins involved in precursor biosynthesis was detected. Production and localization of Alg8 and Alg44 in heterologous

hosts was confirmed. Therefore, we would suggest that functional activity of these membrane proteins must be assessed in *in vitro* conditions as the critical step for proving the establishment of the polymerization event. This step can be completed by the assessment of AlgE production and localization in *E. coli* strains, required for alginate secretion. However, post-translational modifications at the protein level and post-translational regulation such as in the role of c-di-GMP can be important to consider for achieving this goal.

OUTLOOK

Traditionally, polysaccharides have been largely utilized in food, agricultural, cosmetic, and pharmaceutical industries as thickeners, stabilizers, viscosifiers, additives, gel-and film-formers, and fertilizers (244). Bacteria are major polysaccharide producers in nature. To bacteria, polysaccharide production is vital because they take part in the formation of the bacterial envelope or participate in biofilm formation (10). Therefore, studying bacterial polysaccharides is important not only due to their potential for being harnessed for industrial applications, but also for delineating their role in the biology of bacteria particularly in the context of pathogenesis and human health. This study focused on understanding the role of polysaccharides in biofilm formation of two species of *Pseudomonas* i.e. *P. aeruginosa* and *P. syringae* causing infections in human and plant, respectively. This study showed that *Pseudomonas* species like other bacteria take the same strategy for surviving harsh conditions and polysaccharides are biologically important as major part of their biofilm matrix. Our analysis resulted in identification of two novel polysaccharides from *P. syringae* containing different ratios of rhamnose, fucose, and glucose. This study suggests analysing further physicochemical properties of these novel polysaccharides for use in appropriate industrial applications. Furthermore, rhamnose and fucose are rare sugars and their occurrence in the structure of polysaccharides brings new biological and physiochemical properties (245). Also, we suggest investigating the biosynthesis pathway of rhamnose, fucose, and glucose containing polysaccharides in *P. syringae* as a model organism. Similar to the alginate biosynthesis pathway in *P. aeruginosa*, studying the biosynthesis pathway of such polysaccharides not only informs drug development but also aids in the production of tailor-made polysaccharides.

Based on our findings, we suggest that assessment of anti-biofilm efficacy of kasugamycin and chlorine dioxide against other bacterial biofilms.

Many aspects of alginate biosynthesis have been understood but there are still some aspects that remain unknown. Therefore, we suggest that future research must focus on understanding the poorly understood acetylation mechanism with the involvement of AlgF, AlgI and AlgJ. It is still unclear how these essential proteins for acetylation link to the multi-protein complex or assemble into this complex and play roles in acetylating alginate.

Alginates have been of the most widely applied biopolymers in various industries due to their unique physiochemical properties (246). The most relevant criteria which have made alginates appropriate for biomedical and pharmaceutical purposes are associated with their non-toxicity, biocompatibility, inertness and straightforward modification. Hence, nowadays, various types of alginates and their derivatives have earned their reputation in drug delivery, cell encapsulation and enzyme immobilization (51, 247-249). However, development of some high value products from alginates and their derivatives may require desired and defined composition and properties of alginates which might not exist in algal alginates or may not be achievable via chemical modifications. Therefore, bacterial alginates which display different characteristics from algal alginates can potentially meet the required criteria for advanced biomedical purposes. Most importantly, our study showed that in contrast to algal alginates whose biosynthesis pathways and lab production has not yet been achieved, obtaining various alginates with pre-determined and unique properties from bacteria is achievable in the laboratory. However, bacterial production of alginates is still at an early stage, as the biosynthesis/modification pathways need to be fully understood. More importantly, these pathways are tightly controlled by bacterial regulatory systems which may be an obstacle for the establishment of laboratory production of alginates. Therefore, understanding the minimal protein requirements for bacterial production of alginates in homologous and heterologous hosts should be a future research goal. To date most research has focussed on the opportunistic human pathogen *P. aeruginosa*, therefore we suggest establishing the production of various alginates in non-pathogenic bacteria and non-virulent strains.

REFRENCES

1. **Dumitriu S.** 2004. Polysaccharides: structural diversity and functional versatility. CRC press.

2. **Schmid J, Sieber V, Rehm B.** 2015. Bacterial exopolysaccharides: biosynthesis pathways and engineering strategies. Front Microbiol **6:**496.

3. **Lapasin R, Pricl S.** 1995. Industrial applications of polysaccharides, p 134-161, Rheology of Industrial Polysaccharides: Theory and Applications doi:10.1007/978-1-4615-2185-3_2. Springer US, Boston, MA.

4. **Nwodo UU, Green E, Okoh AI.** 2012. Bacterial exopolysaccharides: functionality and prospects. Int J Mol Sci **13:**14002-14015.

5. **Harshey RM.** 2003. Bacterial motility on a surface: many ways to a common goal. Annual Reviews in Microbiology **57:**249-273.

6. **Marykwas DL, Schmidt SA, Berg HC.** 1996. Interacting components of the flagellar motor of *Escherichia coli* revealed by the two-hybrid system in yeast. J Mol Biol **256:**564-576.

7. **Branda SS, Vik S, Friedman L, Kolter R.** 2005. Biofilms: the matrix revisited. Trends in microbiology **13:**20-26.

8. **Costerton JW, Lewandowski Z, Caldwell DE, Korber DR, Lappin-Scott HM.** 1995. Microbial biofilms. Annual Reviews in Microbiology **49:**711-745.

9. **Moradali MF, Ghods S, Rehm BHA.** 2017. *Pseudomonas aeruginosa* Lifestyle: A Paradigm for Adaptation, Survival, and Persistence. Frontiers in Cellular and Infection Microbiology **7:**39.

10. **Costerton JW, Cheng KJ, Geesey GG, Ladd TI, Nickel JC, Dasgupta M, Marrie TJ.** 1987. Bacterial biofilms in nature and disease. Annu Rev Microbiol **41:**435-464.

11. **Donlan RM, Costerton JW.** 2002. Biofilms: survival mechanisms of clinically relevant microorganisms. Clinical Microbiology Reviews **15:**167-193.

12. **Gacesa P, Russell NJ.** 1990. Pseudomonas infection and alginates : biochemistry, genetics, and pathology, 1st ed. Chapman and Hall, London ; New York.

13. **Mazzaglia A, Studholme DJ, Taratufolo MC, Cai R, Almeida NF, Goodman T, Guttman DS, Vinatzer Ba, Balestra GM.** 2012. *Pseudomonas syringae* pv. *actinidiae* (PSA) isolates from recent bacterial canker of kiwifruit outbreaks belong to the same genetic lineage. PloS one **7:**e36518-e36518.

14. **Ude S, Arnold DL, Moon CD, Timms-Wilson T, Spiers AJ.** 2006. Biofilm formation and cellulose expression among diverse environmental Pseudomonas isolates. Environmental microbiology **8:**1997-2011.

15. **Takikawa Y, Serizawa S, Ichikawa T, Goto M, Takanashi K.** 1989. *Pseudomonas syringae* pv. *actinifiae* pv. nov.: the causal of canker bacterium of canker of kiwifruit in Japan. Ann Phytopath Soc Japan **55:**437-444.

16. **Koh Y, Chung H, Cha B, Lee D.** 1994. Outbreak and spread of bacterial canker in kiwifruit. Korean Journal of Plant Pathology (Korea Republic).

17. **Balestra GM, Mazzaglia A, Quattrucci A, Renzi M, Rossetti A.** 2009. Current status of bacterial canker spread on kiwifruit in Italy. Australasian Plant Disease Notes **4:**34-36.

18. **Ferrante P, Scortichini M.** 2010. Molecular and phenotypic features of *Pseudomonas syringae* pv. *actinidiae* isolated during recent epidemics of bacterial canker on yellow kiwifruit (*Actinidia chinensis*) in central Italy. Plant Pathology **59:**954-962.

19. **Young JM.** 2012. *Pseudomonas syringae* pv.*actinidiae* in New zealand. Journal of Plant Pathology **94:**5-10.

20. **McCann HC, Rikkerink EH, Bertels F, Fiers M, Lu A, Rees-George J, Andersen MT, Gleave AP, Haubold B, Wohlers MW.** 2013. Genomic analysis of the kiwifruit pathogen *Pseudomonas syringae* pv. *actinidiae* provides insight into the origins of an emergent plant disease. PLoS Pathog **9:**e1003503.

21. **Chapman JR, Taylor RK, Weir BS, Romberg MK, Vanneste JL, Luck J, Alexander BJR.** 2012. Phylogenetic relationships among global populations of *Pseudomonas syringae* pv. *actinidiae*. Phytopathology **102:**1034-1044.

22. **Quiñones B, Dulla G, Lindow SE.** 2005. Quorum sensing regulates exopolysaccharide production, motility, and virulence in *Pseudomonas syringae*. Molecular Plant-Microbe Interactions **18:**682-693.

23. **Von Bodman SB, Bauer WD, Coplin DL.** 2003. Quorum sensing in plant-pathogenic bacteria. Annual review of phytopathology **41:**455-482.

24. **Renzi M, Copini P, Taddei AR, Rossetti A, Gallipoli L, Mazzaglia A, Balestra GM.** 2012. Bacterial canker on kiwifruit in Italy: anatomical changes in the wood and in the primary infection sites. Phytopathology **102:**827-840.

25. **Chen X, Stewart PS.** 2000. Biofilm removal caused by chemical treatments. Wat Res **34:**4229-4233.

26. **Dow JM, Crossman L, Findlay K, He Y-Q, Feng J-X, Tang J-L.** 2003. Biofilm dispersal in *Xanthomonas campestris* is controlled by cell-cell signaling and is required for full virulence to plants. Proceedings of the National Academy of Sciences of the United States of America **100:**10995-11000.

27. **Levitan AA.** 1967. In vitro antibacterial activity of kasugamycin. Applied microbiology **15:**750-753.

28. **Suhara Y, Maeda K, Umezawa H.** 1966. Chemical studies on kasugamycin. V. The structure of kasugamycin. Tetrahedron letters **12:**1239-1244.

29. **Suvorov A, Van Gemen B, Van Knippenberg P.** 1988. Increased kasugamycin sensitivity in *Escherichia coli* caused by the presence of an inducible erythromycin resistance (erm) gene of *Streptococcus pyogenes*. Mol Gen Genet **215:**152-155.

30. **Umezawa H, Okami Y, Hashimoto T, Sukara M, Hamada M, Takeuchi T.** 1965. A new antibiotic, Kasugamycin. Journal of Antibiotic (Tokyyo) Ser A **18:**101-103.

31. **Aieta EM, James DB.** 2014. A Review of Chlorine Dioxide in Drinking Water Treatment. American Water Works Association **78:**62-72.

32. **Behnke S, Camper AK.** 2012. Chlorine dioxide disinfection of single and dual species biofilms, detached biofilm and planktonic cells. Biofouling **28:**635-647.

33. **United States Environmental Protection Agency.** 1999. Alternative Disinfectants and Oxidants Guidance Manual. Chapter 4. chlorine dioxide.1-41.

34. **Masschelein WJ, Rice RG.** 1979. Chlorine dioxide: chemistry and environmental impact of oxychlorine compounds. Ann Arbor Science Publ Ann Arbor, Mich**:**190-190.

35. **Mayack LA, Soracco RJ, Wilde EW, Pope DH.** 1984. Comparative effectiveness of chlorine and chlorine dioxide biocide regimes for biofouling control. Water Research **18:**593-599.

36. **Hay ID, Wang Y, Moradali MF, Rehman ZU, Rehm BH.** 2014. Genetics and regulation of bacterial alginate production. Environ Microbiol **16:**2997-3011.

37. **Rehm BH, Valla S.** 1997. Bacterial alginates: biosynthesis and applications. Appl Microbiol Biotechnol **48:**281-288.

38. **Skjak-Braek G, Grasdalen H, Larsen B.** 1986. Monomer sequence and acetylation pattern in some bacterial alginates. Carbohydr Res **154:**239-250.

39. **Kobayashi H.** 2005. Airway biofilms: implications for pathogenesis and therapy of respiratory tract infections. Treat Respir Med **4:**241-253.

40. **Bayer AS, Speert DP, Park S, Tu J, Witt M, Nast CC, Norman DC.** 1991. Functional role of mucoid exopolysaccharide (alginate) in antibiotic-induced and polymorphonuclear leukocyte-mediated killing of *Pseudomonas aeruginosa*. Infect Immun **59:**302-308.

41. **Slack MPE, Nichols WW.** 1981. The penetration of antibiotics through sodium alginate and through the exopolysaccharide of a mucoid strain of *Pseudomonas aeruginosa*. Lancet **2:**502-503.

42. **Simpson JA, Smith SE, Dean RT.** 1989. Scavenging by alginate of free radicals released by macrophages. Free Radic Biol Med **6:**347-353.

43. **Rehm, B. H. A.** 2002. Alginates from bacteria, p. 179–211. In E. J. Vandamme, S. DeBaets, and A. Steinbu¨chel (ed.), Biopolymers, vol. polysaccharides. Wiley VCH, New York, N.Y.

44. **Moradali MF, Donati I, Sims IM, Ghods S, Rehm BH.** 2015. Alginate polymerization and modification are linked in *Pseudomonas aeruginosa*. MBio **6:**e00453-00415.

45. **Douthit SA, Dlakic M, Ohman DE, Franklin MJ.** 2005. Epimerase active domain of *Pseudomonas aeruginosa* AlgG, a protein that contains a right-handed β-helix. Journal of bacteriology **187:**4573-4583.

46. **SkjÅk-Bræk G, Paoletti S, Gianferrara T.** 1989. Selective acetylation of mannuronic acid residues in calcium alginate gels. Carbohydrate Research **185:**119-129.

47. **Windhues T, Borchard W.** 2003. Effect of acetylation on physico-chemical properties of bacterial and algal alginates in physiological sodium chloride solutions investigated with light scattering techniques. Carbohydrate polymers **52:**47-52.

48. **Mørch ÝA, Donati I, Strand BL, Skjåk-Bræk G.** 2006. Effect of Ca2+, Ba2+, and Sr2+ on alginate microbeads. Biomacromolecules **7:**1471-1480.

49. **Onsøyen E.** 1997. Alginates, p 22-44, Thickening and gelling agents for food. Springer.

50. **McHugh DJ.** 1987. Production, properties and uses of alginates. Production and Utilization of Products from Commercial Seaweeds FAO Fish Tech Pap **288:**58-115.

51. **Smith AM, Miri T.** 2010. 6 Alginates in Foods. Practical Food Rheology: An Interpretive Approach**:**113.

52. **Tønnesen HH, Karlsen J.** 2002. Alginate in Drug Delivery Systems. Drug Development and Industrial Pharmacy **28:**621-630.

53. **Lesser MA.** 1947. Alginates in drugs and cosmetics. Drug Cosmet Ind **61:**761-842.

54. **Skaugrud Ø, Hagen A, Borgersen B, Dornish M.** 1999. Biomedical and pharmaceutical applications of alginate and chitosan. Biotechnology and genetic engineering reviews **16:**23-40.

55. **Bhattarai N, Li Z, Edmondson D, Zhang M.** 2006. Alginate- based nanofibrous scaffolds: Structural, mechanical, and biological properties. Advanced Materials **18:**1463-1467.

56. **Douglas KL, Piccirillo CA, Tabrizian M.** 2006. Effects of alginate inclusion on the vector properties of chitosan-based nanoparticles. Journal of Controlled Release **115:**354-361.

57. **Cook W.** 1986. Alginate dental impression materials: chemistry, structure, and properties. Journal of biomedical materials research **20:**1-24.

58. **Craig R.** 1988. Review of dental impression materials. Advances in dental research **2:**51-64.

59. **Groves A, Lawrence J.** 1986. Alginate dressing as a donor site haemostat. Annals of the Royal College of Surgeons of England **68:**27.

60. **Barnett S, Varley S.** 1987. The effects of calcium alginate on wound healing. Annals of the Royal College of Surgeons of England **69:**153.

61. **Hrynyk M, Martins-Green M, Barron AE, Neufeld RJ.** 2012. Alginate-PEG sponge architecture and role in the design of insulin release dressings. Biomacromolecules **13:**1478-1485.

62. **Barbetta A, Barigelli E, Dentini M.** 2009. Porous alginate hydrogels: synthetic methods for tailoring the porous texture. Biomacromolecules **10:**2328-2337.

63. **Andersen T, Melvik JE, Gåserød O, Alsberg E, Christensen BE.** 2012. Ionically gelled alginate foams: physical properties controlled by operational and macromolecular parameters. Biomacromolecules **13:**3703-3710.

64. **Shin S-J, Park J-Y, Lee J-Y, Park H, Park Y-D, Lee K-B, Whang C-M, Lee S-H.** 2007. "On the fly" continuous generation of alginate fibers using a microfluidic device. Langmuir **23:**9104-9108.

65. **Daemi H, Barikani M, Barmar M.** 2013. Highly stretchable nanoalginate based polyurethane elastomers. Carbohydrate polymers **95:**630-636.

66. **Senuma Y, Lowe C, Zweifel Y, Hilborn J, Marison I.** 2000. Alginate hydrogel microspheres and microcapsules prepared by spinning disk atomization. Biotechnology and bioengineering **67:**616-622.

67. **Bodmeier R, Chen H, Paeratakul O.** 1989. A novel approach to the oral delivery of micro-or nanoparticles. Pharmaceutical research **6:**413-417.

68. **Kierstan M, Bucke C.** 1977. The immobilization of microbial cells, subcellular organelles, and enzymes in calcium alginate gels. Biotechnology and bioengineering **19:**387-397.

69. **Palmieri G, Giardina P, Desiderio B, Marzullo L, Giamberini M, Sannia G.** 1994. A new enzyme immobilization procedure using copper alginate gel: application to a fungal phenol oxidase. Enzyme and microbial technology **16:**151-158.

70. **Fukushima Y, Okamura K, Imai K, Motai H.** 1988. A new immobilization technique of whole cells and enzymes with colloidal silica and alginate. Biotechnology and bioengineering **32:**584-594.

71. **Zhang W, Zhang Z, Zhang Y.** 2011. The application of carbon nanotubes in target drug delivery systems for cancer therapies. Nanoscale research letters **6:**555.

72. **Barreto JA, O'Malley W, Kubeil M, Graham B, Stephan H, Spiccia L.** 2011. Nanomaterials: applications in cancer imaging and therapy. Advanced Materials **23**.

73. **Serp D, Cantana E, Heinzen C, Von Stockar U, Marison I.** 2000. Characterization of an encapsulation device for the production of monodisperse alginate beads for cell immobilization. Biotechnology and bioengineering **70:**41-53.

74. **Baruch L, Machluf M.** 2006. Alginate–chitosan complex coacervation for cell encapsulation: Effect on mechanical properties and on long- term viability. Biopolymers **82:**570-579.

75. **Orive G, Hernandez R, Gascon A, Igartua M, Pedraz J.** 2003. Survival of different cell lines in alginate-agarose microcapsules. European journal of pharmaceutical sciences **18:**23-30.

76. **Shapiro L, Cohen S.** 1997. Novel alginate sponges for cell culture and transplantation. Biomaterials **18:**583-590.

77. **de Vos P, Faas MM, Strand B, Calafiore R.** 2006. Alginate-based microcapsules for immunoisolation of pancreatic islets. Biomaterials **27:**5603-5617.

78. **Kulseng B, Skjåk-Bræk G, Ryan L, Andersson A, King A, Faxvaag A, Espevik T.** 1999. Transplantation of Alginate Microcapsules: Generation of Antibodies Against Alginates and Encapsulated Porcine Islet-Like Cell Clusters1. Transplantation **67:**978-984.

79. **Li Z, Ramay HR, Hauch KD, Xiao D, Zhang M.** 2005. Chitosan–alginate hybrid scaffolds for bone tissue engineering. Biomaterials **26:**3919-3928.

80. **Kuo CK, Ma PX.** 2001. Ionically crosslinked alginate hydrogels as scaffolds for tissue engineering: part 1. Structure, gelation rate and mechanical properties. Biomaterials **22:**511-521.

81. **Drury JL, Mooney DJ.** 2003. Hydrogels for tissue engineering: scaffold design variables and applications. Biomaterials **24:**4337-4351.

82. **Lee J, Cuddihy MJ, Kotov NA.** 2008. Three-dimensional cell culture matrices: state of the art. Tissue Engineering Part B: Reviews **14:**61-86.

83. **Perka C, Spitzer RS, Lindenhayn K, Sittinger M, Schultz O.** 2000. Matrix- mixed culture: New methodology for chondrocyte culture and preparation of cartilage transplants. Journal of Biomedical Materials Research Part A **49:**305-311.

84. **Murphy WL, Mooney DJ.** 1999. Controlled delivery of inductive proteins, plasmid DNA and cells from tissue engineering matrices. Journal of periodontal research **34:**413-419.

85. **Kwiatek MA, Roman S, Fareeduddin A, Pandolfino JE, Kahrilas PJ.** 2011. An alginate-antacid formulation (Gaviscon Double Action Liquid) can eliminate or displace the postprandial 'acid pocket'in symptomatic GERD patients. Alimentary pharmacology & therapeutics **34:**59-66.

86. **Washington N.** 1990. Investigation into the barrier action of an alginate gastric reflux suppressant, liquid Gaviscon®. Drug Investigation **2:**23-30.

87. **Michel G, Tonon T, Scornet D, Cock JM, Kloareg B.** 2010. The cell wall polysaccharide metabolism of the brown alga Ectocarpus siliculosus. Insights into the evolution of extracellular matrix polysaccharides in Eukaryotes. New Phytologist **188:**82-97.

88. **Rehm BHA.** 2010. Bacterial polymers: biosynthesis, modifications and applications. Nat Rev Micro **8:**578-592.

89. **Chitnis CE, Ohman DE.** 1993. Genetic analysis of the alginate biosynthetic gene cluster of *Pseudomonas aeruginosa* shows evidence of an operonic structure. Mol Microbiol **8:**583-593.

90. **Schurr MJ, Martin DW, Mudd MH, Hibler NS, Boucher JC, Deretic V.** 1993. The algD promoter: regulation of alginate production by *Pseudomonas aeruginosa* in cystic fibrosis. Cell Mol Biol Res **39:**371-376.

91. **Shankar S, Ye RW, Schlictman D, Chakrabarty A.** 1995. Exopolysaccharide Alginate Synthesis in *Pseudomonas seruginosa*: Enzymology and Regulation of Gene Expression. Advances in enzymology and related areas of molecular biology **70:**221-255.

92. **Lynn AR, Sokatch JR.** 1984. Incorporation of isotope from specifically labeled glucose into alginates of *Pseudomonas aeruginosa* and *Azotobacter vinelandii*. J Bacteriol **158:**1161-1162.

93. **Narbad A, Russell NJ, Gacesa P.** 1988. Radiolabelling patterns in alginate of *Pseudomonas aeruginosa* synthesized from specifically-labelled 14C-monosaccharide precursors. Microbios **54:**171-179.

94. **Tatnell PJ, Russell NJ, Gacesa P.** 1994. GDP-mannose dehydrogenase is the key regulatory enzyme in alginate biosynthesis in *Pseudomonas aeruginosa*: evidence from metabolite studies. Microbiology **140 (Pt 7):**1745-1754.

95. **Rehm BHA, Remminghorst U, Hay ID.** 2009. Molecular characterization of Alg8, a putative glycosyltransferase, involved in alginate polymerisation. J Biotechnol **140:**176-183.

96. **Lory S, Merighi M, Lee VT, Hyodo M, Hayakawa Y.** 2007. The second messenger bis-(3 '-5 ')-cyclic-GMP and its PilZ domain-containing receptor Alg44 are required for alginate biosynthesis in *Pseudomonas aeruginosa*. Mol Microbiol **65:**876-895.

97. **Rehm BHA, Remminghorst U.** 2006. In vitro alginate polymerization and the functional role of Alg8 in alginate production by *Pseudomonas aeruginosa*. Appl Environ Microbiol **72:**298-305.

98. **Rehman ZU, Wang Y, Moradali MF, Hay ID, Rehm BH.** 2013. Insights into the assembly of the alginate biosynthesis machinery in *Pseudomonas aeruginosa*. Appl Environ Microbiol **79:**3264-3272.

99. **Rehman ZU, Wang Y, Moradali MF, Hay ID, Rehm BH.** 2013. Insights into the assembly of the alginate biosynthesis machinery in *Pseudomonas aeruginosa*. Applied and environmental microbiology **79:**3264-3272.

100. **Hay ID, Schmidt O, Filitcheva J, Rehm BH.** 2012. Identification of a periplasmic AlgK–AlgX–MucD multiprotein complex in *Pseudomonas aeruginosa* involved in biosynthesis and regulation of alginate. Applied microbiology and biotechnology **93:**215-227.

101. **Franklin MJ, Douthit SA, McClure MA.** 2004. Evidence that the algI/algJ gene cassette, required for O acetylation of *Pseudomonas aeruginosa* alginate, evolved by lateral gene transfer. Journal of bacteriology **186:**4759-4773.

102. **Everett KR, Taylor RK, Romberg MK, Rees-George J, Fullerton RA, Vanneste JL, Manning MA.** 2011. First report of *Pseudomonas syringae* pv. *actinidiae* causing kiwifruit bacterial canker in New Zealand. Australasian Plant Disease Notes **6:**67-71.

103. **Greer G, Saunders C.** 2012. The costs of Psa-V to the New Zealand kiwifruit industry and the wider community. Agribusiness and Economics Research Unit Report, Lincoln University.

104. **King EO, Ward MK, Raney DE.** 1954. Two simple media for the demonstration of pyocyanin and fluorescin. The Journal of laboratory and clinical medicine **44:**301-307.

105. **Hay ID, Remminghorst U, Rehm BH.** 2009. MucR, a novel membrane-associated regulator of alginate biosynthesis in *Pseudomonas aeruginosa*. Appl Environ Microbiol **75:**1110-1120.

106. **Ghafoor A, Hay ID, Rehm BH.** 2011. Role of exopolysaccharides in *Pseudomonas aeruginosa* biofilm formation and architecture. Appl Environ Microbiol **77:**5238-5246.

107. **Blumenkrantz N, Asboe-Hansen G.** 1973. New method for quantitative determination of uronic acids. Analytical biochemistry **489:**484-489.

108. **Hay ID, Rehman ZU, Rehm BH.** 2010. Membrane topology of outer membrane protein AlgE, which is required for alginate production in *Pseudomonas aeruginosa*. Appl Environ Microbiol **76:**1806-1812.

109. **Yemm E, Willis A.** 1954. The estimation of carbohydrates in plant extracts by anthrone. Biochemical journal **57:**508.

110. **Bradford MM.** 1976. A rapid and sensitive method for the quantitation of microgram quantities of protein utilizing the principle of protein-dye binding. Analytical biochemistry **72:**248-254.

111. **Stoscheck CM.** 1990. Quantitation of protein. Methods in Enzymology **182:**50-68.

112. **Laemmli UK.** 1970. Cleavage of structural proteins during the assembly of the head of bacteriophage T4. Nature **227:**680-685.

113. **Jan S, Roblot C, Goethals G, Courtois J, Courtois B, Saucedo JN, Seguin J-P, Barbotin J-N.** 1995. Study of parameters affecting poly (3-hydroxybutyrate) quantification by gas chromatography. Analytical biochemistry **225:**258-263.

114. **De Ruiter GA, Schols HA, Voragen AG, Rombouts FM.** 1992. Carbohydrate analysis of water-soluble uronic acid-containing polysaccharides with high-performance anion-exchange chromatography using methanolysis combined with TFA hydrolysis is superior to four other methods. Analytical biochemistry **207:**176-185.

115. **Wee MS, Matia-Merino L, Carnachan SM, Sims IM, Goh KK.** 2014. Structure of a shear-thickening polysaccharide extracted from the New Zealand black tree fern, Cyathea medullaris. International journal of biological macromolecules **70:**86-91.

116. **Ciucanu I, Kerek F.** 1984. A simple and rapid method for the permethylation of carbohydrates. Carbohydrate research **131:**209-217.

117. **Carnachan SM, Bootten TJ, Mishra S, Monro JA, Sims IM.** 2012. Effects of simulated digestion in vitro on cell wall polysaccharides from kiwifruit (Actinidia spp.). Food Chemistry **133:**132-139.

118. **Sims IM, Furneaux RH.** 2003. Structure of the exudate gum from *Meryta sinclairii*. Carbohydrate polymers **52:**423-431.

119. **Kuehn M, Hausner M, Bungartz HJ, Wagner M, Wilderer PA, Wuertz S.** 1998. Automated confocal laser scanning microscopy and semiautomated image processing for analysis of biofilms. Appl Environ Microbiol **64:**4115-4127.

120. **Merritt JH, Kadouri DE, O'Toole GA.** 2005. Growing and analyzing static biofilms. Current protocols in microbiology **Chapter 1:**1B. 1.

121. **Everett K.** 2011. Product screening test for kasumin and phyton (Plant & Food Research *Pseudomonas syringae* pv. *actinidiae* (Psa) research note). Plant & Food Research, Mt Albert, Auckland, New Zealand.

122. **Hall III JW, Orth Jr E.** 1962. Actinospectacin: an in vitro study of effectiveness against pathogenic bacteria. The American journal of the medical sciences **244:**30-39.

123. **Spitali M, Patel M, Smith A.** 1995. Structures of Lipopolysaccharide Side- chains of NCPPB 2995, the Neopathotype Strain of *Pseudomonas syringae* pv. *morsprunorum* and Three Other Strains, in Relation to O- serogroup. Journal of Phytopathology **143:**671-677.

124. **Zdorovenko EL, Ovod VV, Zatonsky GV, Shashkov AS, Kocharova NA, Knirel YA.** 2001. Location of the O-methyl groups in the O polysaccharide of *Pseudomonas syringae* pv. *phaseolicola*. Carbohydrate research **330:**505-510.

125. **Senchenkova SyN, Huang X, Laux P, Knirel YA, Shashkov AS, Rudolph K.** 2002. Structures of the O-polysaccharide chains of the lipopolysaccharides of *Xanthomonas*

campestris pv *phaseoli* var fuscans GSPB 271 and *X.campestris* pv *malvacearum* GSPB 1386 and GSPB 2388. Carbohydrate research **337:**1723-1728.

126. **Ovod VV, Knirel YA, Samson R, Krohn KAIJ.** 1999. Immunochemical characterization and taxonomic evaluation of the O- polysaccharides of the lipopolysaccharides of *Pseudomonas syringae* serogroup O1 strains. Journal of bacteriology **181:**6937-6947.

127. **Smith A, Munro S, Wait R, Hignett R.** 1994. Effect on lipopolysaccharide structure of aeration during growth of a plum isolate of *Pseudomonas syringae* pv. *morsprunorum*. Microbiology **140:**1585-1593.

128. **Veremeichenko S, Zdorovenko G, Zdorovenko E, Zatonskii G.** 2005. Characterization of Lipopolysaccharides from *Pseudomonas fluorescens* IMB 2108 (Biovar II) and IMB 2111 (Biovar IV) with O-Chains Represented by α-Glucan. Microbiology **74:**549-556.

129. **Knirel YA, Shashkov AS, Senchenkova SyN, Ajiki Y, Fukuoka S.** 2002. Structure of the O-polysaccharide of *Pseudomonas putida* FERM P-18867. Carbohydrate research **337:**1589-1591.

130. **Sato N, Nakazawa F, Ito T, Hoshino T, Hoshino E.** 2003. The structure of the antigenic polysaccharide produced by *Eubactrium saburreum* T15. Carbohydrate research **338:**923-930.

131. **Kaczynski Z, Karapetyan G, Evidente A, Iacobellis NS, Holst O.** 2006. The structure of a putative exopolysaccharide of *Burkholderia gladioli* pv. *agaricicola*. Carbohydrate research **341:**285-288.

132. **Pieretti G, Nicolaus B, Poli A, Corsaro MM, Lanzetta R, Parrilli M.** 2009. Structural determination of the O-chain polysaccharide from the haloalkaliphilic *Halomonas alkaliantarctica* bacterium strain CRSS. Carbohydrate research **344:**2051-2055.

133. **Leivers S, Hidalgo-Cantabrana C, Robinson G, Margolles A, Ruas-Madiedo P, Laws AP.** 2011. Structure of the high molecular weight exopolysaccharide produced by *Bifidobacterium animalis* subsp. *lactis* IPLA-R1 and sequence analysis of its putative eps cluster. Carbohydrate research **346:**2710-2717.

134. **Morris CE, Monier J-M.** 2003. The ecological significance of biofilm formation by plant-associated bacteria. Annual review of phytopathology **41:**429-453.

135. **Ramey BE, Koutsoudis M, von Bodman SB, Fuqua C.** 2004. Biofilm formation in plant–microbe associations. Current opinion in microbiology **7:**602-609.

136. **Leveau JH, Lindow SE.** 2001. Appetite of an epiphyte: quantitative monitoring of bacterial sugar consumption in the phyllosphere. Proceedings of the National Academy of Sciences **98:**3446-3453.

137. **Monier J-M.** 2002. Biological Significance of Bacterial Aggregation on Leaf Surfaces: The Social Life of Epiphytic Bacteria,University of California, Berkeley.

138. **Morris CE.** 2001. Phyllosphere. In Encyclopedia for Life Sciences, http:// wwwelsnet London: Nat Publ Group.

139. **Steinberger R, Allen A, Hansma H, Holden Pm.** 2002. Elongation correlates with nutrient deprivation in *Pseudomonas aeruginosa* unsaturated biofilms. Microbial ecology **43:**416-423.

140. **Prigent-Combaret C, Vidal O, Dorel C, Lejeune P.** 1999. Abiotic surface sensing and biofilm-dependent regulation of gene expression in *Escherichia coli*. Journal of bacteriology **181:**5993-6002.

141. **Davey ME, O'toole GA.** 2000. Microbial biofilms: from ecology to molecular genetics. Microbiology and molecular biology reviews **64:**847-867.

142. **Watnick P, Kolter R.** 2000. Biofilm, city of microbes. Journal of bacteriology **182:**2675-2679.

143. **van Casteren WH, Dijkema C, Schols HA, Beldman G, Voragen AG.** 2000. Structural characterisation and enzymic modification of the exopolysaccharide produced by *Lactococcus lactis* subsp. *cremoris* B39. Carbohydrate research **324:**170-181.

144. **Mankin A.** 2006. Antibiotic blocks mRNA path on the ribosome. Nature structural & molecular biology **13:**858-860.

145. **Benarde MA, Snow WB, Olivieri VP, Davidson B.** 1967. Kinetics and mechanism of bacterial disinfection by chlorine dioxide. Applied microbiology **15:**257-265.

146. **Rehm BH, Grabert E, Hein J, Winkler UK.** 1994. Antibody response of rabbits and cystic fibrosis patients to an alginate-specific outer membrane protein of a mucoid strain of *Pseudomonas aeruginosa*. Microb Pathog **16:**43-51.

147. **Pedersen SS, Hoiby N, Espersen F, Koch C.** 1992. Role of alginate in infection with mucoid *Pseudomonas aeruginosa* in cystic fibrosis. Thorax **47:**6-13.

148. **Hay I, Rehman, Z., Ghafoor, A., and Rehm, B.** 2010. Bacterial biosynthesis of alginates. J Chem Technol Biotechnol **85:**752-759.

149. **Hay ID, Ur Rehman Z, Moradali MF, Wang Y, Rehm BH.** 2013. Microbial alginate production, modification and its applications. Microb Biotechnol **6:**637-650.

150. **Franklin MJ, Nivens DE, Weadge JT, Howell PL.** 2011. Biosynthesis of the *Pseudomonas aeruginosa* extracellular polysaccharides, Alginate, Pel, and Psl. Front Microbiol **2:**167.

151. **Moradali MF, Donati I, Sims IM, Ghods S, Rehm BH.** 2015. Alginate polymerization and modification are linked in *Pseudomonas aeruginosa*. mBio **6**.

152. **Rehm BHA, Hay ID, Remminghorst U.** 2009. MucR, a Novel Membrane-Associated Regulator of Alginate Biosynthesis in *Pseudomonas aeruginosa*. Applied and Environmental Microbiology **75:**1110-1120.

153. **Baker P, Ricer T, Moynihan PJ, Kitova EN, Walvoort MT, Little DJ, Whitney JC, Dawson K, Weadge JT, Robinson H, Ohman DE, Codee JD, Klassen JS, Clarke AJ, Howell PL.** 2014. *P. aeruginosa* SGNH hydrolase-like proteins AlgJ and AlgX have similar topology but separate and distinct roles in alginate acetylation. PLoS Pathog **10:**e1004334.

154. **Franklin MJ, Ohman DE.** 2002. Mutant analysis and cellular localization of the AlgI, AlgJ, and AlgF proteins required for O acetylation of alginate in *Pseudomonas aeruginosa*. J Bacteriol **184:**3000-3007.

155. **Riley LM, Weadge JT, Baker P, Robinson H, Codee JD, Tipton PA, Ohman DE, Howell PL.** 2013. Structural and functional characterization of *Pseudomonas aeruginosa* AlgX: role of AlgX in alginate acetylation. The Journal of Biological Chemistry **288:**22299-22314.

156. **Jain S, Franklin MJ, Ertesvag H, Valla S, Ohman DE.** 2003. The dual roles of AlgG in C-5-epimerization and secretion of alginate polymers in *Pseudomonas aeruginosa*. Mol Microbiol **47:**1123-1133.

157. **Schiller NL, Robles-Price A, Wong TY, Sletta H, Valla S.** 2004. AlgX is a periplasmic protein required for alginate biosynthesis in *Pseudomonas aeruginosa*. J Bacteriol **186:**7369-7377.

158. **Bakkevig K, Sletta H, Gimmestad M, Aune R, Ertesvag H, Degnes K, Christensen BE, Ellingsen TE, Valla S.** 2005. Role of the *Pseudomonas fluorescens* alginate lyase (AlgL) in clearing the periplasm of alginates not exported to the extracellular environment. J Bacteriol **187:**8375-8384.

159. **Keiski CL, Harwich M, Jain S, Neculai AM, Yip P, Robinson H, Whitney JC, Riley L, Burrows LL, Ohman DE, Howell PL.** 2010. AlgK is a TPR-containing protein and the periplasmic component of a novel exopolysaccharide secretin. Structure **18:**265-273.

160. **Rehman ZU, Rehm BH.** 2013. Dual roles of *Pseudomonas aeruginosa* AlgE in secretion of the virulence factor alginate and formation of the secretion complex. Applied and Environmental Microbiology **79:**2002-2011.

161. **Douthit SA, Dlakic M, Ohman DE, Franklin MJ.** 2005. Epimerase active domain of *Pseudomonas aeruginosa* AlgG, a protein that contains a right-handed beta-helix. J Bacteriol **187:**4573-4583.

162. **Albrecht MT, Schiller NL.** 2005. Alginate lyase (AlgL) activity is required for alginate biosynthesis in *Pseudomonas aeruginosa*. J Bacteriol **187:**3869-3872.

163. **Hay ID, Schmidt O, Filitcheva J, Rehm BH.** 2012. Identification of a periplasmic AlgK-AlgX-MucD multiprotein complex in *Pseudomonas aeruginosa* involved in biosynthesis and regulation of alginate. Applied Microbiology and Biotechnology **93:**215-227.

164. **Remminghorst U, Rehm BHA.** 2006. Alg44, a unique protein required for alginate biosynthesis in *Pseudomonas aeruginosa*. FEBS Lett **580:**3883-3888.

165. **Remminghorst U, Hay ID, Rehm BHA.** 2009. Molecular characterization of Alg8, a putative glycosyltransferase, involved in alginate polymerisation. J Biotechnol **140:**176-183.

166. **Gutsche J, Remminghorst U, Rehm B.** 2006. Biochemical analysis of alginate biosynthesis protein AlgX from *Pseudomonas aeruginosa*: purification of an AlgX-MucD (AlgY) protein complex. Biochimie **88:**245-251.

167. **Schlegel HG, Kaltwasser H, Gottschalk G.** 1961. A submersion method for culture of hydrogen-oxidizing bacteria: growth physiological studies. Arch Mikrobiol **38:**209-222.

168. **Mathee K, Ciofu O, Sternberg C, Lindum PW, Campbell JI, Jensen P, Johnsen AH, Givskov M, Ohman DE, Molin S, Hoiby N, Kharazmi A.** 1999. Mucoid conversion of *Pseudomonas aeruginosa* by hydrogen peroxide: a mechanism for virulence activation in the cystic fibrosis lung. Microbiology **145 (Pt 6):**1349-1357.

169. **Rehm BHA, Remminghorst U.** 2006. Alg44, a unique protein required for alginate biosynthesis in *Pseudomonas aeruginosa*. Febs Letters **580:**3883-3888.

170. **Rehm BHA, Gutsche J, Remminghorst U.** 2006. Biochemical analysis of alginate biosynthesis protein AlgX from *Pseudomonas aeruginosa*: purification of an AlgX-MucD (AlgY) protein complex. Biochimie **88:**245-251.

171. **Simon R PU, Pühler A.** 1983. A broad host range mobilization system for *in vivo* genetic engineering: transposon mutagenesis in Gram-negative bacteria. Nat Biotechnol **1:**784 - 791.

172. **Kovach ME, Elzer PH, Hill DS, Robertson GT, Farris MA, Roop RM, 2nd, Peterson KM.** 1995. Four new derivatives of the broad-host-range cloning vector pBBR1MCS, carrying different antibiotic-resistance cassettes. Gene **166:**175-176.

173. **Hoang TT, Karkhoff-Schweizer RR, Kutchma AJ, Schweizer HP.** 1998. A broad-host-range Flp-FRT recombination system for site-specific excision of chromosomally-located DNA sequences: application for isolation of unmarked *Pseudomonas aeruginosa* mutants. Gene **212:**77-86.

174. **Grasdalen H, Larsen B, Smidsrod O.** 1979. Pmr study of the composition and sequence of uronate residues in alginates. Carbohydr Res **68:**23-31.

175. **Donati IP, S. .** 2009. Material Properties of Alginates in Alginates; Biology and Applications; Rhem, B. H. A. Ed.; Springer-Verlag; Berlin Heidelberg.1-53.

176. **Pawar SN, Edgar KJ.** Chemical modification of alginates in organic solvent systems. Biomacromolecules **12:**4095-4103.

177. **Williams MAK VR, Pinder DN, Hemar Y.** 2008. Microrheological studies offer insights into polysaccharide gels. Journal of Non-Newtonian Fluid Mechanics **149:**63-70.

178. **Hemar Y, Pinder DN.** 2006. DWS microrheology of a linear polysaccharide. Biomacromolecules **7:**674-676.

179. **Mansel BW; Keen SAJ PP, Hemar Y, Williams MAK.** 2013. A practical review of microrheological techniques. Rheology - new concepts, applications and methods, Rajkumar Durairaj, InTech, Rijeka Croatia.

180. **Rogers SS, Waigh TA, Zhao X, Lu JR.** 2007. Precise particle tracking against a complicated background: polynomial fitting with Gaussian weight. Phys Biol **4:**220-227.

181. **Mason TG GK, van Zanten JH, Wirtz D, Kuo SC** 1997. Particle tracking microrheology of complex fluids. Physical Review Letters **79:**3282-3285.

182. **Campisano A, Schroeder C, Schemionek M, Overhage J, Rehm BH.** 2006. PslD is a secreted protein required for biofilm formation by *Pseudomonas aeruginosa*. Appl Environ Microbiol **72:**3066-3068.

183. **Heydorn A, Nielsen AT, Hentzer M, Sternberg C, Givskov M, Ersboll BK, Molin S.** 2000. Quantification of biofilm structures by the novel computer program COMSTAT. Microbiology **146 (Pt 10):**2395-2407.

184. **Schurr MJ, Deretic V.** 1997. Microbial pathogenesis in cystic fibrosis: co-ordinate regulation of heat-shock response and conversion to mucoidy in *Pseudomonas aeruginosa*. Molecular Microbiology **24:**411-420.

185. **Ma L, Conover M, Lu H, Parsek MR, Bayles K, Wozniak DJ.** 2009. Assembly and development of the *Pseudomonas aeruginosa* biofilm matrix. PLoS Pathog **5:**e1000354.

186. **Billings N, Millan M, Caldara M, Rusconi R, Tarasova Y, Stocker R, Ribbeck K.** 2013. The extracellular matrix component Psl provides fast-acting antibiotic defense in *Pseudomonas aeruginosa* biofilms. PLoS Pathog **9:**e1003526.

187. **Wolfram F, Kitova EN, Robinson H, Walvoort MT, Codee JD, Klassen JS, Howell PL.** 2014. Catalytic mechanism and mode of action of the periplasmic alginate epimerase AlgG. The Journal of Biological Chemistry **289:**6006-6019.

188. **Galindo E, Pena C, Nunez C, Segura D, Espin G.** 2007. Molecular and bioengineering strategies to improve alginate and polydydroxyalkanoate production by *Azotobacter vinelandii*. Microb Cell Fact **6:**7.

189. **Tielen P, Strathmann M, Jaeger KE, Flemming HC, Wingender J.** 2005. Alginate acetylation influences initial surface colonization by mucoid *Pseudomonas aeruginosa*. Microbiol Res **160:**165-176.

190. **Gloag ES, Javed MA, Wang H, Gee ML, Wade SA, Turnbull L, Whitchurch CB.** 2013. Stigmergy: A key driver of self-organization in bacterial biofilms. Commun Integr Biol **6:**e27331.

191. **Rehm BHA, Valla S.** 1997. Bacterial alginates: biosynthesis and applications. Appl Microbiol and Biotechnol **48:**281-288.

192. **Donlan RM, Costerton JW.** 2002. Biofilms: survival mechanisms of clinically relevant microorganisms. Clin Microbiol Rev **15:**167-193.

193. **Ghafoor A, Hay ID, Rehm BHA.** 2011. Role of exopolysaccharides in *Pseudomonas aeruginosa* biofilm formation and architecture. Appl Environ Microbiol **77:**5238-5246.

194. **Wood SR, Firoved AM, Ornatowski W, Mai T, Deretic V, Timmins GS.** 2007. Nitrosative stress inhibits production of the virulence factor alginate in mucoid *Pseudomonas aeruginosa*. Free Radic Res **41:**208-215.

195. **May TB, Shinabarger D, Maharaj R, Kato J, Chu L, DeVault JD, Roychoudhury S, Zielinski NA, Berry A, Rothmel RK, et al.** 1991. Alginate synthesis by *Pseudomonas aeruginosa*: a key pathogenic factor in chronic pulmonary infections of cystic fibrosis patients. Clin Microbiol Rev **4:**191-206.

196. **Hay ID, Schmidt O, Filitcheva J, Rehm BH.** 2011. Identification of a periplasmic AlgK-AlgX-MucD multiprotein complex in *Pseudomonas aeruginosa* involved in biosynthesis and regulation of alginate. Appl Microbiol Biotechnol **93:**215-227.

197. **Römling U, Gomelsky M, Galperin MY.** 2005. C-di-GMP: the dawning of a novel bacterial signalling system. Molecular Microbiology **57:**629-639.

198. **Pultz IS, Christen M, Kulasekara HD, Kennard A, Kulasekara B, Miller SI.** 2012. The response threshold of *Salmonella* PilZ domain proteins is determined by their binding affinities for c-di-GMP. Mol microbiol **86:**1424-1440.

199. **Whitney JC, Whitfield GB, Marmont LS, Yip P, Neculai AM, Lobsanov YD, Robinson H, Ohman DE, Howell PL.** 2015. Dimeric c-di-GMP is required for post-translational regulation of alginate production in *Pseudomonas aeruginosa*. J Biol Chem **290:**12451-12462.

200. **Morgan JL, McNamara JT, Zimmer J.** 2014. Mechanism of activation of bacterial cellulose synthase by cyclic di-GMP. Nat Struct Mol Biol **21:**489-496.

201. **Morgan JLW, Strumillo J, Zimmer J.** 2012. Crystallographic snapshot of cellulose synthesis and membrane translocation. Nature **493:**181-186.

202. **Schweizer HP, Chuanchuen R.** 2001. Small broad-host-range *lacZ* operon fusion vector with low background activity. Biotechniques **31:**1258-1262.

203. **Hay ID, Gatland K, Campisano A, Jordens JZ, Rehm BH.** 2009. Impact of alginate overproduction on attachment and biofilm architecture of a supermucoid *Pseudomonas aeruginosa* strain. Appl Environ Microbiol **75:**6022-6025.

204. **Chou SH, Galperin MY.** 2016. Diversity of c-di-GMP-binding proteins and mechanisms. J Bacteriol **198:**32-46.

205. **Kelley LA, Sternberg MJ.** 2009. Protein structure prediction on the Web: a case study using the Phyre server. Nat Protoc **4:**363-371.

206. **Kelley LA, Mezulis S, Yates CM, Wass MN, Sternberg MJ.** 2015. The Phyre2 web portal for protein modeling, prediction and analysis. Nat Protoc **10:**845-858.

207. **Wang Y, Hay ID, Rehman ZU, Rehm BH.** 2015. Membrane-anchored MucR mediates nitrate-dependent regulation of alginate production in *Pseudomonas aeruginosa*. Appl Microbiol Biotechnol **99:**7253-7265.

208. **Oglesby LL, Jain S, Ohman DE.** 2008. Membrane topology and roles of *Pseudomonas aeruginosa* Alg8 and Alg44 in alginate polymerization. Microbiology **154:**1605-1615.

209. **Jain S, Ohman DE.** 2005. Role of an Alginate Lyase for Alginate Transport in Mucoid *Pseudomonas aeruginosa*. Infection and Immunity **73:**6429-6436.

210. **Remminghorst U, Rehm BHA.** 2006. In vitro alginate polymerization and the functional role of Alg8 in alginate production by *Pseudomonas aeruginosa*. Appl Environ Microbiol **72:**298-305.

211. **Snapp EL, Aronson DA, D. E., Costantini LM.** 2011. Superfolder GFP is fluorescent in oxidizing environments when targeted via the sec translocon. Traffic **12:**543-548.

212. **Dinh T, Bernhardt TG.** 2011. Using superfolder green fluorescent protein for periplasmic protein localization studies. J Bacteriol **193:**4984-4987.

213. **Pedelacq JD, Cabantous S, Tran T, Terwilliger TC, Waldo GS.** 2006. Engineering and characterization of a superfolder green fluorescent protein Nat Biotechnol **24:**1170-1170.

214. **Ayers M, Sampaleanu LM, Tammam S, Koo J, Harvey H, Howell PL, Burrows LL.** 2009. PilM/N/O/P proteins form an inner membrane complex that affects the stability of the *Pseudomonas aeruginosa* type IV pilus secretin. J Mol Biol **394:**128-142.

215. **Matsuyama BY, Krasteva PV, Baraquet C, Harwood CS, Sondermann H, Navarro MV.** 2016. Mechanistic insights into c-di-GMP-dependent control of the biofilm regulator FleQ from *Pseudomonas aeruginosa*. Proc Natl Acad Sci U S A **113:**E209-218.

216. **Jitrapakdee S, Wallace JC.** 2003. The biotin enzyme family: conserved structural motifs and domain rearrangements. Curr Protein Pept Sci **4:**217-229.

217. **Taylor JD, Matthews SJ.** 2015. New insight into the molecular control of bacterial functional amyloids. Front Cell Infect Microbiol **5:**33.

218. **Palumaa P.** 2013. Copper chaperones. The concept of conformational control in the metabolism of copper. FEBS Lett **587:**1902-1910.

219. **Puig S, Rees EM, Thiele DJ.** 2002. The ABCDs of periplasmic copper trafficking. Structure **10:**1292-1295.

220. **Bagos PG, Nikolaou EP, Liakopoulos TD, Tsirigos KD.** 2010. Combined prediction of Tat and Sec signal peptides with hidden Markov models. Bioinformatics **26:**2811-2817.

221. **du Plessis DJ, Nouwen N, Driessen AJ.** 2011. The Sec translocase. Biochim Biophys Acta **1808:**851-865.

222. **Maleki S, Almaas E, Zotchev S, Valla S, Ertesvag H.** 2015. Alginate biosynthesis factories in *Pseudomonas fluorescens*: localization and correlation with alginate production level. Appl Environ Microbiol **82:**1227-1236.

223. **Christen M, Kulasekara HD, Christen B, Kulasekara BR, Hoffman LR, Miller SI.** 2010. Asymmetrical distribution of the second messenger c-di-GMP upon bacterial cell division. Science **328:**1295-1297.

224. **Kulasekara BR, Kamischke C, Kulasekara HD, Christen M, Wiggins PA, Miller SI.** 2013. c-di-GMP heterogeneity is generated by the chemotaxis machinery to regulate flagellar motility. Elife **2**.

225. **Ryan RP, Fouhy Y, Lucey JF, Dow JM.** 2006. Cyclic di-GMP signaling in bacteria: recent advances and new puzzles. J Bacteriol **188:**8327-8334.

226. **Bullock WO FJ, Stuart JM.** 1987. XL1-Blue: a high efficiency plasmid transforming *recA Escherichia coli* strain with β-galactosidase selection. BioTechniques **5:**376–379.

227. **Becher A, Schweizer HP.** 2000. Integration-proficient *Pseudomonas aeruginosa* vectors for isolation of single-copy chromosomal *lacZ* and *lux* gene fusions. Biotechniques **29:**948-950, 952.

228. **Nunez C, Moreno S, Soberon-Chavez G, Espin G.** 1999. The *Azotobacter vinelandii* response regulator AlgR is essential for cyst formation. J Bacteriol **181:**141-148.

229. **Moradali MF, Ghods S, Rehm BH.** 2017. Activation Mechanism and Cellular Localization of Membrane-Anchored Alginate Polymerase in *Pseudomonas aeruginosa*. Applied and Environmental Microbiology **83:**e03499-03416.

230. **Tenhaken R, Voglas E, Cock JM, Neu V, Huber CG.** 2011. Characterization of GDP-mannose dehydrogenase from the brown alga *Ectocarpus siliculosus* providing the precursor for the alginate polymer. Journal of Biological Chemistry **286:**16707-16715.

231. **Hancock RE, Nikaido H.** 1978. Outer membranes of Gram-negative bacteria. XIX. Isolation from *Pseudomonas aeruginosa* PAO1 and use in reconstitution and definition of the permeability barrier. J Bacteriol **136:**381-390.

232. **Ewis HE, Lu C-D.** 2005. Osmotic shock: a mechanosensitive channel blocker can prevent release of cytoplasmic but not periplasmic proteins. FEMS microbiology letters **253:**295-301.

233. **Pier GB, Boyer D, Preston M, Coleman FT, Llosa N, Mueschenborn-Koglin S, Theilacker C, Goldenberg H, Uchin J, Priebe GP.** 2004. Human monoclonal antibodies to *Pseudomonas aeruginosa* alginate that protect against infection by both mucoid and nonmucoid strains. The Journal of Immunology **173:**5671-5678.

234. **Pier GB, Desjardins D, Aguilar T, Barnard M, Speert D.** 1986. Polysaccharide surface antigens expressed by nonmucoid isolates of *Pseudomonas aeruginosa* from cystic fibrosis patients. Journal of clinical microbiology **24:**189-196.

235. **Rehm BHA.** 1998. Alginate lyase from *Pseudomonas aeruginosa* CF1/M1 prefers the hexameric oligomannuronate as substrate. Fems Microbiology Letters **165:**175-180.

236. **Shibukawa M, Terashima H, Nakajima H, Saitoh K.** 2004. Evaluation of the surface charge properties of porous graphitic carbon stationary phases treated with redox agents. Analyst **129:**623-628.

237. **Törnkvist A, Markides KE, Nyholm L.** 2003. Chromatographic behaviour of oxidised porous graphitic carbon columns. Analyst **128:**844-848.

238. **Pabst M, Grass J, Fischl R, Léonard R, Jin C, Hinterkörner G, Borth N, Altmann F.** 2010. Nucleotide and nucleotide sugar analysis by liquid chromatography-electrospray ionization-mass spectrometry on surface-conditioned porous graphitic carbon. Analytical chemistry **82:**9782-9788.

239. **Wittchen K-D, Meinhardt F.** 1995. Inactivation of the major extracellular protease from *Bacillus megaterium* DSM319 by gene replacement. Applied microbiology and biotechnology **42:**871-877.

240. **Vu B, Chen M, Crawford RJ, Ivanova EP.** 2009. Bacterial extracellular polysaccharides involved in biofilm formation. Molecules **14:**2535-2554.

241. **Steiner S, Lori C, Boehm A, Jenal U.** 2013. Allosteric activation of exopolysaccharide synthesis through cyclic di-GMP-stimulated protein-protein interaction. EMBO J **32:**354-368.

242. **Hay ID, Ur Rehman Z, Ghafoor A, Rehm BHA.** 2010. Bacterial biosynthesis of alginates. Journal of Chemical Technology & Biotechnology **85:**752-759.

243. **Remminghorst U, Rehm BH.** 2006. Alg44, a unique protein required for alginate biosynthesis in Pseudomonas aeruginosa. FEBS letters **580:**3883-3888.

244. **Hay ID, Rehman ZU, Moradali MF, Wang Y, Rehm BH.** 2013. Microbial alginate production, modification and its applications. Microbial biotechnology **6:**637-650.

245. **Roca C, Alves VD, Freitas F, Reis MA.** 2015. Exopolysaccharides enriched in rare sugars: bacterial sources, production, and applications. Front Microbiol **6:**288.

246. **Donati I, Paoletti S.** 2009. Material Properties of Alginates doi:10.1007/978-3-540-92679-5-1, p 1-53. Springer Science + Business Media.

247. **Skjåk-Bræk G, Donati, I., and Paoletti, S. .** 2015. Alginate hydrogels: properties and applications. In *P. Matricardi* FA, and T. Coviello (ed), Polysaccharide Hydrogels: Characterization and Biomedical Applications. Pan Stanford Publishing Pte Ltd, Singapore.

248. **Thomas S.** 2000. Alginate dressings in surgery and wound management, part 1. J Wound Care **9:**56-60.

249. **Tonnesen HH, Karlsen J.** 2002. Alginate in drug delivery systems. Drug Dev Ind Pharm **28:**621-630.

APPENDIX

RESEARCH ARTICLE

Alginate Polymerization and Modification Are Linked in *Pseudomonas aeruginosa*

M. Fata Moradali,[a] Ivan Donati,[b] Ian M. Sims,[c] Shirin Ghods,[a] Bernd H. A. Rehm[a,d]

Institute of Fundamental Sciences, Massey University, Palmerston North, New Zealand[a]; Department of Life Sciences, University of Trieste, Trieste, Italy[b]; The Ferrier Research Institute, Victoria University of Wellington, Lower Hutt, Wellington, New Zealand[c]; MacDiarmid Institute for Advanced Materials and Nanotechnology, Massey University, Palmerston North, New Zealand[d]

ABSTRACT **The molecular mechanisms of alginate polymerization/modification/secretion by a proposed envelope-spanning multiprotein complex are unknown. Here, bacterial two-hybrid assays and pulldown experiments showed that the catalytic subunit Alg8 directly interacts with the proposed copolymerase Alg44 while embedded in the cytoplasmic membrane. Alg44 additionally interacts with the lipoprotein AlgK bridging the periplasmic space. Site-specific mutagenesis of Alg44 showed that protein-protein interactions and stability were independent of conserved amino acid residues R17 and R21, which are involved in c-di-GMP binding, the N-terminal PilZ domain, and the C-terminal 26 amino acids. Site-specific mutagenesis was employed to investigate the c-di-GMP-mediated activation of alginate polymerization by the $PilZ_{Alg44}$ domain and Alg8. Activation was found to be different from the proposed activation mechanism for cellulose synthesis. The interactive role of Alg8, Alg44, AlgG (epimerase), and AlgX (acetyltransferase) on alginate polymerization and modification was studied by using site-specific deletion mutants, inactive variants, and overproduction of subunits. The compositions, molecular masses, and material properties of resulting novel alginates were analyzed. The molecular mass was reduced by epimerization, while it was increased by acetylation. Interestingly, when overproduced, Alg44, AlgG, and the nonepimerizing variant AlgG(D324A) increased the degree of acetylation, while epimerization was enhanced by AlgX and its nonacetylating variant AlgX(S269A). Biofilm architecture analysis showed that acetyl groups promoted cell aggregation while nonacetylated polymannuronate alginate promoted stigmergy. Overall, this study sheds new light on the arrangement of the multiprotein complex involved in alginate production. Furthermore, the activation mechanism and the interplay between polymerization and modification of alginate were elucidated.**

IMPORTANCE **This study provides new insights into the molecular mechanisms of the synthesis of the unique polysaccharide, alginate, which not only is an important virulence factor of the opportunistic human pathogen *Pseudomonas aeruginosa* but also has, due to its material properties, many applications in medicine and industry. Unraveling the assembly and composition of the alginate-synthesizing and envelope-spanning multiprotein complex will be of tremendous significance for the scientific community. We identified a protein-protein interaction network inside the multiprotein complex and studied its relevance with respect to alginate polymerization/modification as well as the c-di-GMP-mediated activation mechanism. A relationship between alginate polymerization and modification was shown. Due to the role of alginate in pathogenesis as well as its unique material properties harnessed in numerous applications, results obtained in this study will aid the design and development of inhibitory drugs as well as the commercial bacterial production of tailor-made alginates.**

Received 17 March 2015 **Accepted** 7 April 2015 **Published** 12 May 2015

Citation Fata Moradali M, Donati I, Sims IM, Ghods S, Rehm BHA. 2015. Alginate polymerization and modification are linked in *Pseudomonas aeruginosa.* mBio 6(3):e00453-15. doi:10.1128/mBio.00453-15.

Invited Editor Mark Nitz, University of Toronto **Editor** Gerald B. Pier, Harvard Medical School

Address correspondence to Bernd H. A. Rehm, B.Rehm@massey.ac.nz.

Pseudomonas aeruginosa is an opportunistic human pathogen which can become life-threatening in immunocompromised patients. It is the leading cause of morbidity and mortality in cystic fibrosis patients. This is due mainly to its ability to colonize lungs by forming structured biofilms which consist of bacterial cells embedded in a complex matrix predominantly composed of alginate. Bacterial cells in biofilms are protected against the immune system and antibiotics (1, 2). Alginates are anionic exopolysaccharides composed of variable proportions of 1,4-linked β-D-mannuronic acid (M) and its C-5 epimer α-L-guluronic acid (G). The alginate derived from *P. aeruginosa* is naturally acetylated and lacks consecutive G residues (GG-blocks) (3). Alginates exhibit unique gel-forming properties suitable for numerous medical and industrial applications (3, 4). The alginate structure strongly impacts its material properties. Hence, the development of bioengineering approaches to control the alginate structure will enable production of alginates with new material properties toward novel applications.

For many years, *P. aeruginosa* has been the model organism to study various aspects of alginate biosynthesis, such as polymerization, epimerization, acetylation, secretion, and regulation. Thirteen proteins are directly involved in the biosynthesis of alginate,

and except for *algC*, their encoding genes are clustered in the alginate biosynthesis operon (*algD*, *alg8*, *alg44*, *algK*, *algE*, *algG*, *algX*, *algL*, *algI*, *algJ*, *algF*, *algA*) (5, 6). Except for soluble cytoplasmic proteins AlgA, AlgC, and AlgD, which are responsible for providing the activated nucleotide sugar precursor, GDP-mannuronic acid, proteins encoded by the operon are proposed to constitute an envelope-spanning multiprotein complex. Two cytoplasmic membrane-anchored proteins, the glycosyltransferase, Alg8, and the proposed copolymerase, Alg44, are necessary for alginate polymerization (7–9). The MucR sensor protein, a diguanylate cyclase (DGC)/phosphodiesterase (PDE) embedded in the cytoplasmic membrane, was proposed to provide c-di-GMP for binding to the cytoplasmic PilZ domain of Alg44 by which alginate polymerization is activated (10). Translocation of nascent alginate across the periplasm is coupled with modification processes, including *O*-acetylation and epimerization. *O*-Acetylation is independently catalyzed by AlgJ and AlgX (11), while the acetyl group donor is provided by AlgI and AlgF (12, 13). The AlgG epimerase converts M residues to G residues in the nascent alginate chain. AlgG, AlgX, and AlgK were suggested to form a periplasmic scaffold for guiding alginate through the periplasm for secretion via the outer membrane protein AlgE (14–19). It was also suggested that if alginate is misguided into the periplasm, then degradation would be mediated by the periplasmic AlgL lyase (20). Previous studies on protein-protein interactions and mutual stabilities of proposed subunits of the multiprotein biosynthesis machinery provided evidence of binary protein interactions, including AlgE-AlgK, AlgX-AlgK, AlgX-MucD (a serine protease), Alg44-AlgX, and Alg8-AlgG (21, 22). However, more experimental evidence is needed to map all protein-protein interactions within the multiprotein complex, in particular toward unraveling the molecular mechanisms of alginate polymerization, molecular mass control, and the relationship of modification events to polymerization.

In this study, protein-protein interactions within the multiprotein complex were investigated using the bacterial two-hybrid technique and pulldown assays. The proposed interacting protein surface of Alg44 was probed, and the molecular mechanism of c-di-GMP-mediated activation was studied (23, 24). The role of Alg8, Alg44, AlgG, and AlgX with respect to polymerization and modification was studied by analyzing the composition and material properties of alginates produced by various strains. We employed a constitutively alginate-producing strain of *P. aeruginosa*, PDO300, to generate isogenic single- and double-gene knockouts of *alg8*, *alg44*, *algG*, and *algX*. This allowed studying the role of the respective proteins in alginate polymerization and/or modifications by introducing additional copy numbers of subunits or their variants in *trans*. The impact of various alginate structures on motility, biofilm formation, and architecture was investigated.

RESULTS

Protein-protein interaction of membrane-anchored Alg8 and Alg44 toward constitution of an active alginate polymerase subunit. The two cytoplasmic membrane-anchored proteins Alg8 and Alg44 were previously shown to be necessary for alginate polymerization. Alg8 is a glycosyltransferase catalyzing alginate polymerization, using the substrate GDP-mannuronic acid, while the c-di-GMP-binding PilZ domain containing Alg44 was proposed as copolymerase (9, 25). However, the functional and structural interactions of Alg8 and Alg44 had not been elucidated. Therefore, the marker-free isogenic double-gene-knockout PDO300Δ*alg8*Δ*alg44* mutant was generated. This mutant lost the mucoid phenotype, while introduction of plasmid pBBR1MCS-5:*alg44*:*alg8* restored alginate production and the mucoid phenotype.

In order to investigate the proposed interaction of Alg8 and Alg44, functional His-tagged variants (Alg44-6His and Alg8-6His) were subjected to pulldown experiments under native conditions and to bacterial two-hybrid system assays. In pulldown experiments, wild-type Alg44 and Alg8 without His tag served as negative controls. To address possible stoichiometric effects, i.e., effects of increased copy numbers of individual subunits on the integrity of the multiprotein complex, single genes encoding Alg8-6His or Alg44-6His under the control of their native promoter were integrated into the genome. In contrast, in *trans* genes were present on plasmids in multiple copies under control of the strong constitutive *lac* promoter. Immunoblots showed that Alg44 with an apparent molecular mass of 41.8 kDa was copurified with Alg8-6His produced either from in *trans* or in *cis* encoding genes, and similarly Alg8 (~53 kDa) was copurified with Alg44-6His, while respective proteins were not detected for complemented mutants with native Alg44 and Alg8 as well as in double-knockout mutants with single Alg8-6His or Alg44-6His (Fig. 1A and B).

In addition, the bacterial two-hybrid system showed that the chimeric enzyme adenylate cyclase was reconstituted when its two complementary fragments (T18/T25) were brought together by Alg8 and Alg44 interaction. β-Galactosidase activity in those cells harboring two plasmids producing fusion proteins of Alg8 and Alg44 (pKNT25:*alg8*-pUT18:*alg44*) was on average 11-fold (672 U/mg [cellular dry weight]) greater than the negative controls without the fusion protein partner (background control) or compared with single fusion protein Alg8 or Alg44 (58 to 66 U/mg [cellular dry weight]) as well as the vice versa combination (pKNT25:*alg44*-pUT18:*alg8*), which showed a β-galactosidase activity of 160 U/mg (cellular dry weight) (Fig. 1C). Analysis of cytoplasmic membrane proteins by immunoblotting confirmed that both proteins were localized to the cytoplasmic membrane of *Escherichia coli* (Fig. 1D). These results provided the first experimental evidence for the direct interaction between the membrane-anchored proposed alginate polymerase (glycosyltransferase) Alg8 and the copolymerase Alg44.

Cytoplasmic membrane-anchored Alg44 interacts with outer membrane-anchored AlgK, while Alg44 is critical for structural integrity of the multiprotein alginate biosynthesis machinery. To assess whether Alg8 and Alg44 interact with other proposed subunits of the multiprotein complex, pulldown assays under native conditions were employed using Alg8-6His and Alg44-6His proteins followed by immunoblotting using anti-AlgX, -AlgK, and -AlgE antibodies. Additionally, to rule out indirect interactions, appropriate double-gene-knockout mutants harboring individual genes in *trans* [PDO300Δ*alg8*Δ*alg44* (pBBR1MCS5:*alg8*-6His), PDO300Δ*alg8*Δ*alg44*(pBBR1MCS5:*alg44*-6His), and PDO300Δ*alg44*Δ*algX*(pBBR1MCS5:*alg44*-6His) mutants] were included. To address stoichiometric effects, complemented PDO300Δ*alg8* and PDO300Δ*alg44* mutants, respectively, were used to generate single-gene-copy complementation strains by integrating *alg8*-6His and *alg44*-6His into the bacterial genome. The mutants producing native Alg8 and Alg44 proteins were used as negative controls. Resultant immunoblots (Fig. 2A and B) showed AlgK and AlgX but not AlgE were independently

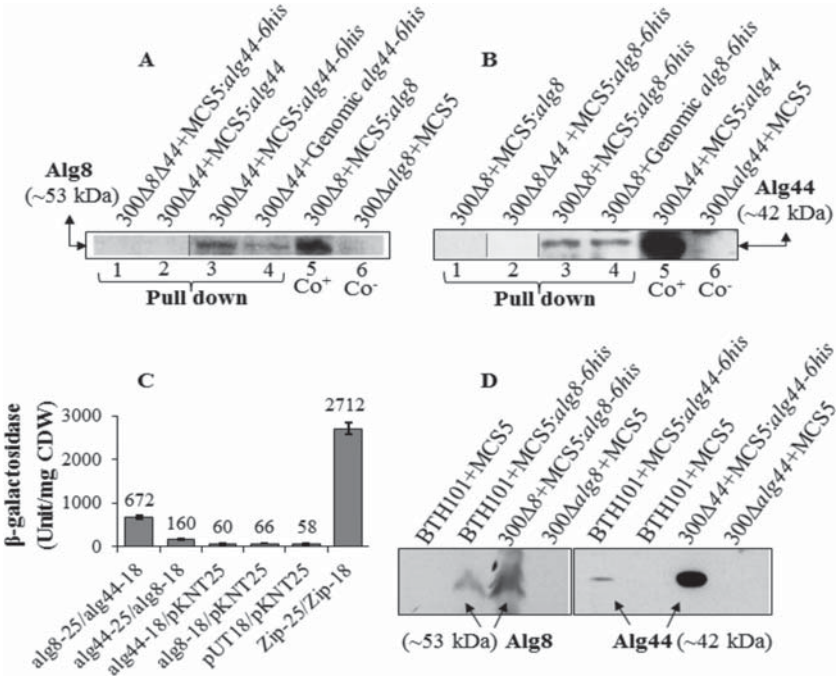

FIG 1 Alg8-Alg44 protein-protein interaction. (A and B) His tag-based pulldown assays (lanes 1 to 4) and immunoblotting using anti-Alg8 antibodies (A) and anti-Alg44 antibodies (B) show protein-protein interaction between Alg8 and Alg44. Alg8 and Alg44 interaction was detected by respective copurification of the non-His-tagged interacting protein partner encoded by genes either integrated into the genome or localized on a plasmid (lanes 3 and 4). Lanes 1 and 2 belong to negative controls (proteins without His tag or present individually in double-gene-knockout mutants) (see Materials and Methods). (C) In bacterial two-hybrid analysis, the appropriate pUT18 and pKNT25 derivatives were cotransferred into *E. coli* BTH101. The pUT18 and pKNT25 vectors were used as a negative control (background) in addition to transformants with one of the constructs and one empty vector, while the pUT18c-Zip and pKT25-Zip plasmid pair was used as a positive control. Upon induction with 0.5 mM isopropyl-β-D-thiogalactopyranoside (IPTG), 4-fold β-galactosidase activity higher than background was regarded as evidence for protein-protein interaction. (D) Immunoblots developed using anti-His tag antibodies show production and subcellular localization of Alg8 and Alg44 to the cytoplasmic membrane of *E. coli* BTH101 (see Materials and Methods). 300, PDO300; 8 and 44, Alg8 and Alg44; MCS5, pBBR1MCS-5; Co+/−, positive/negative control; CDW, cellular dry weight; −18, pUT18; −25, pKNT25. An irrelevant lane was deleted between lanes 2 and 3 in blot A, as indicated by a thin line. Lane 2 in blot B was inserted as a representative control blot lane, as it was obscured by artificial stains in the original bot. Insertion of lane 2 is indicated by thin lines. Between dividing lines in blot B, a representative control blot lane was inserted from a separate blot, because in the original blot, it was obscured by artificial dots/development artifacts.

pulled down with Alg44-6His, both when *alg44*-6His was provided in *trans* or in *cis*. Hence, experimental evidence is provided, as previously proposed (21), that a protein-protein interaction network spanning the periplasm and constituted by Alg8-Alg44-AlgK-AlgE interactions exists.

Cross-linking experiments using a DSG cross-linking reagent with a spacer arm length of 7.7 Å followed by Alg44-6His pulldown under denaturing conditions showed a protein with an apparent molecular mass of ~84 kDa, which was detected only by the anti-Alg44 antibody. In addition, the previously shown Alg44-AlgX (21) interaction was confirmed by detecting a cross-linked protein with an apparent molecular mass of ~90 kDa binding both anti-Alg44 and anti-AlgX antibodies. The ~84-kDa protein was detected only in pulldown elution fractions obtained from genomic expression of *alg44*-6His but not from the plasmid-borne gene, while Alg44-AlgX interactions were found to be independent of the stoichiometry of the individual proteins (Fig. 2C and D). These proteins were not detected in elution fractions when the native protein Alg44 was present and in the negative control treated with dimethyl sulfoxide (DMSO).

Alg44 variants with a truncated PilZ domain and C terminus were stable and maintained integrity of protein-protein interactions within the alginate biosynthesis multiprotein complex. Previously, it was demonstrated that site-directed mutagenesis of the putative c-di-GMP-binding motifs (R17XXXR21) of the PilZ domain and a C-terminal truncation of Alg44 completely abolished alginate production (26). In comparison, it was shown that c-di-GMP binds directly to both PgaC and PgaD, the two cytoplasmic membrane components of the *E. coli* poly-β-1,6-*N*-acetylglucosamine synthesis machinery, which stimulated their glycosyltransferase activity by stabilizing their interaction (27). Here, it was investigated whether c-di-GMP binding to the PilZ domain of Alg44 and the C-terminal part itself impacts on protein-protein interactions and ultimately alginate polymerization.

His pulldown experiments under native conditions as described above were applied using His-tagged Alg44 variants [Alg44(R21D), Alg44(Δ40–74aa$_{PilZ}$), and C-terminally truncated Alg44(Δ364–389aa)] (Fig. 3A). As shown in Fig. 3B, Alg44-6His variants were all found in the envelope fraction, which suggested their localization and stability were not affected. Interestingly, the abovementioned protein interaction network was confirmed, which signifies neither protein stability nor the interaction of Alg44 with AlgK and AlgX was disrupted by its defective PilZ domain or the C-terminal truncation. However, the C-terminal truncation of Alg44 impacted on the stability of Alg8 (Fig. 3C, lane 1), while the other variants of Alg44 did not (Fig. 3C).

C-di-GMP levels and growth mode impact on Alg44 stability. Previous studies showed that introducing high copy numbers of

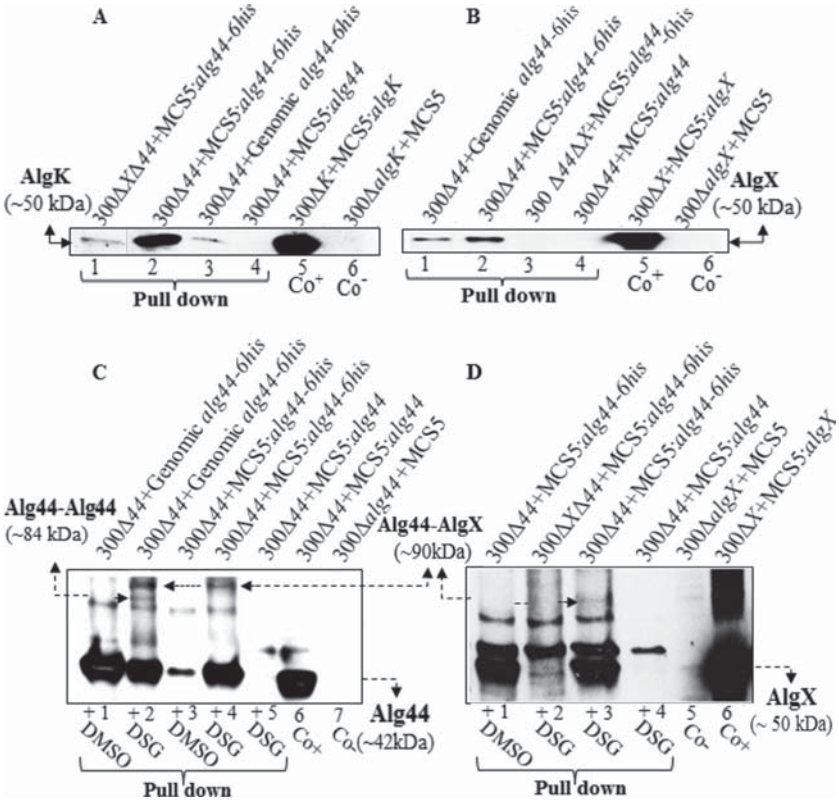

FIG 2 Protein-protein interaction analysis indicates interaction of Alg44-AlgK, Alg44-AlgX, and probable Alg44-Alg44 (dimer). (A and B) His tag-based pulldown assays and immunoblotting using anti-AlgK (A) and anti-AlgX (B) antibodies show interactions of Alg44-AlgK and Alg44-AlgX (A and B, lanes 1 to 4). These interactions were detected in both cases of in *trans* and in *cis* complementation of mutants with *alg44*-6His (lanes 2 and 3 of blot A; lanes 1 and 2 of blot B). AlgK was pulled down using His-tagged Alg44 in the absence of AlgX (lane 1, blot A). The elution fraction derived from complemented mutants producing non-His-tagged protein lacked AlgK and AlgX (lane 4 in blots A and B). (C and D) Immunoblots suggesting *in vivo* Alg44 dimerization and Alg44-AlgX interaction using stabilization of interaction by chemical cross-linking combined with His-tagged Alg44-mediated pulldown assays under denaturing conditions (see Materials and Methods). A presumable Alg44 dimer band (~84 kDa) reacted only with anti-Alg44 antibody (blot C, lane 2) while the *alg44*-AlgX band (~90 kDa) reacted with Alg44 and AlgX antibodies in both blots (blot C, lanes 2 and 4; blot D, lane 3). These bands were not detected in the elution fraction derived from mutants with native Alg44 with DSG and Alg44-6His treated with DMSO as negative controls (blot C, lanes 1, 3, and 5; blot D, lanes 1 and 4). 300, PDO300; MCS5, BBR1MCS-5; Co+/−, positive/negative control. An irrelevant lane was deleted between lanes 1 and 2 in blot A, as indicated by a thin line.

mucR in the PDO300Δ*mucR* mutant resulted in greater production of alginate than found in the wild type, while increased copy numbers of *rocR* encoding a c-di-GMP-degrading phosphodiesterase (PDE) led to strongly reduced alginate production, presumably due to reduction in c-di-GMP levels. Therefore, it was suggested that MucR plays a specific role in the regulation of alginate biosynthesis by colocalizing with Alg44 and providing a localized c-di-GMP pool (10). Here, it was tested if Alg44 copy numbers in the envelope fraction might be affected by the presence or absence of MucR or RocR, respectively, i.e., by different c-di-GMP levels and within different physiological conditions, such as planktonic and biofilm growth modes. Immunoblotting analysis of envelope fractions of the various mutants showed the amount of Alg44 was not significantly affected by the absence of MucR in biofilm mode, while it was reduced in the envelope fraction of biofilm cells with a high copy number of *rocR* in the absence of MucR (see Fig. S1 in the supplemental material), indicating that the small amount of Alg44 corresponded with low c-di-GMP levels. However, the amount of Alg44 in the same mutants growing in planktonic mode did not significantly differ.

Is alginate polymerization controlled by an autoinhibition mechanism, as shown for the bacterial cellulose synthase? Alg8 and BcsA of bacterial cellulose synthase both belong to the glycosyltransferase family 2 (GT-2), and they share the same conserved signature motifs and residues experimentally known as critical for production of alginate and cellulose, respectively (28, 29). Recently, the structure of the bacterial cellulose synthase BcsA-BcsB complex was resolved. It was shown that the PilZ domain in this complex was in proximity to the catalytic site of BcsA (30). The first arginine of the PilZ domain's R580XXXR584 motif formed a salt bridge with E371 preceding the RW motif (a signature of the glycosyltransferase family 2), consequently tethering the gating loop in the resting status and blocking the catalytic site. This steric hindrance was called the autoinhibiting mechanism, which was proposed to be eliminated upon c-di-GMP binding to R580, opening up the gate for precursors to enter into the catalytic site.

Accordingly, informed by the BcsA-BcsB structure and implementing bioinformatics analysis using the Phyre2 Protein Fold Recognition Server, an *in silico* structural model of Alg8 fused with the C-terminal $PilZ_{Alg44}$ domain was developed (31). A structural model homologous to BcsA (confidence, 100%; coverage, 93%) showed the PilZ domain in proximity to the catalytic site of Alg8 and close to the E322, H323, and E326 residues located on the BcsA-homologous loop preceding motif RW (residues 339 and

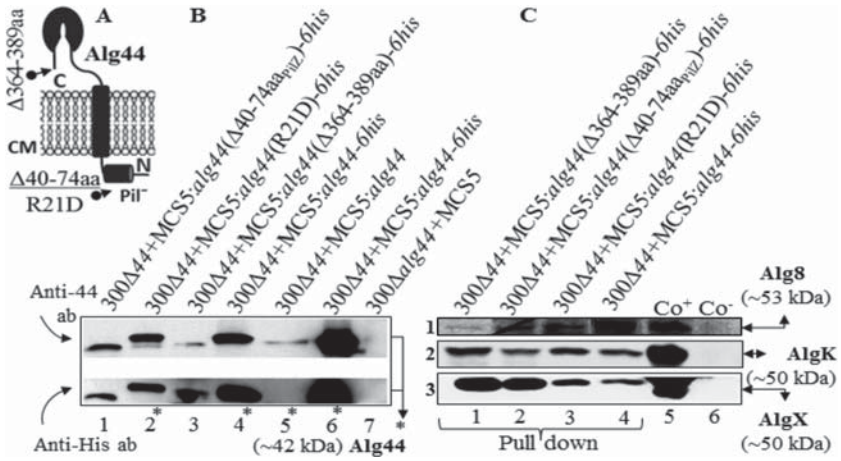

FIG 3 Localization, stability, and protein-protein interaction of Alg44 variants. (A) Schematic view of the deleted or point-mutated region of Alg44. (B) Immunoblots of the envelope fraction developed using anti-Alg44 (upper) and anti-His tag (lower) antibodies showed with the various Alg44 variants localized to the envelope fraction (immunoblot B, lanes 1 to 3). Lanes 4 to 7 represent negative and positives controls (blot C, lanes 1 to 4). Immunoblots suggested protein-protein interaction of Alg44 variants with Alg8, AlgK, and AlgX by using pulldown experiments using His-tagged variants of Alg44. C-terminal deletion of Alg44 had a destabilizing effect on Alg8. Immunoblots were developed using anti-Alg8 (1), anti-AlgK (2), and anti-AlgX (3) antibodies, respectively. Asterisks indicate full-length Alg44. 300, PDO300; MCS5, pBBR1MCS-5; ab, antibody; Co+/−, positive/negative control.

340), a site potentially involved in salt bridge formation (Fig. 4A to C). The impact of alanine substitutions of these residues, individually and in combination with R17 and/or R21 of Alg44's RXXXR (residues 17 to 21) motif at different c-di-GMP levels (i.e., the presence or absence of overproduced c-di-GMP degrading RocR), on *in vivo* activity of respective Alg8 and Alg44 variants was assessed. The overproduction of RocR was confirmed to significantly reduce alginate production in the wild-type strain and complemented mutants. Substitution of R residues in the PilZ$_{Alg44}$ domain RXXXR motif (amino acids 17 to 21) and the E322 resi-

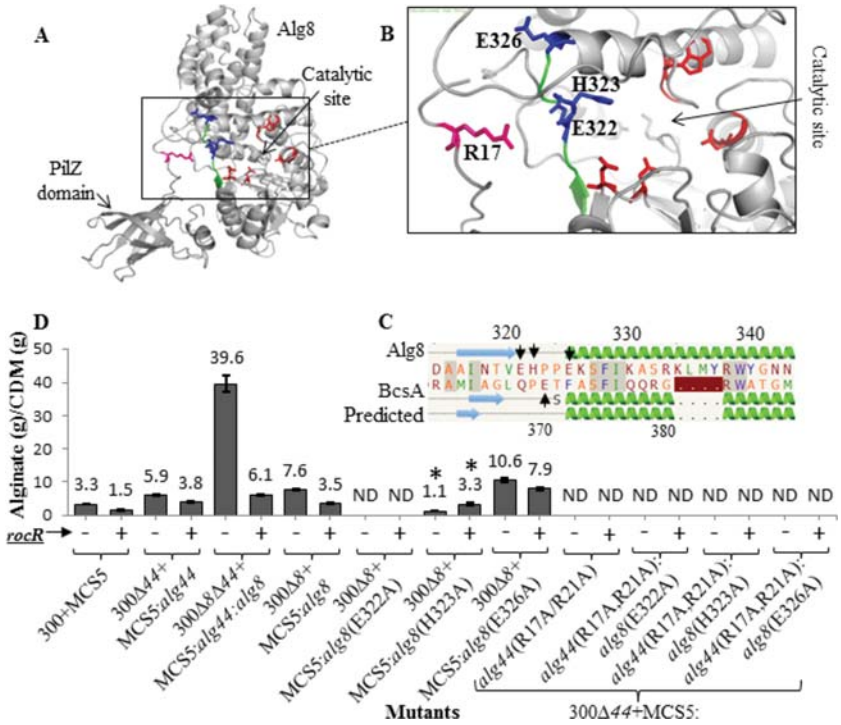

FIG 4 Bacterial cellulose synthase-associated autoinhibiting mechanism does not play a role in alginate polymerization. (A) *In silico* fusion of Alg8-PilZ$_{Alg44}$ was modeled using the Phyre2 server. (B) Highly conserved amino acids (blue sticks; E322, H323, and E326 are labeled with arrows in pairwise alignment of Alg8 with BcsA [C]) were identified in a similar position to that of BcsA and could form a salt bridge with R residues of the PilZ$_{Alg44}$ domain R17XXXR21 motif and were chosen to be replaced by alanine using site-specific mutagenesis. (D) Alginate quantification of PDO300Δ*alg8*, PDO300Δ*alg44*, and PDO300Δ*alg8*Δ*alg44* transformants with plasmids harboring respective site-specific mutants of *alg8* and *alg44* with (+) and without (−) the *rocR* gene. Alg8's mutated residue which positively responded to c-di-GMP level alteration by RocR is labeled with an asterisk. 300, PDO300; ND, not detectable; MCS5, pBBR1MCS-5.

TABLE 1 Composition and molecular mass analyses of alginate produced by different mutants[a]

No.	Mutant description	F_G	F_M	$F_{GM/MG}$	F_{MM}	Ac. %	Wt avg molecular mass (kDa)	No. avg molecular mass (kDa)	PI	Alginate yield (g)/CDM (g)
1	300+MCS5	0.3	0.7	0.29	0.41	32	3,927 (±0.864%)	3,832 (±0.842%)	1.025 (±1.2%)	1.3 ± 0.03
2	300Δ*8*+MCS5:*alg8*	0.18	0.82	0.17	0.65	11.3	3,045 (±0.556%)	3,037 (±0.551%)	1.003 (±0.7%)	12.8 ± 1.03
3	300Δ*44*+MCS5:*alg44*	0.18	0.82	0.18	0.64	26.8	3,831 (±0.963%)	3,650 (±0.950%)	1.05 (±1.3%)	8.7 ± 0.53
4	300Δ*44*Δ*8*+MCS5:*alg44*:*alg8*	0.17	0.83	0.17	0.66	11	3,369 (±0.839%)	3,352 (±0.821%)	1.005 (±1.1%)	41.5 ± 4.9
5	300Δ*X*+MCS5:*algX*	0.36	0.64	0.36	0.28	9.8	2,460 (±0.932%)	2,447 (±0.913%)	1.005 (±1.3%)	104.1 ± 5.5
6	300Δ*X*+MCS5:*algX*(S269A)	0.36	0.64	0.36	0.28	0	2,086 (±0.960%)	2,065 (±0.944%)	1.010 (±1.3%)	125.8 ± 9.9
7	300Δ*G*+MCS5:*algG*	0.32	0.68	0.32	0.36	23.3	2,755 (±1.041%)	2,726 (±0.986%)	1.011 (±1.4%)	2.6 ± 0.04
8	300Δ*G*+MCS5:*algG*(D324A)	0	1	0	1	25.2	4,653 (±1.097%)	4,575 (±1.117%)	1.017 (±1.5%)	7.6 ± 0.57
9	300Δ*X*Δ*G*+MCS5:*algX*:*algG*	0.34	0.66	0.34	0.32	28.4	3,076 (±1.051%)	3,044 (±1.029%)	1.011 (±1.4%)	67.42 ± 4.8
10	300Δ*X*Δ*G*+MCS5:*algX*(S269A):*algG*(D324A)	0	1	0	1	0	1,811 (±0.884%)	1,716 (±0.888%)	1.055 (±1.2%)	8.7 ± 0.42
11	300Δ*44*Δ*G*+MCS5:*alg44*+*algG*	0.22	0.78	0.22	0.56	14.5	2,907 (±0.966%)	2,861 (±0.944%)	1.016 (±1.3%)	9.0 ± 0.3

[a] 300, PDO300; MCS5, pBBR1MCS-5; F_G, molar fraction of guluronate (G) residue; F_M, molar fraction of mannuronate (M) residue; $F_{GM/MG}$, molar fraction of two consecutive G and M residues; F_{MM}, molar fraction of two consecutive M residues; Ac, acetylation; PI, polydispersity index; CDM, cell dry mass.

due of Alg8 with alanine completely abolished alginate production. The mutagenesis of H323 [i.e., PDO300Δ*alg8*(pBBR1MCS-5:*alg8*(H323A) mutant] lowered alginate production by 6.9-fold compared to that of the PDO300Δ*alg8*(pBBR1MCS-5:*alg8*) mutant. Interestingly, RocR-mediated reduced intracellular c-di-GMP levels restored alginate production to PDO300Δ*alg8* (pBBR1MCS-5:*alg8:rocR*) mutant levels (Fig. 4D, labeled with asterisk). Replacement of E326 by alanine in Alg8 increased alginate production by 1.3-fold compared with that of the PDO300Δ*alg8*(pBBR1MCS-5:*alg8*) mutant. RocR production in this mutant background mediated decreased alginate production by about 2-fold compared to that of wild-type Alg8 (Fig. 4D). In summary, conserved R residues of Alg44 proposed to be involved in autoinhibition via salt bridge formation inactivated alginate polymerization. However, the replacement of H323 or E326 of Alg8 still mediated alginate production, while reduced levels of c-di-GMP did cause less or no reduction of alginate production compared to that of the reference strain [PDO300Δ*alg8* (pBBR1MCS-5:*alg8*) mutant].

Interplay of alginate polymerizing (Alg8-Alg44) and modifying (AlgG-AlgX) units on alginate composition and molecular mass. In order to investigate the relationship between alginate polymerization and modification, single- and double-gene-knockout mutants of *P. aeruginosa* PDO300 were generated and followed by individual and combinatorial in *trans* complementation using relevant genes, including *alg8-alg44* (encoding alginate-polymerizing proteins), *algX-algX*(S269A) (encoding alginate-acetylating/non-acetylating AlgX), and *algG-algG*(D324A) (encoding alginate-epimerizing/nonepimerizing AlgG). Generated knockout mutants lost mucoidy, while mucoidy was restored upon in *trans* complementation with relevant genes. In order to shed light on the functional interaction between alginate-polymerizing and -modifying subunits, the polymerization degree, epimerization degree, and acetylation level of resulting alginates were assessed. The composition and the molecular masses of the respective alginates are summarized in Table 1. Figure 5A shows in descending order the values obtained in regard to epimerization, acetylation, and polymerization degree. ^{1}H-nuclear magnetic resonance (NMR) spectra of compositional analysis of alginates are shown in Fig. S2 in the supplemental material. In order to investigate whether Alg8 and Alg44 are directly involved in polymannuronate synthesis, additional copies of both Alg8 and its interacting partner Alg44 were introduced into respective mutant backgrounds. Additional copies of Alg8 and/or Alg44 had a similar effect on alginate production, such as resulting in high molecular masses with reduced epimerization and acetylation compared to those of the wild-type control (Fig. 5A; Table 1). The same effect of Alg8 and Alg44 on alginate polymerization supported the hypothesis that both subunits constitute the alginate polymerase.

AlgF, AlgI, and AlgJ were proposed to form a protein complex constituting the alginate acetyltransferase/acetylesterase (12, 32, 33). Recently, AlgX was demonstrated to play an independent role in alginate acetylation. AlgX is a two-domain protein, including a domain with acetyltransferase activity and a carbohydrate-binding domain. Replacement of amino acid residues S269, H176, and D174, which were proposed to constitute the catalytic site, resulted in nonacetylated alginate (13). AlgG, the epimerase, contains a conserved DPHD motif (residues 324 to 327) (14, 19, 34, 35), the proposed active site involved in epimerization. Replacement of amino acid residues in this motif was shown to result in nonepimerized alginate, while modified AlgG retained its protective role on nascent alginate against degradation in the periplasm. Here, we used catalytically inactive variants of AlgX(S269A) and AlgG(D324A). When only the inactive AlgX variant was present, the resulting alginate was nonacetylated. Interestingly, additional copies of active AlgX or inactive AlgX resulted in the highest epimerization values of molar fraction of G residue (F_G) = 0.36. Additional copies of both AlgG and AlgX or inactive variants increased the degree of epimerization of the resulting alginate (Fig. 5A). Additional copies of both AlgX and AlgG increased the degree of acetylation compared to additional copies of only AlgX (Fig. 5A). Interestingly, additional copies of Alg44 enhanced acetylation 2.7-fold compared to AlgX.

The correlation between the molecular mass of alginate and alginate modification, such as acetylation and epimerization, was assessed (Fig. 5B). The molecular mass of the various alginates was determined by size exclusion chromatography-multiangle laser light scattering (SEC-MALLS) (Table 1; see also Fig. S3 in the supplemental material). The highest molecular mass (4,653 ± 1.1% kDa, corresponding to about 22,876 uronic acid residues) was detected in alginates from strains with additional copies of the catalytically inactive epimerase variant AlgG(D324A). This was about a 70% increase in molecular mass compared to alginate produced from strains with additional copies of epimerizing

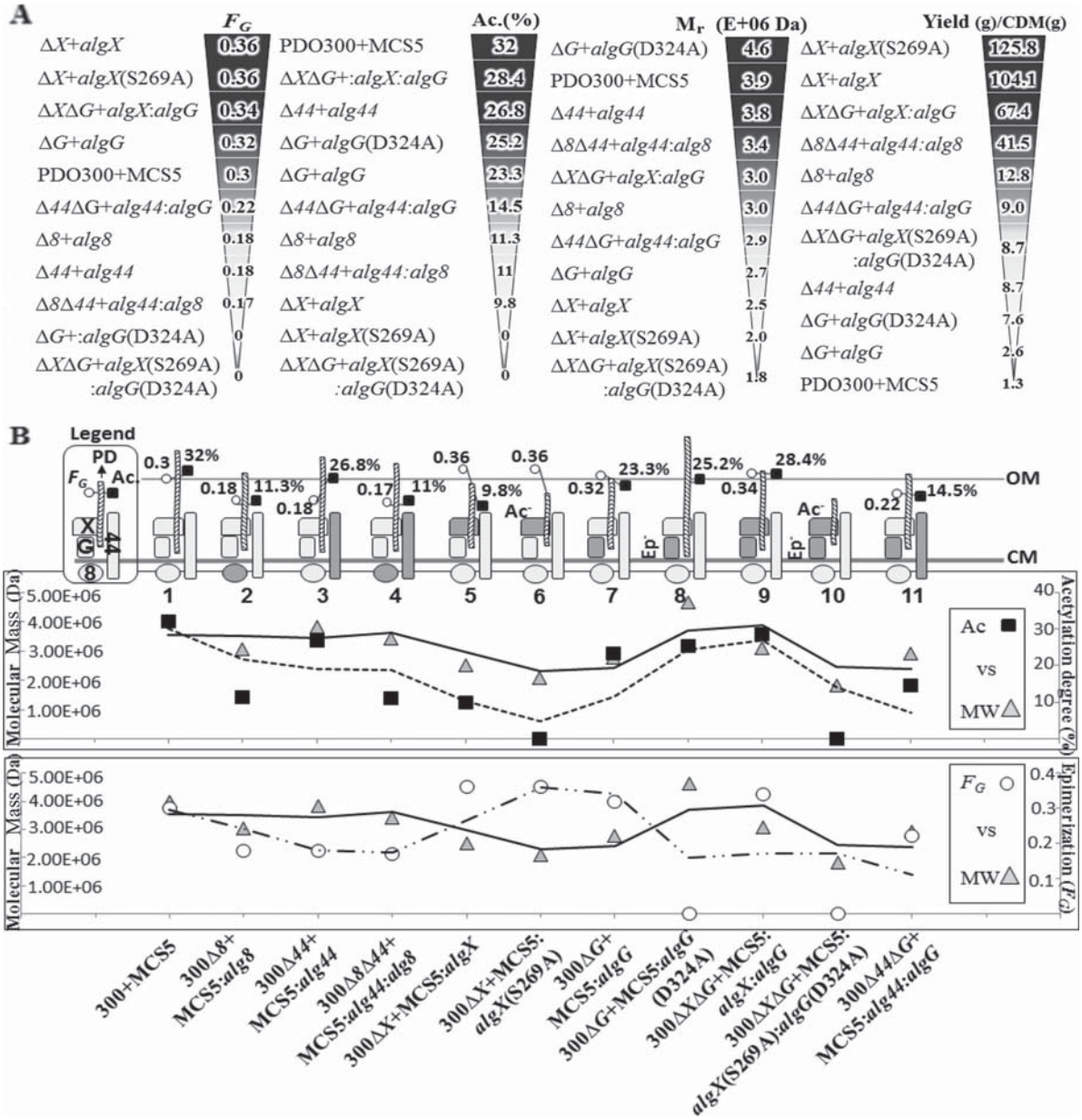

FIG 5 Impact of putative alginate polymerase subunits on alginate polymerase activity, alginate polymerization, and composition and correlation between polymerization and modification. (A) The values of molar fraction of G residue (F_G), acetylation degrees (Ac. %), mean molecular masses, and alginate yield are aligned with the strains producing the respective alginates. (B) Correlation between degree of acetylation, epimerization, and molecular mass of alginate. Presumable features (no. 1 to 11) show protein complexes constituted by Alg8, Alg44, AlgG, and AlgX (see the legend at the top left corner of the plot). The subunit produced upon in *trans* complementation is shown as darker shape(s). Inactive AlgX(S269A) and AlgG(D324A) proteins are labeled as (Ac⁻) and (Ep⁻), respectively. The length of various alginates (PD) with respect to acetylation (Ac. %) and epimerization (F_G) degrees are presented and proportionally illustrated for each feature. 300, PDO300; MCS5, pBBR1MCS-5; PD, polymerization degree; OM, outer membrane; CM, cytoplasmic membrane.

AlgG. The lowest-molecular-weight alginates were produced by strains harboring additional copies of those subunits contributing the highest levels of epimerization, i.e., AlgX ($F_G = 0.36$) and AlgX(S269A) ($F_G = 0.36$), along with the lowest levels of acetylation (9.8% and 0). Nonacetylated and nonepimerized alginates ($F_G = 0$, acetylation = 0%) showed the lowest molecular mass (1,811 ± 0.9% kDa). Since ^{1}H-NMR spectra of the various alginates did not provide evidence for double bonds (between the C-4 and C-5 carbons, leading to 4-deoxy-L-erythro-hex-4-enopyranosyluronic acid), which are introduced by alginate lyase-mediated degradation, the alginate lyase presumably did not influence the polymerization degree. Additional copies of Alg8 and Alg44 gave rise to increased molecular masses ranging from 3,000 to 3,800 kDa, supporting their direct involvement in alginate chain synthesis. These data suggested that the alginate molecular mass is inversely correlated with alginate epimerization but positively correlated with acetylation (Fig. 5B). Alginates produced by the various strains showed a narrow mo-

lecular mass distribution with a polydispersity index close to 1 (Table 1).

***In vivo* alginate polymerase activity.** Alginate produced by the various strains was isolated and quantified (Fig. 5A; Table 1). Although additional copies of the various proteins increased the amount of alginate produced compared to the PDO300 (pBBR1MCS-5) reference strain, a significant variation of alginate productivity, i.e., alginate polymerase activity, was detected. Interestingly, additional copies of nonacetylating AlgX(S269A) and native AlgX mediated production of the largest amounts of alginate, while epimerizing and nonepimerizing AlgG mediated the lowest level of production (Fig. 5A). Pairwise comparison of these four strains showed that more alginate is produced in the absence of modification events. The enhancing role of AlgX in alginate production was further supported when additional copies of AlgX together with AlgG led to a strong production of alginate. However, the nonacetylating and nonepimerizing pair of them resulted in a much lower quantity (Fig. 5A). Furthermore, all attempts to restore alginate production in the PDO300Δ*alg44*Δ*algX* mutant with pBBR1MCS-5:*alg44*:*algX* failed. The mucoid phenotype of this double-gene-knockout mutant was restored only when one of the introduced complementing genes, either *alg44* or *algX*, was integrated into the genome (in *cis* complementation using mini-CTX) and the other one presented in *trans*, resulting in alginate production of 1.9 g/cell dry mass (CDM) (g).

Microrheological analysis of various alginates. Particle-tracking microrheology was applied to assess the viscoelastic properties of the various resulting alginates. All alginates showed viscoelastic properties in which the solid-like elastic modulus G' was greater than the liquid-like viscous modulus G'' ($G' > G''$). The plot of particle mean square displacement (MSD) versus correlation time showed MSD curves of the alginates are distributed in four distinct categories (see Fig. S4 in the supplemental material). In the first category, the alginates produced from the PDO300Δ*algG*(pBBR1MCS-5:*algG*(D324A)) and PDO300Δ*alg8* (pBBR1MCS-5:*alg8*) mutants, without G residues and with the highest molar fraction of MM-blocks, respectively, and both with very high molecular mass, showed the highest and quite similar viscoelastic properties ($G' = 0.41$, $G'' = 0.3$; $G' = 0.40$, $G'' = 0.28$, respectively). Interestingly, the alginates from the PDO300Δ*alg44* (pBBR1MCS-5:*alg44*), PDO300Δ*algG*(pBBR1MCS-5:*algG*), and PDO300(pBBR1MCS-5) strains dropped into the second category with lower viscoelastic property. In the third category, showing lower viscoelastic properties, those alginates with a molecular mass of ≤2,000 kDa produced by PDO300Δ*algX*(pBBR1MCS-5:*algX*(S269A)) and PDO300Δ*algX*Δ*algG*(pBBR1MCS-5:*algX*(S269A):*algG*(D324A)) mutants were found. Surprisingly, acetylated alginate from the PDO300Δ*algX*(pBBR1MCS-5:*algX*) mutant was the only member of the fourth category, with the lowest viscoelastic property among all analyzed samples. These results suggested that viscoelasticity was positively impacted by the molecular mass combined with high M content, while the presence of G residues and acetyl groups in the alginate chain lowered viscoelasticity. All these polymers showed greater elasticity than viscosity ($G' > G''$).

The impact of various alginates on biofilm formation. *P. aeruginosa* is capable of different modes of motility, such as twitching, swarming, and swimming, which are controlled by various regulatory pathways and environmental factors. These play an important role in biofilm formation and dispersal. Here, motility assays were conducted with strains capable of producing different alginates in order to assess the relationship between alginate composition/molecular mass, i.e., material properties, and motility, ultimately impacting on biofilm formation (see Fig. S5 in the supplemental material). All strains with alginate production greater than that of PDO300 (pBBR1MCS-5) showed lower twitching motility, while non-alginate-producing knockout mutants showed greater twitching values. The lowest twitching motility among all strains was found for the PDO300Δ*alg44*(pBBR1MCS-5:*alg44*) mutant. Twitching motility differences between the PDO300Δ*algX* (pBBR1MCS-5:*algX*) and PDO300Δ*algX*(pBBR1MCS-5:*algX* (S269A) mutants or between the PDO300Δ*algG*(pBBR1MCS-5:*algG*) and PDO300Δ*algG*(pBBR1MCS-5:*algG*(D324A)) mutants were insignificant (see Fig. S5 in the supplemental material).

Swarming motility, which occurs on semisolid surfaces and is regulated by quorum sensing, was assessed as being lower in alginate-producing strains than in their respective knockout mutants, except for the PDO300Δ*alg8*(pBBR1MCS-5:*alg8*) mutant, which showed slightly greater swarming motility than the PDO300Δ*alg8*(pBBR1MCS-5) mutant. Among the alginate-producing strains, the greatest value of swarming motility was found for the PDO300Δ*alg44*(pBBR1MCS-5:*alg44*) mutant (11.33 mm) and the PDO300Δ*algX*(pBBR1MCS-5:*algX*) mutant (11.0 mm). The PDO300Δ*algG*(pBBR1MCS-5:*algG*(D324A)) mutant (6.83 mm) showed slightly greater swarming motility than the PDO300Δ*algG*(pBBR1MCS-5:*algG*) mutant (6.0 mm).

Swimming, which occurs in aqueous environments, was tested, and the values obtained varied significantly among the strains. Generally, alginate-producing strains showed lower swimming capability than knockout mutants, except for the PDO300 Δ*alg8*(pBBR1MCS-5:*alg8*) and PDO300Δ*alg8*(pBBR1MCS-5) mutants (see Fig. S5 in the supplemental material).

Confocal laser-scanning microscopy images of biofilms formed by the PDO300Δ*algX*(pBBR1MCS-5:*algX*) mutant and its nonacetylating counterpart, the PDO300Δ*algX*(pBBR1MCS-5:*algX*(S269A)) mutant, highlighted the crucial role of acetylation of alginate for developing biofilms and cellular arrangements (Fig. 6). Comparison of the two strains revealed significant differences in elevated structures and the distribution of microcolonies. For example, the structures formed by strains producing acetylated alginates were perfectly shaped and developed with a biovolume of $5.5 \pm 1.26\ \mu m^3 \cdot \mu m^{-2}$ and a maximum height of 83 μm, while those formed with nonacetylated alginate showed a smaller biovolume of $3.9 \pm 0.2\ \mu m^3 \cdot \mu m^{-2}$ and a reduced height of 26 μm, with irregular architecture. Interestingly, the strain producing acetylated alginate did not produce a multicellular base layer, and cells were organized in pillar-shaped architectures, similar to structures described for the architectures of the Psl-overproducing strain (i.e., *P. aeruginosa* WFPA801) (36, 37). In contrast, the strain producing nonacetylated alginate formed a biofilm with disordered and scattered microcolonies (Fig. 6, frame 3). Furthermore, the PDO300Δ*algX*(pBBR1MCS-5:*algX*) mutant formed a biofilm with 1.5-fold more compactness and 31% more live cells than the biofilm formed by the PDO300Δ*algX* (pBBR1MCS-5:*algX*(S269A))mutant(Table2).ThePDO300Δ*algX* (pBBR1MCS-5) mutant did not form a structured biofilm (Fig. 6, frame 4) but did form a multicellular layer with a thickness of 6 μm.

The PDO300Δ*algG*(pBBR1MCS-5:*algG*(D324A)) mutant,

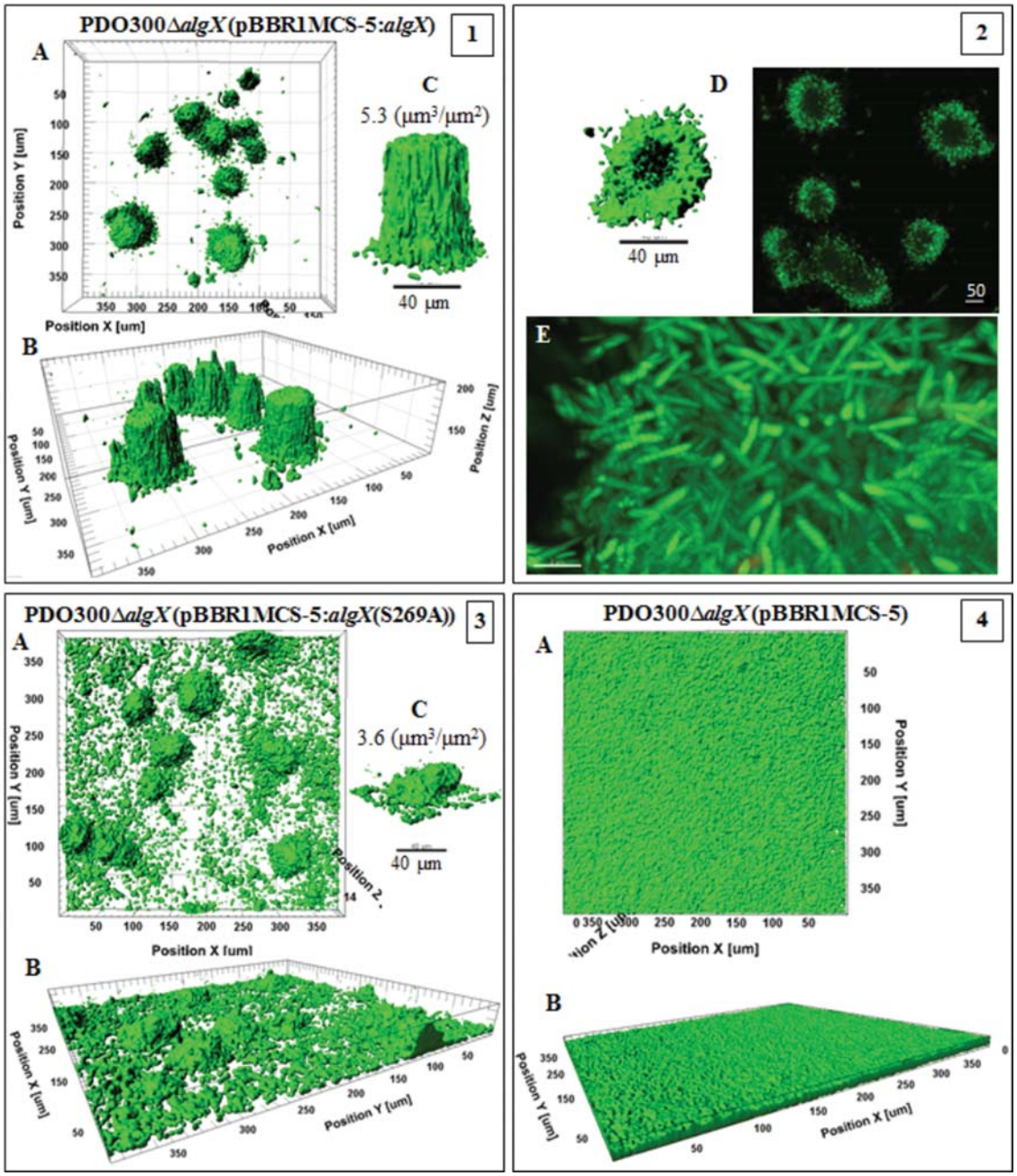

FIG 6 Biofilm architecture of mutants producing acetylated and nonacetylated alginates. This figure shows biofilm formation and architecture of the PDO300Δ*algX*(pBBR1MCS-5:*algX*) (frames 1 and 2) and PDO300Δ*algX*(pBBR1MCS-5:*algX*(S269A)) (frame 3) mutants, which produce acetylated and nonacetylated alginates, respectively, and the PDO300Δ*algX*(pBBR1MCS-5) (frame 4) mutant with no alginate production. In all frames, A, B, and C show top views, side views, and a representative of typical highly structured cell community, respectively. The cell community dimensions are provided as $\mu m^3 \cdot \mu m^{-2}$.

which produced a high-molecular-mass, acetylated polymannuronate with strong viscoelasticity, acquired the largest biovolume of $6.0 \pm 0.22\ \mu m^3 \cdot \mu m^{-2}$ (Fig. 7, frame 3). Interestingly, adjacent structures were networked with horizontal appendages, with void spaces and channels formed underneath whole structures, likely to constitute water channels (Fig. 7, frame 4). On the other hand, the PDO300Δ*algG*(pBBR1MCS-5:*algG*) mutant, which produced lower-molecular-mass, acetylated, and G residue-containing alginate, formed elevated but less developed structures with less biovolume, $4.8 \pm 0.22\ \mu m^3 \cdot \mu m^{-2}$ (Fig. 7, frame 1). The base layers formed by both strains were dense and covered the whole area of the surface. The biofilm of the PDO300Δ*algG*(pBBR1MCS-5) mutant was a homogenous layer of cells (7-μm thickness) without elevated structures (Fig. 7, frame 2).

The PDO300Δ*algG*Δ*algX*(pBBR1MCS-5:*algX*(S269A):*algG* (D324A)) mutant produced a nonacetylated polymannuronate with a low molecular mass, and the respective biofilm was composed of very long and narrowly elevated structures (Fig. 8, frames

TABLE 2 Compactness and dead/live ratio calculated for analyzed biofilms

Mutant description[c]	Compactness[a]	Dead/live ratio[b]
300Δ*8*+MCS5:*alg8*	6.09E+02	1.43 ± 0.10
300Δ*44*+MCS5:*alg44*	4.43E+02	1.17 ± 0.04
300Δ*G*+MCS5:*algG*	2.77E+02	0.70 ± 0.06
300Δ*G*+MCS5:*algG*(D324A)	1.68E+02	0.97 ± 0.04
300Δ*X*+MCS5:*algX*	3.00E+02	0.42 ± 0.02
300Δ*X*+MCS5:*algX*(S269A)	2.20E+02	0.55 ± 0.02
300Δ*G*Δ*X*+MCS5:*algG*(D324A):*algX*(S269A)	1.20E+03	0.49 ± 0.03
300+MCS5	4.46E+02	2.40 ± 0.29
300Δ*8*+MCS5	1.39E+02	1.46
300Δ*44*+MCS5	1.42E+02	0.7
300Δ*G*+MCS5	8.90E+01	1.01
300Δ*X*+MCS5	1.16E+02	0.94

[a] Total fluorescence per volume of biofilm.
[b] Ratio between red and green fluorescence shown by each biofilm-forming mutant.
[c] 300, PDO300; MCS5, pBBR1MCS-5.

1 and 2). The biovolume was 1.5 ± 0.2 $\mu m^3 \cdot \mu m^{-2}$), which was less than for all the other investigated strains (Table 2).

The PDO300Δ*alg8*(pBBR1MCS-5:*alg8*) and PDO300Δ*alg44* (pBBR1MCS-5:*alg44*) strains established heterogeneous highly structured biofilms (Fig. 9). The former formed a biovolume of 3.95 ± 0.43 $\mu m^3 \cdot \mu m^{-2}$ and compactness of 6.09E+02, while the latter generated very dense and large structures with a biovolume of 5.8 ± 0.43 $\mu m^3 \cdot \mu m^{-2}$ but less compactness (4.43E+02). Both mutants showed higher numbers of dead cells than all applied mutants but fewer dead cells than the wild type (Table 2). Conversely, the PDO300Δ*alg8*(pBBR1MCS-5) and PDO300 Δ*alg44*(pBBR1MCS-5) strains generated homogenous biofilm without elevated or highly structured architectures. Compactness values and dead/live ratios are summarized in Table 2.

DISCUSSION

In this study, we investigated the relationship between alginate polymerization and modification, the functional role of the subunits Alg8, Alg44, AlgG, and AlgX, and their physical and functional interaction. A range of alginate compositions and molecular masses exhibiting various material properties were produced by engineered *P. aeruginosa* strains, and their impact on motility and biofilm formation was assessed. This study revealed protein-protein interaction between Alg8 and Alg44, proposed as alginate polymerase and copolymerize (Fig. 1). Alg44 was found to interact with AlgK (Fig. 2A), which is an outer membrane lipoprotein that aids the correct localization of the AlgE porin to the outer membrane. This study provides experimental evidence for the previously suggested presence of an Alg8-Alg44-AlgX-AlgK-AlgE multiprotein complex bridging the cell envelope forming the alginate polymerization/modification/secretion machinery (21). The absence of the previously observed AlgK-X interaction after DSG cross-linking and anti-AlgX immunoblotting (Fig. 2D) was presumable due to a lack of suitable cross-linking sites (K residues 7 Å apart from each other) (22). In addition, immunoblotting/cross-linking data suggested that Alg44 forms a dimer. However, this dimer was not observed when Alg44 was overproduced from a plasmid, indicating that Alg44 dimerization might be susceptible to changes in stoichiometry (Fig. 2C and D). Bioinformatics analysis of the periplasmic part of Alg44 suggests the presence of coil-coiled structures (Coil/Pcoils-based score of 0.4), which have been described for membrane fusion proteins (MFPs) such as MexA and polysaccharide copolymerases (PCPs) to contribute to oligomerization (38). Here, it was demonstrated that Alg44 localization, stability, and protein-protein interaction were not impacted by altering the c-di-GMP level or by non-c-di-GMP binding variants (Fig. 3; see also Fig. S1 in the supplemental material). Our results indicated that the c-di-GMP-mediated activation mechanism of alginate polymerization differs from the activation mechanism of cellulose synthase in which c-di-GMP releases an autoinhibited state by breaking a salt bridge (30). However, residue H323 of Alg8 might be involved in c-di-GMP-dependent activation of alginate polymerase, as reduced c-di-GMP levels did not impair *in vivo* Alg8 activity (Fig. 4).

The first experimental evidence was obtained that AlgX and AlgG exhibit a mutually auxiliary behavior, suggesting that the two modification events (acetylation and epimerization) are not competitive but linked (35). In addition, we propose a new auxiliary role for Alg44 in acetylation besides being necessary for c-di-GMP-dependent activation of alginate polymerization (Table 1; Fig. 5A). Failed attempts in complementing the PDO300Δ*alg44* Δ*algX* mutant with pBBR1MCS-5:*alg44*:*algX*, but successful complementation if one gene was present in *cis* and the other in *trans*, suggested that the stoichiometry of these two proteins is critical for proper performance of the multiprotein complex.

This study revealed how alginate polymerization (Alg8, Alg44) is aligned with alginate modification (AlgG, AlgX). As shown in Fig. 5A, additional copies of active or inactive AlgX acetyltransferase significantly increased the molar fraction of G residues as well as productivity, which appeared inversely correlated with the alginate molecular mass (Fig. 5A; Table 1). This suggests a new role of AlgX in epimerization and a periplasmic scaffold protein playing a key role in efficient translocation of the alginate chain across the periplasm. Recently, it was reported that AlgX binds to polymannuronic acid in a length-dependent manner and acts as a terminal acetyltransferase (11).

Interestingly, restoration of alginate production of the AlgG-negative mutant by an inactive variant of AlgG led to a significantly increased alginate molecular mass compared to that of active AlgG, suggesting that AlgG as a scaffold subunit is critical for processivity of alginate polymerization, while the actual epimerization event interferes with processivity (Fig. 5A and B). Furthermore, the role of AlgG-mediated epimerization on alginate length might be due to AlgG-mediated alginate degradation, as polysaccharide epimerases show a reaction mechanism similar to that of polysaccharide lyases (35). This finding might also explain why algal alginates with a high molar fraction of G residues introduced by epimerases have very low molecular masses (39). Acetylation was correlated with the molecular mass, suggesting that there was no impact on processivity of alginate polymerization (Fig. 5B).

In general, additional copies of any subunit increased alginate production compared to that of the reference strain, indicating that the stoichiometry of the various subunits is less critical for the activity of the multiprotein complex (Table 1). Based on these results with regard to the roles of the investigated subunits in alginate synthesis and modification, a revised model of the alginate biosynthesis multiprotein complex was proposed (Fig. 10).

To shed light on the structure-function relationship of the various alginates, their viscoelasticity was assessed. The presence of

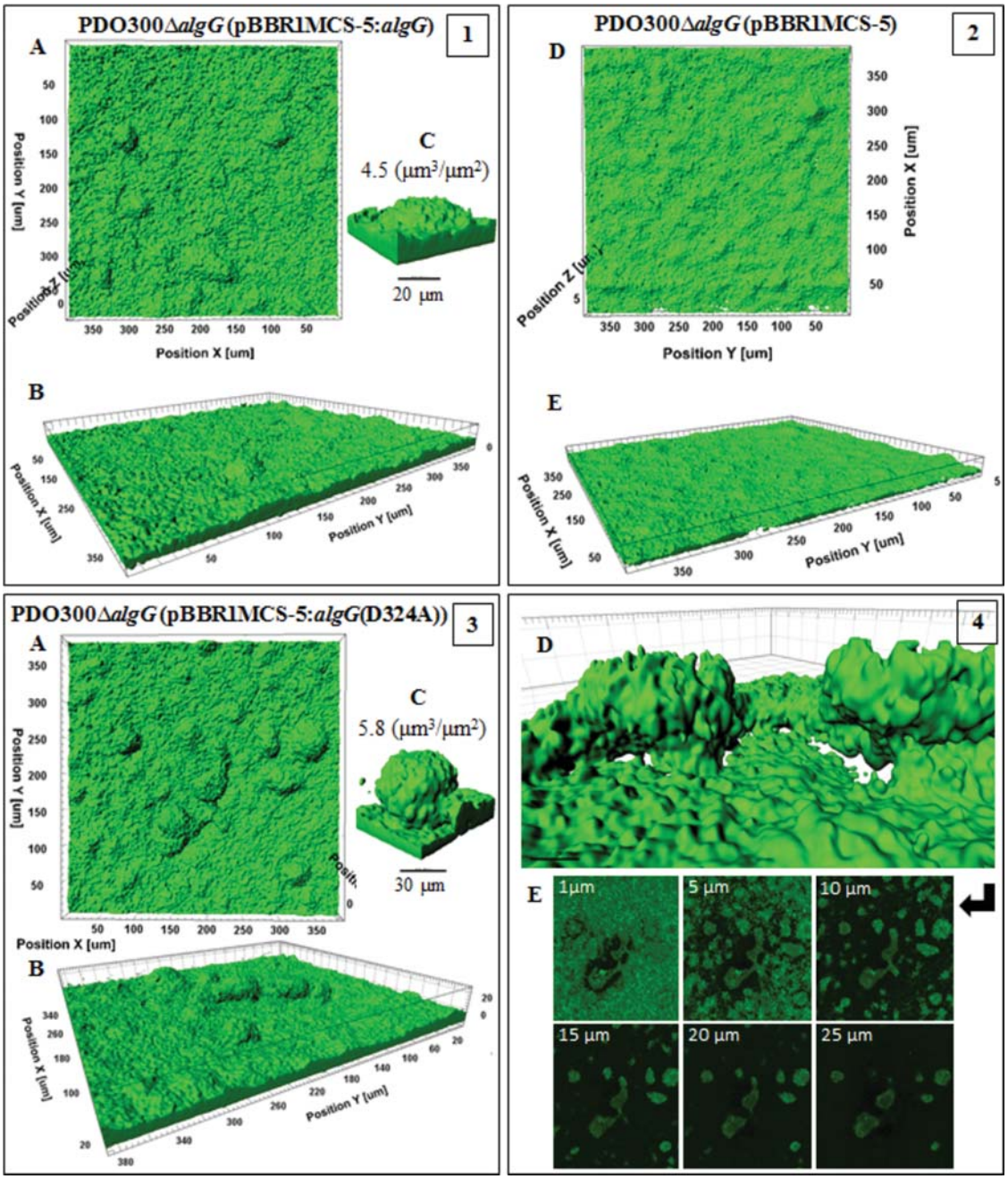

FIG 7 Biofilm architecture of mutants producing epimerized and nonepimerized alginates. This figure shows biofilm formation and architecture of the PDO300Δ*algG*(pBBR1MCS-5:*algG*) (frame 1) and PDO300Δ*algG*(pBBR1MCS-5:*algG*(D324A)) (frames 3 and 4) mutants, which produce, respectively, epimerized [poly(MG)] and nonepimerized [poly(M)] alginates, and the PDO300Δ*algG*(pBBR1MCS-5) (frame 2) mutant with no alginate production. In all frames, A, B, and C show, respectively, top views, side views, and a representative of typical highly structured cell communities for that mutant with biovolume-per-area ($\mu m^3 \cdot \mu m^{-2}$) ratio. In frame 3, poly(M) alginate-based biofilm is more highly developed than poly(MG) alginate-based biofilm in frame 1, presenting larger biovolume and biovolume-per-area ratios. Cells of both mutants covered the entire cover slide surface. Frames 4D and E represent the architecture of poly(M) alginate-based microcolonies in which two adjacent structures are connected with horizontal appendages and free-cell void cavities channeled underneath of microcolonies. Frame 4E shows 6 different slices of microcolonies with connected structures at the middle of the figures surrounded by free-cell and matrix areas. Frame 2 represents the homogenous cell community of a nonmucoid mutant without highly structured architecture.

acetyl groups lowered viscoelasticity by possibly interfering with intermolecular alginate chain interactions (see Fig. S4 in the supplemental material). In contrast, increasing molar fractions of MM-blocks and higher molecular masses increased viscoelasticity (see Fig. S4 in the supplemental material). Acetylated alginates gave rise to well-developed and highly organized heterogeneous architectures and promoted cell aggregations (Fig. 6), which was consistent with previous studies (40), but these findings suggested viscoelasticity is not critical for biofilm architecture formation. Figure 7 shows that nonepimerized alginate (polymannuronate)

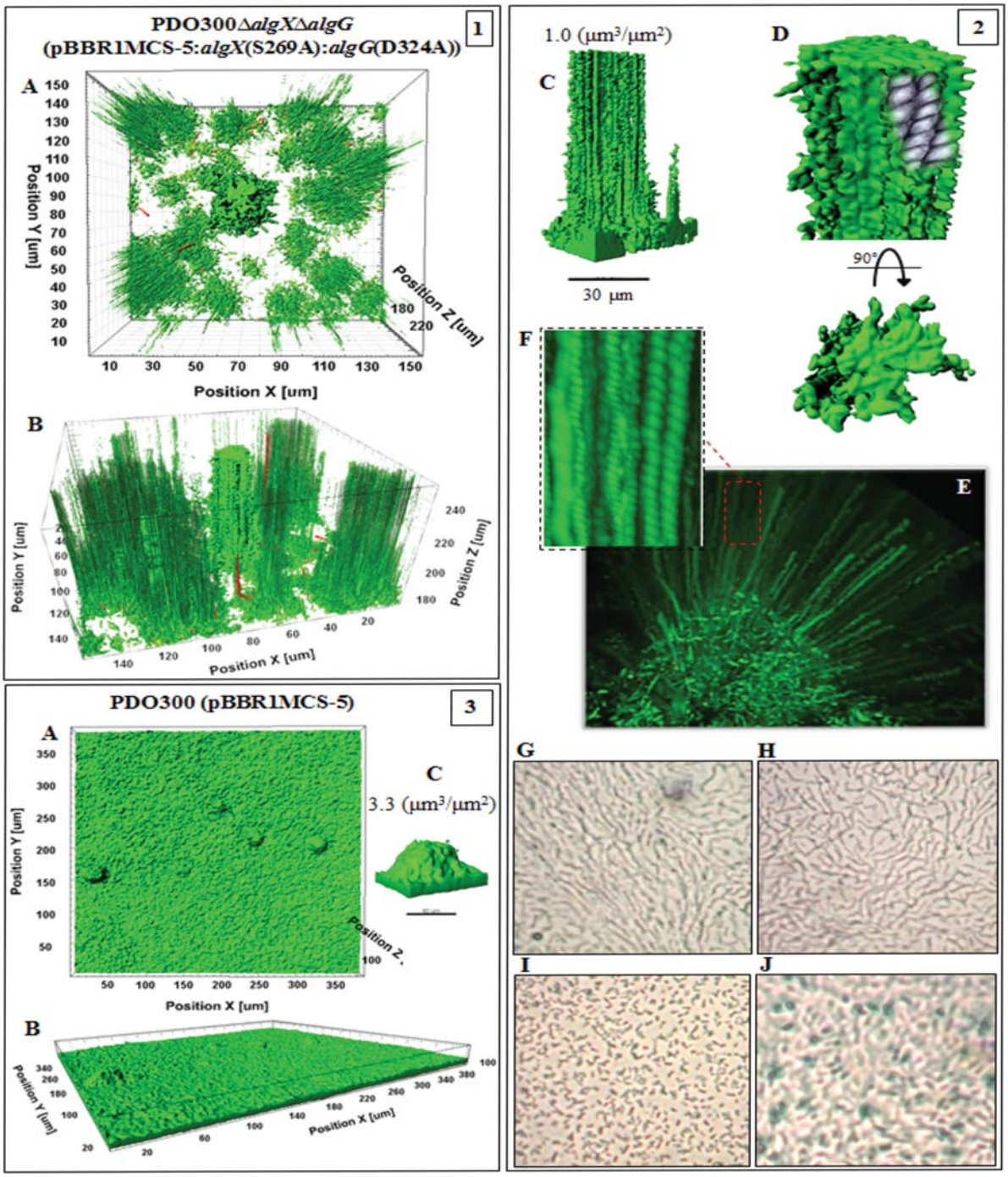

FIG 8 Biofilm architecture of mutant-producing nonepimerized and nonacetylated alginates and the wild type. This figure shows biofilm formation and architecture of the PDO300Δ*algX*Δ*algG*(pBBR1MCS-5:*algX*(S269A):*algG*(D324A)) (frames 1 and 2) and PDO300(pBBR1MCS-5) (frame 3) mutants. In all frames, A, B, and C show, respectively, top views, side views, and a representative of typical highly structured cell communities for that mutant with biovolume-per-area ($\mu m^3 \cdot \mu m^{-2}$) ratio. The biofilm architecture visualized for the mutant producing nonacetylated poly(M) alginate (frames 1and 2) was remarkably different from that of other applied mutants. Affected by alginate properties, emerging biofilm consists of very narrow but long elevated microcolonies representing longitudinal cell trails or strips indicating stigmergic self-organization and adaptation of cells in weak matrices. Frames 2D to F represent close side and top views of one of the microcolonies and cell trails, and cell-cell interactions in each cell trail are depicted in sketches. Frames 2G to J show micrographs (×40 magnification) of the edge (H and I) and surface (G and J) of mucoid colonies of the PDO300Δ*algX*Δ*algG*(pBBR1MCS-5:*algX*(S269A):*algG*(D324A)) (G and H) and PDO300(pBBR1MCS-5) (I and J) mutants forming a thin layer on PIA medium after incubation at 37°C for 18 h. Organization of cells of the PDO300Δ*algX*Δ*algG*(pBBR1MCS-5:*algX*(S269A):*algG*(D324A)) mutant showed a linear filamentous aggregation pattern. Wild-type biofilm architecture is presented in frame 3.

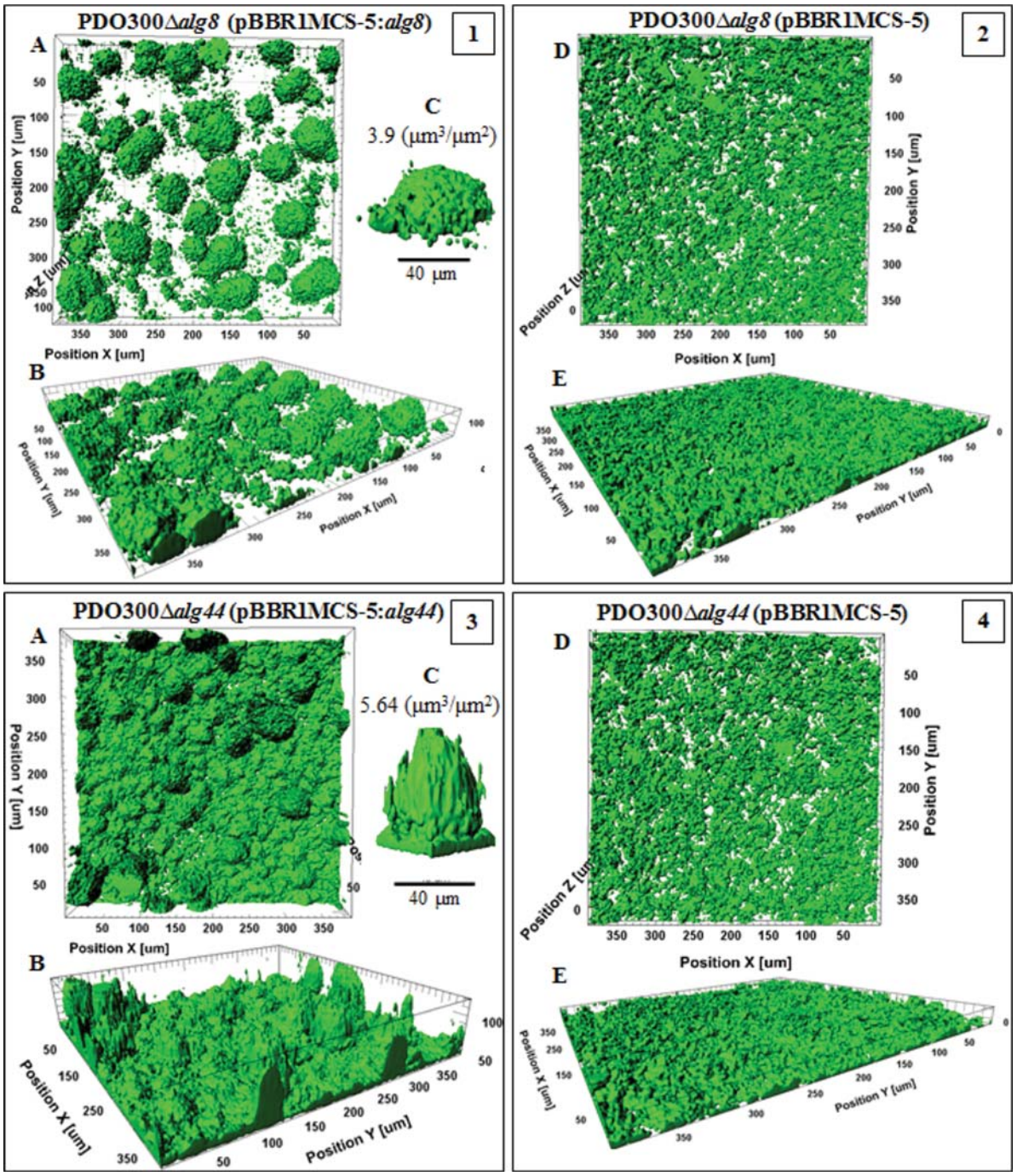

FIG 9 Biofilm architecture of a mutant producing a high mannuronate molar fraction and M-block. This figure shows biofilm formation and architecture of the PDO300Δ*alg8*(pBBR1MCS-5:*alg8*) (frame 1) and PDO300Δ*alg44*(pBBR1MCS-5:*alg44*) (frame 3) mutants and nonmucoid mutants (frames 2 and 4). In all frames, A, B, and C show, respectively, top views, side views, and a representative of typical highly structured cell communities for that mutant with biovolume-per-area ($\mu m^3 \cdot \mu m^{-2}$) ratio. Both mutants produce alginates with the highest degree of M-block occurrence but very different degrees of acetylation. The PDO300Δ*alg44*(pBBR1MCS-5:*alg44*) (frame 3) mutant, which produces highly acetylated alginate, established very dense and highly developed and larger microcolonies than the PDO300Δ*alg8*(pBBR1MCS-5:*alg8*) (frame 1) mutant. One explanation for this significance difference is the presence of an additional copy of Alg44 which senses c-di-GMP, which is a common secondary messenger in the cells governing the physiological condition of cells during colonization. However, nonmucoid mutants did not establish highly structured biofilm and microcolonies.

with high molecular mass and the strong viscoelasticity supported the establishment of these biofilm features and that by controlling the molar fraction of G residue biofilm architecture, characteristics could be adapted to various environments. We showed that the lack of G residues and acetyl groups caused the formation of undeveloped and narrow microcolonies, which were supported by specific long trails or strips of cells emerging from stigmergic self-organization of cells affected by this particular alginate

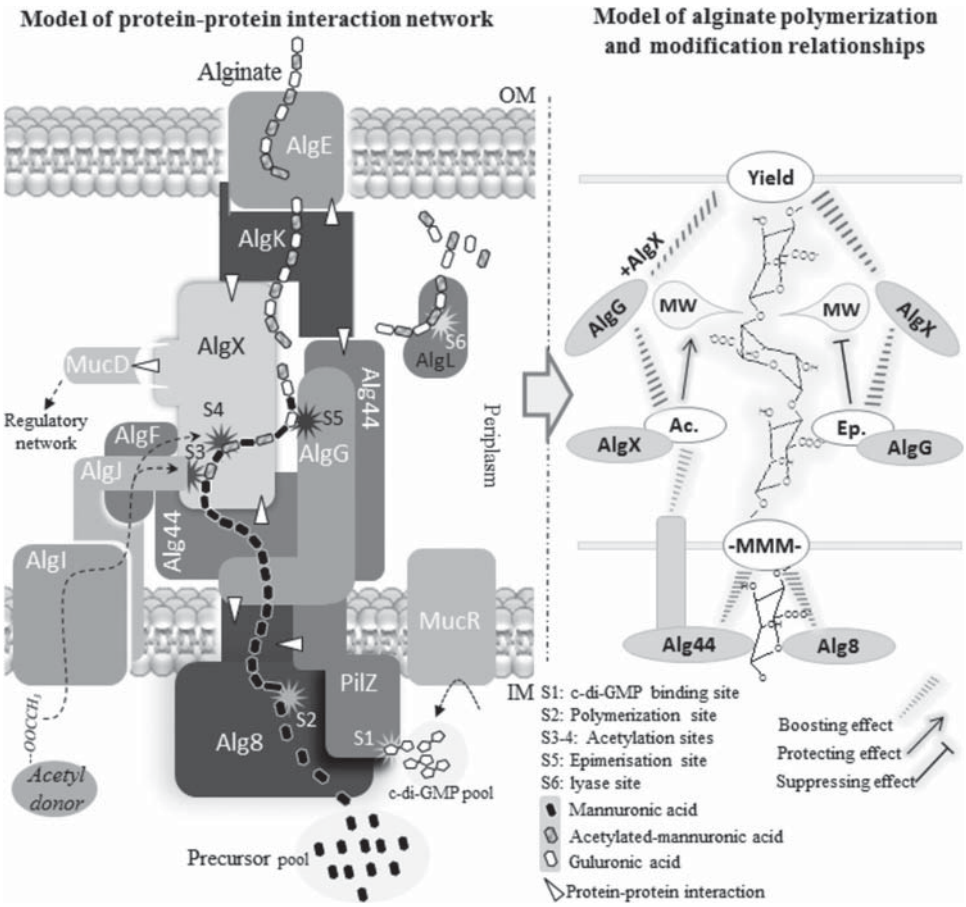

FIG 10 A new proposed model of alginate biosynthesis machinery complex and interactive performances of protein functionality over alginate polymerization, acetylation, epimerization, and length determination. Based on experimental results obtained in the current study, functional and physical interactions of subunits (left side of figure) were modeled into a multiprotein complex. In this model, different binary interactions are marked with white triangles. Our finding of Alg8-Alg44 and Alg44-AlgK interactions together with the previously discovered interaction of AlgK-AlgE (21) constitute the periplasmic part of the multiprotein complex connecting the cytoplasmic membrane with the outer membrane. The model also includes the following interactions, Alg44-AlgX, Alg8-AlgG, and MucD-AlgX-AlgK (21, 22, 49), in support of the periplasmic scaffold guiding nascent alginate for translocation and secretion. This model shows alginate production is positively regulated by c-di-GMP binding to Alg44 (S1) which targets the catalytic site of Alg8 polymerase (S2) through an unknown mechanism. Then, translocation across the periplasmic scaffold is coupled with interactive functional performances of modification events and proteins (right side of model) for alginate length regulation and a series of associated modification events (S3 to S5). AlgL is responsible for degrading misguided alginate accumulating in periplasm (S6). MucD protein links the complex with the posttranslational alginate regulatory network via an interaction with AlgX.

(Fig. 8) (41). This was further evidence for the role of alginate material properties on the formation of particular biofilm architectures and cellular aggregation patterns.

Motility mediated by twitching, swarming, and swimming was assessed using strains producing various alginates. These motilities are critical for biofilm development and dispersal (42). Here, we showed that overproduction of alginate interferes with motility. Previously, it was shown that high levels of c-di-GMP reduced motility while increasing production of various exopolysaccharides and biofilm formation (43). Moreover, our results showed these motilities are independent of the acetyl group and G residue content of the respective alginate (see Fig. S5 in the supplemental material). Overall, this study led to updating the protein-protein interaction network constituting the proposed alginate polymerization/modification/secretion multiprotein complex in *P. aeruginosa* and the development of strains producing a range of alginates, enabling the analysis of structure-function relationships from a material property and biological function perspective, such as demonstrating that viscoelasticity of alginate contributed to enhanced cell aggregation during biofilm formation.

MATERIALS AND METHODS

Bacterial strains, plasmids, and growth conditions. Strains and plasmids used in this study are summarized in Table S1 in the supplemental material. *P. aeruginosa* and *Escherichia coli* strains were grown at 37°C. For those assays designed for studying alginate production, bacterial phenotype, and protein-protein interaction and stability, Difco *Pseudomonas* isolation agar (PIA) medium was used. To rule out the effect of growth condition and media on alginate composition and quantity, all experiments were conducted under the same conditions and using the same batch culture at the same time (see the supplemental material).

Construction of isogenic mutants with single- and double-gene knockouts of *alg8*, *alg44*, *algG*, and *algX* genes. The *P. aeruginosa* PDO300 strain was used to generate isogenic mutants with single- and double-gene knockouts of *alg8*, *alg44*, *algG*, and *algX* genes through two events of homologous recombination using suicide plasmid pEX100T containing knockout genes which were disrupted by the *aacC1* gene (en-

coding gentamicin acetyltransferase) flanked by two *FRT* sites (see the supplemental material).

In *trans* complementation of single- and double-gene-knockout mutants and chromosomal integrations. Relevant genes encoding Alg8, Alg44, AlgG, and AlgX (with and without the 6His tag) were individually or in combination transferred into generated mutants using the pBBR1MCS-5 plasmid and also incorporated into the genome using mini-CTX-*lacZ* plasmid (see the supplemental material). The pBBR1MCS-5 plasmid containing the various alginate genes was considered to study the impact on production of alginates and their characteristics in order to more sensitively detect changes in the alginates due to additional copy numbers of the respective alginate protein under investigation.

Site-specific mutations and deletions of *alg44* and *alg8*. Site-specific mutations and deletions of *alg44* and *alg8* genes were performed using the QuikChange II site-directed mutagenesis kit (Stratagene) or by DNA synthesis (GenScript), resulting in genes encoding the Alg8(E322A/H323/E326A) protein, Alg44(R17A/R21A/R21D) protein, and Alg44's N- and C-terminal truncation (see the supplemental material).

***In vivo* detection of the protein-protein interaction network.** *In vivo* detection of protein-protein interaction was performed by employing pulling down 6His-tagged proteins under native conditions, *in vivo* chemical cross-linking, and bacterial two-hybrid assay (see the supplemental material).

Assessment of the stability of Alg44 variants in the presence and absence of MucR (DGC/PDE)/RocR (PDE). Previously generated mutants, including the PDO300Δ*mucR*, PDO300Δ*mucR*(pBBR1MCS-5:*mucR*), PDO300(pBBR1MCS-5:*rocR*), and PDO300Δ*mucR*(pBBR1MCS-5:*rocR*) mutants, were shown to positively or negatively regulate alginate production through c-di-GMP synthesis (by MucR) or degradation (by RocR) (24). Also to use presumably nonfunctional Alg44 in binding to c-di-GMP and/or in alginate polymerization (8, 26), the PDO300Δ*alg44*(pBBR1MCS-5:*alg44*(R21D)-6His), PDO300Δ*alg44*(pBBR1MCS-5:*alg44*-6His(Δ40-74aa$_{PilZ}$)), and PDO300Δ*alg44*(pBBR1MCS-5:*alg44*-6His(Δ364-389aa)) mutants were generated. Using these mutants, we examined the direct effect of c-di-GMP and defective variants of Alg44 on its localization and stability in planktonic and biofilm cells. Cells grown on solid media or in liquid cultures as described above were washed twice with saline. Enzymatic cell lysis was performed using the abovementioned lysis buffer prepared in buffer A followed by sonication and isolation of the cell envelope fraction by ultracentrifugation at 100,000 × *g* for 1 h at 4°C. Pellets were solubilized with buffer A for protein analysis.

Isolation of cytoplasmic membrane and general protein analysis. To confirm the localization of Alg8 and Alg44 in the cytoplasmic membrane of *E. coli* BTH101, the cytoplasmic membrane fraction was isolated as described previously with some modifications (44) (see supplemental material).

Protein samples were generally analyzed utilizing SDS-PAGE (8% acrylamide gels) and immunoblotting (see the supplemental material).

Alginate purification and quantification. Two milliliters of bacterial overnight culture grown in LB medium supplemented with the appropriate antibiotic was sedimented, and cells were washed twice with saline solution. Cells were suspended in 1 ml of saline solution, and 200 μl of cell suspension was plated onto PIA medium (in triplicates) containing 300 $\mu g \cdot ml^{-1}$ of gentamicin and then incubated at 37°C for 72 h. Cells of each agar plate were scraped off and suspended in saline solution until the biomass was completely suspended. Then, suspensions were pelleted and alginates in supernatants were precipitated with equal volume of ice-cold isopropanol. The alginate precipitants were freeze-dried and then redissolved in 50 mM Tris-HCl (pH 7.4) and 10 mM $MgCl_2$ to a final concentration of 0.5% (wt/vol), followed by incubation with 15 $\mu g \cdot ml^{-1}$ DNase I and 15 $\mu g \cdot m \cdot liter^{-1}$ RNase I at 37°C for 6 h. Then, pronase E was added to a final concentration of 20 $\mu g \cdot ml^{-1}$ and incubated for a further 18 h at 37°C. Alginate solutions were dialyzed (12- to 14-kDa molecular mass cutoff; ZelluTrans/Roth mini dialyzer; Carl Roth GmbH & Co.) against 5 liters of ultrapure H_2O for 48 h. Finally, alginates were precipitated with an equal volume of ice-cold isopropanol and freeze-dried for uronic acid assay and biochemical analysis (see the supplemental material).

The analysis of molecular mass, composition, and viscoelastic properties of the alginates. Various alginates produced by different complemented mutants were subjected to molecular mass analysis using size exclusion chromatography-multiangle laser light scattering (SEC-MALLS) and compositional analysis utilizing ^{1}H-nuclear magnetic resonance (NMR) spectroscopy and Fourier transform infrared (FTIR) spectrometry (see Text S1 in the supplemental material. Microrheological analysis was used to measure the viscoelastic property of the alginates in which the mean square displacement (MSD) of probe particles embedded in the samples and in turn the viscoelastic moduli (*G*' [elastic] and *G*" [viscose]) were measured (see the supplemental material).

Continuous-culture flow cell biofilms, quantitative analysis, and motility assays. Biofilm architecture analysis was performed for those mutants producing alginates with very distinct composition and properties from each other, including the PDO300(pBBR1MCS-5), PDO300Δ*alg8*(pBBR1MCS-5:*alg8*), PDO300Δ*alg44*(pBBR1MCS-5:*alg44*), PDO300Δ*algG*(pBBR1MCS-5:*algG*), PDO300Δ*algG*(pBBR1MCS-5:*algG*(D324A)), PDO300Δ*algX*(pBBR1MCS-5:*algX*), PDO300Δ*algX*(pBBR1MCS-5:*algX*(S269A)), and PDO300Δ*algX*Δ*algG*(pBBR1MCS-5:*algX*(S269A):*algG*(D324A)) mutants. Each mutant was grown in continuous-culture flow cells (channel dimensions of 4 mm by 40 mm by 1.5 mm) at 37°C (45). The flow cells were then incubated at 37°C for 24 h. Biofilms were stained utilizing the LIVE/DEAD BacLight bacterial viability kit (Molecular Probes) and visualized using confocal laser scanning microscopy (Leica SP5 DM6000B). For quantitative analysis of biofilms, IMARIS image analysis software (Bitplane) was employed. Biofilm architecture and appearance, biovolume (μm^3), the ratio of biovolume per unit area ($\mu m^3 \cdot \mu m^{-2}$), dead-to-live ratio, compactness, and thickness of base layers were analyzed (46–48). Motilities, including twitching, swarming, and swimming, were assessed by the method explained by Pang et al. (42) with modification. Full experimental details are provided in the supplemental materials.

SUPPLEMENTAL MATERIAL

Supplemental material for this article may be found at http://mbio.asm.org/lookup/suppl/doi:10.1128/mBio.00453-15/-/DCSupplemental.

Text S1, PDF file, 0.1 MB.
Figure S1, TIF file, 1 MB.
Figure S2, TIF file, 2.8 MB.
Figure S3, TIF file, 1.2 MB.
Figure S4, TIF file, 2.3 MB.
Figure S5, TIF file, 2.5 MB.
Table S1, PDF file, 0.1 MB.

ACKNOWLEDGMENTS

We are thankful to Lynne Howell from the University of Toronto and Dennis E. Ohman from Virginia Commonwealth University for providing antibodies and Iain D. Hay for advice and technical assistance, the Manawatu Microscopy and Imaging Centre (MMIC) of Massey University, and especially Matthew Savoian for microscopic technical assistance and Martin A. K. Williams and Bradley W. Mansel for assisting us with microrheology analysis.

This work was supported by grants from the Massey University Research Fund and the MacDiarmid Institute of Advanced Materials and Nanotechnology (New Zealand) to B.H.A.R. M.F.M. is funded by a Massey University doctoral scholarship.

REFERENCES

1. **Rehm BH, Grabert E, Hein J, Winkler UK**. 1994. Antibody response of rabbits and cystic fibrosis patients to an alginate-specific outer membrane protein of a mucoid strain of *Pseudomonas aeruginosa*. Microb Pathog **16:**43–51. http://dx.doi.org/10.1006/mpat.1994.1004.
2. **Pedersen SS, Høiby N, Espersen F, Koch C**. 1992. Role of alginate in

infection with mucoid *Pseudomonas aeruginosa* in cystic fibrosis. Thorax **47:**6–13. http://dx.doi.org/10.1136/thx.47.1.6.
3. **Hay ID, Ur Rehman Z, Ghafoor A, Rehm BHA.** 2010. Bacterial biosynthesis of alginates. J Chem Technol Biotechnol **85:**752–759. http://dx.doi.org/10.1002/jctb.2372.
4. **Hay ID, Ur Rehman Z, Moradali MF, Wang Y, Rehm BH.** 2013. Microbial alginate production, modification and its applications. Microb Biotechnol **6:**637–650. http://dx.doi.org/10.1111/1751-7915.12076.
5. **Franklin MJ, Nivens DE, Weadge JT, Howell PL.** 2011. Biosynthesis of the *Pseudomonas aeruginosa* extracellular polysaccharides, alginate, Pel, and Psl. Front Microbiol **2:**167. http://dx.doi.org/10.3389/fmicb.2011.00167.
6. **Chitnis CE, Ohman DE.** 1993. Genetic analysis of the alginate biosynthetic gene cluster of *Pseudomonas aeruginosa* shows evidence of an operonic structure. Mol Microbiol **8:**583–593. http://dx.doi.org/10.1111/j.1365-2958.1993.tb01602.x.
7. **Rehm BHA, Remminghorst U, Hay ID.** 2009. Molecular characterization of Alg8, a putative glycosyltransferase, involved in alginate polymerisation. J Biotechnol **140:**176–183. http://dx.doi.org/10.1016/j.jbiotec.2009.02.006.
8. **Lory S, Merighi M, Lee VT, Hyodo M, Hayakawa Y.** 2007. The second messenger bis-(3′-5′)-cyclic-GMP and its PilZ domain-containing receptor Alg44 are required for alginate biosynthesis in *Pseudomonas aeruginosa*. Mol Microbiol **65:**876–895. http://dx.doi.org/10.1111/j.1365-2958.2007.05817.x.
9. **Rehm BHA, Remminghorst U.** 2006. *In vitro* alginate polymerization and the functional role of Alg8 in alginate production by *Pseudomonas aeruginosa*. Appl Environ Microbiol **72:**298–305. http://dx.doi.org/10.1128/AEM.72.1.298-305.2006.
10. **Rehm BHA, Hay ID, Remminghorst U.** 2009. MucR, a novel membrane-associated regulator of alginate biosynthesis in *Pseudomonas aeruginosa*. Appl Environ Microbiol **75:**1110–1120. http://dx.doi.org/10.1128/AEM.02416-08.
11. **Baker P, Ricer T, Moynihan PJ, Kitova EN, Walvoort MT, Little DJ, Whitney JC, Dawson K, Weadge JT, Robinson H, Ohman DE, Codée JD, Klassen JS, Clarke AJ, Howell PL.** 2014. *P. aeruginosa* SGNH hydrolase-like proteins AlgJ and AlgX have similar topology but separate and distinct roles in alginate acetylation. PLoS Pathog **10:**e1004334. http://dx.doi.org/10.1371/journal.ppat.1004334.
12. **Franklin MJ, Ohman DE.** 2002. Mutant analysis and cellular localization of the AlgI, AlgJ, and AlgF proteins required for O acetylation of alginate in *Pseudomonas aeruginosa*. J Bacteriol **184:**3000–3007. http://dx.doi.org/10.1128/JB.184.11.3000-3007.2002.
13. **Riley LM, Weadge JT, Baker P, Robinson H, Codée JD, Tipton PA, Ohman DE, Howell PL.** 2013. Structural and functional characterization of *Pseudomonas aeruginosa* AlgX: role of AlgX in alginate acetylation. J Biol Chem **288:**22299–22314. http://dx.doi.org/10.1074/jbc.M113.484931.
14. **Jain S, Franklin MJ, Ertesvåg H, Valla S, Ohman DE.** 2003. The dual roles of AlgG in C-5-epimerization and secretion of alginate polymers in *Pseudomonas aeruginosa*. Mol Microbiol **47:**1123–1133. http://dx.doi.org/10.1046/j.1365-2958.2003.03361.x.
15. **Schiller NL, Robles-Price A, Wong TY, Sletta H, Valla S.** 2004. AlgX is a periplasmic protein required for alginate biosynthesis in *Pseudomonas aeruginosa*. J Bacteriol **186:**7369–7377. http://dx.doi.org/10.1128/JB.186.21.7369-7377.2004.
16. **Bakkevig K, Sletta H, Gimmestad M, Aune R, Ertesvåg H, Degnes K, Christensen BE, Ellingsen TE, Valla S.** 2005. Role of the *Pseudomonas fluorescens* alginate lyase (AlgL) in clearing the periplasm of alginates not exported to the extracellular environment. J Bacteriol **187:**8375–8384. http://dx.doi.org/10.1128/JB.187.24.8375-8384.2005.
17. **Keiski CL, Harwich M, Jain S, Neculai AM, Yip P, Robinson H, Whitney JC, Riley L, Burrows LL, Ohman DE, Howell PL.** 2010. AlgK is a TPR-containing protein and the periplasmic component of a novel exopolysaccharide secretin. Structure **18:**265–273. http://dx.doi.org/10.1016/j.str.2009.11.015.
18. **Rehman ZU, Rehm BH.** 2013. Dual roles of *Pseudomonas aeruginosa* AlgE in secretion of the virulence factor alginate and formation of the secretion complex. Appl Environ Microbiol **79:**2002–2011. http://dx.doi.org/10.1128/AEM.03960-12.
19. **Douthit SA, Dlakic M, Ohman DE, Franklin MJ.** 2005. Epimerase active domain of *Pseudomonas aeruginosa* AlgG, a protein that contains a right-handed beta-helix. J Bacteriol **187:**4573–4583. http://dx.doi.org/10.1128/JB.187.13.4573-4583.2005.
20. **Albrecht MT, Schiller NL.** 2005. Alginate lyase (AlgL) activity is required for alginate biosynthesis in *Pseudomonas aeruginosa*. J Bacteriol **187:**3869–3872. http://dx.doi.org/10.1128/JB.187.11.3869-3872.2005.
21. **Rehman ZU, Wang Y, Moradali MF, Hay ID, Rehm BH.** 2013. Insights into the assembly of the alginate biosynthesis machinery in *Pseudomonas aeruginosa*. Appl Environ Microbiol **79:**3264–3272. http://dx.doi.org/10.1128/AEM.00460-13.
22. **Hay ID, Schmidt O, Filitcheva J, Rehm BH.** 2012. Identification of a periplasmic AlgK-AlgX-MucD multiprotein complex in *Pseudomonas aeruginosa* involved in biosynthesis and regulation of alginate. Appl Microbiol Biotechnol **93:**215–227. http://dx.doi.org/10.1007/s00253-011-3430-0.
23. **Kulasakara H, Lee V, Brencic A, Liberati N, Urbach J, Miyata S, Lee DG, Neely AN, Hyodo M, Hayakawa Y, Ausubel FM, Lory S.** 2006. Analysis of *Pseudomonas aeruginosa* diguanylate cyclases and phosphodiesterases reveals a role for bis-(3′-5′)-cyclic-GMP in virulence. Proc Natl Acad Sci U S A **103:**2839–2844. http://dx.doi.org/10.1073/pnas.0511090103.
24. **Hay ID, Remminghorst U, Rehm BH.** 2009. MucR, a novel membrane-associated regulator of alginate biosynthesis in *Pseudomonas aeruginosa*. Appl Environ Microbiol **75:**1110–1120. http://dx.doi.org/10.1128/AEM.02416-08.
25. **Rehm BHA, Remminghorst U.** 2006. Alg44, a unique protein required for alginate biosynthesis in *Pseudomonas aeruginosa*. FEBS Lett **580:**3883–3888. http://dx.doi.org/10.1016/j.febslet.2006.05.077.
26. **Ohman DE, Oglesby LL, Jain S.** 2008. Membrane topology and roles of *Pseudomonas aeruginosa* Alg8 and Alg44 in alginate polymerization. Microbiology **154:**1605–1615. http://dx.doi.org/10.1099/mic.0.2007/015305-0.
27. **Steiner S, Lori C, Boehm A, Jenal U.** 2013. Allosteric activation of exopolysaccharide synthesis through cyclic di-GMP-stimulated protein-protein interaction. EMBO J **32:**354–368. http://dx.doi.org/10.1038/emboj.2012.315.
28. **Rehm B.** 2009. Microbial production of biopolymers and polymer precursors: applications and perspectives. Caister Academic, Wymondham, United Kingdom.
29. **Morgan JL, Strumillo J, Zimmer J.** 2013. Crystallographic snapshot of cellulose synthesis and membrane translocation. Nature **493:**181–186. http://dx.doi.org/10.1038/nature11744.
30. **Morgan JL, McNamara JT, Zimmer J.** 2014. Mechanism of activation of bacterial cellulose synthase by cyclic di-GMP. Nat Struct Mol Biol **21:**489–496. http://dx.doi.org/10.1038/nsmb.2803.
31. **Kelley LA, Sternberg MJ.** 2009. Protein structure prediction on the Web: a case study using the Phyre server. Nat Protoc **4:**363–371. http://dx.doi.org/10.1038/nprot.2009.2.
32. **Franklin MJ, Ohman DE.** 1993. Identification of *algF* in the alginate biosynthetic gene cluster of *Pseudomonas aeruginosa* which is required for alginate acetylation. J Bacteriol **175:**5057–5065.
33. **Franklin MJ, Ohman DE.** 1996. Identification of *algI* and *algJ* in the *Pseudomonas aeruginosa* alginate biosynthetic gene cluster which are required for alginate O acetylation. J Bacteriol **178:**2186–2195.
34. **Franklin MJ, Chitnis CE, Gacesa P, Sonesson A, White DC, Ohman DE.** 1994. *Pseudomonas aeruginosa* AlgG is a polymer level alginate C5-mannuronan epimerase. J Bacteriol **176:**1821–1830.
35. **Wolfram F, Kitova EN, Robinson H, Walvoort MT, Codée JD, Klassen JS, Howell PL.** 2014. Catalytic mechanism and mode of action of the periplasmic alginate epimerase AlgG. J Biol Chem **289:**6006–6019. http://dx.doi.org/10.1074/jbc.M113.533158.
36. **Ma L, Conover M, Lu H, Parsek MR, Bayles K, Wozniak DJ.** 2009. Assembly and development of the *Pseudomonas aeruginosa* biofilm matrix. PLoS Pathog **5:**e1000354. http://dx.doi.org/10.1371/journal.ppat.1000354.
37. **Billings N, Millan M, Caldara M, Rusconi R, Tarasova Y, Stocker R, Ribbeck K.** 2013. The extracellular matrix component Psl provides fast-acting antibiotic defense in *Pseudomonas aeruginosa* biofilms. PLoS Pathog **9:**e1003526. http://dx.doi.org/10.1371/journal.ppat.1003526.
38. **Cuthbertson L, Mainprize IL, Naismith JH, Whitfield C.** 2009. Pivotal roles of the outer membrane polysaccharide export and polysaccharide copolymerase protein families in export of extracellular polysaccharides in Gram-negative bacteria. Microbiol Mol Biol Rev **73:**155–177. http://dx.doi.org/10.1128/MMBR.00024-08.
39. **Galindo E, Peña C, Núñez C, Segura D, Espín G.** 2007. Molecular and bioengineering strategies to improve alginate and polydydroxyalkanoate production by *Azotobacter vinelandii*. Microb Cell Fact **6:**7. http://dx.doi.org/10.1186/1475-2859-6-7.
40. **Tielen P, Strathmann M, Jaeger KE, Flemming HC, Wingender J.** 2005.

Alginate acetylation influences initial surface colonization by mucoid *Pseudomonas aeruginosa*. Microbiol Res **160:**165–176. http://dx.doi.org/10.1016/j.micres.2004.11.003.

41. **Gloag ES, Javed MA, Wang H, Gee ML, Wade SA, Turnbull L, Whitchurch CB**. 2013. Stigmergy: a key driver of self-organization in bacterial biofilms. Commun Integr Biol **6:**e27331. http://dx.doi.org/10.4161/cib.27331.
42. **Pang CM, Hong P, Guo H, Liu WT**. 2005. Biofilm formation characteristics of bacterial isolates retrieved from a reverse osmosis membrane. Environ Sci Technol **39:**7541–7550. http://dx.doi.org/10.1021/es050170h.
43. **Hengge R**. 2009. Principles of c-di-GMP signalling in bacteria. Nat Rev Microbiol **7:**263–273. http://dx.doi.org/10.1038/nrmicro2109.
44. **Hancock RE, Nikaido H**. 1978. Outer membranes of Gram-negative bacteria. XIX. Isolation from *Pseudomonas aeruginosa* PAO1 and use in reconstitution and definition of the permeability barrier. J Bacteriol **136:**381–390.
45. **Campisano A, Schroeder C, Schemionek M, Overhage J, Rehm BH**. 2006. PslD is a secreted protein required for biofilm formation by *Pseudomonas aeruginosa*. Appl Environ Microbiol **72:**3066–3068. http://dx.doi.org/10.1128/AEM.72.4.3066-3068.2006.
46. **Ghafoor A, Hay ID, Rehm BH**. 2011. Role of exopolysaccharides in *Pseudomonas aeruginosa* biofilm formation and architecture. Appl Environ Microbiol **77:**5238–5246. http://dx.doi.org/10.1128/AEM.00637-11.
47. **Kuehn M, Hausner M, Bungartz HJ, Wagner M, Wilderer PA, Wuertz S**. 1998. Automated confocal laser scanning microscopy and semiautomated image processing for analysis of biofilms. Appl Environ Microbiol **64:**4115–4127.
48. **Heydorn A, Nielsen AT, Hentzer M, Sternberg C, Givskov M, Ersbøll BK, Molin S**. 2000. Quantification of biofilm structures by the novel computer program COMSTAT. Microbiology **146:**2395–2407.
49. **Hay ID, Schmidt O, Filitcheva J, Rehm BH**. 2012. Identification of a periplasmic AlgK-AlgX-MucD multiprotein complex in *Pseudomonas aeruginosa* involved in biosynthesis and regulation of alginate. Appl Microbiol Biotechnol **93:**215–227. http://dx.doi.org/10.1007/s00253-011-3430-0.